COMILLAS
UNIVERSIDAD PONTIFICIA
ICAI

GRADO EN INGENIERÍA EN TECNOLOGÍAS INDUSTRIALES (GITI)

DESIGN OF A MODULAR ROCKET TO PASS THE THREE LEVELS OF THE TRIPOLI ROCKETRY ASSOCIATION WITH A CANSAT PAYLOAD

Autor: Ignacio Victoria Rodríguez

Director: Dr. Francisco José López Valdés

A mi familia.

≪ ***"Hey Buzz! You are flying!"***

"This isn't flying, this is falling with style."

"To infinity and beyond" ≫

-Toy Story (1995)

AUTORIZACIÓN PARA LA DIGITALIZACIÓN, DEPÓSITO Y DIVULGACIÓN EN RED DE PROYECTOS FIN DE GRADO, FIN DE MÁSTER, TESINAS O MEMORIAS DE BACHILLERATO

1º. Declaración de la autoría y acreditación de la misma.

El autor D. Ignacio Victoria Rodríguez

DECLARA ser el titular de los derechos de propiedad intelectual de la obra: "Designo f a modular rocket to pass the three levels of the Tripoli Rocketry Association with a CanSat payload", que ésta es una obra original, y que ostenta la condición de autor en el sentido que otorga la Ley de Propiedad Intelectual.

2º. Objeto y fines de la cesión.

Con el fin de dar la máxima difusión a la obra citada a través del Repositorio institucional de la Universidad, el autor **CEDE** a la Universidad Pontificia Comillas, de forma gratuita y no exclusiva, por el máximo plazo legal y con ámbito universal, los derechos de digitalización, de archivo, de reproducción, de distribución y de comunicación pública, incluido el derecho de puesta a disposición electrónica, tal y como se describen en la Ley de Propiedad Intelectual. El derecho de transformación se cede a los únicos efectos de lo dispuesto en la letra a) del apartado siguiente.

3º. Condiciones de la cesión y acceso

Sin perjuicio de la titularidad de la obra, que sigue correspondiendo a su autor, la cesión de derechos contemplada en esta licencia habilita para:

a) Transformarla con el fin de adaptarla a cualquier tecnología que permita incorporarla a internet y hacerla accesible; incorporar metadatos para realizar el registro de la obra e incorporar "marcas de agua" o cualquier otro sistema de seguridad o de protección.
b) Reproducirla en un soporte digital para su incorporación a una base de datos electrónica, incluyendo el derecho de reproducir y almacenar la obra en servidores, a los efectos de garantizar su seguridad, conservación y preservar el formato.
c) Comunicarla, por defecto, a través de un archivo institucional abierto, accesible de modo libre y gratuito a través de internet.
d) Cualquier otra forma de acceso (restringido, embargado, cerrado) deberá solicitarse expresamente y obedecer a causas justificadas.
e) Asignar por defecto a estos trabajos una licencia Creative Commons.
f) Asignar por defecto a estos trabajos un HANDLE (URL *persistente)*.

4º. Derechos del autor.

El autor, en tanto que titular de una obra tiene derecho a:

a) Que la Universidad identifique claramente su nombre como autor de la misma
b) Comunicar y dar publicidad a la obra en la versión que ceda y en otras posteriores a través de cualquier medio.
c) Solicitar la retirada de la obra del repositorio por causa justificada.
d) Recibir notificación fehaciente de cualquier reclamación que puedan formular terceras personas en relación con la obra y, en particular, de reclamaciones relativas a los derechos de propiedad intelectual sobre ella.

5º. Deberes del autor.

El autor se compromete a:

a) Garantizar que el compromiso que adquiere mediante el presente escrito no infringe ningún derecho de terceros, ya sean de propiedad industrial, intelectual o cualquier otro.
b) Garantizar que el contenido de las obras no atenta contra los derechos al honor, a la intimidad y a la imagen de terceros.
c) Asumir toda reclamación o responsabilidad, incluyendo las indemnizaciones por daños, que pudieran ejercitarse contra la Universidad por terceros que vieran infringidos sus derechos e

intereses a causa de la cesión.

d) Asumir la responsabilidad en el caso de que las instituciones fueran condenadas por infracción de derechos derivada de las obras objeto de la cesión.

6º. Fines y funcionamiento del Repositorio Institucional.

La obra se pondrá a disposición de los usuarios para que hagan de ella un uso justo y respetuoso con los derechos del autor, según lo permitido por la legislación aplicable, y con fines de estudio, investigación, o cualquier otro fin lícito. Con dicha finalidad, la Universidad asume los siguientes deberes y se reserva las siguientes facultades:

- La Universidad informará a los usuarios del archivo sobre los usos permitidos, y no garantiza ni asume responsabilidad alguna por otras formas en que los usuarios hagan un uso posterior de las obras no conforme con la legislación vigente. El uso posterior, más allá de la copia privada, requerirá que se cite la fuente y se reconozca la autoría, que no se obtenga beneficio comercial, y que no se realicen obras derivadas.
- La Universidad no revisará el contenido de las obras, que en todo caso permanecerá bajo la responsabilidad exclusive del autor y no estará obligada a ejercitar acciones legales en nombre del autor en el supuesto de infracciones a derechos de propiedad intelectual derivados del depósito y archivo de las obras. El autor renuncia a cualquier reclamación frente a la Universidad por las formas no ajustadas a la legislación vigente en que los usuarios hagan uso de las obras.
- La Universidad adoptará las medidas necesarias para la preservación de la obra en un futuro.
- La Universidad se reserva la facultad de retirar la obra, previa notificación al autor, en supuestos suficientemente justificados, o en caso de reclamaciones de terceros.

Madrid, a 7 de julio de 2020

ACEPTA

Fdo………………………………………………………

Motivos para solicitar el acceso restringido, cerrado o embargado del trabajo en el Repositorio Institucional:

Declaro, bajo mi responsabilidad, que el Proyecto presentado con el título “Design of a modular rocket to pass the three lecels of the Tripoli Rocketry Association with a CanSat payload”

en la ETS de Ingeniería - ICAI de la Universidad Pontificia Comillas en el curso académico 2019/2020 es de mi autoría, original e inédito y

no ha sido presentado con anterioridad a otros efectos. El Proyecto no es plagio de otro, ni total ni parcialmente y la información que ha sido tomada de otros documentos está debidamente referenciada.

Fdo.: Ignacio Victoria Rodríguez Fecha: 07/ 07/ 2020

Autorizada la entrega del proyecto

EL DIRECTOR DEL PROYECTO

LOPEZ VALDES FRANCISCO JOSE - 09437440B

Firmado digitalmente por LOPEZ VALDES FRANCISCO JOSE - 09437440B
Fecha: 2020.07.08 17:37:33 +02'00'

Fdo.: Francisco José López Valdés Fecha: 07/ 07/ 2020

Este proyecto contiene los siguientes documentos:

DOCUMENTO 1: MEMORIA	pág. 1 a 170 170 páginas
DOCUMENTO 2: PLANOS	pág. 1 a 54 54 páginas
DOCUMENTO 3: PLIEGO DE CONDICIONES	pág. 1 a 31 31páginas

This Project contains the following documents:

DOCUMENT 1: MEMOIR	pág. 1 a 170 170 páginas
DOCUMENT 2: BLUEPRINTS	pág. 1 a 54 54 páginas
DOCUMENT 3: CONDITIONS AND REQUIREMENTS	pág. 1 a 31 31páginas

DOCUMENT 1: MEMOIR

Index

Table of Figures ... 3

Table of tables ... 7

Resumen del Proyecto ... 10

Project Summary ... 25

Introduction ... 40

- **Motivation** ... 41
- **State of the Art** ... 41

Requirements ... 44

Modular connector ... 45

- **Mechanical design** ... 45
- **Gluing Length** ... 51
- **Design Result** ... 54

Composite Tubes ... 55

- **Tube Sizing** ... 55
- **Tube characterization** ... 59
- **Service deformations** ... 60

Nosecone ... 62

- **Adimensional approximation** ... 62
- **Nosecone selection** ... 63
- **First Characterization of the Drag Forces as a function of time** ... 71
- **System overview** ... 71

Recovery system ... 73

- **System's discussion** ... 73
- **Single Event Recovery System** ... 75
- **Double Event Recovery System** ... 77
- **System rundown and operation** ... 78
- **Electromagnetic joint** ... 78

Avionics and Payload Module ... 81

- **Structural Design** ... 81
  - **Beam Design** ... 81
  - **Coupler modification** ... 92
  - **Structure Assembly** ... 93
- **Payload bay mechanism** ... 93
  - **Payload system assembly** ... 108

Motor Characterization ... 109
Level 1 motor characterization ... 109
Level 2 motor characterization ... 114
Level 3 motor characterization ... 121
Multivariate adaptative regression splines ... 126
Engine Bay ... 129
Mis-fire safety system ... 129
Hydrodynamic circuit ... 132
Thrust plate design ... 137
Engine bay configuration ... 141
Boat tail ... 142
Fins ... 144
Rocket Overview ... 157
Level 1 ... 157
Level 2 ... 158
Level 3 ... 159
Flight Simulations ... 160
Level 1 rocket ... 160
Level 2 Rocket ... 161
Level 3 Rocket ... 162
Naming ... 164
Millennium developments goals ... 165
Outlook ... 166
References ... 167

Table of Figures

Figure 1 | Conector 11
Figure 2 | Disposición capas 12
Figure 3 | Distribución de presiones y velocidades entorno a la ojiva Von Kármán 15
Figure 4 | Sección Montaje Ojiva 15
Figure 5 | Evento único y doble evento con y sin tubo interno 16
Figure 6 | Plastificación de una sección con solicitaciones internas previas 19
Figure 7 | Tensiones y deformaciones viga aviónica 20
Figure 8 | Diseño correa, tornillo sin fin y montaje en el módulo 20
Figure 9 | Simulaciones Thrust Plates 22
Figure 10 | Sección aleta 23
Figure 11 | Simulaciones de vuelo 24
Figure 12 | Simulación Nivel 3 control electrónico y Nivel 1 sin aviónica ni carga 24
Figure 13 | Coupleur render 26
Figure 14 | Layer alignment 27
Figure 15 | Hack series c=0 pressure and velocity distributions 30
Figure 16 | Nosecone assembly cross-section 30
Figure 17 | Single event, double event with and without the phenolique tube 31
Figure 18 | elastic limit saturation cross-section 34
Figure 19 | Stress and deformation beam simulation 35
Figure 20 | Belt assembly, worm gear-wheel pair and their assembly in the module 35
Figure 21 | Thrust plates simulations 2 operational and all 3 operational 37
Figure 22 | Fin cross-section 38
Figure 23 | Worst case scenarios flight simulations 39
Figure 24 | Follow up simulations Levels 3 and 1 39
Figure 25 | EPFL Rocket Team, Eiger I (2020) 40
Figure 26|Hydra Experiencing Fin Flutter (2016) 41
Figure 27 | Connector threaded insert cross-section 45
Figure 28 | Thread cross-section (Fastenings, 2020) 45
Figure 29 | Screw-beam equivalent 48
Figure 30 | Connector load transfer cross-section 48
Figure 31 | Threaded insert-cantilever equivalent Figure 32 | Screw cantilever .. 48
Figure 33 | Strain and moment diagrams of a cantilever under a uniformly distributed charge . 49
Figure 34 | Full connector assembly cross-section 50
Figure 35 | Contact cross-section coupleurs 50
Figure 36 Schematic view of a single lap shear joint 51
Figure 37 Distribution of stresses calculated as presented in the reference 51
Figure 38 Stress distribution along the gluing surface 52
Figure 39 Adhesive axial shear stress distribution as represented in the literature 53
Figure 40 Interfacial radial stress distribution as represented in the reference 53
Figure 41 | Coupleur render 54
Figure 42 | Layer alignment 59
Figure 43|Elliptical nose cone cross-section (Senthiil, 2018) 64
Figure 44 | Tangent nose cone cross-section (Sr., 1996) 64
Figure 45 | Parabolic nose cone cross-section (Department of Defence, United States of America, 1996) 64
Figure 46 | Haack series nose cone cross-section (Sr., 1996) 65
Figure 47 | Elliptical nosecone pressure distribution 68

Figure 48 | Parabolic nosecone pressure distribution 68
Figure 49| Haack c=0 nosecone pressure distribution 69
Figure 50 | Haack nosecone c=1/3 pressure distribution 69
Figure 51 | Haack c=0 velocity distribution 69
Figure 52 | Haack c=1/3 velocity distribution 70
Figure 53 | Elliptical velocity distribution 70
Figure 54 | Parabolic velocity distribution 70
Figure 55 | Nosecone assembly cross-section 71
Figure 56 | Nosecone front view 72
Figure 57 | Nosecone lower view (eye bolt detail) 72
Figure 58 | Parachute sketch (Fruity Chutes Inc., 2019) 74
Figure 59 | Single Event Recovery internal system 77
Figure 60 | Double Event Recovery system detail 77
Figure 61 | Equivalent magnetic circuit 80
Figure 62 | beam cross-section 82
Figure 63| Beam cross-section with pre-constraints 83
Figure 64|Elastic deformation of the beam with pre-constraints 84
Figure 65 | Beam simulation load distribution 90
Figure 66 | Normal force beam simulation 90
Figure 67 | Torsional moment beam simulation 91
Figure 68 | Flexural moment along the y axis beam simulation 91
Figure 69 | Flexural moment along the z axis beam simulation 91
Figure 70 | Mesh Beam Simulation 91
Figure 71 | Stress distribution beam simulation 92
Figure 72| Unitary deformations beam simulation 92
Figure 73 | Gluing surface AV/PL module 93
Figure 74 | AV/PL module structure 93
Figure 75 | Gear Teeth detail 94
Figure 76 | Cylindrical Worm Right Hand Helix (KHK Gears, s.f.) 95
Figure 77 | Cylindrical Worm Gear pair (KHK Gears, s.f.) 95
Figure 78 | Trapezoidal belt cross-section 98
Figure 79 | Belt length scheme (Soubielle, Transmissions à courroies III, 2020) 99
Figure 80 | Belt-Puller induced stress (Soubielle, Transmission à courroies I, 2020) 99
Figure 81 | Sections of a belt-assembly (Soubielle, Transmission à courroies I, 2020) 100
Figure 82 | Initial tension schema (Soubielle, Transmission à courroies I, 2020) 101
Figure 83 | Differential Section-Belt (Soubielle, Transmission à courroies I, 2020) 102
Figure 84 | Operation limits Belt (Soubielle, Transmission à courroies I, 2020) 103
Figure 85 | Stress distribution in the belt (Soubielle, Transmission par courroies, 2020) 103
Figure 86 | Simple 2 pulley system 105
Figure 87 | Pulley-Belt assembly 105
Figure 88 | Net magnetic dipole beams 107
Figure 89 | Net electromagnetic dipole pusher 107
Figure 90 | Payload deployment system assembly 108
Figure 91 | I218R characteristic curve 110
Figure 92 | Non-linear regression ascending arm Level 1 results 110
Figure 93 | Residual analysis ascending arm Level 1 111
Figure 94 | Level 1 ascending arm model 111
Figure 95 | Non-linear regression descending arm Level 1 results 112

Figure 96 | Residual analysis descending arm Level 1 112
Figure 97 | Level 1 ascending arm model 113
Figure 98 | Level 1 motor characterization 114
Figure 99 | L1100 characteristic curve (National Association of Rocketry, 2004) 115
Figure 100 | Non-linear regression ascending section Level 2 results 115
Figure 101 | Residual analysis ascending arm Level 2 116
Figure 102 | Level 2 ascending arm model 116
Figure 103 | Non-linear regression plateau Level 2 results 117
Figure 104 | Residual analysis plateau Level 2 117
Figure 105 | Level 2 plateau arm 118
Figure 106 | Non-linear regression descending arm Level 2 results 118
Figure 107 | Residual analysis descending arm Level 2 119
Figure 108 | Level 2 descending arm model 120
Figure 109 | Level 2 motor characterization 120
Figure 110 | M650W characteristic curve (National Association of Rockertry, 2007) 121
Figure 111 | Level 3 ascending arm boxplot 121
Figure 112 | Non-linear regression descending arm Level 3 results 122
Figure 113 | Residual analysis ascending arm Level 3 122
Figure 114 | Level 3 ascending arm model 123
Figure 115 | Non-linear regression descending arm Level 3 results 123
Figure 116 | Residual analysis descending arm Level 3 124
Figure 117 | Level 3 descending arm model 124
Figure 118 | Level 3 motor characterization 125
Figure 119 | Good modelling output tests 126
Figure 120 | Level 1 model complexity graph 127
Figure 121 | Level 1 modelling results vs data 127
Figure 122 | Level 3 Model Complexity Graph 128
Figure 123 | Level 3 model vs data 128
Figure 124 | Converging and diverging flows (Vasava, 2007) 133
Figure 125 | Nozzle-fuel tube interaction 134
Figure 126 | Forces distribution stand-alone simulation 137
Figure 127 | Thrust plate mesh stand-alone simulation 138
Figure 128 | Thrust plate stress distribution stand-alone simulation 138
Figure 129 | Thrust plate unitary deformation stand-alone simulation 139
Figure 130 | Thrust plate deformations stand-alone simulation 139
Figure 131 | Load distribution thrust plate service simulation 139
Figure 132 | Thrust plate mesh service simulation 140
Figure 133 | Thrust plate stress distribution service simulation 140
Figure 134 | Thrust plate unitary deformation service simulation 140
Figure 135 | Thrust plate deformations service simulation 141
Figure 136 | Engine bay configuration 141
Figure 137 | Thrust Plate assembly details 141
Figure 138 | Fins retainer assembly 142
Figure 139 | Boat tail assembly detail 143
Figure 140 | End height-Fin length plot Level ·1 145
Figure 141 | End height-Fin length plot Level ·2 146
Figure 142 | End height-Fin length plot Level ·3 146
Figure 143|Fin cross-section (Nakka, Fins, 2001) 147

Figure 144 | Fin NACA cross-section 151
Figure 145 | Stress distribution on a Level 1 fin 152
Figure 146 | Stress distribution in a Level 2 fin 152
Figure 147 | Stress distribution on a Level 3 fin 153
Figure 148 | Hydra Fins flutter 156
Figure 149 | Level 1 rocket assembly 157
Figure 150 | Level 2 rocket assembly 158
Figure 151 | Level 3 rocket assembly 159
Figure 152 | Level 1 simulation configuration 160
Figure 153 | Level 1 simulation results 160
Figure 154 | Alternative Level 1 configuration 161
Figure 155 | Alternative Level 1 simulation 161
Figure 156 | Level 2 simulation configuration 161
Figure 157 | Level 2 simulation results 162
Figure 158 | Level 3 simulation configuration 162
Figure 159 | Level 3 simulation results 163
Figure 160 | Level 3 alternative simulation results 163

Table of tables

Table 1 | Requisitos Tripoli 10
Table 2 | Calidad Tornillos 11
Table 3 | Deformaciones de servicio 13
Table 4 | Coeficientes de arrastre 14
Table 5 | Sección y montaje de la viga de aviónica 18
Table 6 | Diseño tornillo sin fin-rueda dentada 21
Table 7 | Composición motores 21
Table 8 | Prérdidas circuito hidráulico 22
Table 9 | Composición aletas y velocidad de resonancia 23
Table 10 | Tripoli Requirements 25
Table 11 | Screw quality 26
Table 12 | Maximum Service Deformations 28
Table 13 | Cross-section drag coefficients 29
Table 14 | Beam characterization 33
Table 15 | Worm gear-wheel design 36
Table 16 | Engine composition 36
Table 17 | Hydraulic circuit losses 37
Table 18 | Fin composition and flutter speed 38
Table 19 | Tripoli Requirements 44
Table 20 | Commercial screw quality comparison 49
Table 21 | Maximum efforts calculations 61
Table 22| Adimensionally calculated drag coefficients 67
Table 23| Simulated drag coefficients 68
Table 24 | Tripoli Recovery Requirements 73
Table 25 | Cable characterization 80
Table 26 | Torsional Constant Coefficient 82
Table 27 | Beam cross-section dimensions 83
Table 28 | Teeth stress 94
Table 29 | Worm gear-Wheel design 96
Table 30 | Wheel check 97
Table 31 | Motor characteristics 109
Table 32 | Engine impulse 126
Table 33 | Engine composition 130
Table 34 | Magnesium hydroxide calculations 131
Table 35 | Magnesium hydroxide concentration and density 131
Table 36 | Valve Loss Coefficient 132
Table 37| Casing nozzle values 134
Table 38| Energy loss calculations 136
Table 39|Fin size approximation 145
Table 40 | Aspect Ratio per Level 150
Table 41 | Centre of gravity of each fin type 150
Table 42 | Maximum Stress on the fins per axise 153
Table 43 | Composition percentages of each fin 154
Table 44 | fins fluttering results 156
Table 45 | Level 1 modules 157
Table 46 | Level 1 characteristics 157
Table 47 | Level 2 modules 158

Table 48 | Level 2 characteristics 158
Table 49 | Level 3 modules 159
Table 50 | Level 3 characteristics 159

DISEÑO Y SIMULACIÓN DE UN COHETE MODULAR CAPAZ DE SUPERAR LOS 3 NIVELES DE LA TITULACIÓN TRIPOLI CON UNA CARGA CANSAT

Autor: Victoria rodríguez, Ignacio.

Director: López Valdés, Francisco José.

Entidad Colaboradora: ICAI Rocket Team

Resumen del Proyecto

Objetivo

Diseño y simulación de un cohete modular (diámetro interno 120mm) capaz de obtener los 3 niveles de la Certificación Trípoli.

Requisitos

Certificación Tripoli	Nivel 1	Nivel 2	Nivel 3
Máximo impulse permitido	640N-s	5120N-s	>5120N-s
Cuerpo del cohete	Diseño convencional (cohete balístico). El Centro de Presiones debe estar claramente mercado en el exterior de la estructura- Los cohetes concebidos y construidos por el piloto pueden contener elementos comerciales.		
Sistemas de paracaídas	Sistema estándar de paracaídas, evento único o doble evento (En caso de tener un doble evento el primer evento puede tener diferentes iteraciones siempre y cuando el segundo sea un paracaídas clásico).		Sin especificar.
Motores autorizados	Un único motor de clase I o H (impulso total comprobado experimentalmente entre 160.01 y 640.00 N-s). Cohetes por fases o grupos de motores no están permitidos.	Un único motor de clase J, K o L (impulso total comprobado experimentalmente entre 640.01 y 5120.00 N-s). Cohetes por fases o grupos de motores no están permitidos.	Un único motor de clase M o superior (impulso total comprobado experimentalmente mayor de 5120.01 N-s). Cohetes por fases o grupos de motores no están permitidos.
Electrónica y aviónica	No es necesaria. Antes de obtener el permiso para realizar el vuelo para obtener el nivel de certificación 3 el piloto debe haber demostrado que es capaz de operar un sistema de paracaídas controlado electrónicamente en un cohete de nivel 2		El vehículo debe tener al menos 2 sistemas electrónicos separados con fuentes de alimentación independientes y elementos de ignición separados para el paracaídas principal y el paracaídas de emergencia.
Otros	El cohete puede ser comprado o construido por el piloto		El cohete debe ser construido por el piloto
Referencias	(Tripoli Rocketry Association, 2020)	(Tripoli Rocketry Association, 2020)	(Tripoli Rocketry Association, 2020)

Table 1 | Requisitos Tripoli

Diseño del conector

El conector es la pieza mEás importante del cohete, no solo porque es la que más veces se repite a lo largo de la estructura (a excepción de elementos normalizados como los tornillos) si no porque permite variar la configuración del vehículo.

Figure 1 | Conector

De acuerdo con las normas de la SpacePort America Cup los elementos estructurales deben poder aguantar solicitaciones de hasta 30mg, (considerando la masa del cohete de nivel 3 30kg). El conector se diseñó con esos parámetros, de tal manera que los 6 roscados M6 de las lengüetas disponen de un coeficiente de seguridad de 1.37 y su construcción los hace autoblocantes, por lo que no hay peligro de que se suelten en mitad del vuelo.

Los taladros y roscados perpendiculares al eje principal disponen de un coeficiente de seguridad de 4.32 en total (1.44 por cada pareja de tornillos), por lo tanto, pueden fallar hasta 4 y mantener la integridad estructural (con calidad 10.9), frente a una solicitación máxima de:$|\sigma| = 391.35MPa$.

Calidad tornillos	Limite rotura (MPa)	Limite Élastico (MPa)	OK
4.6	400	240	No
5.6	500	300	No
8.8	800	640	Marginalmente
10.9	1000	900	Sí
12.9	1200	1080	Sí

Table 2 | Calidad Tornillos

Y la superficie de contacto entre conectores permite pasar los esfuerzos de compresión con un coeficiente de seguridad de hasta 10.66.

La superficie de pegado se calculó de acuerdo con la referencia (Aimmanee, 2017), aplicando simultáneamente efectos de torsión y solicitaciones axiales, llegando al caso límite donde la tensión equivalente máxima era de 13.335MPa, considerando un limite de 15MPa para pegamentos epoxy, otorga un coeficiente de seguridad de:

$$n = \frac{\sigma_{adm}}{\sigma_{max}} \rightarrow n = \frac{15}{13.335} = 1.12$$

Finalmente, los conectores permiten únicamente el desplazamiento axial de los ensamblajes (por construcción), el cual recae sobre los tornillos pasantes. Debido a la construcción hay una rotación de 30º entre conectores.

Diseño de los tubos

Los tubos se diseñaron mediante un método iterativo para obtener la orientación de las diferentes capas de fibra de vidrio para aumentar sus resistencias y módulos de Young longitudinales y transversales, donde se consideraron 3 eventos donde se combinaban los siguientes casos:

- Una fuerza radial aplicada en lo alto del cohete (30mg) cuando se despliega el paracaidas si el paracaidas se desplegase radialmente) combinado con una diferencia de presiones de 1MPa debido a los cartuchos de dióxido de carbono (aproximadamente 10 atmósferas); un momento de torsión debido al empuje en las aletas causado por la desviación del cohete (considerado como $3mgR_{ext}$).
- Despliegue axial del paracaídas (30mg) combinado con el aumento de presión en los tubos y el momento torsor ya mencionados.
- Finalmente un esfuerzo de compresión que experimentará durante el vuelo, combinado con el momento torsor debido a la desviación y un aumento de la presión interna (simulando el disparo temprano de los cartuchos de dióxido de carbono).

Se procedió a la caracterización del cohete como un tubo de 3 metros de longitud, diámetro interno 120mm y diámetro externo 125mm y empotrado en 1 de los lados para maximizar los esfuerzos, tal que:

$$I_x = I_z = 1.805 * 10^6 \ mm^4$$

$$I_y = 3.610 * 10^6 \ mm^4$$

$$W_x = W_z = 28.887 * 10^3 \ mm^3$$

$$W_y = 57.774 * 10^3 \ mm^3$$

$$S_x = 58.920 * 10^3 mm^3$$

Con un esfuerzo máximo (alcanzado en el primer supuesto) de:

$$\sigma = \sqrt{\left(\sigma_{flex} + \sigma_{rad}\right)^2 \ + 4\tau_{tor}^2} \rightarrow \sigma = 306.6422MPa$$

Lo cual, tras calcular el alineamiento de 8 capas de fibra de vidrio de clase E como:

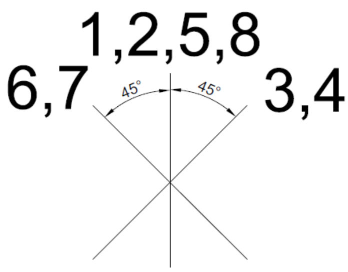

Figure 2 | Disposición capas

Otorgando por lo tanto unas fracciones másicas tales que el esfuerzo máximo siempre esté por debajo del límite de proporcionalidad del material compuesto:

$$\sigma_{yC} = 1.1\sigma_{max} = \left[1 + \frac{V_f E_f}{V_m E_m}\right] V_m \sigma_{ym} \rightarrow \begin{cases} V_m = 0.1872 \\ V_f = 0.8128 \end{cases}$$

De donde se pueden obtener los límites de servicio de los tubos:

Evento	Fórmula	Máxima deformación en servicio
Tracción (m)	$L = L_o e^{\frac{F}{AE}}$	$L = 3.00045$
Compresión (m)	$L = Le^{\frac{F}{AE}}$	$L = 2.99955$
Flexión debida a un esfuerzo puntual en un extremo (m)	$w = \frac{FL^3}{3EI_x}$	$w = 0.72780$
Ángulo de la deformada debido a un esfuerzo puntual en un extremo (rad)	$\theta = \frac{FL^2}{2EI_x}$	$\theta = 0.36390$
Deformación debida a un esfuerzo distribuido uniformemente (m)	$w = \frac{qL^4}{8EI_x}$	$w = 0.27293$
Ángulo de la deformada debido a un esfuerzo uniformemente distribuido (rad)	$\theta = \frac{qL^3}{6EI_x}$	$\theta = 0.1213$
Ángulo de deformación debido a la torsión(rad)	$\theta = \frac{M_t}{I_y G} L$	$\theta = 0.00189$
Máxima presión interna (MPa)	$P = \frac{2t\sigma_{max}}{D_{ext}}$	$P = 24.45154$

Table 3 | Deformaciones de servicio

Diseño, optimización y simulación de la ojiva

El morro u ojiva del cohete tiene como cometido principal reducir el arrastre del cuerpo principal del cohete, existen 2 grandes familias de ojivas:

- Construcción geométrica
- Concepción matemática

Las de construcción geométrica son las más empleadas común mente debido a su simpleza y facilidad de construcción, los principales perfiles son.

Sección elíptica:

$$y = R\sqrt{1 - \frac{x^2}{L^2}}$$

La sección de la ojiva es claramente una semi-elipse y de acuerdo con la literatura consultada, es la sección geométrica con menor arrastre para vuelos subsónicos 0.4≤ Ma ≤0.8 (Senthiil, 2018).

Otra construcción popular es la de sección tangencial, cuyo uso explican las referencias es puramente situacional (Filho, 2019):

$$y = \sqrt{\rho^2 - (L - x)^2} + R - \rho \mid \rho = \frac{R^2 + L^2}{2R}$$

La última de las secciones geométricas es la ojiva de sección parabólica:

$$y = R\left(2\frac{x}{L} - \left(\frac{x}{L}\right)^2\right)$$

Finalmente, las ojivas de concepción matemática, o series de Haack (Haack, 1941), se obtienen de la minimización de las ecuaciones de arrastre para una construcción cilíndrica y son comúnmente empleadas en vuelos trans-sónicos (Ma>1). Estas ojivas están compuestas por una serie de formas continuas determinadas por un factor C de los cuales 2 son de especial interés (Stroick, Nose Cone and Fin Optimization, 2011):

- LD (C=0): Arrastre se minimiza para una longitud y un diámetro especificados (también conocido como la ojiva de Von Kármán).
- LV (C=1/3): Arrastre minimizado para una longitud y un volumen predeterminados

Su principal problema es que no son tangentes al cilindro al que se acoplan, sin embargo, es una imperfección tan pequeña que suele obviarse:

$$y = \frac{R}{\sqrt{\pi}}\sqrt{\theta - \frac{\sin(2\theta)}{2} + C\sin^3(\theta)}\,|\theta = \arccos\left(1 - \frac{2x}{L}\right)$$

Así mismo el aspect ratio óptimo para vuelos subsónicos es de 5:

$$AR = \frac{L}{2R} \rightarrow L = 10R$$

Para realizar un primer estudio de los coeficientes de arrastre de las diferentes ojivas se empleó una definición derivada de números adimensionales:

$$F_d = \frac{1}{2}\rho u^2 C_d A \rightarrow C_d = 2\frac{A_w}{A_f}\frac{Be}{Re_L^2}$$

De la cual, empleando diferentes definicones y teoremas (Bernoulli, Froude) se obtuvo la definición:

$$C_d = \frac{4}{Fr^2}\frac{\int_0^L f(x)\sqrt{\left(f'(x)\right)^2 + 1}\,dx}{R_{ext}^2}$$

Por lo tanto, minimizar la integral del numerador implica minimizar el arrastre, además, estos resultados se corroboraron con una serie de simulaciones de flujo externo alrededor de las diferentes ojivas (v=30m/s; ρ=1.214kg/m^3):

Sección	Arrastre calculado	Arrastre simulado
Elíptica	0.215	0.242962
Tangencial	14.03	Did not converge
Parabolica	0.1823	0.359210
Haack (C=0)	0.047	0.205910
Haack (C=1/3)	1.418	0.234925

Table 4 | Coeficientes de arrastre

Pese a que los resultados no se corroboran con los obtenidos si que demuestran que la aproximación de números adimensionales si demuestran que la más apropiada es la ojiva de Von Kármán, con el siguiente perfil presiones (derecha), aplicando Bernoulli se puede calcular también las velocidades (izquierda):

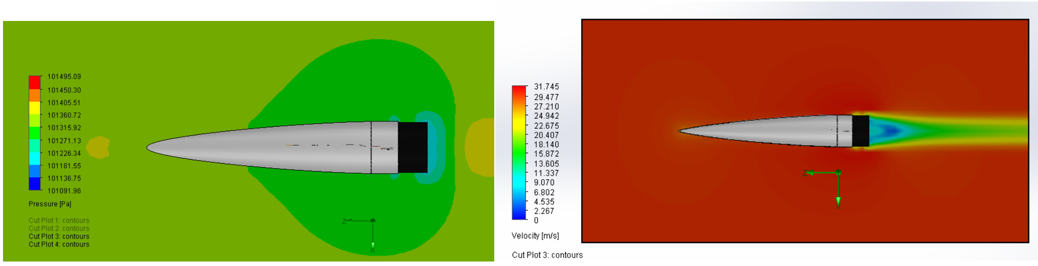

Figure 3 | Distribución de presiones y velocidades entorno a la ojiva Von Kármán

Para mantener la ojiva pegada al cohete durante el vuelo y una vez desplegado el paracaídas se diseñó un subsistema tal que la cuerda de conexión se ataba a una argolla y éste a una placa sujeta por un cilindro interno, para transmitir los esfuerzos (evitando así saliente de fibra de vidrio ya que curvas con radios pequeños en materiales compuestos comprometen seriamente su resistencia, además que así se puede dimensionar simplemente a tracción y no es necesario considerar flexión):

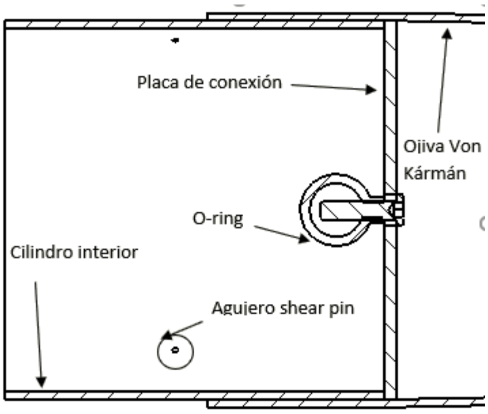

Figure 4 | Sección Montaje Ojiva

Así mismo, el cilindro interno tiene 3 agujeros para pasar 3 shear pins (pasadores de plástico dimensionados para romper cuando experimentan una fuerza cortante superior a 15MPa) de tal modo que se mantiene pegado en el ascenso y cuando se libera el dióxido de carbono aumenta la presión y rompen.

Diseño de los sistemas de paracaídas

Se diseñaron 2 sistemas de paracaídas (para que la velocidad al aterrizar fuese 4m/s):

- Evento único: Para el vuelo del nivel 1 y paracaídas secundario del nivel 3.
- Evento doble: Vuelos de nivel 2 y 3.

El evento único dispone de un paracaídas plano de forma hexagonal accionado por las cargas de dióxido de carbono, las cuales aumentan la presión y generan una fuerza de tracción en la placa del paracaídas integrada en la ojiva, la cual genera la cortante necesaria en los shear pins, rompiéndolos y desplegando el paracaídas. Así mismo, hay 3 pilares de los cuales 1 puede fallar y la seguridad estructural seguiría garantizada (evento único, izquierda y evento doble medio y derecha).

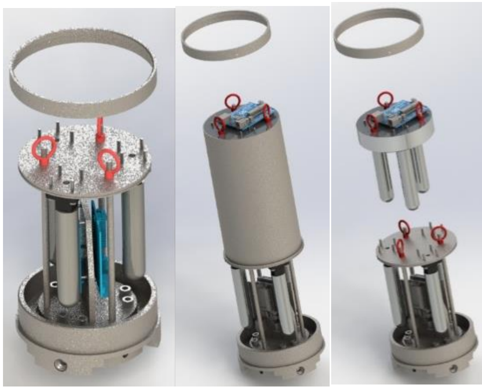

Figure 5 | Evento único y doble evento con y sin tubo interno

El anillo de aluminio en lo alto del tubo (hecho invisible en el renderizado) sirve como mera protección de la fibra para evitar su delaminación (debida a la fuerza ejercida por el cable) cuando se despliega el paracaídas.

Existe una redundancia tanto en la electrónica (2 controladores y 2 altímetros) como en las cargas de dióxido de carbono (existen 3 las cuales pueden ser accionadas por cualquiera de los 2 controladores, siendo solo 2 necesarios para desplegar el paracaídas).

La electrónica se basa en la señal de los altímetros para liberar el CO_2, cuando éstos detectan un aumento de la presión a lo largo de varios segundos (lo cual implica que el cohete ya ha alcanzado el apogeo y está cayendo), se mandan las señales a los micro-controladores que liberan el CO_2.

Tradicionalmente los cartuchos de CO_2 son perforados por punzones que son propulsados por una carga de pólvora negra, para evitar elementos inflamables dentro del cohete éstos han sido sustituidos por unas válvulas solenoides controladas por los micro-controladores.

De igual manera, se han considerado micro-controladores Arduino UNO debido a su gran tamaño, para que si en un futuro se deciden cambiar, haya espacio para montar unos más pequeños.

Para el sistema de evento doble el sistema es igual, se duplican las cargas de dióxido de carbono ya que 3 pasan de estar integradas en la base inferior a estar dentro de un tubo que contiene el segundo paracaídas, de tal modo que primero se accionan las cargas en el tubo interior de fenólico para propulsar el paracaídas pequeño (o de drogue, que frena la caída a 10m/s aproximadamente) y más tarde tras la señal del segundo set de altímetros se despliega el paracaídas principal que frena el cohete hasta 4m/s para aterrizar de manera segura.

Para evitar el despliegue del paracaídas principal antes de tiempo la estructura metálica en lo alto del tubo de fenólico está conectada a un imán que está en un conector imán-electroimán para transferir la fuerza directamente a la base del módulo, debido a la presencia de electrónica in jaula de Faraday la imantación es débil y por lo tanto, no se puede emplear la reversión del electroimán para propulsar el despliegue del paracaídas principal.

Para el vuelo de nivel 3, donde se necesita un sistema de paracaídas de emergencia, se montará el evento doble sobre el único y se juntarán mediante una pareja imán electroimán (más potente que la descrita anteriormente) la cual se puede revertir la corriente en el electroimán para desplegar el paracaídas de emergencia, ignorando si se puede dañar la electrónica, dado que si debe desplegarse implica que está en peligro la totalidad del cohete y se aplica el mal menor. Resolviendo la ecuación de dipolos magnéticos en coordenadas cilíndricas se obtiene:

$$\vec{\boldsymbol{F}}(\vec{r}, \overrightarrow{m_1}, \overrightarrow{m_2}) = \frac{-3\mu_o m_1 m_2}{2\pi z^4}\,\overrightarrow{e_3}$$

Y aplicando el teorema de superposición junto con el teorema de la mano derecha se puede obtener la corriente necesaria como función de la fuerza del imán permanente (considerando la resistencia de cable y una fuente de baja tensión, 5 V):

$$\overrightarrow{m_{elec}} = \pm inA\overrightarrow{e_3} \mid I = \frac{5}{0.028\,\frac{2n45\pi}{r^2\pi}}$$

Diseño, optimización y simulación de la estructura de los módulos de aviónica y carga

Debido a que el módulo de aviónica debe tener las antenas cilíndricas en la superficie y el de la carga debe abrirse, el tubo en dichas secciones no puede ser estructural, por lo tanto se procedió a diseñar un sistema de conectores y vigas para transferir los esfuerzos de manera segura.

Las vigas se diseñaron con el supuesto de que solo 2 estarían operativas, dotando así de mayor seguridad a la construcción. Se consideraron los siguientes esfuerzos:

- Tracción (despliegue del paracaídas 30mg).
- Compresión (en el despegue, 20mg según las normas de la SpacePort America Cup, para los cálculos se ha considerado 30mg para otorgar más seguridad).

$$F_{tract} = -F_{comp} = 30mg = 30^3 * 9.81 = 8829N$$

- Torsion (durante el vuelo, debido a la desviación del cohete, $3mgR_{ext}$).

$$M_{tor} = 3mgR_{ext}t = 3 * 30 * 9.81 * 62.5 * 10^{-3} = 55.18125Nm$$

- Momento flector debido a una fuerza radial aplicada en el extremo del módulo, con una magnitud de 30mg (la masa del módulo es de 5kg aplicado al final de la viga de 200mm).

$$M_{module} = 30mgL = 30 * 5 * 9.81 * 0.2 = 294.3Nm$$

Para dimensionar la torsión se consideró la referencia (Nussbaumer, 2015), de donde se obtuvo:

$$K_{beam} = 1.2 * 863.232 = 1035.878mm^4$$

Y el perfil de la viga (con sus valores respectivos):

Nombre	Simbolo	Valor		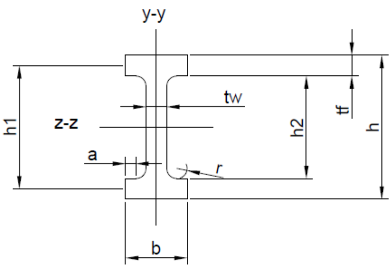
Altura	h	28		
Ancho	b	12		
Longitud equivalente del alma	h_1	24		
Espesor alma	t_w	4		
Web height	h_2	20		
Espesor patín	t_f	4		
Radio	r	-		
Patín útil	a	-		

Table 5 | Sección y montaje de la viga de aviónica

El radio y el patín útil no se pudieron dimensionar ya que depende del radio mínimo de la fibra empleada el cual depende del fabricante.

De tal modo que la viga quedaba caracterizada como:

$$A = t_w h_1 + 2bt_f \rightarrow A = 192mm^2$$

$$I_z = \frac{1}{12}h_1^3 t_w + 2\left(\frac{1}{12}bt_f^3 + b * t_f * \left(\frac{h_1}{2}\right)^2\right) \rightarrow I_z = 16618.667mm^4$$

$$I_y = \frac{1}{12}t_w^3 h_1 + \frac{1}{12}t_f b^3 \rightarrow I_y = 1258.667mm^4$$

$$W_z = \frac{I_z}{\frac{h}{2}} \rightarrow W_z = 1187.0476mm^3$$

$$W_y = \frac{I_y}{\frac{b}{2}} \rightarrow W_y = 209.778mm^3$$

$$S_z = \frac{A}{2}\frac{\frac{bt_f h_1}{2} + \frac{h_1}{2}t_w \frac{h_1}{4}}{bt_f + \frac{h_1}{2}t_w} \rightarrow S_z = 864mm^3$$

Debido a la falta de referencias sobre vigas de materiales compuestos se optó por seguir la norma SIA263 donde se hace referencia a la platificación de las secciones de una viga y como estás no afectan al límite élastico de la misma (para optimizar el ratio resistencia-tamaño).

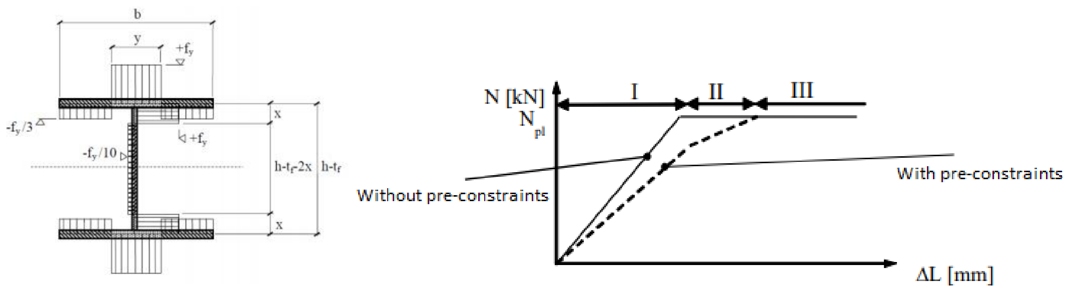

Figure 6 | Plastificación de una sección con solicitaciones internas previas

Por consiguiente, el límite de proporcionalidad de los materiales compuestos puede obviarse y trabajar directamente con los límites elásticos.

De acuerdo con los cálculos, la tensión máxima equivalente en la viga, permitía calcular las fracciones másicas (siendo el límite elástico un 25% superior a la máxima solicitación):

$$\sigma_{eq} = \sqrt{\sigma^2 + 4\tau^2} = 1018MPa \rightarrow Re = V_m Re_m + V_f Re_f \rightarrow V_m = 0.551, V_f = 0.449$$

De lo cual se obtuvo la longitud debida al fallo de torsión y el momento requiro para tal fallo:

$$L_{cr} = 2.7 * 9.3 * (1 - 0.5 * 0) * \sqrt{\frac{17.031 * 10^3}{1272.104}} = 92.602mm$$

$$M_D = 707.4273Nm \geq \frac{294.3}{2} Nm = \frac{M_{module}}{2} = M_{beam}$$

Si bien la longitud es menor a la de la viga y por tanto está en peligro de fallo, el momento es mucho menor al requerido, sin embargo, por precaución se introdujeron soportes intermedios de acero (cada 25mm), de tal modo que:

$$L_{cr} = 2.7 * 9.304(1 - 0.5\Psi) \sqrt{\frac{17.031 * 10^3}{1272.104}} \rightarrow \begin{cases} L_{cr1} = 91.916mm \geq \frac{L_D}{1.1} = \frac{50}{1.1} mm \\ L_{cr2} = 68.937mm \geq \frac{L_D}{1.1} = \frac{50}{1.1} mm \\ L_{cr3} = 61.278mm \geq \frac{L_D}{1.1} = \frac{50}{1.1} mm \\ L_{cr4} = 57.448mm \geq \frac{L_D}{1.1} = \frac{50}{1.1} mm \end{cases}$$

Y su fallo debido a pandeo (considerado como viga bi-empotrada):

$$P_{crit_y} = \frac{\pi^2 E I_y}{L_k^2 A} = \frac{\pi^2 17.031 * 10^9 * 1258.667 * 10^{-12}}{(0.5 * 0.2)^2 * 192 * 10^{-6}} >> 30mg = 8829N$$

$$P_{crit_z} = \frac{\pi^2 E I_z}{L_k^2 A} = \frac{\pi^2 17.031 * 10^9 * 16618.667 * 10^{-12}}{(0.5 * 0.2)^2 * 192 * 10^{-6}} >> 30mg = 8829N$$

Para corroborar los resultados se simuló la viga obteniendo una tensión máxima de 1006MPa (izquierda) con una deformación unitaria de 0.0032 (derecha).

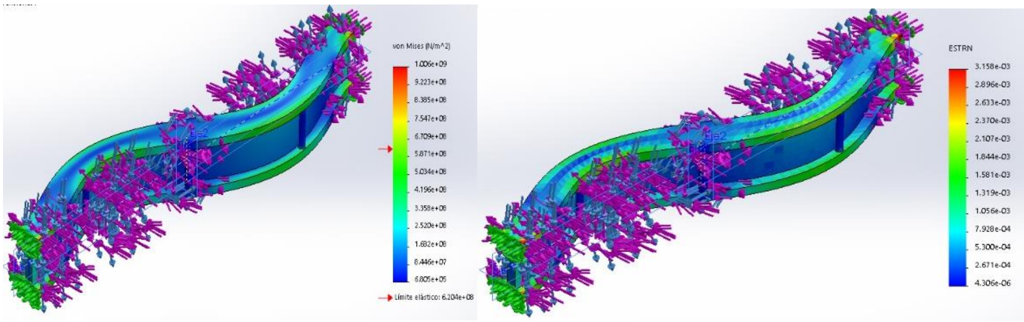

Figure 7 | Tensiones y deformaciones viga aviónica

Diseño del mecanismo de despliegue de la carga

Para desplegar el CanSat se emplean unas parejas engranaje-tornillos sin fin movidos por un sistema de poleas (correas de poliamida pura), de las cuales se obtiene una fuerza útil y una tensión de:

$$T_o \geq T_c + \frac{1}{2}\frac{e^{\alpha_g \mu} + 1}{e^{\alpha_g \mu} - 1} F_U | \; T_c = \rho A_o V^2$$

$$T_o = 1.14 * 19.86 * 10^{-6} * 0.744^2 + \frac{1}{2}\frac{e^{\frac{11}{180}*\pi*0.8*3.4} + 1}{e^{\frac{11}{180}*\pi*0.8*3.4} - 1} 1.413 = 1.384N$$

$$F_U = 1.413N \leq 2(T_o - 1.14 * 19.86 * 10^{-6} * 0.744^2)\frac{e^{\frac{11}{180}*\pi*0.8*3.4} + 1}{e^{\frac{11}{180}*\pi*0.8*3.4} - 1} = 10.837N$$

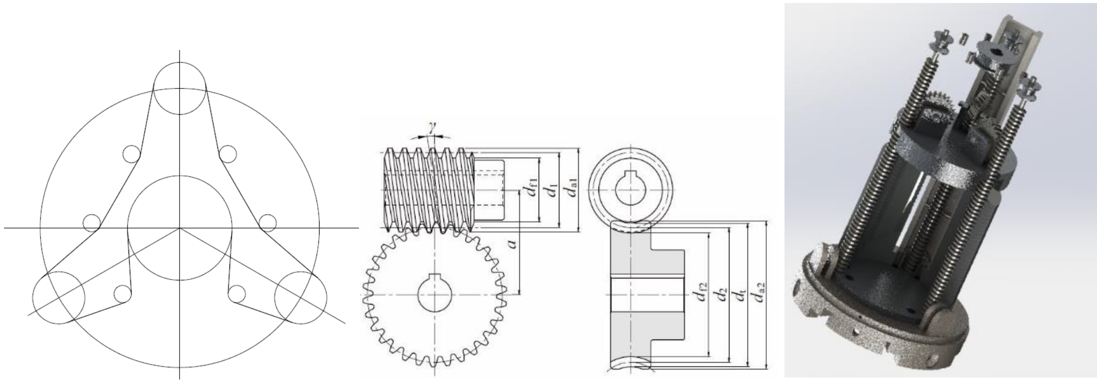

Figure 8 | Diseño correa, tornillo sin fin y montaje en el módulo

Lo cual permite diseñar el tornillo sin fin y el engranaje tal que:

Item	Símbolo	Tornillo (1)	Rueda (2)
Modulo normal (mm)	m_n	1	
Ángulo de presión (º)	α_n	20	
Número de dientes	Z	1	12
Dimaetro primitivo (mm)	d_1	8	-
Normal Profile Shift Coefficient	X_{n2}	-	-0.1414
Ángulo en el cilindro (º)	Y	7.1808	
Diametro primitivo piñón (mm)	d_2	-	24
Distancia entre centros (mm)	a	15.8586	
Addendum (mm)	h_{ai}	1	0.8586
Altura diente (mm)	h	2.25	
Dimetro externo (mm)	d_{ai}	10	27
Dimáetro garganta (mm)	d_t	-	25.7172
Radio garganta diente (mm)	r_i	-	3
Diámetro mínimo (mm)	d_{fi}	5.5	21.2172

Table 6 | Diseño tornillo sin fin-rueda dentada

Al rotar éstos, mueven verticalmente un carrito con una velocidad de 0.05m/s, el cual libera el CanSat que es empujado por unos carritos con electroimanes descritos por:

$$\overrightarrow{m_{elec-push}} = \pm 3420.85 * 10^{-6} ni * 2 * \frac{\sqrt{2}}{2}\overrightarrow{e_1}$$

Diseño de las bahías de los motores

El combustible sólido de los motores es una mezcla de aluminio y perclorato de amonio suspendido en una matriz de caucho tal que al reaccionar:

$$10Al + 6NH_4ClO_4 \rightarrow 4Al_2O_3 + 2AlCl_3 + 3N_2 + 12H_2O$$

De haber un fallo en la secuencia de despegue se debe neutralizar el aluminio con un compuesto que contenga metal más reactivo y cuya parte no-metálica genere menos gases, por lo tanto se ha optado por el hydroxido de magnesio ya que no es toxico y es comúnmente empleado en la lucha contra incendios:

$$Mg(OH)_2 + 2NH_4ClO_4 \rightarrow 2NH_3 + 2H_2O + MgCl_2O_8$$

Considerando los diferentes tipos de motores seleccionados se necesita, por tanto (depósito de 0.7L):

	I218R	L1100	M650W
Masa de combustible (g)	172.7	1346	3351
Masa de aluminio (g)	47.804	372.579	927.573
Masa perclorato de amonio(g)	124.896	973.421	2423.427
Concentración de $Mg(OH)_2$ (mol/L)	0.6767	5.2745	13.1314

Table 7 | Composición motores

Y se puede dimensionar el circuito hidráulico necesario para extinguir en 2 segundos el combustible:

Elemento	Características	K_v	Caudal (m^3/s)	Pérdidas (J)
Salida depósito	$D_1 = 10mm$ $D_2 = 100mm$	0.495	$2.567 * 10^{-3}$	264.391
Válvula	$\Theta = 5º$	0.05	$2.567 * 10^{-3}$	26.706
Unión en Y	$\alpha = 45º$ $V_o = V_1$	1.349	$2.567 * 10^{-3}$	720.533
Triple separación	$\alpha = 60º$ $V_o = 3V_1$	$3K_v = 3 * 1.254$	$\frac{2.567 * 10^{-3}}{3}$	223.264
Codo	$\theta = 60º$ $D = 10mm$ $r = 20mm$	$3K_v = 3 * 0.0969$	$\frac{2.567 * 10^{-3}}{3}$	17.252
Tubería	$L = 0.9m$ $Re = 2300$ $K_s = 1.5E - 6m$	$3K_v = 3 * 2.776$	$\frac{2.567 * 10^{-3}}{3}$	494.243
Codo	$\theta = 85.796º$ $D = 10mm$ $r = 20mm$	$3K_v = 3 * 0.1386$	$\frac{2.567 * 10^{-3}}{3}$	24.677
Tobera	$D_1 = 5mm$ $D_2 = 10mm$	$3K_v = 3 * 0.75$	$\frac{2.567 * 10^{-3}}{3}$	133.531
Total pérdidas				1904.597

Table 8 | Prérdidas circuito hidráulico

Lo cual permite seleccionar las bombas necesarias.

El sistema está diseñado para que pueda operarlo 1 de las 2 bombas y el caudal por 1 de las 3 toberas sea suficiente para extinguir el combustible, ya que en el caso de fallo en el despegue peligra todo el cohete.

Para transferir la potencia del motor al tuve se emplean las thrust plates, las cuales, debido a su geometría se deben dimensionar mediante simulaciones. Se simularon en 2 casos, bajo condiciones de servicio y otro considerando que 1 de las 3 había fallado, obteniendo así unas tensiones máximas de 15MPa para el fallo de 1 de ellas (izquierda) y 5MPa cuando las 3 están operacionales (derecha) ambas debajo de su límite elástico de 27MPa:

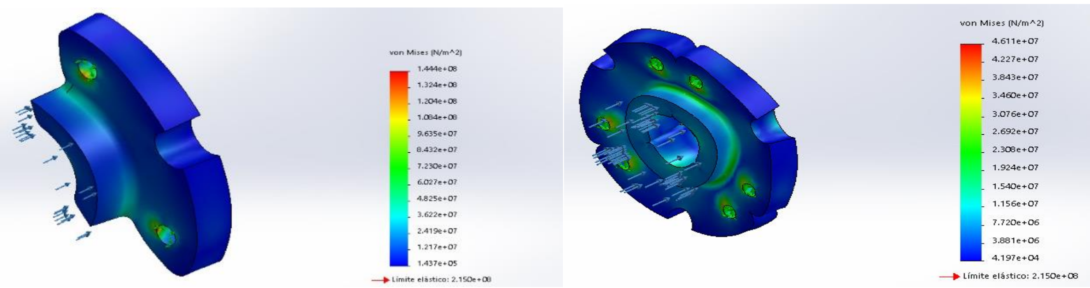

Figure 9 | Simulaciones Thrust Plates

Diseño de las aletas

Las aletas siguen un perfil NACA no estandarizado, guiado por el perfil:

$$y\begin{cases} 5t(z)\left[0.2969\sqrt{\frac{x}{L(z)}}-\frac{0.1260}{L(z)}x-0.3516\left(\frac{x}{L(z)}\right)^2+0.2843\left(\frac{x}{L(z)}\right)^3-0.1015\left(\frac{x}{L(z)}\right)^4\right] & if\ x \leq L(z) \\ \sqrt{(0.0105t(z))^2-(x-L(z))^2} & if\ L(z) \leq x \leq L(z)+0.0105t(z) \end{cases}$$

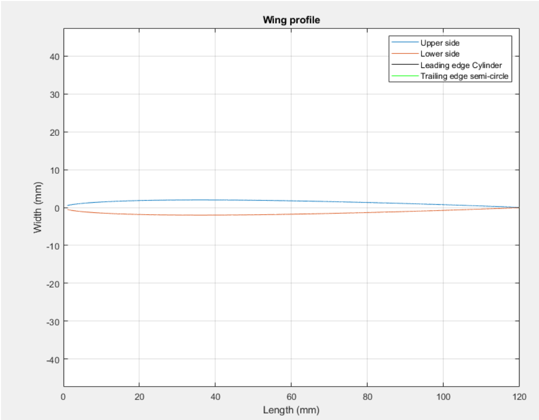

Figure 10 | Sección aleta

Siendo por lo tanto caracterizadas como (en función de su longitud y espesor):

$$I_y^o = \iint_A x^2 dA = \int_0^{L(z)} x^2 * 2 * y_t(x,z)dx = 0.4489190476 * t(z) * [L(z)]^3 mm^4$$

$$I_x^o = \iint_A y^2 dA = \int_0^{L(z)} x * 2 * [y_t(x,z)]^3\, dx$$
$$= 0.0432584113291[L(z)]^2 * [t(z)]^3 mm^4$$

Para dimensionarlas se consideró un esfuerzo distribuido uniformemente a lo largo de la aleta tal que:

$$\sigma\ (x,y) = -\frac{M_x}{W_x}+\frac{M_y}{W_y}\ |\ W_x = \frac{I_x}{\frac{t(z)}{2}}, W_y = \frac{I_y}{\frac{L(z)}{2}}, M_i = 3mgz - \frac{3mgz^2}{2L_{fin}}$$

Lo cual permite saber la composición que deben tener así como la velocidad de resonancia:

	$\sigma_{MAX}\ (MPa)$	V_m	V_f	Densidad(kg/m^3)	$V_{Flutter}$ (m/s)	Evitado
Level 1	15.4711	1	0	1400	-	-
	160.5513	0.811	0.189	1626.8	22244.75	Sí
Level 2	19.3389	1	0	1400	-	-
	200.6892	0.753	0.247	1696.4	182108.67	Sí
Level 3	23.2067	1	0	1400	-	-
	240.8270	0.703	0.297	1756.4	154682.07	Sí

Table 9 | Composición aletas y velocidad de resonancia

Debido a las limitaciones del equipo de simulación no se puedo simular el flujo entorno a las aletas y por tanto no se pudo caracterizar el vórtice de punta de ala, sin embargo, la longitud de las aletas es tal que los vórtices no interactúan con el vehículo, evitando así inestabilidades.

Del mismo modo, su dimensionamiento evita que puedan entrar en resonancia, evitando el fenómeno conocido como “fins fluttering” que ocurre cuando la capa limite se desprende alternativamente de cada lado de las aletas causando un pequeño momento de flexión en ellas que al aumentar la flecha y debido a su interacción con el fluido genera una pareja momento flector-momento torsor en los otros ejes de la aleta.

Simulaciones de vuelo

Al realizar las simulaciones de vuelo en OpenRocket (con un paracaídas de único evento para maximizar la aceleración al abrir el paracaídas y simular al mismo tiempo el evento más nocivo para el nivel 3) se obtuvo (nivel 1, 2 y 3 de izquierda a derecha):

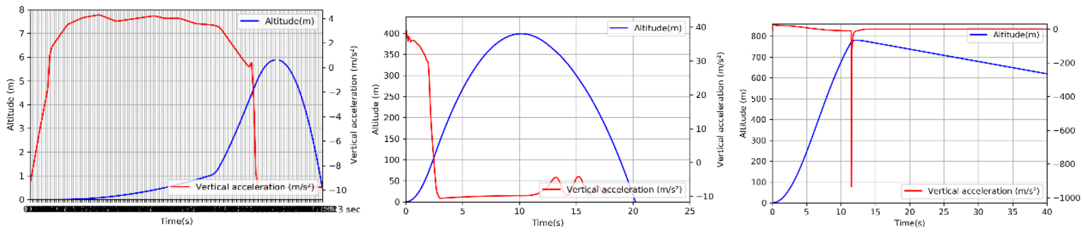

Figure 11 | Simulaciones de vuelo

El nivel 1 apenas vuela dado al gran peso del vehículo (los motores I están destinados a cohetes más simples y ligeros, aproximadamente 5kg) y en los niveles 2 y 3 las altitudes son más que suficientes para obtener las titulaciones Tripoli, por consiguiente se ensayó una nueva iteración del Nivel 1 sin el módulo de aviónica ni el de la carga CanSat. Del mismo modo, los 100g de aceleración en la simulación del Nivel 3 no pueden considerarse definitivos ya que en las simulaciones se considera un despliegue debido al quemado del motor (peor de los casos), por lo tanto, es más lento que un control electrónico y por lo tanto el cohete sufre una mayor inercia, disponiendo un control más rápido (una simulación más fidedigna, manteniendo la velocidad de aterrizaje a 4.4m/s) se obtiene (Nivel 3 izquierda y Nivel 1 derecha):

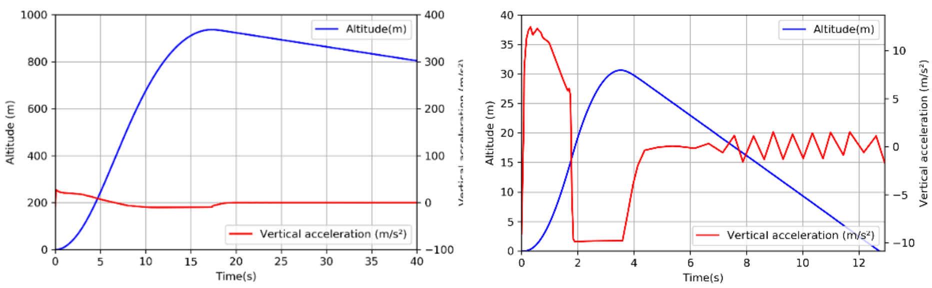

Figure 12 | Simulación Nivel 3 control electrónico y Nivel 1 sin aviónica ni carga

Donde la aceleración del cohete de Nivel 3 está dentro de parámetros y el cohete de Nivel 1 alcanza un apogeo de 30.5m (con una velocidad al aterrizar de 3.37m/s), cumpliendo así las nubes simulaciones con los requisitos.

Project Summary

Objetive

Design and simulate a modular rocket (internal diameter 120mm) capable of passing all 3 levels of the Tripoli Certificate.

Requirements

Tripoli Certificate	Level 1	Level 2	Level 3
Maximum Impulse	640N-s	5120N-s	>5120N-s
Airframe	Conventional design (ballistic rocket). The centre of Pressures must be clearly visible on the outside of the rocket. Scratch-built rockets may contain bought parts		
Recovery System	Standard parachute recovery (Single or Double-event). If the rocket implements a double event the drogue parachute can have a different construction as long as the main parachute is standardized).		No especification
Engines	Single I or H class motor (total tested impulse between 160.01 and 640.00 N-s). Stages or clustered motors will not be permitted.	single J, K or L class motors (total tested impulse between 640.01 y 5120.00 N-s). Stages or clustered motors will not be permitted.	Single M class motor or bigger (total tested impulse greater than 5120.01 N-s). Stages or clustered motors will not be permitted.
Electronics	Not required. Prior to a Level 3 flight the pilot must have proven his/her proficiency with an electronically controlled recovery system in a Level 2 Rocket.		EThe vehicle must have at least 2 separate electronic systems with independent power supplies and ignition to release the main recovery and the back up.
Others	The rocket can be self-built or bought.		The rocket must be self-built.
References	(Tripoli Rocketry Association, 2020)	(Tripoli Rocketry Association, 2020)	(Tripoli Rocketry Association, 2020)

Table 10 | Tripoli Requirements

Coupleur Design

The connector is the most important part of the rocket, not only because it's the most commonly used one (other than standardized elements such as screws) but also because it permits for a modular configuration of the rocket.

Figure 13 | Coupleur render

According to the SpacePort America Cup rules all structural elements must be able to withstand a force of up to 30mg, (Considering the mass of the Level 3 rocket to be 30kg). The connector was design with said parameters in mind such that the 6 M6 threads in the flaps have a security coefficient of 1.37 and thanks to their construction they are self-locking, therefore, they won't come lose during flight.

The holes and threads perpendicular to the main axe have a security margin of 4.32 (1.44 per pair of screws), therefore, up to 4 may fail and the structural integrity would still be guaranteed (with a quality of 10.9), when presented with the maximum stress of: $|\sigma| = 391.35MPa$.

Screw quality	Yield Strength (MPa)	Elastic Limit (MPa)	OK
4.6	400	240	No
5.6	500	300	No
8.8	800	640	Marginally
10.9	1000	900	Yes
12.9	1200	1080	Yes

Table 11 | Screw quality

The contact Surface between both coupleurs permits to safely transfer a compression load with a security coefficient of 10.66.

The gluing surface was calculated based on the reference (Aimmanee, 2017), applying simultaneously torsional efforts and axial stress, reaching a maximum equivalent stress of 13.335MPa, considering commercially available glues to have a service limit of 15MPa yields a security coefficient of:

$$n = \frac{\sigma_{adm}}{\sigma_{max}} \rightarrow n = \frac{15}{13.335} = 1.12$$

Finally, fue to their construction, the coupleurs only allow for axial displacements, which falls upon the passing radial screws to avoid. Due to their geometry they cause a rotation of 30º between coupleurs.

Tube Design

The tubes were design following an iterative process to determine the alignment of the different glass fibre layer and maximize the longitudinal and transversal Young's moduli, considering the following cases:

Radial force applied at the tip of the rocket (30mg), representing the parrachute deploying radialy, paired with a pressure difference of 1MPa due to the CO_2 cartridges (approximately 10 atmospheres); torsional moments due to the lift generated in the fins as a response to the rocket's misalignement (assumed to be $3mgR_{ext}$).

- Axial deployment of the parachute (30mg) paired with the aforementioned pressure difference and torsional moment.
- Finally, a compression effort which the rocket will experience during flight combined with the torsional moment and an increase in the internal pressure (simulating the early release of the carbon dioxide).

The rocket was considered to be a 3 meter tube with and internal diameter of 120mm and an external diameter of 125mm, considered to be cantilevered to maximize the internal stress, such that:

$$I_x = I_z = 1.805 * 10^6 \ mm^4$$

$$I_y = 3.610 * 10^6 \ mm^4$$

$$W_x = W_z = 28.887 * 10^3 \ mm^3$$

$$W_y = 57.774 * 10^3 \ mm^3$$

$$S_x = 58.920 * 10^3 mm^3$$

The maximum stress calculated was (occurred in the first case):

$$\sigma = \sqrt{\left(\sigma_{flex} + \sigma_{rad}\right)^2 + 4\tau_{tor}^2} \rightarrow \sigma = 306.6422MPa$$

Considering 8 layers of E-Glass Fibre, with an alignment such that:

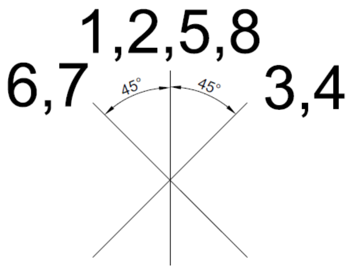

Figure 14 | Layer alignment

To calculate the mass percentages the proportinallity limit was modelled to always be superior to the maximum effort:

$$\sigma_{yC} = 1.1\sigma_{max} = \left[1 + \frac{V_f E_f}{V_m E_m}\right] V_m \sigma_{ym} \rightarrow \begin{cases} V_m = 0.1872 \\ V_f = 0.8128 \end{cases}$$

Therefore, the maximum service deformation of the tubes can be calculated:

Event	Formulae	Maximum service deformation
Traction (m)	$L = L_o e^{\frac{F}{AE}}$	$L = 3.00045$
Compression (m)	$L = Le^{\frac{F}{AE}}$	$L = 2.99955$
Deformation due to a radial effort applied at the tip (m)	$w = \frac{FL^3}{3EI_x}$	$w = 0.72780$
Deformation angle due to due to a radial effort applied at the tip (rad)	$\theta = \frac{FL^2}{2EI_x}$	$\theta = 0.36390$
Deformation due to a radial effort uniformly distributed (m)	$w = \frac{qL^4}{8EI_x}$	$w = 0.27293$
Deformation angle due to a radial effort uniformly distributed (rad)	$\theta = \frac{qL^3}{6EI_x}$	$\theta = 0.1213$
Deformation angle due to a torsional moment (rad)	$\theta = \frac{M_t}{I_y G} L$	$\theta = 0.00189$
Maximum internal pressure (MPa)	$P = \frac{2t\sigma_{max}}{D_{ext}}$	$P = 24.45154$

Table 12 | Maximum Service Deformations

Design, optimization and simulation of the nosecone

The nosecone's main objective is to reduce the drag of the rocket's main body, there are 2 main types of nosecones:

- Geometrical construction
- Mathematical conception

Geometrical construction nosecones are most commonly employed in amateur rockets due to their simplicity and ease of manufacturing, the main cross-sections are:

Elliptical cross-section:

$$y = R\sqrt{1 - \frac{x^2}{L^2}}$$

The cross-section of the nosecone clearly resembles a half-ellipse and according to literature it minimizes drag coefficient (compared with other geometrical nosecones) in subsonic flights 0.4≤ Ma ≤0.8 (Senthiil, 2018).

Other popular construction is the tangential cross-section, which according to a number of references it's purely a situational improvement (Filho, 2019):

$$y = \sqrt{\rho^2 - (L - x)^2} + R - \rho \mid \rho = \frac{R^2 + L^2}{2R}$$

The last of the geometrically built nosecones is the parabolic cross-section:

$$y = R\left(2\frac{x}{L} - \left(\frac{x}{L}\right)^2\right)$$

Finally the mathematically derived nosecones or Haack series (Haack, 1941), are the result of minimizing the drag equations for a cylindrical body and are commonly employed in trans-sonic flights (Ma>1). These nosecones are made out of a series of continuous shapes determined by a factor C, of which, 2 stand out (Stroick, Nose Cone and Fin Optimization, 2011):

- LD (C=0): Minimizing drag for a given length and diameter (also known as Von Kármán Ogive).
- LV (C=1/3): Minimizing drag for a given length and volume.

Their main drawback is that they are not tangent to the cylinder at their base, although it's such a small discontinuity which tends to be disregarded:

$$y = \frac{R}{\sqrt{\pi}}\sqrt{\theta - \frac{\sin(2\theta)}{2} + C\sin^3(\theta)}\,|\theta = \arccos\left(1 - \frac{2x}{L}\right)$$

Moreover, the optimum aspect ratio for subsonic flights is 5, thus:

$$AR = \frac{L}{2R} \rightarrow L = 10R$$

To obtain a first approximation of the drag force each cross-section generates a definition was derived from adimentional numbers:

$$F_d = \frac{1}{2}\rho u^2 C_d A \rightarrow C_d = 2\frac{A_w}{A_f}\frac{Be}{Re_L^2}$$

From which, employing different theorems and definitions (Bernoulli, Froude) the following expression was obtained:

$$C_d = \frac{4}{Fr^2}\frac{\int_0^L f(x)\sqrt{\left(f'(x)\right)^2 + 1}\,dx}{R_{ext}^2}$$

Therefore, to minimize the drag, the integral needs to be minimized, moreover, the results were then checked against a series of external flow simulations around each nosecone (v=30m/s; ρ=1.214kg/m^3):

Cross-section	Estimated drag	Simulated Drag
Elliptical	0.215	0.242962
Tangential	14.03	Did not converge
Parabolic	0.1823	0.359210
Haack (C=0)	0.047	0.205910
Haack (C=1/3)	1.418	0.234925

Table 13 | Cross-section drag coefficients

Although the results do not corroborate the calculated ones they do agree on the Von Kármán ogive being the one which generates less drag with the following pressure (left) and velocity (right) distributions:

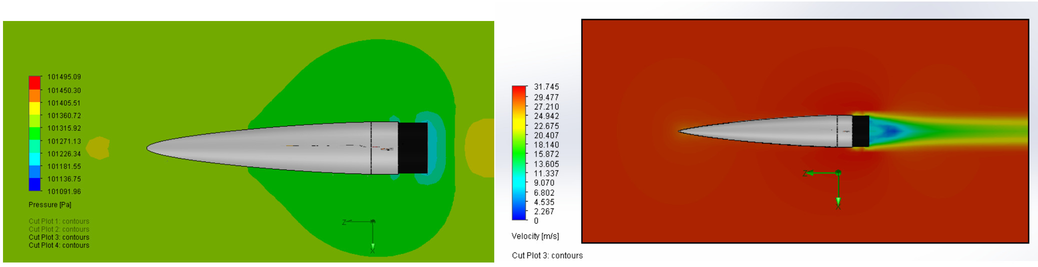

Figure 15 | Hack series c=0 pressure and velocity distributions

To keep the nosecone attached during flight to the main body and once the parachute is deployed, a system was designed so a shock cord was attached to a buckle and itself is attached to a glass fibre sheet which is held in place by an internal cylinder (avoiding any cantilever supports since sharp bends could compromise the fibre's integrity and that way the joint could be modelled to be merely traction and not flexion):

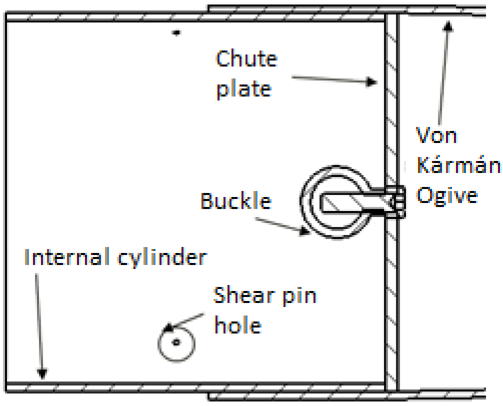

Figure 16 | Nosecone assembly cross-section

Furthermore, there are 3 holes to mount shear pins (plastic dowels sized to break when they suffer a shear stress of 15MPa) such that the nosecone is stuck to the body of the rocket during the ascension and it is released when the carbon dioxide augments the internal pressure and they break.

Recovery system design

2 separate recovery systems were designed (to obtain a touch down speed of 4m/s):

- Single event: For the Level 1 flight and the emergency parachute of the Level 3 rocket.
- Double event: For the Level 2 and Level 3 flights.

The single event consists of a flat hexagonal parachute which is released by the CO_2 cartridges, which augment the pressure inside the tube and thus generate a traction force in the chute plate, which in turn creates the shear stress needed to break the shear pins and deploy the parachute. For redundancy pourposes, there are 3 pilars, of which 1 could fail and the structural integrity could still be preserved (single event, left; double event centre and right).

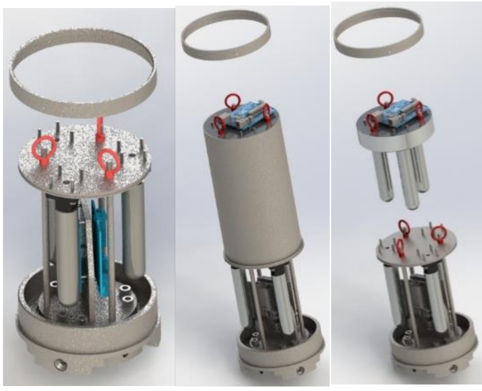

Figure 17 | Single event, double event with and without the phenolique tube

The aluminium ring on top of the tube (which has been hidden in the renders) acts as a protective layer to prevent the fibre from delaminating (due to the force exerted by the parachute upon deployment).

There is a redundancy in the electronics (2 controllers and 2 altimeters) as well as in the cardon dioxide cartridges (there are 3 in total, of which all can be released by either controller and only 2 are needed to deploy the parachute).

The electronic controller depends on the altimeter signals to release the CO_2, when they detect an increase in pressure over a few seconds (which means the rocket has already reached the apogee and is free falling), a signal is sent to the micro-controllers which in turn release the CO_2.

Traditionally the carbon dioxide cartridges are pierced by awl's which are themselves propelled by gunpowder, however, in an effort to reduce the amount of inflammatory elements inside the body of the rocket they have been swapped by solenoid valves controlled by the micro-controllers.

Similarly, the micro-controllers were assumed to be Arduino UNOs due to their size, so that if in the future they are swapped there is space to mount a different controller.

For the double event, the system is similar, duplicating the number of carbon dioxide cartridge and micro-controllers since 3 are integrated within the phonolique tube which contains the main parachute. The cartridges within the phenolique are released so they deploy the drogue parachute and reduce the decent speed to 10m/s and later the CO_2 at the base is released to deploy the main parachute.

To avoid the early deployment of the main parachute, the metallic structure on top of the phenolique tube is connected to an electromagnet-permanent magnet pair to transfer the load directly to the base of the module. Due to the presence of electronic components without a Faraday cage the magnetic force is weak and the electromagnet cannot revert polarities to deploy the main parachute.

For the Level 3 flight an emergency parachute is needed, for which, the Level 1 single event will be mounted underneath the double event and they will be kept together by another magnet-electromagnet pair (stronger than the one previously explained), which will be able to revert the electromagnet's polarity to deploy the single event in case it is needed (since this would mean the rocket is free falling and thus the entirety of the rocket is at risk damaging the electronics is not considered a priority, least damage criteria). Solving the magnetic dipoles equation in cylindrical coordinates yields:

$$\vec{\boldsymbol{F}}(\vec{r}, \overrightarrow{m_1}, \overrightarrow{m_2}) = \frac{-3\mu_o m_1 m_2}{2\pi z^4} \overrightarrow{e_3}$$

Simultaneously applying the superposition teorema and the right hand rule, the current needed to maintain the magnetic link can be expressed as a function of the force (considering a low voltage source, 5 V and the cables inherent resistance):

$$\overrightarrow{m_{elec}} = \pm inA\overrightarrow{e_3} \mid I = \frac{5}{0.028 \frac{2n45\pi}{r^2\pi}}$$

Design, optimization and simulation of the avionics and payload modules

Since the avionics module needs to have the cylindrical antennas mounted on the exterior and the payload bay needs to be able to open mid-flight to deploy the CanSat they cannot be made out of structural tubes, hence a new system of connectors and beams was designed.

The beams were calculated assuming only 2 of the 3 would be operative, thus obtaining a greater margin of security, under the following efforts:

- Traction (parachute deployment at 30mg).
- Compression (during take off, 20mg as per the SpacePort America Cup, however, for the dimensioning of the beam the load was considered to be 30mg to augment the structural security).

$$F_{tract} = -F_{comp} = 30mg = 30^3 * 9.81 = 8829N$$

- Torsion (during flight,caused by the rocket's misalignement, $3mgR_{ext}$).

$$M_{tor} = 3mgR_{ext}t = 3 * 30 * 9.81 * 62.5 * 10^{-3} = 55.18125Nm$$

- Flexing moment due to a force applied at the tipo f the module with a magnitude of 30mg (with the module's mass being 5kg and the point of application at 200mm, the end of the beams).

$$M_{module} = 30mgL = 30 * 5 * 9.81 * 0.2 = 294.3Nm$$

To size the torsional moment, according to the reference (Nussbaumer, 2015):

$$K_{beam} = 1.2 * 863.232 = 1035.878mm^4$$

And the beam's cross-section (with it's respective values in mm):

Name	Symbol	Value		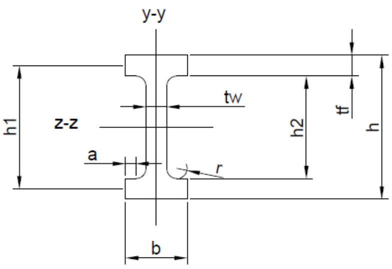
Height	h	28		
Width	b	12		
Web's equivalent length	h_1	24		
Web's thickness	t_w	4		
Web height	h_2	20		
Flange's thickness	t_f	4		
Radius	r	-		
Useable flange	a	-		

Table 14 | Beam characterization

The radius and the useful flange could not be computed since they depend of the fibre's minimum bending radius which depends entirely on the manufacturer.

Hence, the beam was characterized as:

$$A = t_w h_1 + 2bt_f \rightarrow A = 192mm^2$$

$$I_z = \frac{1}{12}h_1^3 t_w + 2\left(\frac{1}{12}bt_f^3 + b * t_f * \left(\frac{h_1}{2}\right)^2\right) \rightarrow I_z = 16618.667mm^4$$

$$I_y = \frac{1}{12}t_w^3 h_1 + \frac{1}{12}t_f b^3 \rightarrow I_y = 1258.667mm^4$$

$$W_z = \frac{I_z}{\frac{h}{2}} \rightarrow W_z = 1187.0476mm^3$$

$$W_y = \frac{I_y}{\frac{b}{2}} \rightarrow W_y = 209.778mm^3$$

$$S_z = \frac{A}{2}\frac{\frac{bt_f h_1}{2} + \frac{h_1}{2}t_w\frac{h_1}{4}}{bt_f + \frac{h_1}{2}t_w} \rightarrow S_z = 864mm^3$$

Due to the lack of literature concerning composite material beams they were sized as per the SIA263 guidelines where it's explained that reaching elastic limit of each part of the cross-section at different loads due to pre-existing constraints does not compromise the total elastic limit of the beam (to optimize the stress-size ratio).

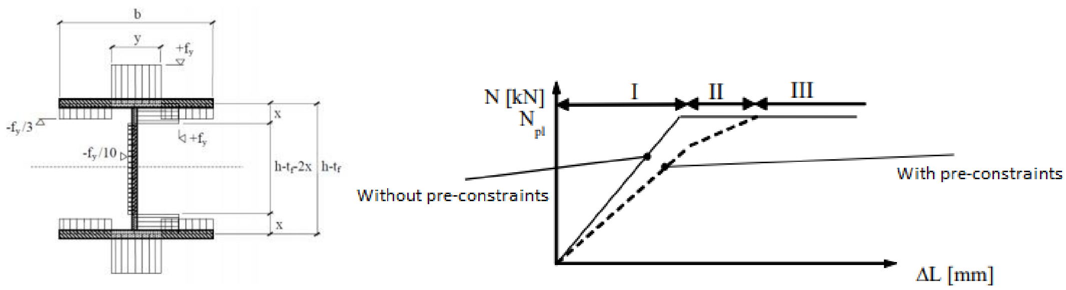

Figure 18 | elastic limit saturation cross-section

Therefore, the proportionality limit of composite materials can be disregarded and work directly with the elastic limits.

As per the calculations, the maximum equivalent stress in the beam would allow for the calculations of the wight percentages (considering the elastic limit to be 25% superior to the maximum stress)

$$\sigma_{eq} = \sqrt{\sigma^2 + 4\tau^2} = 1018MPa \rightarrow Re = V_m Re_m + V_f Re_f \rightarrow V_m = 0.551, V_f = 0.449$$

From which the torsional buckling length and momento can be computed:

$$L_{cr} = 2.7 * 9.3 * (1 - 0.5 * 0) * \sqrt{\frac{17.031 * 10^3}{1272.104}} = 92.602mm$$

$$M_D = 707.4273Nm \geq \frac{294.3}{2}Nm = \frac{M_{module}}{2} = M_{beam}$$

Even thought the length is smaller than that of the beam, the moment required is far superior to the one the beams will experience, however, as a precaution, intermediate steel supports (radisseurs) will be embedded in the beam so that:

$$L_{cr} = 2.7 * 9.304(1 - 0.5\Psi)\sqrt{\frac{17.031 * 10^3}{1272.104}} \rightarrow \begin{cases} L_{cr1} = 91.916mm \geq \frac{L_D}{1.1} = \frac{50}{1.1}mm \\ L_{cr2} = 68.937mm \geq \frac{L_D}{1.1} = \frac{50}{1.1}mm \\ L_{cr3} = 61.278mm \geq \frac{L_D}{1.1} = \frac{50}{1.1}mm \\ L_{cr4} = 57.448mm \geq \frac{L_D}{1.1} = \frac{50}{1.1}mm \end{cases}$$

Finally the buckling load (considering it a doubly embedded beam):

$$P_{crit_y} = \frac{\pi^2 EI_y}{L_k^2 A} = \frac{\pi^2 17.031 * 10^9 * 1258.667 * 10^{-12}}{(0.5 * 0.2)^2 * 192 * 10^{-6}} >> 30mg = 8829N$$

$$P_{crit_z} = \frac{\pi^2 EI_z}{L_k^2 A} = \frac{\pi^2 17.031 * 10^9 * 16618.667 * 10^{-12}}{(0.5 * 0.2)^2 * 192 * 10^{-6}} >> 30mg = 8829N$$

To check the validity of the results, the beam was simulated, obtaining a maximum stress of 1006MPa (left) along with a maximum unitary deformation of 0.0032 (right).

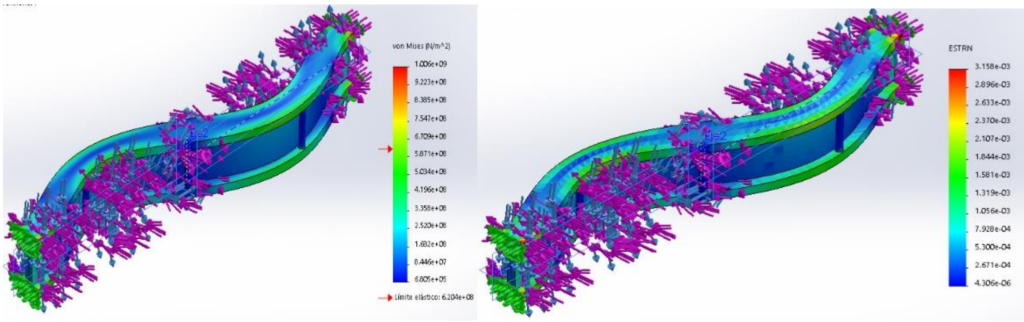

Figure 19 | Stress and deformation beam simulation

Design of the payload deployment mechanism

To deploy the CanSat a worm gear-gear coupling is employed, moved by a belt system (polyamide belt), from which the useful force and tension yield:

$$T_o \geq T_c + \frac{1}{2}\frac{e^{\alpha_g \mu}+1}{e^{\alpha_g \mu}-1}F_U \,|\, T_c = \rho A_o V^2$$

$$T_o = 1.14 * 19.86 * 10^{-6} * 0.744^2 + \frac{1}{2}\frac{e^{\frac{11}{180}*\pi*0.8*3.4}+1}{e^{\frac{11}{180}*\pi*0.8*3.4}-1}1.413 = 1.384N$$

$$F_U = 1.413N \leq 2(T_o - 1.14 * 19.86 * 10^{-6} * 0.744^2)\frac{e^{\frac{11}{180}*\pi*0.8*3.4}+1}{e^{\frac{11}{180}*\pi*0.8*3.4}-1} = 10.837N$$

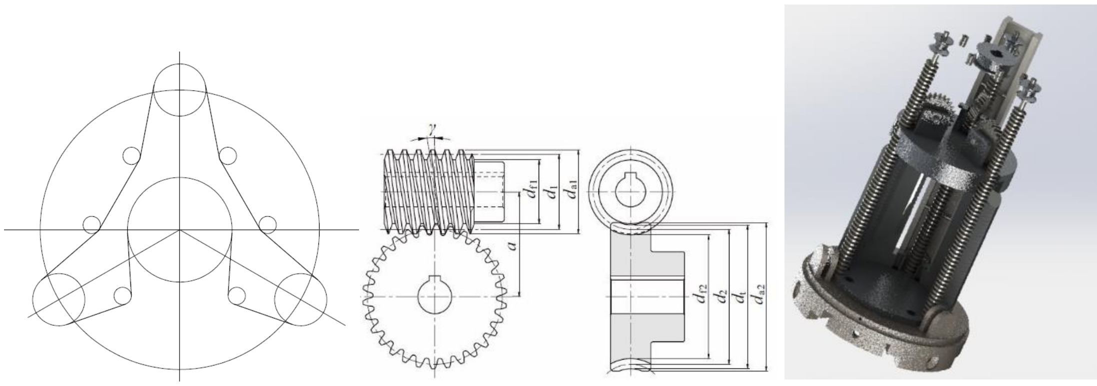

Figure 20 | Belt assembly, worm gear-wheel pair and their assembly in the module

Which allows to sixe the worm gear-gear pair:

Item	Symbol	Worm (1)	Wheel (2)
Normal module (mm)	m_n	1	
Pressure angle (º)	α_n	20	
Number of teeth	Z	1	12
Primitive diametre (mm)	d_1	8	-
Normal Profile Shift Coefficient	X_{n2}	-	-0.1414
Reference Cylinder lead angle (º)	Y	7.1808	
Primitive diameter wheel (mm)	d_2	-	24
Centre distance (mm)	a	15.8586	
Addendum (mm)	h_{ai}	1	0.8586
Tooth depth (mm)	h	2.25	
Tip diametre (mm)	d_{ai}	10	27
Throat diameter (mm)	d_t	-	25.7172
Throat surface radius (mm)	r_i	-	3
Root diameter (mm)	d_{fi}	5.5	21.2172

Table 15 | Worm gear-wheel design

When they rotate they move the slide vertically with a speed of 0.05m/s, which releases the CanSat and it's in turn pushed by a set of electromagnetic slides with a force described as:

$$\overrightarrow{m_{elec-push}} = \pm 3420.85 * 10^{-6} ni * 2 * \frac{\sqrt{2}}{2} \overrightarrow{e_1}$$

Engine Bay Design

Solid fuel rockets are composed of an aluminium-amonium perchlorate mixture suspended in a rubber matrix so that when they react:

$$10Al + 6NH_4ClO_4 \rightarrow 4Al_2O_3 + 2AlCl_3 + 3N_2 + 12H_2O$$

If there ever is a mishap in the take-off procedure, the aluminium needs to be neutralized by a compound which contains a more reactive metal and which it's non-metallic part generates less gasses, therefore, magnesium hydroxide was selected since it's not toxic and it is commonly employing in firefighting:

$$Mg(OH)_2 + 2NH_4ClO_4 \rightarrow 2NH_3 + 2H_2O + MgCl_2O_8$$

Considering the selected engine, the amount of magnesium hydroxide needed is (reservoir of 0.7L):

	I218R	L1100	M650W
Masa de combustible (g)	172.7	1346	3351
Masa de aluminio (g)	47.804	372.579	927.573
Masa perclorato de amonio(g)	124.896	973.421	2423.427
Concentración de $Mg(OH)_2$ (mol/L)	0.6767	5.2745	13.1314

Table 16 | Engine composition

The hydraulic circuit can then be dimensioned to neutralize the fuel within 2 seconds:

Element	Characteristics	K_v	Flow rate (m^3/s)	Losses (J)
Reservoir exit	$D_1 = 10mm$ $D_2 = 100mm$	0.495	$2.567 * 10^{-3}$	264.391
Valve	$\Theta = 5º$	0.05	$2.567 * 10^{-3}$	26.706
Y-union	$\alpha = 45º$ $V_o = V_1$	1.349	$2.567 * 10^{-3}$	720.533
Triple split	$\alpha = 60º$ $V_o = 3V_1$	$3K_v = 3 * 1.254$	$\frac{2.567 * 10^{-3}}{3}$	223.264
Elbow	$\theta = 60º$ $D = 10mm$ $r = 20mm$	$3K_v$ $= 3 * 0.0969$	$\frac{2.567 * 10^{-3}}{3}$	17.252
Tube	$L = 0.9m$ $Re = 2300$ K_s $= 1.5E - 6m$	$3K_v = 3 * 2.776$	$\frac{2.567 * 10^{-3}}{3}$	494.243
Elbow	$\theta = 85.796º$ $D = 10mm$ $r = 20mm$	$3K_v$ $= 3 * 0.1386$	$\frac{2.567 * 10^{-3}}{3}$	24.677
Nozzle	$D_1 = 5mm$ $D_2 = 10mm$	$3K_v = 3 * 0.75$	$\frac{2.567 * 10^{-3}}{3}$	133.531
Total losses				1904.597

Table 17 | Hydraulic circuit losses

This, in turn, provides the guidelines to select the pump.

The system is designed so that with only 1 of the2 pumps operational and 2 of the nozzles blocked the flow rate through that remaining nozzle is enough to extinguish the fuel, since if there is an ignition mishap the entirety of the rocket is at risk.

To transfer the thrust from the engine 3 thrust plates are employed, which due to their geometry are sized by simulations. 2 main cases were considered, one were all 3 were operational and another where 1 failed, when only 2 were operational the maximum stress was found to be 15MPa (left) and when all 3 were operational the maximum stress was 5MPa (right) both below the elastic limit of 27MPa:

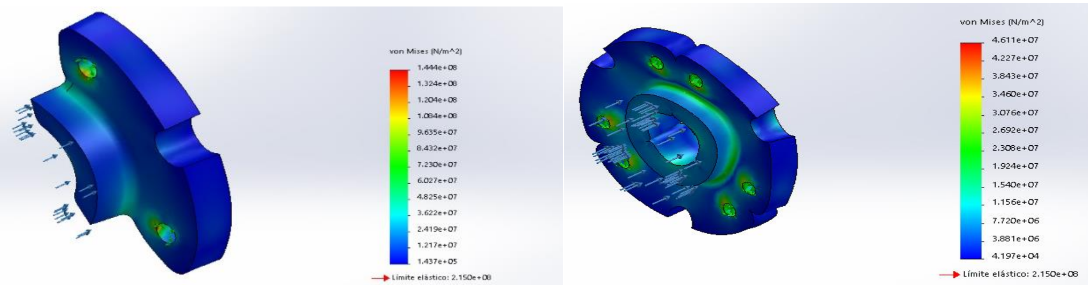

Figure 21 | Thrust plates simulations 2 operational and all 3 operational

Fin design

The fins followed a non-standarized NACA profile with guided by the equation:

$$y\begin{cases} 5t(z)\left[0.2969\sqrt{\frac{x}{L(z)}}-\frac{0.1260}{L(z)}x-0.3516\left(\frac{x}{L(z)}\right)^2+0.2843\left(\frac{x}{L(z)}\right)^3-0.1015\left(\frac{x}{L(z)}\right)^4\right] & if\ x\leq L(z) \\ \sqrt{(0.0105t(z))^2-(x-L(z))^2}\ if\ L(z)\leq x\leq L(z)+0.0105t(z) \end{cases}$$

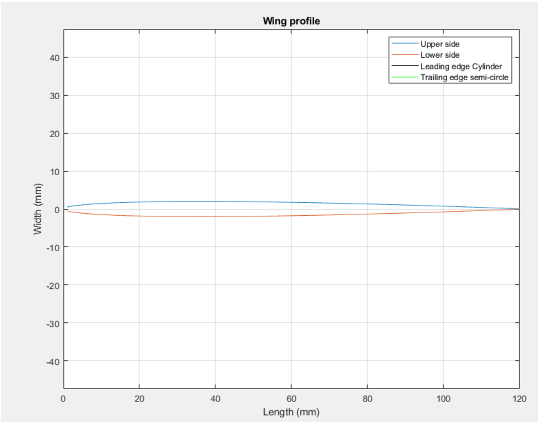

Figure 22 | Fin cross-section

Being therefore characterized as (dependent on their length and thickness):

$$I_y^o=\iint_A x^2dA=\int_0^{L(z)}x^2*2*y_t(x,z)dx=0.4489190476*t(z)*[L(z)]^3mm^4$$

$$I_x^o=\iint_A y^2dA=\int_0^{L(z)}x*2*[y_t(x,z)]^3\,dx$$
$$=0.0432584113291[L(z)]^2*[t(z)]^3mm^4$$

To size them, an evenly distributed effort was considered along the fin such that:

$$\sigma\,(x,y)=-\frac{M_x}{W_x}+\frac{M_y}{W_y}\mid W_x=\frac{I_x}{\frac{t(z)}{2}},W_y=\frac{I_y}{\frac{L(z)}{2}},M_i=3mgz-\frac{3mgz^2}{2L_{fin}}$$

Which allows for the composition to be calculated and the fluttering speed:

	$\sigma_{MAX}\ (MPa)$	V_m	V_f	Density (kg/m^3)	$V_{Flutter}$ (m/s)	Avodied
Level 1	15.4711	1	0	1400	-	-
	160.5513	0.811	0.189	1626.8	22244.75	Yes
Level 2	19.3389	1	0	1400	-	-
	200.6892	0.753	0.247	1696.4	182108.67	Yes
Level 3	23.2067	1	0	1400	-	-
	240.8270	0.703	0.297	1756.4	154682.07	Yes

Table 18 | Fin composition and flutter speed

Due to computational limitations the external flow around the fins could not be computed and thus the wing tip vortex could not be characterized, however, due to the wing's length the vortex will never be able to interact with the body of the rocket, thus avoiding perturbations.

Similarly, the sizing avoids the fin's flutter, which occurs when the limit-most layer of fluid detaches, causing a small flexion moment which's deformation is amplified by the interaction with the fluid and can degenerate in a pair flexion moment-torsinal moment in the other axe.

Flight simulations

The flight simulations were performed in OpenRocket (with a single event parachute to maximize the accelerations upon the parachute deployment and simulate Level 3's worst case scenario) which yielded (Levels 1, 2 and 3 from left to right):

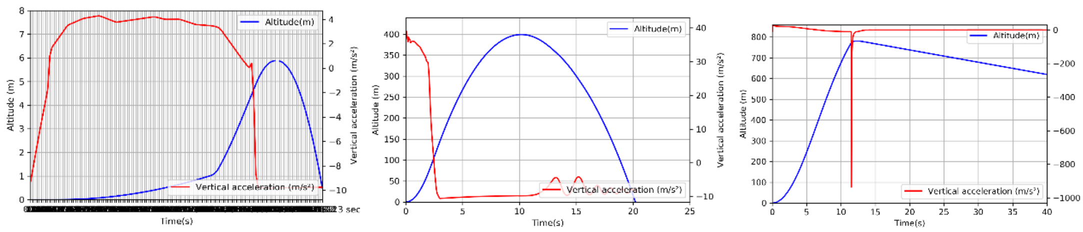

Figure 23 | Worst case scenarios flight simulations

The level 1 rocket barely gains any altitude due to it's weight (I class engines are destined for smaller, simpler rockets with an approximate mass of 5kg) and for the remaining levels the altitude is more than eneought to obtaine the Tripoli Certificate. Thus the Level 1 was re-simulated without the avionics nor the payload module to reduce the weight. Similarly, the 100g acceleration the Level 3 rocket experiences cannot be considered to be realsitic since it depends on a fuse burnout recovery (worst case scenario, no electronics), therefore, it's slower than an electronically driven recovey and thus the rockets gains more inertia prior to the parachute opening a new simulation with a quicker control (maintaining the landing speed at 4.4m/s) yields (Level 3 left and Level 1 right):

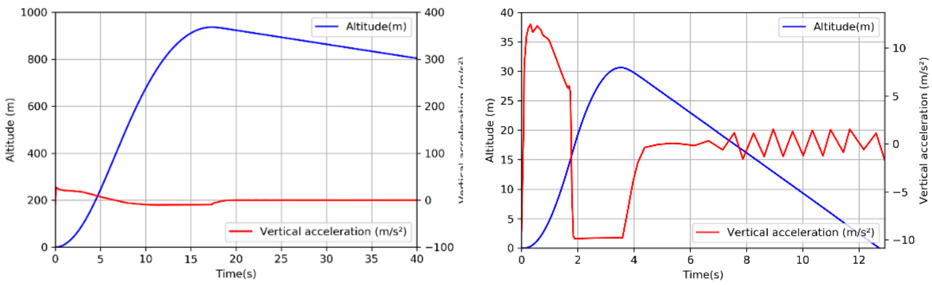

Figure 24 | Follow up simulations Levels 3 and 1

Where the vertical acceleration of the rocket is within the design parameters and the Level 1 rocket reaches an apogee of 30.5m (with a landing speed of 3.37m), thus fulfilling all the requirements.

Introduction

The project consists on the design of a modular rocket capable of passing all three certificate levels imposed by the Tripoli Rocketry Association (or the American equivalent: National Rocketry Association) whilst carrying a CanSat payload.

A conventional ballistic rocket is made up of the following Sub-Systems:

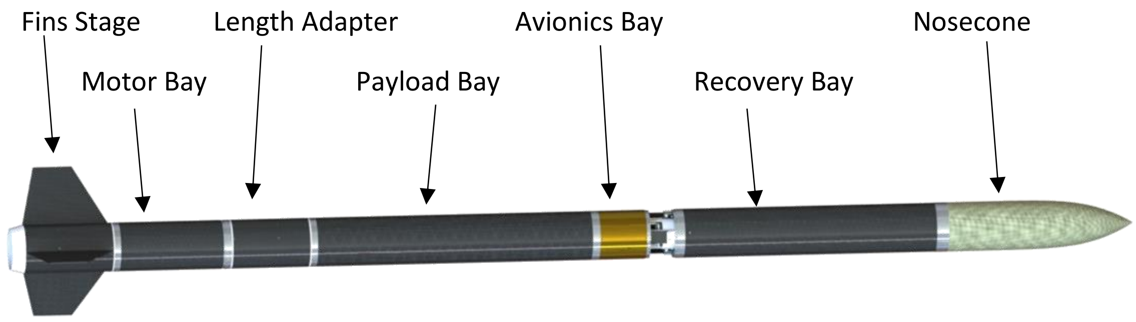

Figure 25 | EPFL Rocket Team, Eiger I (2020)

The Fins Stage is the main passive control of the rocket, ensuring it can withstand side winds and still fly upwards.

The Motor Bay contains the solid fuel engine, the diameters and impulse vary with each category.

The Length adapter is commonly employed to fly different motors in the same structure, since each motor category (A-M) has different dimensions.

The Payload Bay integrates the payload of the rocket, often a small scientific experiment or ballast to mimic space missions.

The Avionics Bay contains most of the circuitry and controls of the launch vehicle it may also contain antennas to communicate with a ground station.

The Recovery Bay, in a classically built rocket, contains the parachute to control the descent of the rocket after it's reached the apogee,

The Nosecone aims to reduce the drag force of the rocket and detaches prior to the deployment of the parachute, to which it's attached with a shock cord.

The structure of the rockets is normally made of aluminium parts and composite materials to reduce weight whilst maximizing the yield strength of the launch vehicle.

There are two main standardized payload designs:

- CubeSat: constructed by assembling cubes with a side of 100mm and a total mass of 1330g (California Polytechnic State University, 2014) first proposed in 1999 by Stanford University and California Polytechnic State University (Alen Space, 2020) and greatly encouraged by NASA (National Aeronautics and Space Administration, 2017).
- CanSat: a nano satellite with the dimensions of a soda can (115 mm height and 66 mm diameter and a mass ranging from 300g to 325g), first specified at

1998's University Space Systems Symposium and greatly encouraged by the European Space Agency (European Space Agency, 2020).

Motivation
Rocketry pairs to of the key features any engineer should poses, ingenuity and attention to detail.

It paires vastly different fields such as data analysis and stress and strain or fluid mechanics, just make a mass rise for a few hundred meters prior to falling with style.

Amateur rocketry has been consistently growing ever since the Space Race of the 60s and it is commonly employed to either test prior knowledge or to get a feel for tougher challenges in the research and development world, this project serves just that goal.

Furthermore, it promotes European science since not only does it comply to European norms, but it implements a CanSat, which is the nano satellite promoted by the European Space Agency to increase it's outreach towards the general public.

Moreover, it permits to get a feel for the world of composite materials, which will become imperative in the foreseeable future for any engineer who wises to design high performance systems.

State of the Art
Amateur rockets often suffer of fins fluttering, compromising the structural integrity of the Fins Bay and the security of the flight.

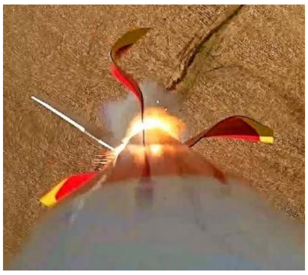

It's caused due to aeroelastic flutter, defined as "a dynamic instability associated with the interaction of aerodynamic, elastic and inertial forces." (Apogee Rockets, 2011) it's caused by the detachment of the boundary layer of the fluid which creates a small vibration in the fin, causing it to gain an undesired "camber", thus torsion strains appear in the wing, which are amplified with the speed of the incoming flow against the asymmetrical cross-section.

Figure 26|Hydra Experiencing Fin Flutter (2016)

To reduce the grad force the fins experience it's common practice to follow NACA airfoil guidelines and give them an aerodynamic shape (Ira H. Abbott, 1945).

The Motor Bay contains the engine along with centering rings and the thrust plates to transmit the force to the structure.

Since often amateur rockets re-use parts, a length adapter is often required to accept different motor types, since maintaining the diameter of the motor casing and adding additional flue cells will only increase the length.

Usually bigger diameter rockets incorporate CubeSat type payloads, however, since this is a smaller diameter rocket it will incorporate a payload following CanSat standards, it's specified by the European Space Agency that CanSat modules require at least

45mm of extra space atop the nanosatellite to accommodate the parachute and the antennas (European Space Agency, 2020).

The Avionics Bay incorporates the electronics and in some cases the antennas which allow the launch vehicle to communicate with the ground system. As a safety measure, normally the electronic systems are design to be redundant and thus have at least 2 systems completely independent acting in parallel.

The Recovery Bay integrates the parachute and the means to deploy it. It can be often done in 2 ways:

- A short fuse ignited by the motor which burns until the apogee thus, requires extensive calculation, simulations and testing for the time between motor burnout and the apogee, since the fuse's length-burn time is non-linear it requires prior testing, it's main drawback is however, that it fixes the Recovery Bay on top of the Motor Bay.
- The second system, employed in bigger more powerful rockets (since it allows for a greater module flexibility) is an electronic recovery, usually required to be completely independent of the rocket's electronics, it relies on altimeters to deploy the parachutes.

The parachute is ejected with a small blast which releases the nosecone and allows for the parachute deployment.

The nosecone has an aerodynamic shape to reduce drag and it's attached to the main body of the rocket by means of shear pins which are broken when the blast goes off and releases the nosecone to allow for the parachute deployment and thus a controlled descent.

The internal structure of the rocket is normally made of a mixture of aluminium parts as well as carbon and glass fibre sections glued or bolted together, thus it's especially critical the gluing calculations and simulations.

Furthermore, since most commercially available screws are made of steel, it's fairly common for threads to strip, so it's common to used Heli-coil® to ensure an even load distribution amongst the thread, since in standardized threads usually the first thread takes approximately 30% of the load.

It is common practice to perform as well several test prior to launching a rocket, amongst which 3 stand out:

- Static Tests: Commonly employed to test and characterized self-built engines and/or rocket fuel, the engine is set up on a stand with the thrust plates and several gauges and sensors to measure the impulse curve, temperature and time-to-burnout of the engine and/or rocket fuel. Standardized motors, such as the ones sold commercially and employed in the Certification Flights do not require Static Tests.
- Ground Tests: They are a prerequisite for Drop Tests, in these tests the recovery ejection system is tested on its own.

- Drop Test: These are employed to test the Recovery System that will be employed by the rocket. Normally the Recovery System is attached to a ballast of equivalent mass to that of the assembled rocket and it’s dropped from a height equivalent to the apogee of the rocket.

Often Rocketry Associations rent Static Test Stands and have contracts with different site managers to perform drop tests.

Under the current legislation, a flyer requires a Tripoli Rocketry Association or NAR (National Association of Rocketry) certificate if they aim to fly with any of the sub-classes (National Fire Protection Association 1122: Code for Model Rocketry, 2018):

- Cluster rockets (models containing multiple motors) with a total impulse of 320.01 N-s or more.
- Single motor model with a total installed impulse greater than 160N-s.
- Rockets with a total weight greater than 1500g.
- Models containing motors that do not comply with NFPA 1122. Most commonly:
    - Average thrust exceeding 80.0N.
    - Propellant mass that exceeds 125g.
    - Hybrid motors.

Requirements

The requirements stipulated for the launch vehicle as per the Tripoli rocketry Association are:

Tripoli Certificate	Level 1	Level 2	Level 3
Maximum Impulse	640N-s	5120N-s	>5120N-s
Airframe	Conventional design (ballistic rocket). The centre of Pressures must be clearly visible on the outside of the rocket. Scratch-built rockets may contain bought parts		
Recovery System	Standard parachute recovery (Single or Double-event). If the rocket implements a double event the drogue parachute can have a different construction as long as the main parachute is standardized).		No especification
Engines	Single I or H class motor (total tested impulse between 160.01 and 640.00 N-s). Stages or clustered motors will not be permitted.	single J, K or L class motors (total tested impulse between 640.01 y 5120.00 N-s). Stages or clustered motors will not be permitted.	Single M class motor or bigger (total tested impulse greater than 5120.01 N-s). Stages or clustered motors will not be permitted.
Electronics	Not required. Prior to a Level 3 flight the pilot must have proven his/her proficiency with an electronically controlled recovery system in a Level 2 Rocket.		EThe vehicle must have at least 2 separate electronic systems with independent power supplies and ignition to release the main recovery and the back up.
Others	The rocket can be self-built or bought.		The rocket must be self-built.
References	(Tripoli Rocketry Association, 2020)	(Tripoli Rocketry Association, 2020)	(Tripoli Rocketry Association, 2020)

Table 19 | Tripoli Requirements

Modular connector

Mechanical design

Since the rocket is modular, the connectors are one of the key pieces within the entirety of the rocket. They ought to follow some basic characteristics to ensure they are properly modelled:

- Only allow axial displacements amongst each other (thus blocking any radial or tangential forces which might happen during flight).
- Simplified geometry for easier manufacturing (since there are plenty within the rocket assembly).
- Flaps to support the innards of the launch vehicle (electronics; parachute assembly; motor casing…).
- Connecting structure to the rest of the load bearing elements (structural outer tubes or beams).

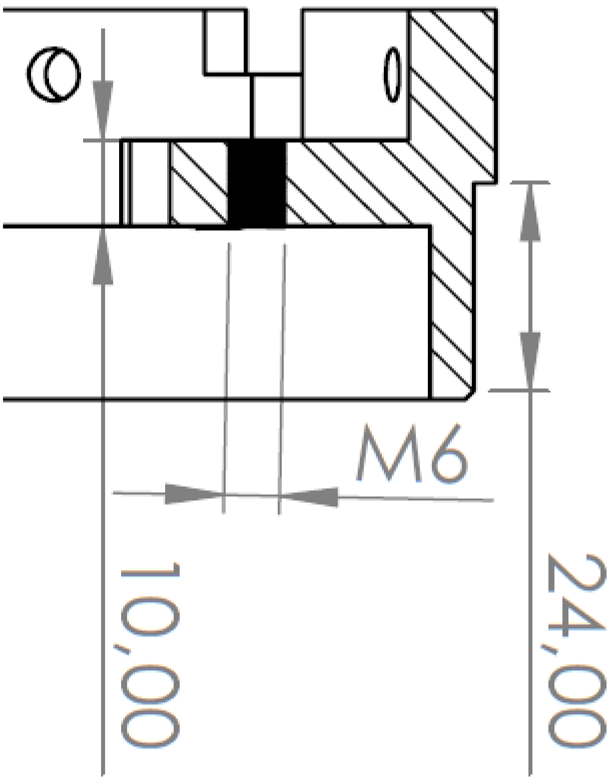

Figure 27 | Connector threaded insert cross-section

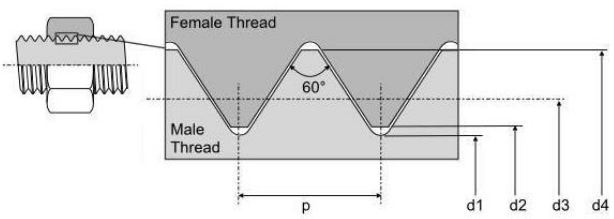

Figure 28 | Thread cross-section (Fastenings, 2020)

The connector has 6 M6 threads which withhold an axial load, hence the load for the thread to strip must be calculated, considering the characteristics of a standardized coarse M6 screw:

- D_1 (Minor Thread diameter, male thread): 4.773
- D_2 (Minor Thread diameter, female thread): 4.917 mm
- D_3 (Pitch diameter): 5.350 mm
- D_4 (Major diameter): 6 mm
- P (pitch): 1 mm

A coarse thread has been selected over a fine thread since they have greater stripping strengths for the same engagement length and have a greater fatigue resistance (Fastenal, 2009).

Since the bolt will be one commercially available and threaded into an aluminium plate, the design shear strength will be 20MPa (below the aluminium's elastic limit R_e=30 MPa). The thread's effective length will be 10mm. as shown in the figure.

Therefore, the pitch diameter will be:

$$d_o = \frac{d_2 + d_3}{2} \rightarrow d_o = 5.1335\, mm$$

The tensile stress area:

$$A_t = \frac{\pi d_o^2}{4} \rightarrow A_t = 20.6975\, mm^2$$

Shear area:

$$A_{th} = \frac{\pi}{2} d_o L_e \rightarrow \; A_{th} = 80.6368\, mm^2$$

Shear strength:

$$F = \sigma_{adm} A_{th} \rightarrow F = 2.01592\, KN$$

Which in turn, yields a stress in the bolt:

$$\sigma_{bolt} = \frac{F}{A_t} \rightarrow \sigma_{bolt} = 97.3992\, MPa$$

Therefore, the maximum strength the six bolts can hold is:

$$F_{tot} = N_{bolt} F \rightarrow 12.09552\, KN$$

Which yields a security margin, considering a maximum force of 30g as per the specifications (with a mass of 30kg):

$$n = \frac{F_{tot}}{30gm} \rightarrow n = 1.37$$

To ensure the assembly does not fall apart during use, the screws should be self-locking:

$$M_S = F\left(\frac{d_2}{2}\tan(\delta' + \alpha_2) + r_m \mu_B\right)$$

Where M_S is the moment required to screw it in, F represents the axial load applied, d_2 represents the pitch diameter between the base and the tip of the thread, δ' is the friction angle, α_2 stands for the thread angle, r_m is the extended diameter (representing the head of the screw and is generally accepted to be 0.7d for normalized screws) and μ_B is the friction of the threads.

The un-screwing moment can be modelled as:

$$M_D = F(tan(-\delta' + \alpha_2) - r_m \mu_0)$$

Where μ_0 is the friction of the head of the screw with the metal

Furthermore, a crew is self-blocking if $\delta' > \alpha_2$, therefore:

$$\delta' = \arctan\left(\frac{\mu}{\cos\left(\frac{\beta}{2}\right)}\right) > \alpha_2 = \arctan\left(\frac{P}{\pi D_2}\right)$$

Where μ is the friction coefficient in between both metals, β is the thread angle and is the P pitch.

With numerical application for a normalized M6 screw with P=1mm, $D_2 = 5.350$mm, $\beta = 60º$ and $\mu = 0.4$ (Tribonet, 2020):

$$\delta' = 24.79º > \alpha_2 = 3.41º$$

Hence the screw is self-locking.

Furthermore, the flap upon which the inner structure will rest, can be described as a cantilever, with an area which follows the function (moving radially and outwards):

$$A = \begin{cases} 0 \; for \; r < 25 \\ for \; 25 \le r < 29.58 \begin{cases} 10 * r^2 + 30^2 - 60rcos(\theta - 21.41º) = 5^2 \; for \; 21.41º < \theta \le 30º \\ 2 * 10 * \dfrac{2\pi * 20.41}{360} r \; for - 20.41º < \theta \le 20.41º \\ 10 * r^2 + 30^2 - 60rcos(\theta + 21.41º) = 5^2 \; for - 30º < \theta \le -21.41º \end{cases} \\ for \; 29.58 \le r < 38.20 \begin{cases} 10 * \dfrac{2\pi * 9.75}{360} r \; for \; 20.25º < \theta \le 30º \\ 10 * \dfrac{2\pi * 10.49}{360} r - A(r,\theta) for \; 9.75º < \theta \le 20.25º \\ 10 * \dfrac{2\pi * 19.5}{360} r \; for - 9.75º < \theta \le 9.75º \\ 10 * \dfrac{2\pi * 10.49}{360} r - B(r,\theta) for - 20.25º < \theta \le -9.75º \\ 10 * \dfrac{2\pi * 9.75}{360} r \; for - 30º < \theta \le -20.25º \end{cases} \\ 10 * \dfrac{2\pi * 60}{360} r \; for \; 38.20 \le r < 45 \end{cases}$$

Such that,

$$A(r,\theta): r^2 + 35^2 - 70rcos(\theta - 15) = 3^2$$
$$B(r,\theta): r^2 + 35^2 - 70rcos(\theta + 15) = 3^2$$

To determine the axial load applied upon assembly, the pre charge to avoid minor displacements must be calculated for each bay.

To transmit the load between 2 connectors there are 2 scenarios, first where the 6 M6 screws will be employed again, therefore, their loads can be calculated:

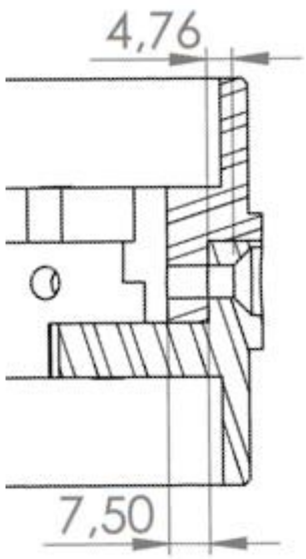

Figure 30 | Connector load transfer cross-section

Hence 2 cases must be studied:

Considering once each side to be fixed and the other a cantilever and a spring to represent the resistance of the surrounding aluminium:

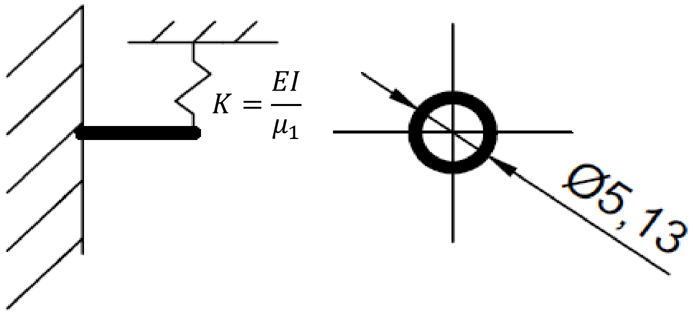

Figure 29 | Screw-beam equivalent

Where E is the aluminium’s Young Modulus, I represents the moment of inertia and finally μ_1 is the linear mass distribution. However, it’s more unfavourable if they are considered as simple cantilevers with a distributed effort such that:

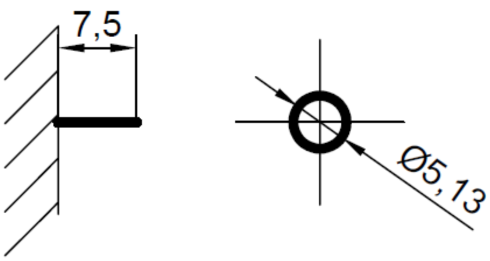

Figure 31 | Threaded insert-cantilever equivalent

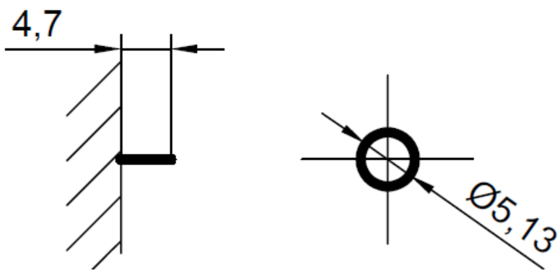

Figure 32 | Screw cantilever

Therefore, the distributed force can be described as:

$$q = \frac{F}{L} = \frac{30mg}{L}$$

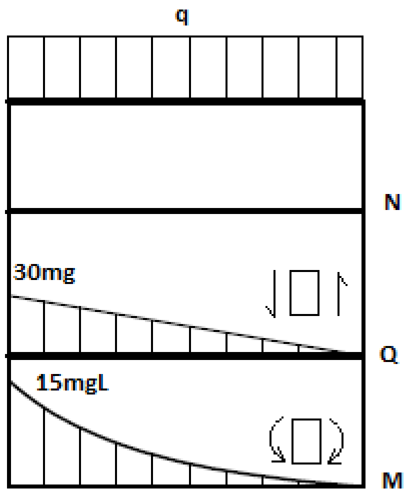

Therefore, following Navier's equation (considering 2 screws will share the load):

$$\sigma = -\frac{M_z}{W_z} = -\frac{15mgL}{\frac{1}{2}\pi r^3}$$

Hence for L=7.5 mm and a mass of 30kg:

$$|\sigma| = 624.50\ MPa$$

And for L=4.7 mm and a mass of 30kg:

$$|\sigma| = 391.35MPa$$

Figure 33 | Strain and moment diagrams of a cantilever under a uniformly distributed charge

Knowing the quality of commercially available screws:

Quality	Rm (MPa)	Re (MPa)	Holds
4.6	400	240	No
5.6	500	300	No
8.8	800	640	Yes (too little margin)
10.9	1000	900	Yes
12.9	1200	1080	Yes

Table 20 | Commercial screw quality comparison

Therefore, considering a screw quality of 10.9, the security coefficient for each screw would be:

$$n = \frac{\sigma_{max}}{\sigma_{screw}} \rightarrow n = 1.44$$

However, since each pair of screws can take all the load the overall security coefficient will be:

$$nN_{pairs} = 1.44 * 3 = 4.32$$

The other extreme scenario is when the load is entirely transmitted by the aluminium connectors, in which case, we can assume the cross-section to be (for the contact amongst the different connectors, with a maximum stress of 20MPa):

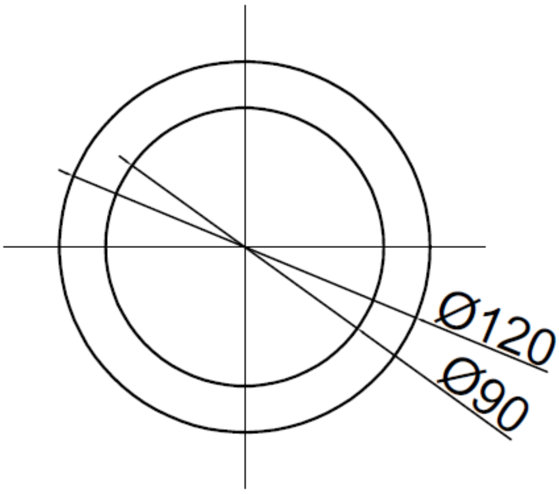

$$\sigma = \frac{N}{A} = \frac{30mg}{\frac{\pi}{4} * 10^{-6} * (120^2 - 90^2)}$$

Hence:

$$\sigma = 1.784MPa$$

Which, when compared to aluminium's Re:

$$n = \frac{\sigma_{max}}{\sigma_{screw}} \rightarrow n = 11.21$$

Figure 34 | Full connector assembly cross-section

Whilst for a single connector the smallest load bearing cross-section will be (with an internal diameter of 90mm and an external one of 120mm):

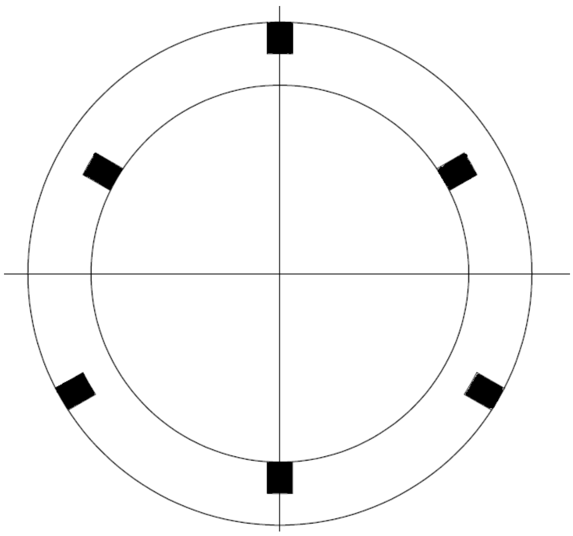

Figure 35 | Contact cross-section coupleurs

Therefore, the net area can be calculated:

$$A_{net} = 4677.86mm^2$$

Alas, the maximum stress can be calculated (with a maximum stress of 20MPa to have a security margin):

$$\sigma = \frac{N}{A} \rightarrow N = 4677.86 * 10^{-6} * 20 * 10^6 = 93.5572KN$$

And thus, the margin of safety can be calculated:

$$n = \frac{N}{30mg} \rightarrow n = 10.60$$

The load carried by the connectors ought to be transmitted through out the structure of the launch vehicle, main to the structure composite tubes, therefore, the gluing length required ought to be calculated.

Gluing Length

The design of the glue joint is based on the Single Lap Joint as described in the literature (Aimmanee, 2017).

Using this approximation, and assuming a gluing thickness of 0.2mm and knowing the length of the lap joint (24mm due to a 1mm chamfer to reduce stress), the maximum shear stress in the glue can be determined.

The calculations takes into account, the thickness and material properties of both materials, as well as the adhesive. By iterating over thickness and maximum shear force, a minimal length of the glue joint can be determined.

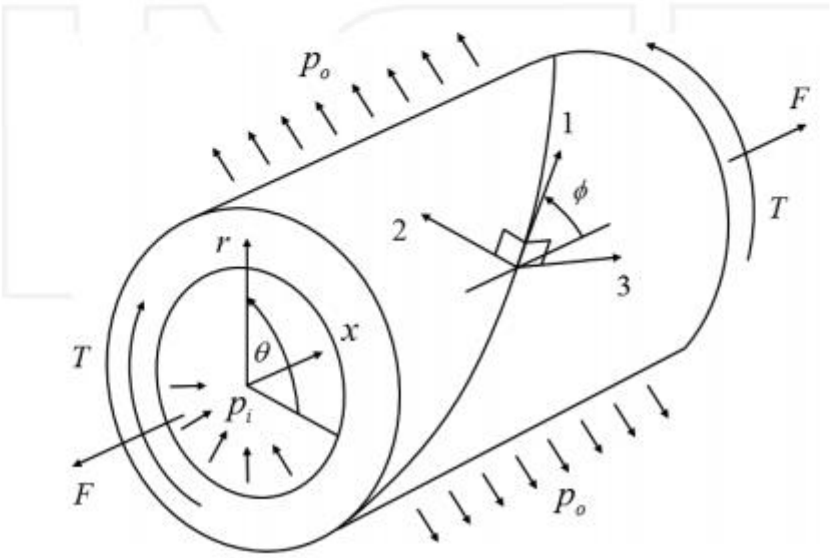

Figure 36 Schematic view of a single lap shear joint

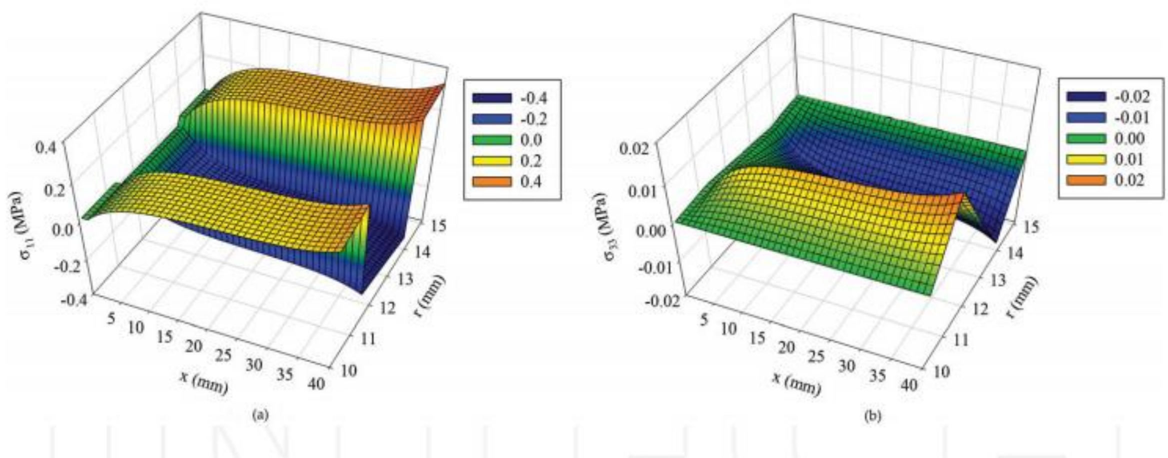

Figure 37 Distribution of stresses calculated as presented in the reference

Using sections 3 and 4.2 in ((Aimmanee, 2017) the effect of an axial loading in the shear stress and the normalized shear stress can be calculated (with a mass of 30kg):

$$\tau_m{}^a = \frac{F}{2\pi RL} = \frac{30mg}{2\pi \frac{0.120}{2} 0.024} = 0.976MPa$$

According to the reference, the relation between the axial force and the stress distribution can be described as (when considering the aerodynamic forces would cause a torsional effort equal to half of the design specifications):

$$\frac{1}{2\pi R}\frac{dF(x)}{dx} = \tau_{xr}{}^a = G^a \gamma_{xr}^a$$

Following the guidelines provided the stress distribution can be represented as:

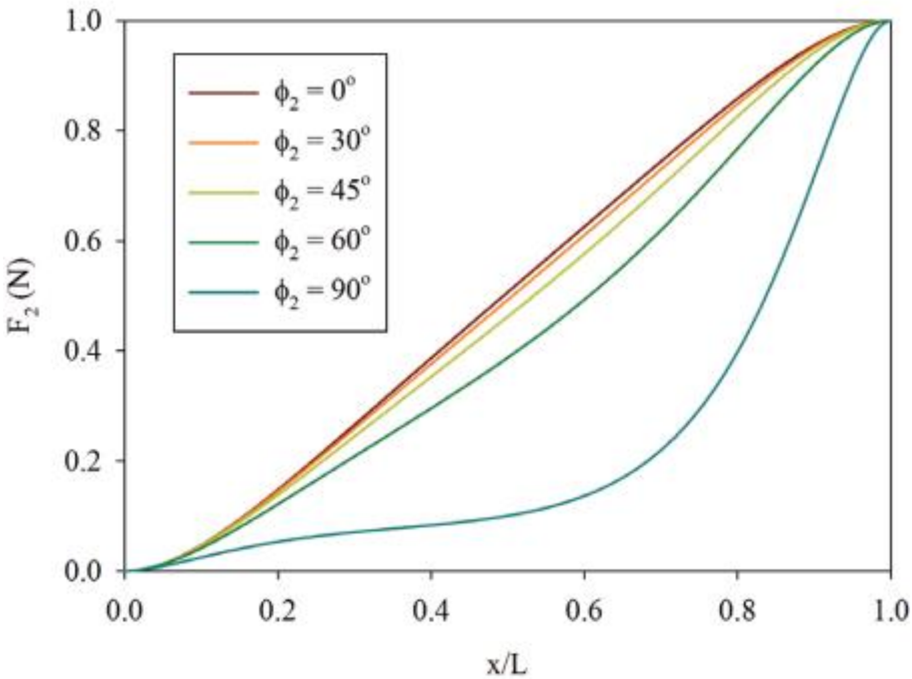

Figure 38 Stress distribution along the gluing surface

Where ϕ_2 represents the gluing angle between the layers (0º in our case).

Thus, the distribution in the Shear Strength and radial stress can also be represented:

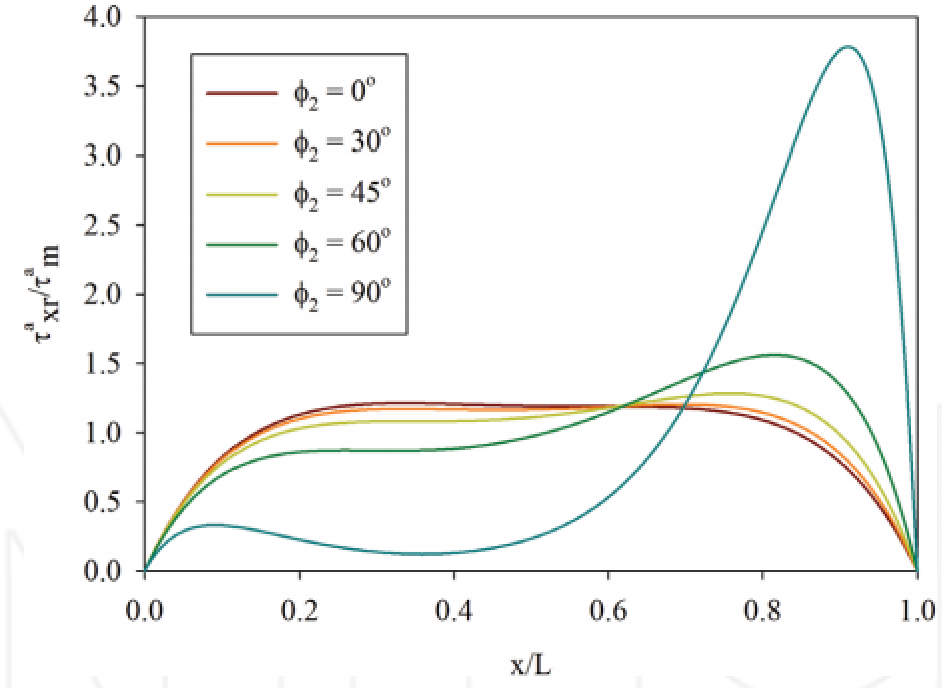

Figure 39 Adhesive axial shear stress distribution as represented in the literature

Furthermore, the torsional loading in the joint ca be computed as bearing 10% of the design requirements (Aimmanee, 2017):

$$\tau_m{}^a = \frac{T}{2\pi R^2 L} = \frac{\frac{30mg}{10}}{2\pi\left(\frac{0.120}{2}\right)^2 0.024} = 1.626MPa$$

Therefore, the module of the sheer stress can be calculated as:

$$|\tau_m{}^a| = \sqrt{1.626^2 + 0.976^2} = 1.896MPa$$

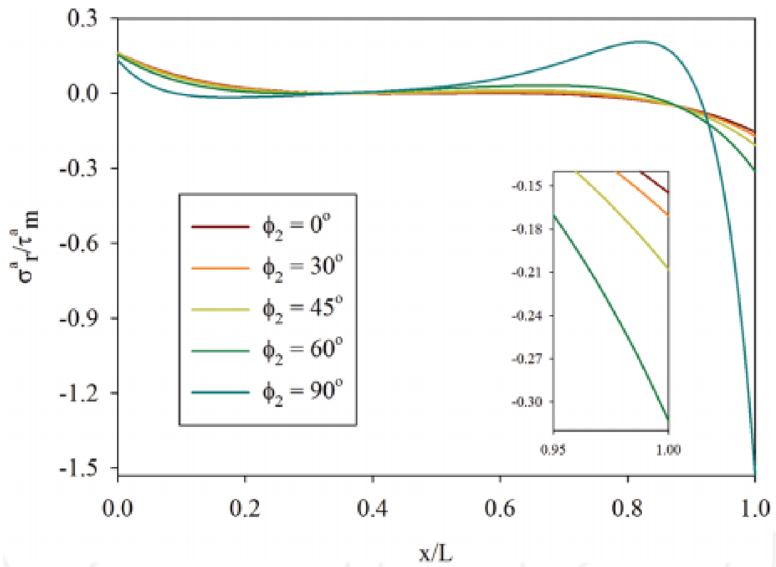

Figure 40 Interfacial radial stress distribution as represented in the reference

Thus, following a conservative approximation, the maximum shear strength will follow the equations (obtaining the maximum value from the graph):

$$\tau_{xr}{}^{a} = |\tau_m{}^{a}| * k = 1.896 * 4 = 7.586MPa$$

Considering k to be the coefficient shown in the graph for ϕ_2=0º since the thread of the inner most layer of the tube is assumed to be aligned with the coupler's main axis.

Afterwards, the maximum radial stress, can be calculated in a similar fashion:

$$\sigma_r{}^{a} = \tau_m{}^{a} * |k| = 7.586 * 0.3 = 2.276MPa$$

Considering k to be the coefficient shown in the graph for ϕ_2=0º.

Finally, if applying Von-Misses:

$$\sigma_{VM} = \sqrt{\sigma^2 + 3\tau^2} = \sqrt{2.276^2 + 3 * 7.586^2} = 13.335MPa$$

Given that most epoxy glues available commercially have a yield strength of 15 MPa approximately, a rough security margin can be estimated:

$$n = \frac{\sigma_{adm}}{\sigma_{max}} \rightarrow n = \frac{15}{13.335} = 1.12$$

Design Result

The resulting geometry has 3 internal flaps with 6 M6 threads capable of withstanding forces of up to 9000N safely.

Said efforts can the be distributed to either the 6 radial M6 screws passing through 2 joined coupleurs to transfer the load to a different sextion of the vehicle or through the gluing surface to the tubes.

Furthermore, the construction of the couplers blocks all movement but axial displacements and permits to align 2 section with a rotation of 30º, so the geometries are not confined to the lower section of the coupler but can exceed somewhat said limit it follows this 30º rule.

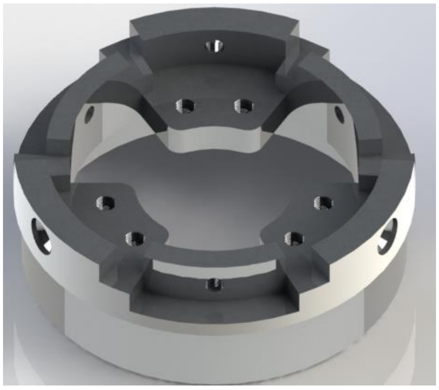

Figure 41 | Coupleur render

Composite Tubes

Tube Sizing

The tubes will be the main load bearing component of the rocket, as such, they ought to be able to withstand 6 main types of efforts (although not all at once):

- Tractions upon the parachute's deployment.
- Compression during the flight.
- Flexion when it misaligns and thus drag forces act upon the body at an angle.
- Torsional effort inherent to flying.
- Radial pressures acting upon the tubes due to pressure differences.
- Deformations due to the own tube's weight.

Therefore, the tubes ought to be designed considering several 3 critical situations:

- A combination of a radial force applied at the very tip of the tubes (30mg) when the parachute deploys (in case the parachute were to deploy radially) combined with an difference in pressure between the interior of the vehicle with the outer atmosphere due to the CO_2 cartridges releasing the gas (which will be considered to be 10atm which is equivalent to 1MPa, roughly); a torsional moment due to the effect of the lift on the wings (which can be considered to be 10% of the modelling radial force times the radius, 3mgR).
- When the Parachute deploys, the pressure within the tube will augment, alas presenting the inner pressure increase of 10atm (1MPa) paired with the torsional moment (3mgR) and a traction effort due to the parachute deploying along the main axis of the rocket (30mg).
- Finally a compression effort need to be considered upon flight where the maximum stress which can be tolerated is reduced due to the pairing of the previously discussed torsional moment (3mgR) and the difference in pressure (10atm or 1MPa) in case some of the cartridges released their content before they are meant to.

Finally, as a merely informational section, the following ought to be calculated as well:

- Maximum deformations upon each study case.
- Individual maximum critical loads during service.

For the calculations, a 3 meter-long tube will be considered (since the rocket is essentially a tube itself), without any intermediary supports (even though the couplers can be considered a rolling support with the properties of a fixed support, not allowing any deformation as it approaches the gluing length whilst still being able to move).

The tube will always be assumed to be a cantilever to augment the internal forces and moments the rocket will experience.

The tubes can be characterized as:

$$I_x = I_z = \iint_A x^2 dA = \frac{\pi}{4}(R_{ext}^4 - R_{int}^4)$$

$$I_y = I_x + I_z = 2I_x \rightarrow I_y = \frac{\pi}{2}(R_{ext}^4 - R_{int}^4)$$

Similarly, the elastic moment of the section can be computed as:

$$W_x = W_z = \frac{I_x}{R_{ext}} \rightarrow W_x = W_z = \frac{\pi(R_{ext}^4 - R_{int}^4)}{4R_{ext}}$$

$$W_y = \frac{I_y}{R_{ext}} = \frac{\pi(R_{ext}^4 - R_{int}^4)}{4R_{ext}} \rightarrow W_y = 2W_x$$

Upon numerical applications (rounding down when needed to augment ever so slightly the tensions the body undergoes),

$$I_x = I_z = 1.805 * 10^6\ mm^4$$

$$I_y = 3.610 * 10^6\ mm^4$$

$$W_x = W_z = 28.887 * 10^3\ mm^3$$

$$W_y = 57.774 * 10^3\ mm^3$$

$$S_x = 58.920 * 10^3 mm^3$$

For the first case discussed (which also happens to be the most extreme), where applying Navier's equations yields a result:

$$\sigma_{flex} = \frac{30mg}{W_y} \rightarrow \sigma = 305.635MPa$$

Adding the shear stress cause by the torsion:

$$\tau_{tor} = \frac{3mgR_{ext}}{W_x} \rightarrow \tau_{tor} = 0.9552MPa$$

When finding the equivalent stress employing Treska's formula (since it slightly overestimates the shear stress over Von-Misses) alongside the radial stress due to the pressure, paired with thin walled tube theory, where the radial pressure causes a tension along the axis of the tube):

$$\sigma = \sqrt{(\sigma_{flex} + \sigma_{rad})^2 + 4\tau_{tor}^2} \rightarrow \sigma = 306.6422MPa$$

The second case to be studied represents the parachute opening axially to the rocket:

$$\sigma_{trac} = \frac{30mg}{A} \rightarrow \sigma = 9.177MPa$$

Adding the shear stress cause by the torsion:

$$\tau_{tor} = \frac{3mgR_{ext}}{W_x} \rightarrow \tau_{tor} = 0.9552MPa$$

When finding the equivalent stress employing Treska's formula (since it slightly overestimates the shear stress over Von-Misses) alongside the radial stress due to the pressure:

$$\sigma = \sqrt{(\sigma_{trac} + \sigma_{rad})^2 + 4\tau_{tor}^2} \rightarrow \sigma = 10.363MPa$$

Finally, the third event, is to take place during flight, assuming a malfunction of the gas cannisters, thus, the calculations result in:

The second case to be studied represents the parachute opening axially to the rocket:

$$\sigma_{comp} = \frac{30mg}{A} \rightarrow \sigma = 9.177MPa$$

Adding the shear stress cause by the torsion:

$$\tau_{tor} = \frac{3mgR_{ext}}{W_x} \rightarrow \tau_{tor} = 0.9552MPa$$

When finding the equivalent stress employing Treska's formula (since it slightly overestimates the shear stress over Von-Misses) alongside the radial stress due to the pressure:

$$\sigma = \sqrt{(-\sigma_{trac} + \sigma_{rad})^2 + 4\tau_{tor}^2} \rightarrow \sigma = 8.233MPa$$

Therefore, to size the tubes a stress of 306.6422MPa will be considered.

Although carbon fibre tends to yield more solid materials it has a main drawback, it prevents electromagnetic waves from entering the Launch Vehicle for frequencies ranging from 1 to 6GHz (Parneix, 2010), due to the free electrons in the carbon creating a Faraday Cage as described in the literature, where upon the carbon facing a surface treatment increases said shielding up to 90dB due to the many reflections caused by the interphases between carbon layers.

Hence, once its paired with the carbon fibre's higher cost, glass fibre becomes the obvious choice.

Composite material must always be at a stress below it's proportionality limit, which can be described as (Princeton University, 2020):

$$\sigma_{yC} = \left[1 + \frac{V_f E_f}{V_m E_m}\right] V_m \sigma_{ym}$$

Where σ_{yC} represents the proportionality limit (in MPa); V_f stands for the percentage of reinforcement by weight (dimensionless); E_f is Young's modulus of the reinforcement (in GPa), V_m is the percentage of matrix by weight (dimensionless), E_m is Young's modulus of the matrix (in GPa) and σ_{ym} is the yield limit of the matrix (in GPa).

Following the data provided for glass fibre (AZO Materials, 2020) it can be characterized as:

$$E = 72 - 85\ GPa$$
$$Re = 2750 - 2850\ MPa$$
$$\rho = 2550 - 2600 \frac{kg}{m^3}$$

$$\nu = 0.21 - 0.23$$

Likewise, the epoxy resin (Simmons ltd, 2020):

$$E = 10.5\ GPa$$
$$Ru = 85\ MPa$$

$\rho = 1100 - 1400\ kg/m^3$ (NetComposites, 2020)

$$\nu = 0.3 - 0.35$$

Since the limit obtained from the literature is the rupture limit, the elastic limit will be considered at 80% of the rupture, alas: $Re = 0.8 * 85 = 68MPa$

Therefore, the proportionality limit can be used (at 110% of the maximum service tension) to determine the percentages of each component required (as a first approximation, considering all the glass fibre to be perfectly aligned with the axis of the cylindre):

$$1.1 * 306.6422 = \left[1 + \frac{V_f * 72}{V_m 10.5}\right] V_m 68 \mid V_m + V_f = 1$$

Resulting in:

$$V_m = 0.3266; V_f = 0.6734$$

Even thought surpassing said proportionality limit does not mean it's elastic limit is surpassed it does imply that the deformations seen by the tube will not follow a linear variation as portrayed by Hooke's Law since the material will no longer resemble a perfect spring.

Furthermore, the Young Modulus of the composite material may vary following the equations for the longitudinal Young Modulus of the composite or the transversal (considering the minimum values of their respective intervals):

$$E_{lon} = V_m E_m + V_f E_f \rightarrow E_{lon} = 51.9141GPa$$
$$E_{trans} = \frac{E_m E_f}{V_m E_f + V_f E_m} = 24.7173GPa$$

Furthermore, the density of the finished tubes can be calculated as (considering the higher end of each interval):

$$\rho_c = V_m \rho_m + V_f \rho_f \rightarrow \rho_c = 2208.08 \frac{kg}{m^3}$$

Most commonly in amateur rocketry an epoxy resin is employed as the matrix and either unidirectional glass fibre or carbon fibre is employed.

Seeing as a tube of any given length will have a linear density:

$$\rho_{lin} = \rho_c * A \rightarrow \rho_{lin} = 2.1244 \frac{kg}{m}$$

Furthermore, glass fibre reinforcements usually come in sheets weighing 520g/m^2 (Castro Composites, 2020), therefore, the amount of square meter can be determined as a step to calculate how many layers of reinforcement will be needed.

For any 1 meter, the mass of glass fibre is:

$$m_{glass} = \rho_{lin} * V_f \rightarrow m_{glass} = 1.4306kg$$

Which when divided by the mass per area and the area (considering the inner diameter as a reference for all):

$$n_{layers} = m_{glass} * \frac{m^2}{520g} * \frac{1}{2\pi * R_{int} * L} | n \in N \rightarrow n_{layers} = 7.29 \rightarrow n_{layers} = 8$$

Although there are several layers of unidirectional fibre, layering them at different angles slightly reduces Young's modulus longitudinally but greatly augments it in all other directions whilst also increasing the cohesion between the layers.

Tube characterization

The proposed plan for the layer alignment is:

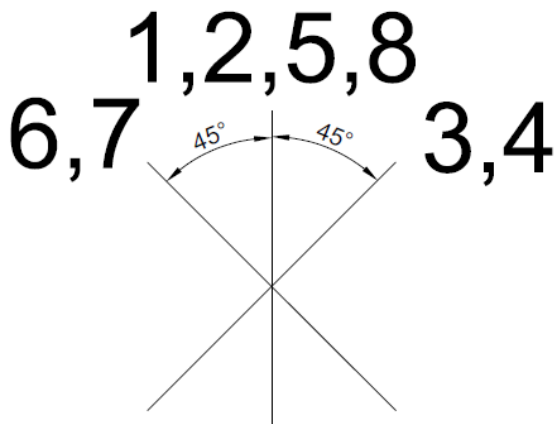

Figure 42 | Layer alignment

Therefore, the new Young's Modulus can be calculated as:

$$E_f = \frac{4E_f + 4E_f \sin(45º)}{8} \rightarrow 61.4558GPa$$

Therefore, the new ratios can be calculated more explicitly (revisiting the equation for the proportionality limit):

$$\sigma_{yC} = \left[1 + \frac{V_f E_f}{V_m E_m}\right] V_m \sigma_{ym} \rightarrow \begin{cases} V_m = 0.1872 \\ V_f = 0.8128 \end{cases}$$

Therefore, the new Young's moduli are:

$$E_{lon} = V_m E_m + V_f E_f \rightarrow E_{lon} = 60.4872GPa$$

$$E_{trans} = \frac{E_m E_f}{V_m E_f + V_f E_m} = 34.3436GPa$$

Since the percentage of glass fibre has increased, so have the moduli.

Employing the previous equations as part of the iterative design process the new densities can be characterized:

$$\rho_c = V_m \rho_m + V_f \rho_f \rightarrow \rho_c = 2375.36 \frac{kg}{m^3}$$

$$\rho_{lin} = \rho_c * A \rightarrow \rho_{lin} = 2.2853 \frac{kg}{m}$$

Similarly, the composite's Poisson's ratio can be calculated employing the homogenization theory (employing the biggest ratios to later minimize the shear modulus and thus maximize the torsion angle):

$$\nu = V_m \nu_m + V_f \nu_f \rightarrow \nu = 0.2525$$

Therefore, the shear modulus is:

$$G = \frac{E_{long}}{2(1+\nu)} \rightarrow G = 24.1466 GPa$$

To fully characterize the tubes, the buckling deformations and maximum critical loads ought to be visited.

Considering buckling (without the reduction due to torsion or internal pressure),

$$P_{crit} = \frac{\pi^2 E I_{min}}{L_p^2}$$

Since for all calculations it's considered to be a cantilever so it will be for the buckling since it maximizes the equivalent length and thus reduces the critical load to it's minimum value:

$$P_{crit} = \frac{\pi^2 * 60.4879 * 10^9 * 1.805 * 10^{-6}}{6^2} = 29.9322 KN$$

Which when considering the mass of the rocket (30kg) the maximum acceleration can be calculated:

$$F = ma \rightarrow a = 997.73838 \frac{km}{s^2} = 101706.26 g$$

Service deformations

Since the maximum critical loads are directly correlated with the maximum deformations they can be expressed as (during service):

Event	Maximum service deformation formulae	Maximum during service
Traction deformation (m)	$L = L_o e^{\frac{F}{AE}}$	$L = 3.00045$
Compression deformation (m)	$L = Le^{\frac{F}{AE}}$	$L = 2.99955$
Flexion deformation due to an effort at the end (m)	$w = \frac{FL^3}{3EI_x}$	$w = 0.72780$
Flexion deformation angle due to an effort at the end (rad)	$\theta = \frac{FL^2}{2EI_x}$	$\theta = 0.36390$
Flexion deformation due to a distributed effort (m)	$w = \frac{qL^4}{8EI_x}$	$w = 0.27293$
Flexion deformation angle due to distributed effort (rad)	$\theta = \frac{qL^3}{6EI_x}$	$\theta = 0.1213$
Torsion deformation angle (rad)	$\theta = \frac{M_t}{I_y G} L$	$\theta = 0.00189$
Internal pressure maximum (MPa)	$P = \frac{2t\sigma_{max}}{D_{ext}}$	$P = 24.45154$

Table 21 | Maximum efforts calculations

Where $F = 30mg$ (where m=30kg); $\sigma_{max} = 305.64422MPa$; $M_t = 3mgR_{ext}$ and $t = 2.5mm$.

The results for flexion with an effort at the end ought to be the same as with the maximum stress since the design maximum is obtained in said case.

Nosecone

Adimensional approximation

The purpose of the nosecone is to reduce the drag force acting on the rocket as it ascends.

The drag force can be described as:

$$F_d = \frac{1}{2}\rho u^2 C_d A$$

Where F_d represents the drag force; ρ is the density of the fluid; u represent the speed of said fluid, C_d is the drag coefficient and A is the cross section of the area perpendicular to the direction of the flow.

Hence to reduce the drag, the drag coefficient must be as small as possible.

The drag coefficient can also be calculated as:

$$C_d = 2\frac{A_w}{A_f}\frac{Be}{Re_L^2}$$

In this equation A_w stands for the wet area; A_f is the cross section of the area perpendicular to the direction of the flow; Be is the Bejan number; Re_L is the Reynolds number over the length of the fluid line.

The Bejan Number represents the pressure drop along a contact between a flow and the boundaries.

$$Be = \frac{\Delta P L^2}{\mu \nu}$$

Here, ΔP stands for the pressure drop along the contact length; ΔL is the contact length; μ is the dynamic viscosity and ν is the kinematic viscosity.

The Reynold Number applied to the fluid line is employed to characterize a fluid's state:

$$Re_L = \frac{\rho u L}{\mu}$$

Having ρ stand for the density of the fluid; u the speed of the flow, L the length of the fluid line and μ stands for the dynamic viscosity of the fluid.

The surface area of a revolution body is defined as:

$$S = 2\pi \int_a^b f(x)\sqrt{(f'(x))^2 + 1}\, dx$$

And the cross section can be expressed as:

$$S = \pi R_{ext}^2$$

Thus, the drag coefficient can be rewritten as:

$$C_d = \frac{4}{\rho u^2}\frac{\int_0^L f(x)\sqrt{\left(f'(x)\right)^2+1}\,dx}{R_{ext}^2}\,\Delta P$$

Applying Bernoulli's equation assuming a conservative state:

$$\frac{P_1}{\rho}+\frac{1}{2}u_1^2+gh_1=\frac{P_2}{\rho}+\frac{1}{2}u_2^2+gh_2$$

And accepting $u_1^2 = u_2^2, h_1 = 0, h_2 = L$

$$\Delta P = \rho g L$$

Applied to the previously obtained approximation:

$$C_d = \frac{4gL}{u^2}\frac{\int_0^L f(x)\sqrt{\left(f'(x)\right)^2+1}\,dx}{R_{ext}^2}$$

Froude's number represents the relation between the inertia and gravity:

$$Fr^2 = \frac{u^2}{gL}$$

Obtaining an approximation completely independent of the fluid's properties and merely relying on the geometry and speed of the fluid.

$$C_d = \frac{4}{Fr^2}\frac{\int_0^L f(x)\sqrt{\left(f'(x)\right)^2+1}\,dx}{R_{ext}^2}$$

Which can be employed to obtain a first approximation of the drag coefficient.

However, it can also be rewritten for simulations as:

$$C_d = \frac{4}{\rho u^2}\frac{\int_0^L f(x)\sqrt{\left(f'(x)\right)^2+1}\,dx}{R_{ext}^2}\frac{dP}{dx}$$

Where the software would only need to calculate the pressure distribution along the body.

Basing the approximations on the previous result:

$$C_d = \frac{4}{Fr^2}\frac{\int_0^L f(x)\sqrt{\left(f'(x)\right)^2+1}\,dx}{R_{ext}^2}$$

Nosecone selection

There are 2 main types of nosecones:

- Geometric design: Those where the cross-section of the nose cone can be derived from geometric shapes, thus being continuous.
- Mathematically derived: obtained by minimizing the drag equations.

According to literature for sub-sonic flights (Ma<1) the best nose cone stemming from a geometric design is that of an elliptical cross section (Stroick, Nose Cone and Fin Optimization, 2011) generating less drag than other geometrically designed nose cones for 0.4≤ Ma ≤0.8 (Senthiil, 2018).

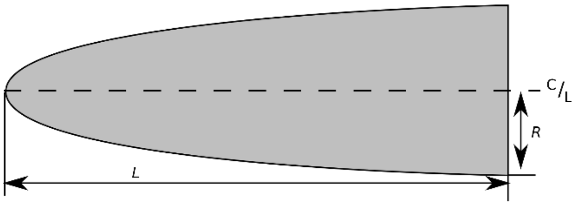

$$y = R\sqrt{1-\frac{x^2}{L^2}}$$

Figure 43|Elliptical nose cone cross-section (Senthiil, 2018)

Where R stands for half of the minor axis of the ellipse (corresponding to the external diameter of the rocket) and L represents half of the major axis of the ellipse (corresponding to the length of the nosecone).

As explained in the literature (Filho, 2019) the implementation of tangent and parabolic shaped nose cones is purely situational and thus for certain case studies it may prove more beneficial.

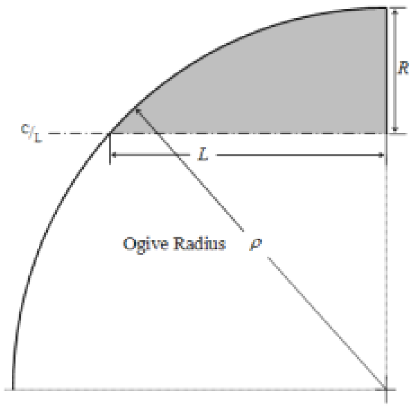

$$y = \sqrt{\rho^2-(L-x)^2}+R-\rho$$

$$\rho = \frac{R^2+L^2}{2R}$$

Figure 44 | Tangent nose cone cross-section (Sr., 1996)

Where R stands for the external diameter of the rocket; L represents the length of the nosecone and ρ corresponds to the radius of the sphere from which the cross-section derives.

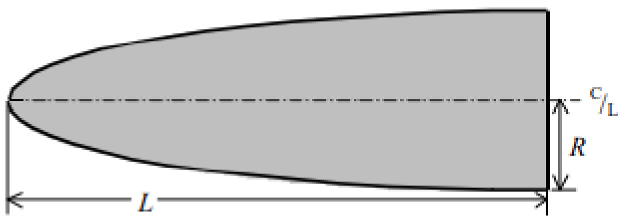

$$y = R\left(2\frac{x}{L}-\left(\frac{x}{L}\right)^2\right)$$

Figure 45 | Parabolic nose cone cross-section (Department of Defence, United States of America, 1996)

Where R stands for the external diameter of the rocket; L corresponds to the length of the nosecone.

Finally, the Haack Series nose cone stems from the mathematical minimization of drag force and are commonly employed in transonic flights (Ma>1), where the series is a set of continuous shapes determined by a factor C, two values of C are particularly important (Stroick, Nose Cone and Fin Optimization, 2011):

- LD ($C = 0$): Where the drag force is minimized for a given length and diameter (Also known as Von Kármán ogive).
- LV ($C = 1/3$): Minimizing drag force for a given length and volume.

It is important to note the Haack series nose cones are not tangent to the tubes, however the imperfection tends to be minimal and thus is generally overlooked (Haack, 1941).

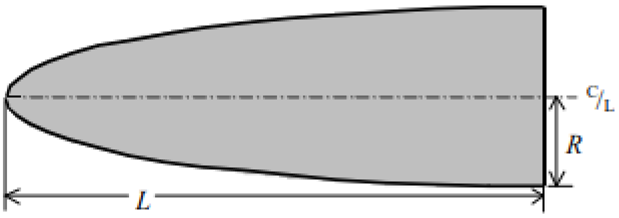

$$y = \frac{R}{\sqrt{\pi}}\sqrt{\theta - \frac{\sin(2\theta)}{2} + C\sin^3(\theta)}$$

$$\theta = \arccos\left(1 - \frac{2x}{L}\right)$$

Figure 46 | Haack series nose cone cross-section (Sr., 1996)

Where R stands for the external diameter of the rocket; L represents the length of the nosecone and C corresponds to the form factor.

The fitness ratio is the ratio between the length of the body and the maximum width its maximum width:

$$AR = \frac{L}{2R}$$

To minimize drag in subsonic (Ma<1) flights an aspect ratio of 5 is critical (Stroick, Nose Cone and Fin Optimization, 2011), therefore, all nose cones designs will adhere to:

$$L = 10R$$

Applying the result obtained in part XX (drag coefficient calculations):

$$C_d = \frac{4}{Fr^2}\frac{\int_0^L f(x)\sqrt{\left(f'(x)\right)^2 + 1}\,dx}{R_{ext}^2}$$

Considering all nose cones will share the same Froude's number and other parameters, the objective function becomes:

$$\min \int_0^L f(x)\sqrt{\left(f'(x)\right)^2 + 1}\,dx$$

Hence for each geometrical cross-section we obtain the following with numerical application:

Elliptical cross-section:

$$\int_0^{625} 62.5\sqrt{1-\frac{x^2}{625^2}}\sqrt{\left(-\frac{62.5\,x}{625^2\sqrt{1\,-\frac{x^2}{625^2}}}\right)^2+1}\,dx = 30821\,mm^2$$

Tangential cross-section:

$$\int_0^{625} (\sqrt{3156.25^2-(625-x)^2}+62.5 - 3156.25)\sqrt{\left(\frac{625\;-\;x}{\sqrt{-(625\;-\;x)^2+\;3156.25^2}}\right)^2+1}\,dx = 2011470.28809\,mm^2$$

Parabolic cross-section:

$$\int_0^{625} 62.5\left(2\frac{x}{625}-\left(\frac{x}{625}\right)^2\right)\sqrt{\left(0.2\left(1-\frac{x}{625}\right)\right)^2+1}\,dx = 26145.4\,mm^2$$

As shown by the calculations, the geometrically built nose cone with the least drag is the parabolic cross-section. As explained in literature, generally the nose cone with the least drag coefficient tends to be the elliptical cross-section but there might be certain application where the tangential or parabolic cross-sections might prove better, as in this case (an aspect ratio $AR = 5$).

However, these results must be validated by the simulations and reduced scale-model testing since with this approximation the fluid-structure coupling is ignored and the pressure variation along the geometry is assumed to be conservative (friction losses are disregarded, due to the application of Bernoulli's equation in its conservative form).

Studying the mathematically built cross-sections:

LD Haack series cross-section:

$$\int_0^{625} \frac{62.5}{\sqrt{\pi}}\sqrt{\arccos\left(1-\frac{2x}{625}\right)-\frac{\sin\left(2\arccos\left(1-\frac{2x}{625}\right)\right)}{2}} * \sqrt{\left(\frac{d}{dx}\left(\frac{62.5}{\sqrt{\pi}}\sqrt{\arccos\left(1-\frac{2x}{625}\right)-\frac{\sin\left(2\arccos\left(1-\frac{2x}{625}\right)\right)}{2}}\right)\right)^2+1}\,dx = 25631.9\,mm^2$$

LV Haack series cross-section:

$$\int_0^{625} \frac{62.5}{\sqrt{\pi}} \sqrt{\arccos\left(1-\frac{2x}{625}\right) - \frac{\sin\left(2\arccos\left(1-\frac{2x}{625}\right)\right)}{2} + \frac{1}{3}\sin^3\left(\arccos\left(1-\frac{2x}{625}\right)\right)}$$
$$* \sqrt{\left(\frac{d}{dx}\left(\frac{62.5}{\sqrt{\pi}} \sqrt{\arccos\left(1-\frac{2x}{625}\right) - \frac{\sin\left(2\arccos\left(1-\frac{2x}{625}\right)\right)}{2} + \frac{1}{3}\sin^3\left(\arccos\left(1-\frac{2x}{625}\right)\right)}\right)\right)^2 + 1}\, dx$$
$$= 203268.9mm^2$$

Therefore, as shown by the calculations, the optimal nosecone to minimize drag is the LV Haack series, with a drag coefficient:

$$C_d = \frac{6.5617664}{Fr^2}$$

Therefore, for a standard, simplified calculation, where(with a s speed of 30m/s and an acceleration of 9.1m/s^2 along with the length of the nosecone):

$$Fr^2 = \frac{v^2}{gl} \rightarrow Fr^2 = \frac{900}{9.81 * 0.625}$$

Which yields a drag coefficient :

$$C_d = \frac{6.5617554}{\frac{900}{9.81 * 0.625}} = 0.047$$

If all the results were to be inserted into a compendium:

Cross-section	Drag coefficient (at 30 m/s over 0.625m)
Elliptical	0.215
Tangential	14.03
Parabolic	0.1823
Haack (C=0)	0.047
Haack (C=1/3)	1.418

Table 22| Adimensionally calculated drag coefficients

Clearly each nosecone cannot have the drag coefficients portrayed in the table above, since, some are far too little other far too big, however, it does serve to have a rough first ranking of their respective drags.

Some present far too high value due to the area-length ratio they present when performing the integral.

Simulations with the same parameters (v=30m/s; ρ=1.214kg/m^3) were performed in SolidWorks 2018 Flow Simulation and the drag coefficients obtained were:

Cross-section	Drag coefficient (Simulation)
Elliptical	0.242962
Tangential	Did not converge
Parabolic	0.359210
Haack (C=0)	0.205910
Haack (C=1/3)	0.234925

Table 23| Simulated drag coefficients

Similarly to the adimensionally calculated drag coefficients the tangential nosecone yields unreasonable results (thus being discarded) whilst the others only portrayed which nosecone yields the least drag overall (Von Kármán ogive) therefore, the method only serves as a rought first approximation.

The pressure distributions for each of the 4 converging simulations were:

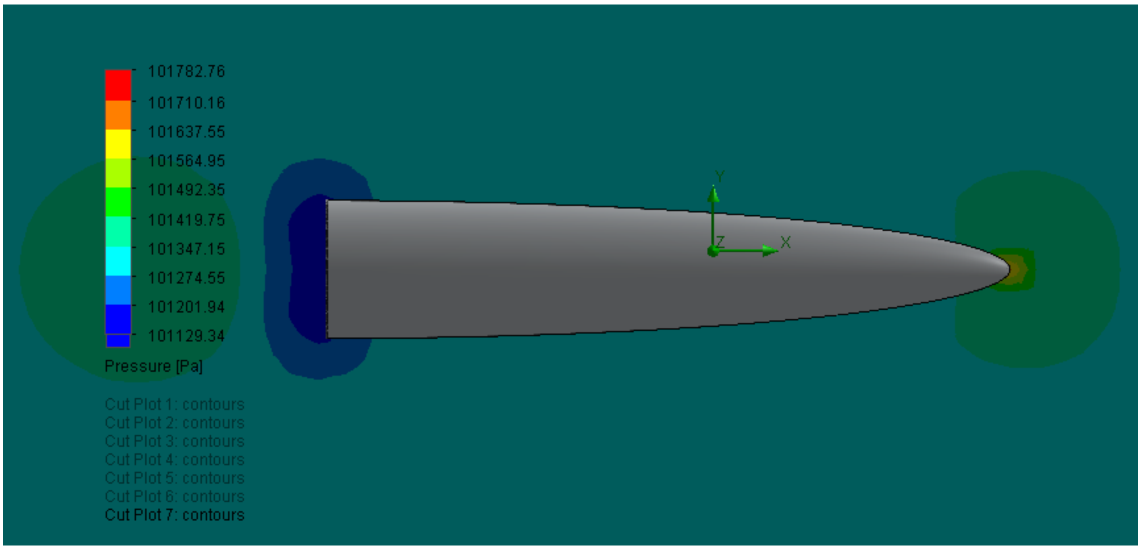

Figure 47 | Elliptical nosecone pressure distribution

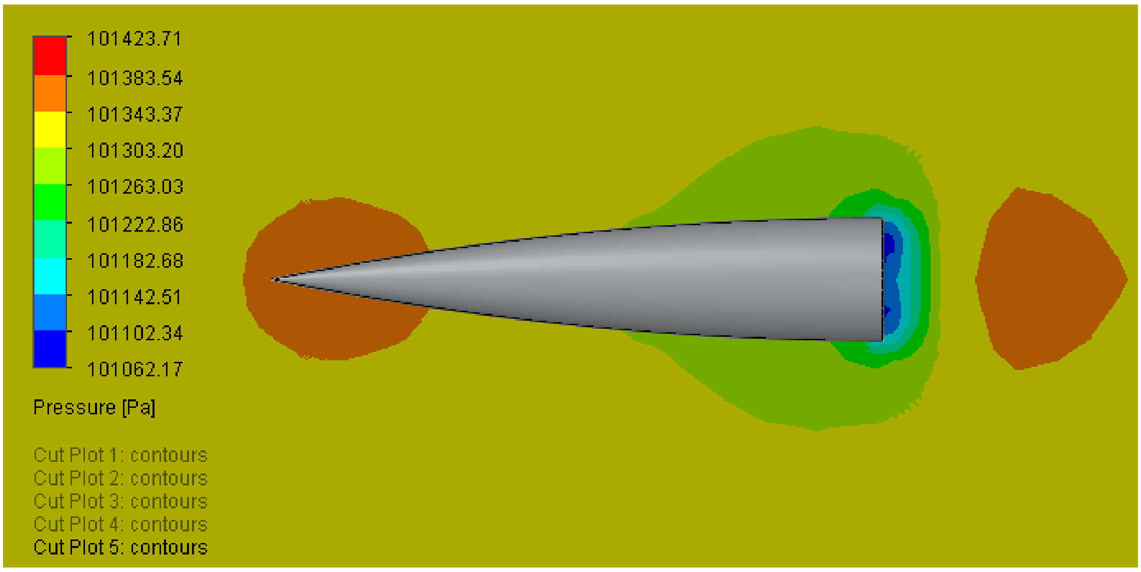

Figure 48 | Parabolic nosecone pressure distribution

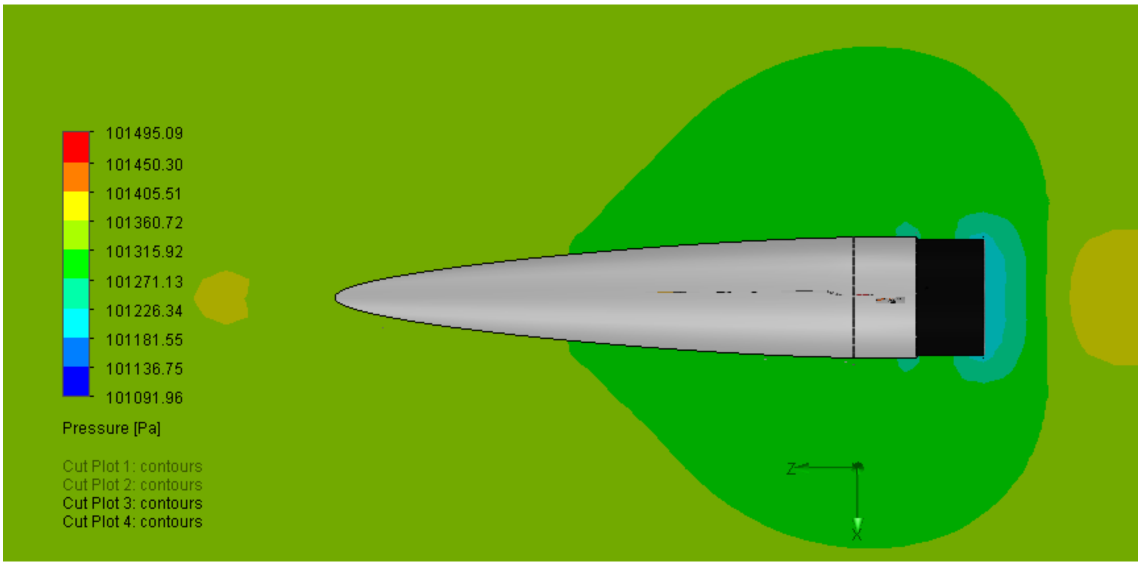

Figure 49| Haack c=0 nosecone pressure distribution

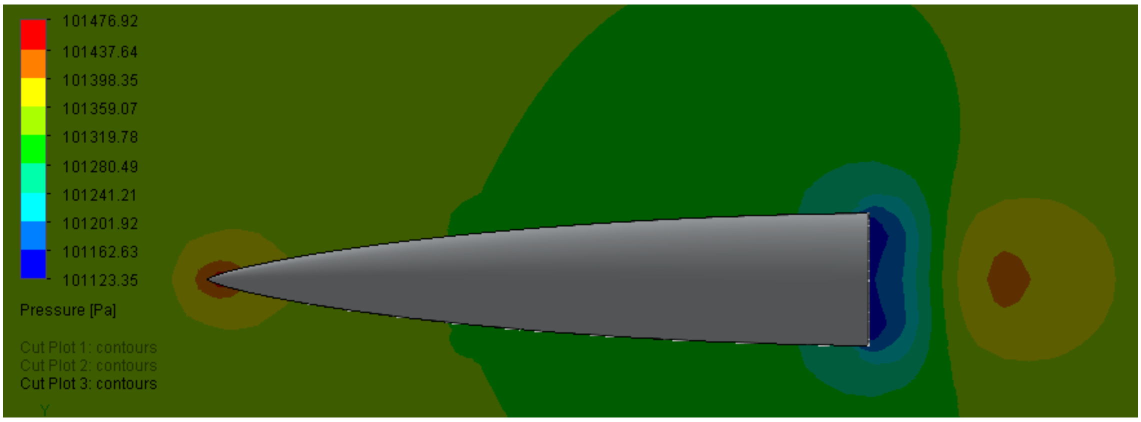

Figure 50 | Haack nosecone c=1/3 pressure distribution

Combining the simulations with Bernoulli, the velocity of the fluid can be obtained:

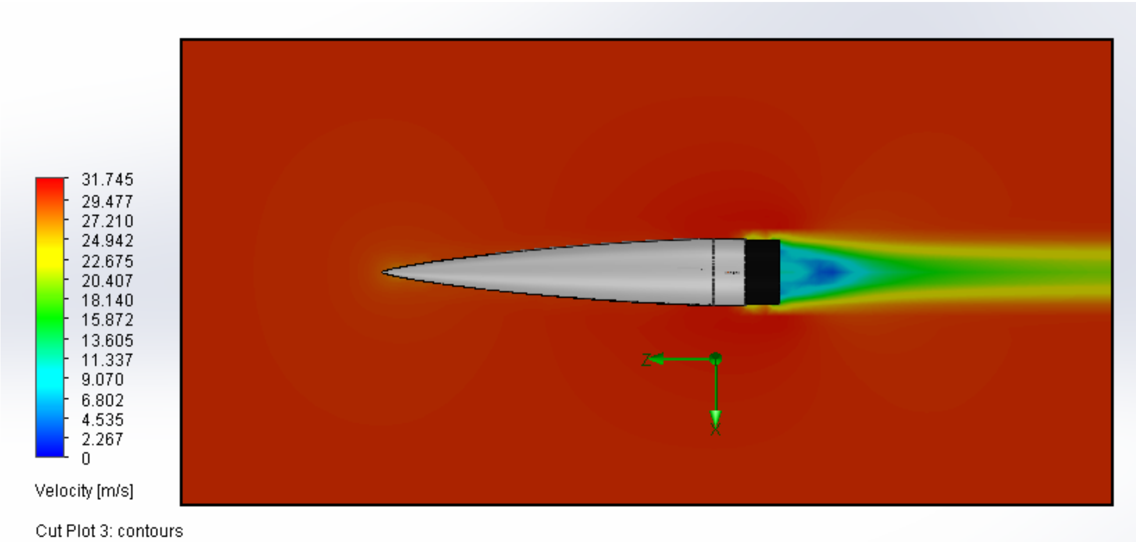

Figure 51 | Haack c=0 velocity distribution

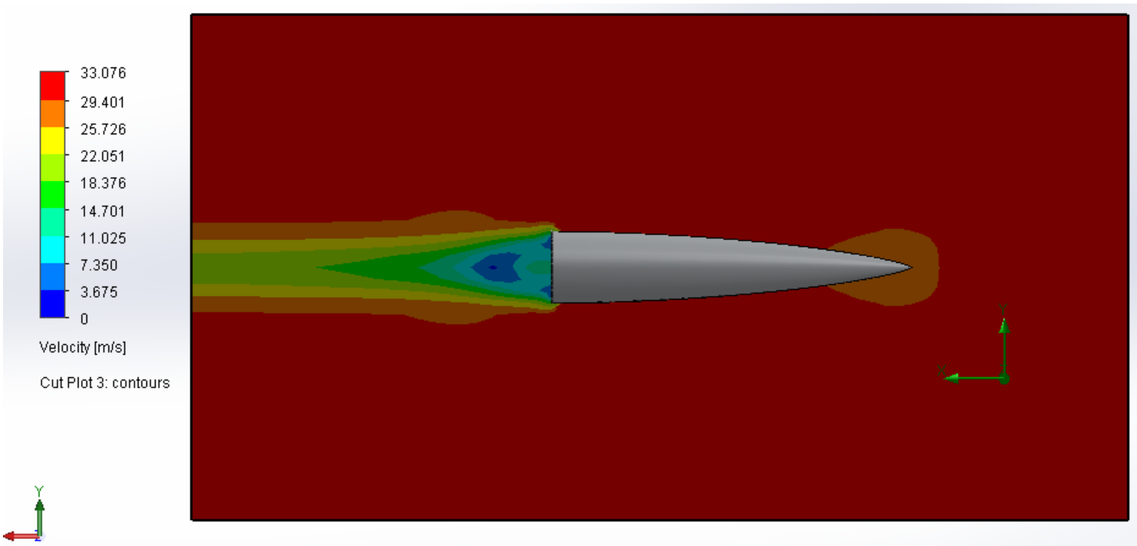

Figure 52 | Haack c=1/3 velocity distribution

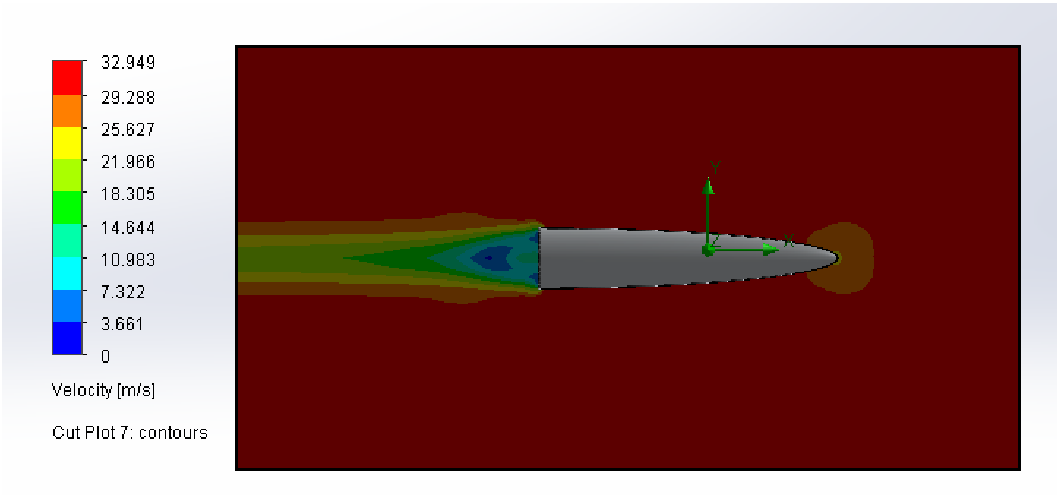

Figure 53 | Elliptical velocity distribution

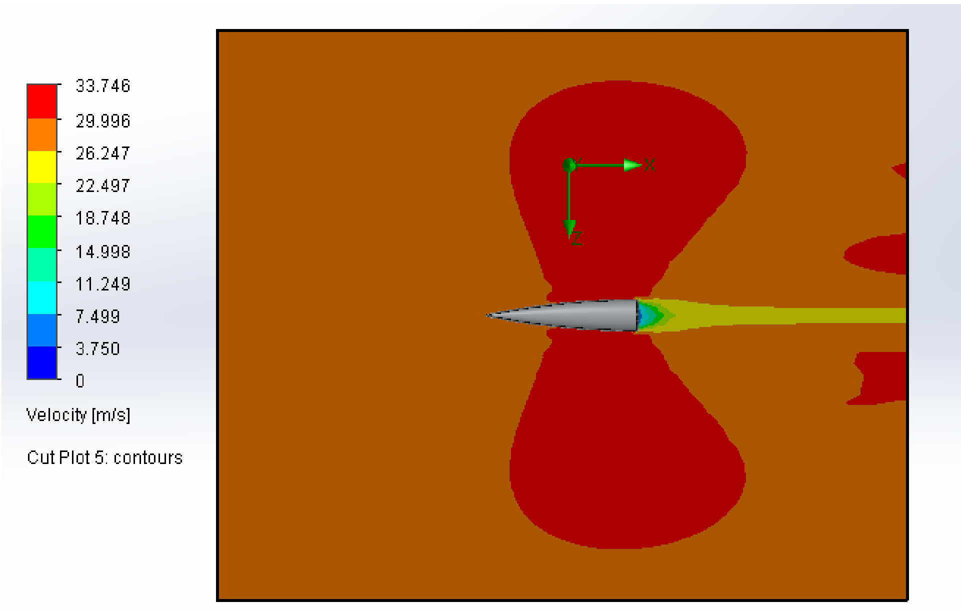

Figure 54 | Parabolic velocity distribution

The lower drag coefficient of the Von Kármán ogive can be explained by the pressure and velocity distributions, since, it does not generate a lower-speed-high-pressure in front of itself when travelling at low speeds (Ma=0.1) unlike all the other cases where the simulations converged.

First Characterization of the Drag Forces as a function of time

Considering the force of gravity to be $g = 9.80665 m/s^2$ (it can be soncidered constant since the variation is minimal for tropospheric flights) and the air density (tropospheric air) as a function of altitude (International Standard Atmosphere):

$$\rho = \frac{p_o M}{R T_o}\left(1 - \frac{Lh}{T_o}\right)^{\frac{gM}{RL}-1}$$

Where p_o is the sea level standard atmospheric pressure ($p_o = 101325$ Pa), T_o is the sea level standard temperature ($T_o = 288.15$ K), M represents the molar mass of dry air ($M = 0.0289654$ kg/mol), R stands for the universal ideal gas constant ($R = 8.31447$J/mol/K), L is the temperature lapse rate ($L = 0.0065$ K/m), finally, h is the altitude.

Thus, considering the different motors for each level, for each it's possible to calculate the variation of the drag coefficient as a function of time:

$$F_{drag} = \frac{AC_D}{2}\frac{p_o M}{R T_o}\left(1 - \frac{L}{T_o}z\right)^{\frac{gM}{RL}-1} * \left(\frac{dz}{dt}\right)^2$$

System overview

To keep the nosecone attached during flight to the main body and once the parachute is deployed, a system was designed so a shock cord was attached to a buckle and itself is attached to a glass fibre sheet which is held in place by an internal cylinder (avoiding any cantilever supports since sharp bends could compromise the fibre's integrity and that way the joint could be modelled to be merely traction and not flexion):

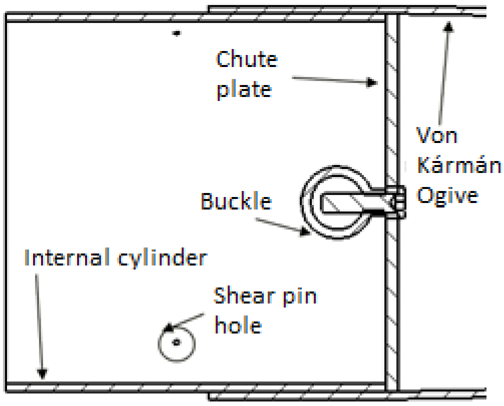

Figure 55 | Nosecone assembly cross-section

Furthermore, there are 3 holes to mount shear pins (plastic dowels sized to break when they suffer a shear stress of 15MPa) such that the nosecone is stuck to the body of the rocket during the ascension and it is released when the carbon dioxide augments the internal pressure and they break.

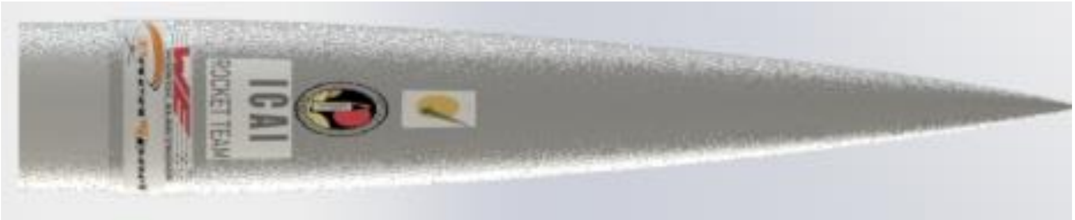

Figure 56 | Nosecone front view

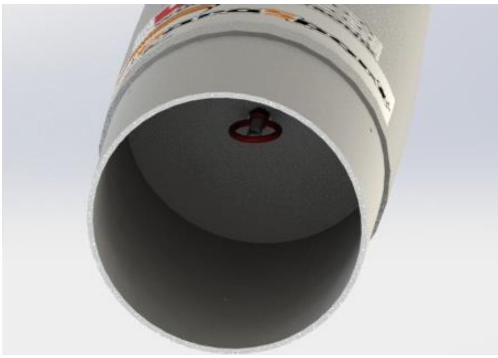

Figure 57 | Nosecone lower view (eye bolt detail)

Recovery system

System’s discussion

The aim of the recovery system is to ensure the rocket can descend and land safely after the motor’s burn out and the launch vehicle has reached the apogee.

According to the Tripoli Rocketry Association, the following are the requirements for each certificate:

<table>
<tr><td>Tripoli Certificate</td><td>Level 1</td><td>Level 2</td><td>Level 3</td></tr>
<tr><td>Recovery requirements</td><td colspan="2">Standard parachute system is demanded, single or double event (ff a double event recovery the first recovery event may be via drogue-less or streamer as long as the second event uses a standard parachute).</td><td>Not specified.</td></tr>
<tr><td>Electronics</td><td colspan="2">Not required.
Prior to a Level 3 Certificate flight the flyer must have proven proficiency with an electronic recovery system at the Level 2 impulse range.</td><td>The launch vehicle must have at least two separate electronic devices, with independent power sources, wire harnesses, and ignition devices for the primary and back-up means of recovery system deployment.</td></tr>
<tr><td>Reference</td><td>(Tripoli Rocketry Association, 2020)</td><td>(Tripoli Rocketry Association, 2020)</td><td>(Tripoli Rocketry Association, 2020)</td></tr>
</table>

Table 24 | Tripoli Recovery Requirements

Traditional Recovery Systems as the ones specified in the Tripoli Requirements are parachute-deployment systems amongst which, the 2 most common are:

- Single Event Recovery Sub-System (for smaller rockets): Consisting of a single parachute and the means to deploy it.
- Double Event Recovery Sub-System: With 2 parachutes which deploy at different altitudes, one at the apogee (commonly known as the drogue parachute) reducing the descent speed (anywhere to 10-20m/s) and afterwards deploying the main parachute at a lower altitude to bring the descent speed of the rocket below 5m/s.

To comply with the Level 3 Requirement, a secondary single event Recovery Sub-System will also need to be designed as the back-up system.

The advantage of employing a double event recovery system is the reduced scatter range of the rocket, greatly facilitating its location upon touchdown.

There exist several methods to deploy the parachute:

- A short fuse ignited by the motor which burns until the apogee when the dying fuse ignites a small charge which forces the upper section of the rocket to separate and deploys the parachute. Thus, this method requires extensive calculation, simulations and testing for the time between motor burnout and the apogee, since the fuse's length-burn time is non-linear it requires prior testing and configuration since there is no form of active control nor feedback in the rocket another drawback is the little flexibility it offers, since it fixes the Recovery Bay atop the Motor Bay, aiming to avoid running the fuse through several compartments and therefore risking an internal burn.

- The second system, employed in bigger more powerful rockets (since it allows for a greater module flexibility and active control) is an electronic recovery, usually required to be completely independent of the rocket's electronics, it relies on altimeters to deploy the parachutes (thus if there ever is a setback in the timing there's no risk of the deployment blast occurring mid-ascent).

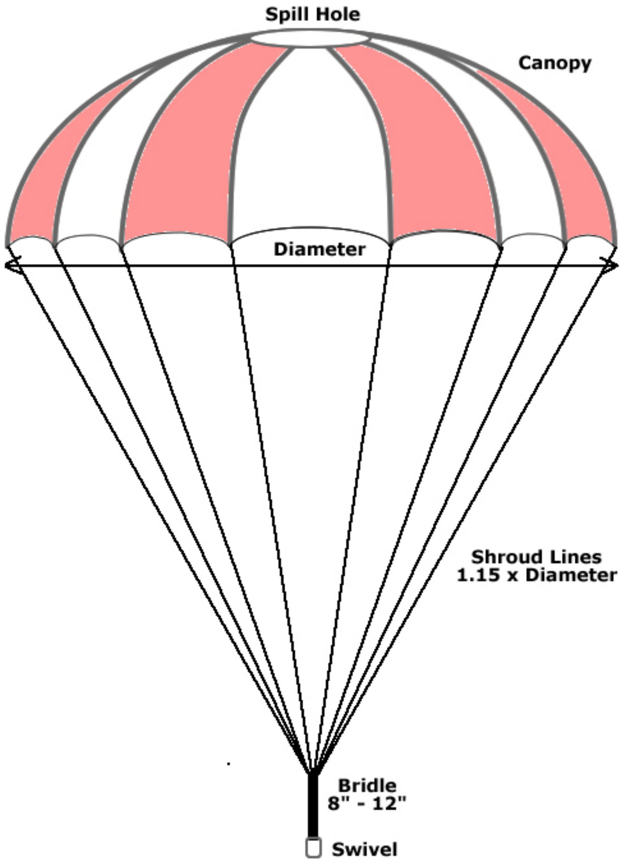

Figure 58 | Parachute sketch (Fruity Chutes Inc., 2019)

The Spill Hole can be found in spherical parachutes and it has a diameter of around 20% of the external diameter (equates to 3% of the area) and it increases the stability of the parachute (preventing it from "puffing").

The canopy can take several shapes and forms but it is always made of sewed fabric.

The diameter is the characteristic dimension of the parachute and allows for its sizing.

The Shroud lines connect the canopy to the bridle.

Finally the Swivel connects it to the falling body, allowing the parachute to rotate without relative to the falling body it's attached to.

Considering the results of the simulations, each certificate flight will have the following recovery system:

- Level 1: Since it's the smallest rocket, it will depend on a single event, electronically driven, recovery system, although it is not required to obtain the certificate, it's far more reliable than employing the fuse ignition system.
- Level 2: Although there are no recovery system requirements to obtain a level 2 certificate, the rocket will have a double event, electronically driven recovery system since prior to the level 3 flight the pilot is required to operate an electronically driven recovery system.

- Level 3: Since the requirements demand a main system and a back-up the rocket will implement both level 1 and level 2 recovery systems, Level 2's double event recovery as its primary system and Level 1's as a back-up.

Single Event Recovery System

Considering the drag coefficient of a parachute to be in the range of 0.8 to 1.2 (Westra, 2020) or less (0.75) if it's a parasheet (Culp, 2008).

Therefore, sizing the parachute:

$$mg = \frac{1}{2}\rho C_d A v^2$$

Where m stands for the mass of the rocket, g represents the gravitational pull, C_d is the drag coefficient, A is the cross-section of the parachute and v is the descent velocity.

Since the parachute will be a flat hexagon with an approximation for the drag coefficient (taking it to be similar to a round canopy) $C_d = 0.75$ (Brohm, 2009) following the instruction specified by the European space Agency (European Space Agency):

$$\begin{cases} A_{para} = \dfrac{2mg}{\rho C_d v^2} \\ A_{hex} = 3\dfrac{\sqrt{3}}{2}r^2 \end{cases} \rightarrow r = \frac{2}{3v}\sqrt{\frac{3mg}{\rho C_d}}$$

Considering a standard (and safe) touchdown speed of 4m/s (Brohm, 2009) at Madrid's average altitude (667m above sea level), thus allowing to calculate the air density (International Standard Atmosphere) upon touchdown:

$$\rho = \frac{p_o M}{R T_o}\left(1 - \frac{Lh}{T_o}\right)^{\frac{gM}{RL}-1}$$

Where p_o is the sea level standard atmospheric pressure ($p_o = 101325$ Pa), T_o is the sea level standard temperature ($T_o = 288.15$ K), M represents the molar mass of dry air ($M = 0.0289654$ kg/mol), R stands for the universal ideal gas constant ($R = 8.31447$J/mol/K), L is the temperature lapse rate ($L = 0.0065$ K/m), finally, h is the altitude.

$$\rho = \frac{101325 * 0.0289654}{8.31447 * 288.15}\left(1 - \frac{0.0065 * 667}{288.15}\right)^{\frac{g0.0289654}{8.31447*0.0065}-1} = 1.1484\frac{kg}{m^3}$$

Hence, the radius of the flat hexagonal parachute (considering the estimated mass of 30kg and a drag coefficient of 0.75):

$$r = \frac{2}{3*4}\sqrt{\frac{3*30g}{1.1484*0.75}} = 5.336m$$

The Shroud lines, according to literature ought to be 1.15 times the diameter, hence:

$$L = 1.15 * 5.336 * 2 = 7.0872m$$

To size the lines the force each will experience must be calculated.

Following the guidelines detailed in the literature

$$\begin{matrix} Forces & Moment \\ \begin{cases} \vec{\imath} \to \sum F = ma \\ \vec{\jmath} \to \sum F = ma \\ \vec{k} \to \sum F = ma \end{cases} & \begin{cases} \vec{\imath} \to \sum M = I\alpha \\ \vec{\jmath} \to \sum M = I\alpha \\ \vec{k} \to \sum M = I\alpha \end{cases} \end{matrix}$$

Due to symmetry, the forces in both $\vec{\imath}$ and $\vec{\jmath}$ will cancel out, just like all the moments due to the forces exerted by the lines. Hence the system will be simplified to:

$$\vec{k} \to F - 6F_{line}\sin(\theta) = 0$$

From a simple geometrical analysis, we can obtain the angle θ, 26.565º

Knowing the requirements specified in the SpacePort rules, where structural parts must be able to withstand a load of 30g upon the chute deployment and the assumed mass of 30kg, we obtain:

$$\vec{k} \to F_{line} = \frac{30mg}{6\sin(\theta)} \to F_{line} = 3290.374N$$

The bridle ought to be (Fruity Chutes Inc., 2019) between 203.2mm and 304.8mm (8-12 inches) and it must be able to withstand a force of 30g upon the parachute's deployment as per the guidelines:

$$\vec{k} \to F_{bridle} = 30mg \to F_{bridle} = 8829N$$

PIA-C-7020, Type II nylon fabric (54.25-118.67 g/m^2) parachute (Small Business Innovation Research, 2020):

$$m_{para} = 3\frac{\sqrt{3}}{2}5.336^2 * 118.67 = 878.584g$$

The biggest load the structure will support, is upon the parachute's deployment, and it will be a traction effort equal to 30mg (as per the literature's specifications), therefore:

$$\sigma = \frac{N}{A} = \frac{4N}{\pi d^2}$$

Designing for a maximum stress of 235MPa (and 2 out of the 3 being operational, whilst never reaching the elastic limit of the S275 bar):

$$\sigma = \frac{N}{A} = \frac{2N}{\pi d^2} \to d = 4.88mm$$

Therefore, the supporting beams will have a diameter of 5mm and will be made out of S275.

There will also need to be a central spine to accept the Arduino controllers, the altimeters and batteries (2 5V PP3 batteries) will be attached to the base with zip-ties

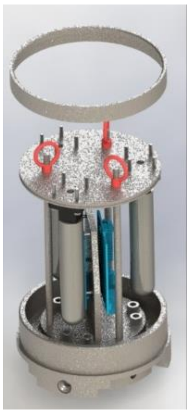

Figure 59 | Single Event Recovery internal system

Double Event Recovery System

The double event consists of 2 parachutes, as previously discussed, which implies only 1 other parachute ought to be sized, the drogue parachute, the smaller one which opens at the apogee.

Generally, they reduce the descent speed to 10m/s, alas:

$$r = \frac{2}{3v}\sqrt{\frac{3mg}{\rho C_d}} \rightarrow r = 0.61m$$

The Shroud lines, according to literature ought to be 1.15 times the diameter, hence:

$$L = 1.15 * 0.611 * 2 = 1.403m$$

And the force on each line:

$$\vec{k} \rightarrow F_{line} = \frac{30mg}{6\sin(\theta)} \rightarrow F_{line} = 3290.374N$$

Maintaining the same bridle for the drogue parachute.

The load is then transferred to the top of the phenolique tube quiche contains the main parachute for later deployment.

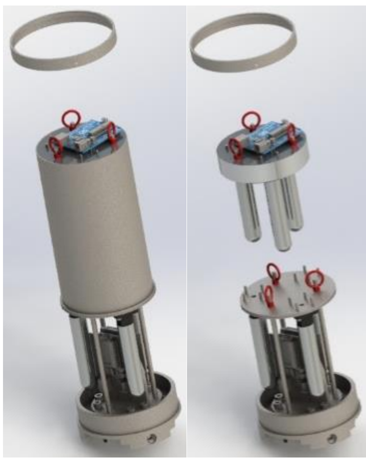

Figure 60 | Double Event Recovery system detail

System rundown and operation

The single event consists of a flat hexagonal parachute which is released by the CO_2 cartridges, which augment the pressure inside the tube and thus generate a traction force in the chute plate, which in turn creates the shear stress needed to break the shear pins and deploy the parachute. For redundancy pourposes, there are 3 pilars, of which 1 could fail and the structural integrity could still be preserved (single event, left; double event centre and right).

The aluminium ring on top of the tube (which has been hidden in the renders) acts as a protective layer to prevent the fibre from delaminating (due to the force exerted by the parachute upon deployment).

There is a redundancy in the electronics (2 controllers and 2 altimeters) as well as in the cardon dioxide cartridges (there are 3 in total, of which all can be released by either controller and only 2 are needed to deploy the parachute).

The electronic controller depends on the altimeter signals to release the CO_2, when they detect an increase in pressure over a few seconds (which means the rocket has already reached the apogee and is free falling), a signal is sent to the micro-controllers which in turn release the CO_2.

Traditionally the carbon dioxide cartridges are pierced by awl's which are themselves propelled by gunpowder, however, in an effort to reduce the amount of inflammatory elements inside the body of the rocket they have been swapped by solenoid valves controlled by the micro-controllers.

Similarly, the micro-controllers were assumed to be Arduino UNOs due to their size, so that if in the future they are swapped there is space to mount a different controller.

For the double event, the system is similar, duplicating the number of carbon dioxide cartridge and micro-controllers since 3 are integrated within the phonolique tube which contains the main parachute. The cartridges within the phenolique are released so they deploy the drogue parachute and reduce the decent speed to 10m/s and later the CO_2 at the base is released to deploy the main parachute.

To avoid the early deployment of the main parachute, the metallic structure on top of the phenolique tube is connected to an electromagnet-permanent magnet pair to transfer the load directly to the base of the module. Due to the presence of electronic components without a Faraday cage the magnetic force is weak and the electromagnet cannot revert polarities to deploy the main parachute.

Electromagnetic joint

The joint between the main recovery bay and the back up (which the level 3 rocket must possess) cannot be designed in the same manner as all the other joints, since, modelling it with merely shear-pins generates too much uncertainty on whether or not the rocket could break in half when deploying the main parachute or not, therefore, a new joint system needs to be created, one which is solid enough to transmit all the efforts within the rocket and can be controlled electronically to whether or not deploy the back-up parachute.

Therefore, the joint will be made up of a magnet-electromagnet pair so the electromagnet can turn it's fields around to either attract or repel and therefore, keep the rocket together or if need be, split it in half to deploy the back up.

According to the literature (Schober, 2018), the force between a magnet-electromagnet pair can be described as a function of their respective magnetic dipole moments and the distance by which they are separated:

$$\vec{\boldsymbol{F}}(\vec{r}, \overrightarrow{m_1}, \overrightarrow{m_2}) = \frac{3\mu_o}{4\pi|\vec{r}|^5}\left(\overrightarrow{m_1}(\overrightarrow{m_2}\cdot\vec{r}) + \overrightarrow{m_2}(\overrightarrow{m_1}\cdot\vec{r}) + \vec{r}(\overrightarrow{m_1}\cdot\overrightarrow{m_2}) - \frac{5\vec{r}}{|\vec{r}|^2}(\overrightarrow{m_1}\cdot\vec{r})(\overrightarrow{m_2}\cdot\vec{r})\right)$$

Which, if considered in cylindrical coordinates with the following vector definitions:

$$\vec{x} = \begin{bmatrix} r\ \overrightarrow{e_1} \\ \theta\ \overrightarrow{e_2} \\ z\ \overrightarrow{e_3} \end{bmatrix} \rightarrow \begin{cases} radial\ axis \\ angular\ axis \\ vertical\ axis \end{cases}$$

And the following vector definitions:

$$\vec{r} = \begin{bmatrix} 0 \\ 0 \\ z \end{bmatrix};\ \overrightarrow{m_1} = \begin{bmatrix} 0 \\ 0 \\ m_1 \end{bmatrix};\overrightarrow{m_2} = \begin{bmatrix} 0 \\ 0 \\ m_2 \end{bmatrix}$$

The formula can be reduced to:

$$\vec{\boldsymbol{F}}(\vec{r}, \overrightarrow{m_1}, \overrightarrow{m_2}) = \frac{-3\mu_o m_1 m_2}{2\pi z^4}\ \overrightarrow{e_3}$$

The electromagnet can be approximated to a magnetic dipole as per the formula (Elster LLC, 2020):

$$\overrightarrow{m_{elec}} = \pm inA\overrightarrow{e_3}$$

Where I stands for the current (in Amps) and A is the area, where the directions of the vector is defined by the right-hand rule and n is the number of times the cable is wound around the perimeter of the surface.

Since the parachute ought to come out of the bay if need be, a ferromagnetic core cannot be put in place and the electromagnet will need to have a ring-like shape and it will attach in the inner overhang of the coupler.

Allowing for a security coefficient of 1.5:

$$|m_1 m_2| = \frac{30mg\pi z^4}{\mu_o}$$

Assuming a maximum separation during flight of 10cm (between both magnetic surfaces):

$$|m_1 m_2| = 2.207KAm^2$$

Knowing the resistance of any cable to be:

$$R = \rho \frac{L}{\pi r^2}$$

Where R is the resistance in Ohms, ρ is the resistance coefficient of the material ($\Omega mm^2/m$) with copper's being 0.028 $\Omega mm^2/m$ and r is the cross-section's radius (considering a circular cross-section).

Furthermore, commercially available cables have a standardized maximum current (Sab Brockskes, 2020):

Cross section (mm^2)	Nominal voltage (KV)	Maximum current (A)
0.75	1	12
1		15
1.5		18
2.5		26
4		34

Table 25 | Cable characterization

To reduce the total current needed to generate the magnetic dipole the cable can be wound several times, alas, the electric circuit can be considered to be:

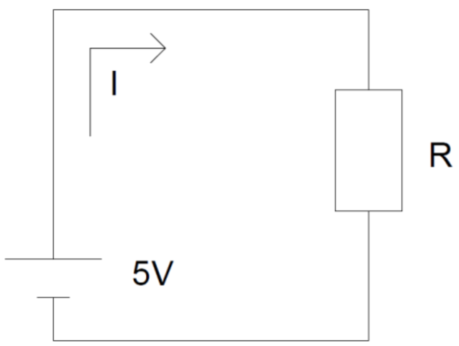

Figure 61 | Equivalent magnetic circuit

Where:

$$I = \frac{5}{0.028 \frac{2n45\pi}{r^2 \pi}}$$

Where r stands for the cross-section of the cable.

To size the current needed, firstly a cheap and strong magnet must be found, since the stronger the magnet, the weaker the induced magnetic field needs to be.

Avionics and Payload Module

Structural Design

Beam Design

Since in both the avionics module and the payload bay the tube walls cannot be load bearing (the avionics module has antenna's on the outside rather than a tube and the payload tube ought to be able to open to deploy the payload and thus the tube cannot be structural) the forces needed t be transmitted by other means.

Therefore, the load will be transmitted by 3 vertical beams to transmit the loads namely:

- Traction (upon the parachute's deployment, 30mg).
- Compression (during take-off and flight, 20mg as per the SpacePort America Cup rules but it will be sized for 30mg).

$$F_{tract} = -F_{comp} = 30mg = 30^3 * 9.81 = 8829N$$

- Torsion (during flight due to the inherent lift which might be produced when the rocket misaligns, $3mgR_{ext}$).

$$M_{tor} = 3mgR_{ext}t = 3 * 30 * 9.81 * 62.5 * 10^{-3} = 55.18125Nm$$

- Flexion moment considering the module to suffer a radial force in the upper-most coupler, with a magnitude of 30mg (the mass of the module, 5kg, applied at the end of the beam, 200mm).

$$M_{module} = 30mgL = 30 * 5 * 9.81 * 0.2 = 294.3Nm$$

According to the literature (Nussbaumer, 2015) the torsional constant of a section can be calculated as (for solid cross-sections):

$$K = \frac{2AT_v}{\oint_\Gamma \tau ds}$$

Where A is the area of the cross-section; T_v stands for the torsional moment; Γ is the perimetre of the cross section and τ represents the shear stress along the perimeter, therefore, when resolved for a rectangular beam there are 2 main solution to consider:

- Saint-Venant's solution (applicable when the cross-section resembles a square or when one of the dimensions is far greater than the other, with y and z the axis of the cross section):

$$K \cong \frac{A^4}{40(I_y + I_z)} \; if \frac{h}{t} \cong 1$$

- Membrane solution (obtained from the integral):

$$K = \begin{cases} K = \beta h t^3 \; if \frac{h}{t} \leq 10 \\ K \approx \frac{1}{3} h t^3 \; if \frac{h}{t} > 10 \end{cases}$$

With the β calculated as:

h/t	1	1.5	2	2.5	3	4	6	8	10
β	0.141	0.196	0.229	0.249	0.263	0.281	0.299	0.307	0.313

Table 26 | Torsional Constant Coefficient

Thus, from said formula, the maximum shear stress can also be computed as:

$$\tau_{max} = \frac{T_v t}{K}$$

And the angle can also be considered:

$$\theta = \frac{T_v * L}{KG}$$

Furthermore, to calculate the total torsion of the module, we need only consider:

$$K = \sum K_i$$

Therefore, the module will require a minimum of 3 beams, to fix the connectors relative to each other in space, therefore:

$$K_{module} = \begin{cases} K_{coupler} \\ 3K_{beams} \\ K_{coupler} \end{cases}$$

Since the requirements on the beams are so big, a section resembling a standardized ought to be employed, hence:

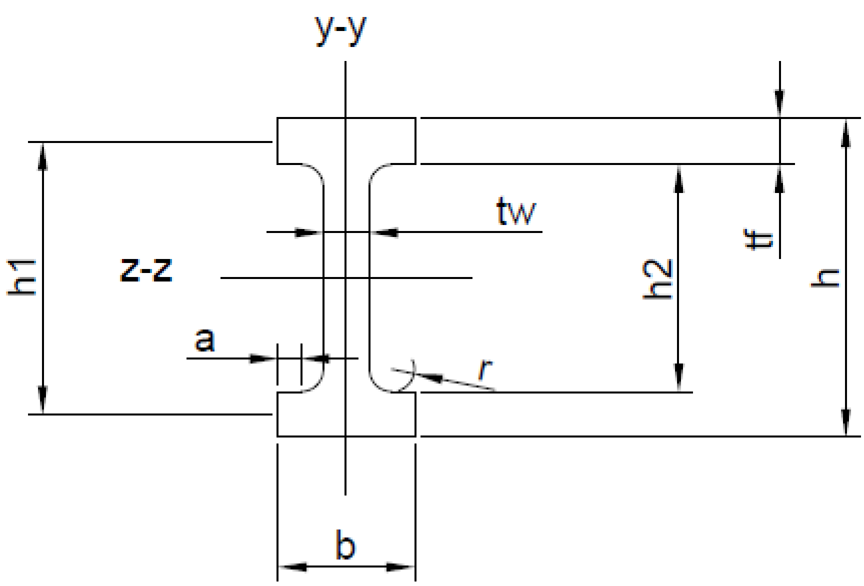

Figure 62 | beam cross-section

With their respective values (all in mm):

Name	Symbol	Equation	Value
Height	h	-	28
Width	b	-	12
Equivalent web length	h_1	$h_1 = h - t_f$	24
Web thickness	t_w	-	4
Web height	h_2	$h_2 = h - 2t_f$	20
Flange width	t_f	-	4
Radius	r	-	-
Usable flange	a	$a = \frac{b - t_w}{2} - r$	-

Table 27 | Beam cross-section dimensions

The radius will be determined by the minimum bending radius of the glass fibre (which depends on the manufacturer's specifications) and the usable flange as well, since it depends on the radius.

Composite materials have a proportionality limit upon which although the section still behaves in an elastic manner, the correlation stress-elongation varies, just like when in metallic structures a section under pre-existing constraints different parts of the cross-section will reach their elastic limit at different moments which varies the stress-elongation coefficient but the overall elastic limit is not affected by it.

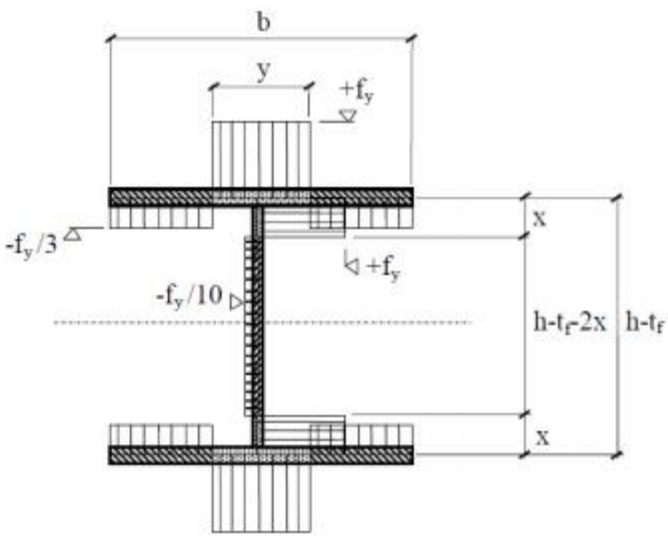

Figure 63| Beam cross-section with pre-constraints

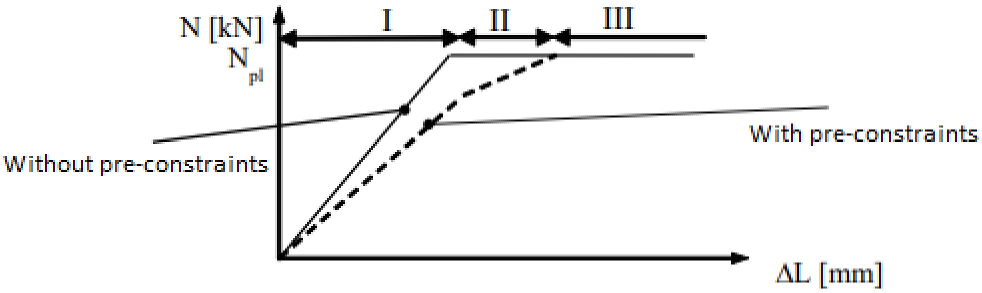

Figure 64|Elastic deformation of the beam with pre-constraints

Therefore from this analogy, a composite beam should be able to be sized following the norms for metallic structures with regards to stability (buckling, warping and torsional buckling) since these parameters are dependent on the cross-section rather than the properties of the material itself.

Since the cross-section has an area which cannot be determined (the added area due to the radius), to compensate the web, in all calculation will be considered to have a height h_1, as it is done with all standardized cross-sections

Since the module is set to have a beam height of 210mm (including the embedment of the beams and the couplers), the torsional constant can be calculated as:

$$K_{beam} = K_{web} + 2K_{flange} = \beta_w h_1 t_w^3 + 2\beta_f b t_f^3 \mid \begin{cases} \beta_w = \beta\left(\frac{24}{4}\right) = 0.299 \\ \beta_f = \beta\left(\frac{12}{4}\right) = 0.263 \end{cases}$$

$$K_{beam} = 863.232mm^4$$

However, as per the reference (Nussbaumer, 2015), double t profiles show to have consistently a torsional constant around 30% higher than the one calculated with the afore mentioned formula, thus (considering only an increase in 20% for security reasons):

$$K_{beam} = 1.2 * 863.232 = 1035.878mm^4$$

Considering, a minimum safety margin of 1.5 (if one of the beams were to fail the remaining 2 would keep the launch vehicle from breaking):

$$\tau_{max} = \frac{\frac{3}{2} mgR_{ext}\frac{h}{2}}{K_{beam}} \rightarrow \tau_{max} = \frac{\frac{3}{2} * 30 * 9.81 * 62.5 * 10^{-3} * \frac{28}{2} * 10^{-3}}{1035.878 * 10^{-12}}$$
$$= 372.890MPa$$

Which, when paired with the compression it will withstand upon the flight:

$$\sigma = \frac{N}{A} - \frac{M_z}{W_z} + \frac{M_y}{W_y}$$

Furthermore, to maximize the moment in the weak axis on both beams and thus the stress induced, the flexion ought to be applied at 120º from either beam (hence, applying the moment where the third beam should be), therefore:

For the first beam,

$$M_{beam} = \begin{cases} M_{z-beam} = \frac{M_{module}}{2}\sin(30º) \\ M_{y-beam} = -\frac{M_{module}}{2}\cos(30º) \end{cases}$$

Likewise, in the second beam we find:

$$M_{beam} = \begin{cases} M_{z-beam} = -\frac{M_{module}}{2}\cos(30º) \\ M_{y-beam} = -\frac{M_{module}}{2}\sin(30º) \end{cases}$$

Then,

$$A = t_w h_1 + 2bt_f \rightarrow A = 192mm^2$$

$$I_z = \frac{1}{12}h_1^3 t_w + 2\left(\frac{1}{12}bt_f^3 + b * t_f * \left(\frac{h_1}{2}\right)^2\right) \rightarrow I_z = 16618.667mm^4$$

$$I_y = \frac{1}{12}t_w^3 h_1 + \frac{1}{12}t_f b^3 \rightarrow I_y = 1258.667mm^4$$

$$W_z = \frac{I_z}{\frac{h}{2}} \rightarrow W_z = 1187.0476mm^3$$

$$W_y = \frac{I_y}{\frac{b}{2}} \rightarrow W_y = 209.778mm^3$$

$$S_z = \frac{A}{2}\frac{\frac{bt_f h_1}{2} + \frac{h_1}{2}t_w\frac{h_1}{4}}{bt_f + \frac{h_1}{2}t_w} \rightarrow S_z = 864mm^3$$

Due to symmetry, its safe to assume each beam will take half of the respective loads, thus, during flight, the efforts experienced will therefore be:

For the first beam:

$$\sigma = \frac{-\frac{30}{2} * 30 * 9.81}{192 * 10^{-6}} - \frac{\frac{294.3}{2}\sin(30º)}{1187.0476 * 10^{-9}} + \frac{-\frac{294.3}{2}\cos(30º)}{209.778 * 10^{-9}} = -692.452MPa$$

Therefore, applying Treska's principle:

$$\sigma_{eq} = \sqrt{\sigma^2 + 4\tau^2} \rightarrow \sigma_{eq} = 1017.683MPa$$

For the second beam:

$$\sigma = \frac{-\frac{30}{2} * 30 * 9.81}{24 * 4 * 10^{-6}} - \frac{-\frac{294.3}{2}\cos(30º)}{1187.0476 * 10^{-9}} + \frac{-\frac{294.3}{2}\sin(30º)}{209.778 * 10^{-9}} = -266.365MPa$$

If they are merged using Treska's principle (since it maximizes the stress caused by the torsion):

$$\sigma_{eq} = \sqrt{\sigma^2 + 4\tau^2} \rightarrow \sigma_{eq} = 791.921MPa$$

Therefore, the beams need to have an elastic limit of at least:

$$Re \geq 1.25 * 1017.683 = 1272.104MPa$$

Following the data provided for glass fibre (AZO Materials, 2020) it can be characterized as:

$$E = 72 - 85\ GPa$$
$$Re = 2750 - 2850\ MPa$$
$$\rho = 2550 - 2600\frac{kg}{m^3}$$
$$\nu = 0.21 - 0.23$$

Likewise, the epoxy resin (Simmons ltd, 2020):

$$E = 10.5\ GPa$$
$$Ru = 85\ MPa$$

$\rho = 1100 - 1400\ kg/m^3$ (NetComposites, 2020)

$$\nu = 0.3 - 0.35$$

Since the limit obtained from the literature is the rupture limit, the elastic limit will be considered at 80% of the rupture, alas: $Re = 0.8 * 85 = 68MPa$

The elastic limit of the composite material can be calculated employing the mixing principle:

$$Re_{comp} = V_m Re_m + V_f Re_f$$

Therefore (employing the lower end of the elastic limit for the glass fibre),

$$Re_{comp} = 1272.104 \rightarrow V_m = 0.551, V_f = 0.449$$

From which result the new Young's moduli can be calculated:

$$E_{lon} = V_m E_m + V_f E_f \rightarrow E_{lon} = 38.111GPa$$
$$E_{trans} = \frac{E_m E_f}{V_m E_f + V_f E_m} = 17.031GPa$$

Furthermore, the density can be calculated (considering the higher end of each interval):

$$\rho_c = V_m \rho_m + V_f \rho_f \rightarrow \rho_c = 1938.749\frac{kg}{m^3}$$

Since it's under such a variety of efforts the stability of the beams ought to be calculated (as per the norm SIA263, tableau 6).

Since the axial effort is less than 15% of the total maximum stress:

$$\frac{N}{A*Re} = 0.036 < 0.15$$

The torsional buckling length can be expressed as (taking Young's Modulus to be the transversal to minimize the required length to cause torsional buckling),

$$L_{cr} = 2.7i_z(1-0.5\Psi)\sqrt{\frac{E}{Re}}|i_z = \sqrt{\frac{I_z}{A}}, \Psi = \frac{M_{min}}{M_{max}}$$

In this case,

$$i_z = \frac{I_z}{A} \rightarrow i_z = 9.304mm$$

$$\Psi = \frac{M_{min}}{M_{max}} = \frac{0}{\frac{M_{flex}}{2}} = 0$$

Therefore,

$$L_{cr} = 2.7*9.3*(1-0.5*0)*\sqrt{\frac{17.031*10^3}{1272.104}} = 92.602mm$$

Therefore, the torsional buckling may happen, since:

$$L_D = 200m \geq 101.862 = 1.1L_{cr}$$

Therefore, the moment at which the torsional buckling occurs can be calculated as (SIA263 section 4.5.2):

$$M_D = \frac{\chi_D W Re}{\gamma}$$

Where,

$$\chi_D = \frac{1}{\phi_D + \sqrt{\phi_D^2 - \overline{\lambda_D}^2}}$$

$$\phi_D = 0.5\left[1 + \alpha_D\left(\overline{\lambda_D} - 0.4\right) + \overline{\lambda_D}^2\right]|\alpha_D = 0.49\ since\ its\ a\ laminated\ profile$$

$$\overline{\lambda_D} = \sqrt{\frac{W}{W_{el}}}$$

However, since it's a set of elastic calculations $W = W_{el}$, therefore,

$$\overline{\lambda_D} = 1$$

$$\phi_D = 0.5[1 + 0.49(1-0.4) + 1] = 1.147$$

$$\chi_D = \frac{1}{1.147 + \sqrt{1.147^2 - 1}} = 0.5852$$

Alas,

$$M_D = \frac{0.5856 * 1187.0476 * 10^{-9} * 1272.104 * 10^{6}}{1.25} = 707.4273Nm$$

Since,

$$M_D = 707.4273Nm \geq \frac{294.3}{2}Nm = \frac{M_{module}}{2} = M_{beam}$$

The beams will not suffer torsional buckling, for security reason, however, 3 stiffeners will be implemented at 1/4 of the beam length each, therefore, the critical torsional buckling length ought to be recalculated for all 4 new segments:

Since the axial effort did not change and its less than 15% of the total maximum stress:

$$\frac{N}{A * Re} = 0.036 < 0.15$$

The torsional buckling length can be expressed as,

$$L_{cr} = 2.7i_z(1 - 0.5\Psi)\sqrt{\frac{E}{Re}} | i_z = \sqrt{\frac{I_z}{A}}, \Psi = \frac{M_{min}}{M_{max}}$$

In this case,

$$i_z = \frac{I_z}{A} \rightarrow i_z = 9.304mm$$

$$\Psi = \frac{M_{min}}{M_{max}} = \begin{cases} segment\ 1 \rightarrow \Psi = \dfrac{0}{\frac{30mgL}{2} * \frac{1}{4}} = 0 \\ segment\ 2 \rightarrow \Psi = \dfrac{\frac{30mgL}{2} * \frac{1}{4}}{\frac{30mgL}{2} * \frac{2}{4}} = \dfrac{1}{2} \\ segment\ 3 \rightarrow \Psi = \dfrac{\frac{30mgL}{2} * \frac{2}{4}}{\frac{30mgL}{2} * \frac{3}{4}} = \dfrac{2}{3} \\ segment\ 3 \rightarrow 4 = \dfrac{\frac{30mgL}{2} * \frac{3}{4}}{\frac{30mgL}{2}} = \dfrac{3}{4} \end{cases}$$

Therefore,

$$L_{cr} = 2.7 * 9.304(1 - 0.5\Psi)\sqrt{\frac{17.031 * 10^3}{1272.104}} \rightarrow \begin{cases} L_{cr1} = 91.916mm \geq \frac{L_D}{1.1} = \frac{50}{1.1}mm \\ L_{cr2} = 68.937mm \geq \frac{L_D}{1.1} = \frac{50}{1.1}mm \\ L_{cr3} = 61.278mm \geq \frac{L_D}{1.1} = \frac{50}{1.1}mm \\ L_{cr4} = 57.448mm \geq \frac{L_D}{1.1} = \frac{50}{1.1}mm \end{cases}$$

With regards to warping of the cross-section, firstly Poisson's coefficient needs to be calculated (considering the maximum values to later reduce the effort at which the section begins warping):

$$\nu = V_m \nu_m + V_f \nu_f \rightarrow \nu = 0.2596$$

Following SIA 263 section 4.5.4, the critical shear stress at which warping starts, can be computed as:

$$\tau_{cr} = k_\tau \frac{\pi^2 E}{12(1 - \nu^2)}\left(\frac{t}{b}\right)^2$$

With the coefficient k_τ being describes as:

$$k_\tau = \begin{cases} 4 + \frac{5.34}{\alpha^2} \ if \ \alpha \leq 1 \mid \alpha = \frac{b}{h} \\ 5.34 + \frac{4}{\alpha^2} \ if \ \alpha > 1 \mid \alpha = \frac{b}{h} \end{cases}$$

Therefore, the critical shear stress can be calculated as:

$$\alpha = \frac{b}{h} = \frac{12}{28} \rightarrow k_\tau = 33.073$$

$$\tau_{cr} = 33.073 \frac{\pi^2 17.031 * 10^9}{12(1 - 0.2596^2)}\left(\frac{4}{12}\right)^2 = 55.194 * 10^3 MPa$$

Which, if Colignon's theorem is applied:

$$\tau = \frac{Q_y S_z}{b(y) I_z} \rightarrow Q_y = \tau * \frac{b(y) I_z}{S_z}$$

Therefore, the load at which the section wraps is:

$$Q_y = 55.194 * 10^9 * \frac{4 * 16618.667 * 10^{-12}}{864 * 10^{-9}} >> 30mg = 8829N$$

Finally, the buckling load is described as:

$$P_{crit} = \frac{\pi^2 EI}{L_k^2 A}$$

For both axis the links to the couplers can be considered a double embedment, thus, $L_k = 0.5L$, which yields:

$$P_{crit_y} = \frac{\pi^2 E I_y}{L_k^2 A} = \frac{\pi^2 17.031 * 10^9 * 1258.667 * 10^{-12}}{(0.5 * 0.2)^2 * 192 * 10^{-6}} >> 30mg = 8829N$$

$$P_{crit_z} = \frac{\pi^2 E I_z}{L_k^2 A} = \frac{\pi^2 17.031 * 10^9 * 16618.667 * 10^{-12}}{(0.5 * 0.2)^2 * 192 * 10^{-6}} >> 30mg = 8829N$$

Undergoing simulations for the most critical case:

- Normal effort (45000N)
- Torsional moment (0.3mgRext)
- Flexing moment on both axe ($M_z = \frac{294.3}{2}\sin(30)$, $M_y = \frac{294.3}{2}\cos(30º)$)

The beam was considered to be doubly embedded (either end-surface was considered to have a deformation of 0 and an angle of 0) since ti maximizes the deformations across the beam

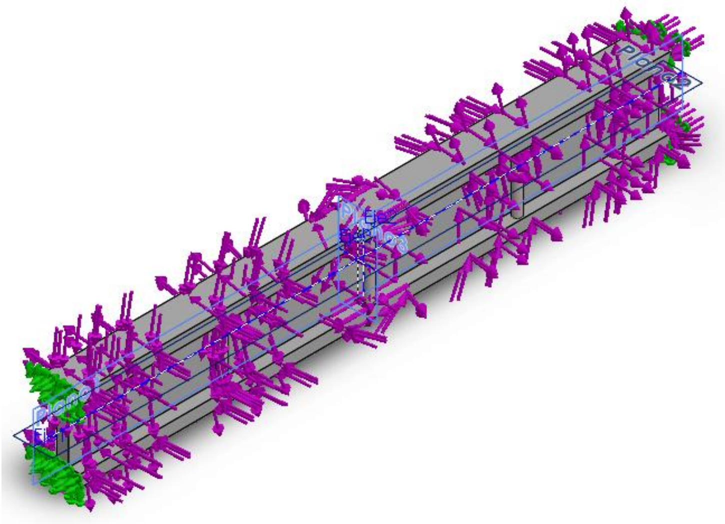

Figure 65 | Beam simulation load distribution

The normal force was applied on the top-most cross section with a total value of 45000N (evenly distributed):

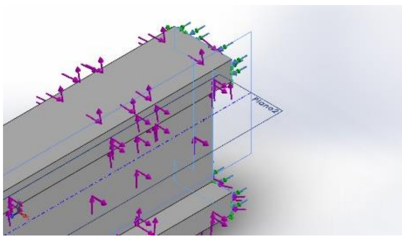

Figure 66 | Normal force beam simulation

It was also paired with a torsional effort along the x axis of the beam and it was considered to affect the entirety of the beam except for the end faces ($M_x = 3mgR_{ext} = 0.386269$ Nm):

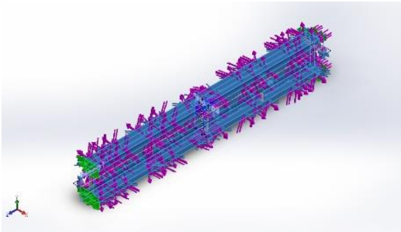

Figure 67 | Torsional moment beam simulation

Another 2 efforts were applied, one on each axis and were considered to apply on the entirety of the beam except the end faces ($M_y = \frac{294.3}{2}\cos(30)\,, M_z = \frac{294.3}{2}\sin(30)$):

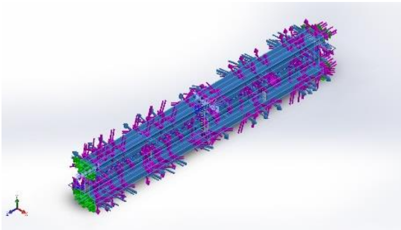

Figure 68 | Flexural moment along the y axis beam simulation

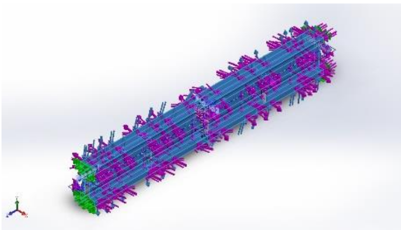

Figure 69 | Flexural moment along the z axis beam simulation

The intermediate supports of the beam were considered to not be affected by the moments nor the normal effort since they behave as supports for said moments.

The mesh generated for the simulations consisted of 16814 nodes with 9221 cubes with a maximum aspect ratio of 6.27603 (96.5% had an aspect ratio greater than 3 but none above 10) and an average size of 3.30453mm and 4 Jacobian points:

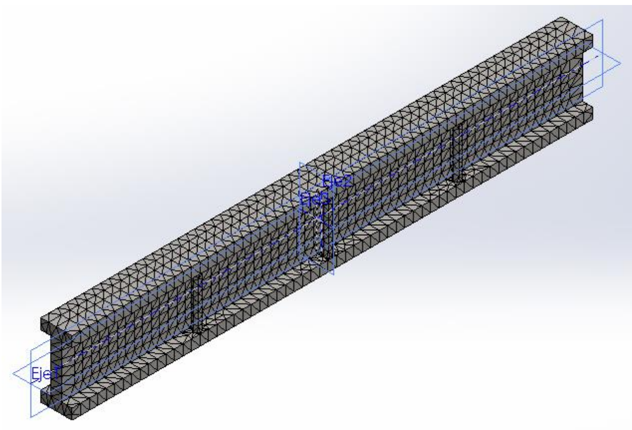

Figure 70 | Mesh Beam Simulation

The maximum stress found was at 1006MPa (10% less than the calculated value), hence validating the results. Said maximum stress is located at the end faces, which would never suffer said stress during their work life since to augment the deviations in the simulations the embedment length has been reduced to merely the end face.

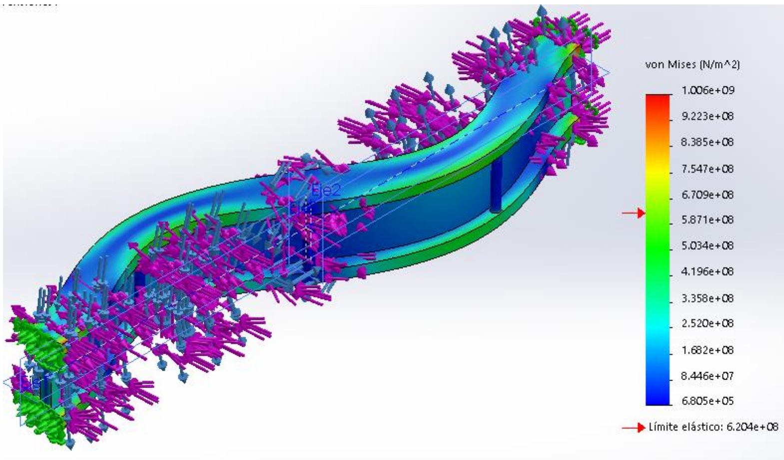

Figure 71 | Stress distribution beam simulation

Likewise, the maximum unitary deformations were found to be in the end faces with a maximum value of 0.0032.

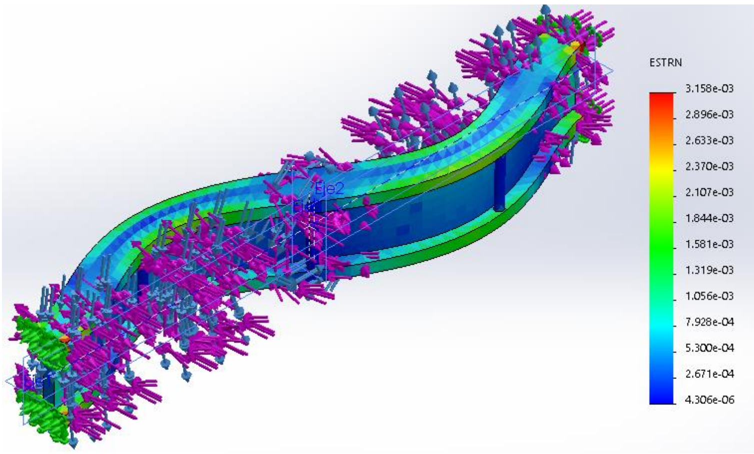

Figure 72| Unitary deformations beam simulation

Coupler modification

Since the load will no longer be transmitted to the tubes, the gluing perimeter can be swapped for a series of extrusions which guarantee an embedment of the beams, whilst also facilitating enough gluing surface for the beams to attach to:

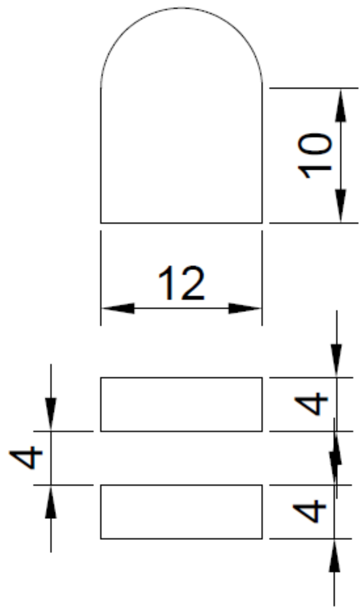

Figure 73 | Gluing surface AV/PL module

Since it's only an embedment, the solicitation can be considered to be merely traction (compression is directly transmitted by contact), therefore, considering a commertially available glue (shear stress 15MPa), with only 2 beams operational:

$$F_{max} = 2 * 15 * 2 * (12 * 10 + \pi * 18 + 2 * 4 * 10) = 15392.92N > 30mg$$

Structure Assembly
Having 2 modified coupleurs facing each other connected by 3 beams the resulting assembly is:

Figure 74 | AV/PL module structure

Payload bay mechanism

The payload will be held in place by a slider which will in turn be guided by 3 pairs of worm gears-gear.

Accepting the similarity of a tooth with a cantilever beam with a force applied on it's end, Navier's equation can be expressed as:

$$\sigma = \frac{M}{I_z} y \rightarrow \sigma = \frac{2.25m * F}{\frac{\Psi m}{12}\left(\frac{\pi m}{2}\right)^3} * \frac{\pi m}{4} | b = \Psi m, e = \frac{\pi m}{2}, h = 2.25m$$

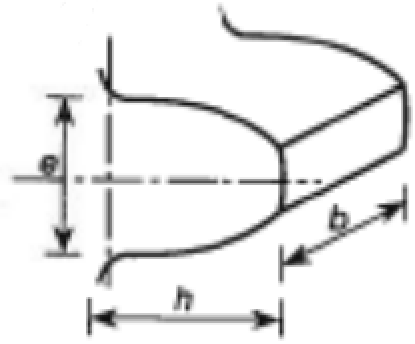

Figure 75 | Gear Teeth detail

Thus, for each module and Ψ (usually around 3 for worm gears) we can calculate the stress on the tooth, considering a force of 30g with a mass of 0.5Kg (in MPa):

		Module (mm)			
		1	2	3	4
Phi	1	805.1082573	201.2770643	89.456473	50.3192661
	2	402.5541287	100.6385322	44.7282365	25.159633
	3	268.3694191	67.09235478	29.8188243	16.7730887
	4	201.2770643	50.31926608	22.3641183	12.5798165
	5	161.0216515	40.25541287	17.8912946	10.0638532
	6	134.1847096	33.54617739	14.9094122	8.38654435

Table 28 | Teeth stress

Assuming the gear will be made of S275steel ($Rp_{0.2\%}$=275MPa>268.3694MPa), the gear will have m_n=1, $\Psi = 3$ and thus b=3mm.

Considering the pair worm-wheel equivalent to that of a helicoidal gear the minimum number of teeth can be computed as ($\beta = 30º, \alpha = 20º$):

$$Z_{min} = \frac{2}{(\sin \alpha)^2} (\cos \beta)^3 \rightarrow 11.1 \rightarrow 12 \; since \; Z \in N$$

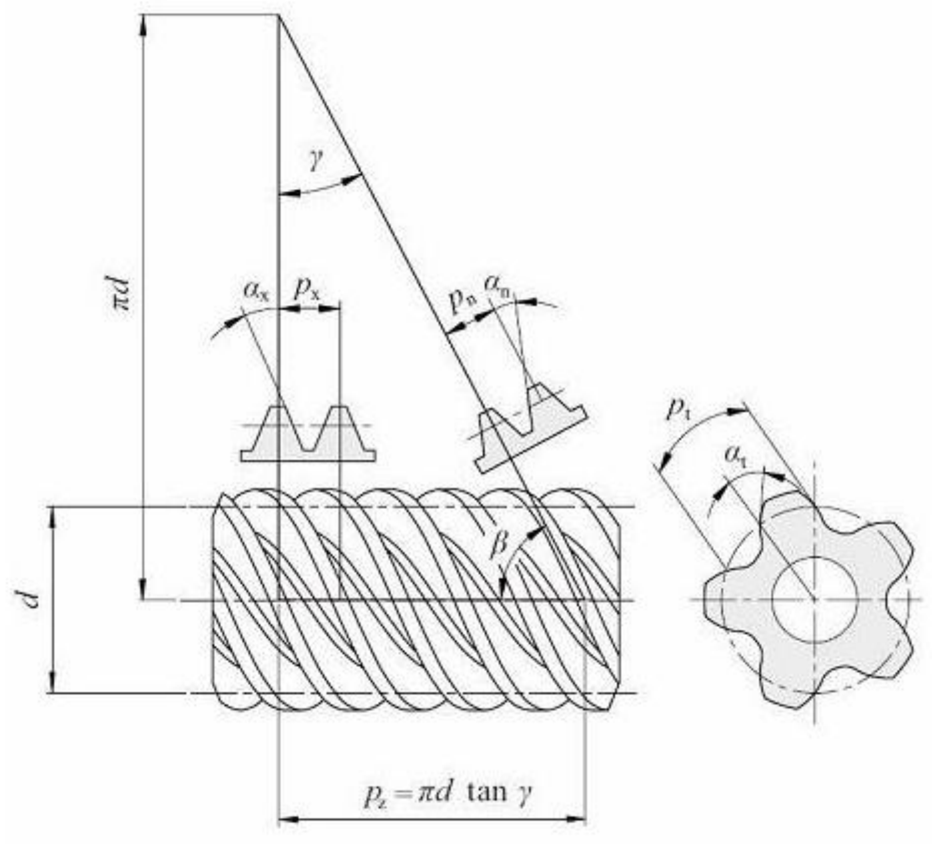

Figure 76 | Cylindrical Worm Right Hand Helix (KHK Gears, s.f.)

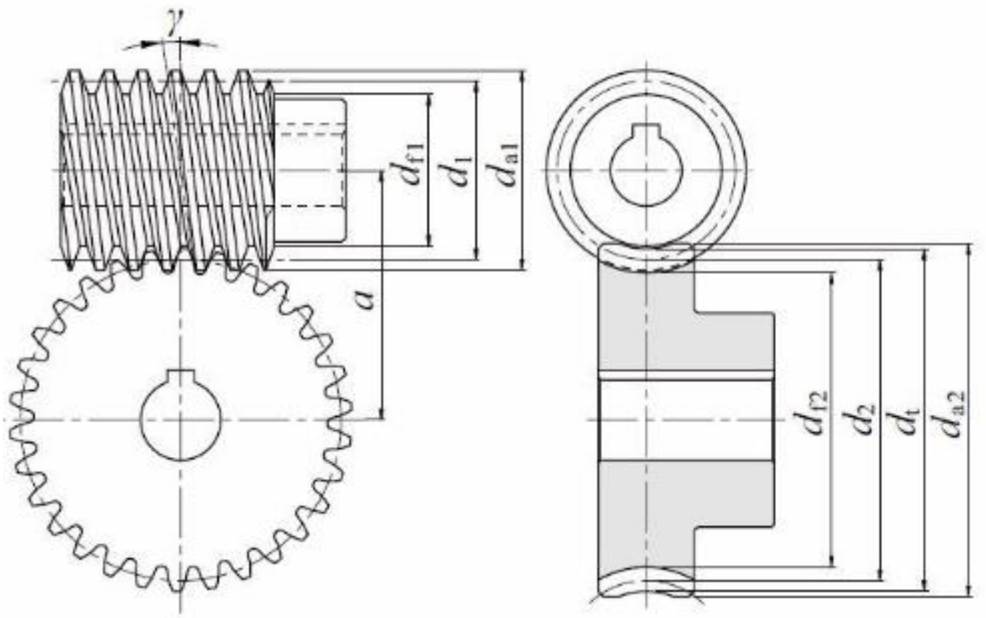

Figure 77 | Cylindrical Worm Gear pair (KHK Gears, s.f.)

Item	Symbol	Formula	Worm (1)	Wheel (2)
Normal module (mm)	m_n	Set Value	1	
Nomall pressure angle (º)	α_n		20	
Number of threads/teeth	Z		1	12
Primitive Diameter (mm)	d_1		8	-
Normal Profile Shift Coefficient	X_{n2}		-	-0.1414
Reference Cylinder lead angle (º)	Y	$\arcsin\left(\frac{Z_1 m_n}{cos\gamma}\right)$	7.1808	
Primitive Diameter Wheel (mm)	d_2	$\frac{Z_2 m_n}{cos\gamma}$	-	24
Centre distance (mm)	a	$\frac{d_1 + d_2}{2} + X_{n2} m_n$	15.8586	
Addendum (mm)	h_{a1} h_{a2}	m_n $(1 + X_{n2}) m_n$	1	0.8586
Tooth depth (mm)	h	$2.25 m_n$	2.25	
Tip diameter (mm)	d_{a1} d_{a2}	$d1 + 2h_{a1}$ $d_2 + 2h_{a1} + m_n$	10	27
Throat diameter (mm)	d_t	$d_2 + 2h_{a2}$	-	25.7172
Throat surface radius (mm)	r_i	$\frac{d_1}{2} - h_{a1}$	-	3
Root diameter (mm)	d_{f1} d_{f2}	$d_{a1} - 2h$ $d_t - 2h$	5.5	21.2172

Table 29 | Worm gear-Wheel design

Thus, now b can be accurately calculated employing simple algebra:

$$\begin{matrix} x^2 + y^2 = r^2 \\ x = a - \frac{d_{ha2}}{2} \end{matrix} \rightarrow \begin{matrix} x^2 + y^2 = 4^2 \\ x = 15.8586 - \frac{27}{2} \end{matrix} \rightarrow \begin{matrix} x = 2.3586 \\ y = 3.2306 \end{matrix}$$

From there the angle of said intersection points can be derived:

$$\theta = \arctan\left(\frac{y}{x}\right) \rightarrow \theta = 53.8675º$$

Finally, b can be calculated as the length of the arch of a circumference:

$$b = \frac{2\pi\theta r}{360} \rightarrow b = \frac{2\pi * 53.8675 * 4}{360} = 3.76mm > b_{estimated} \rightarrow OK$$

With a straight gear design:

The maximum distance between the centres will be 40mm (the sum of both primitive diameters), and the maximum diameter of the pinions will be 10mm (the sum of the pinions primitive dimeter and twice the addendum), thus the geometrical requirements can be expressed as (in mm):

$$\begin{cases} d_1 + d_2 = 40 \rightarrow m(Z_1 + Z_2) = 40 \\ d_2 + 2h_a \leq 10 \rightarrow Z_1 m + 2m \leq 10 \end{cases}$$

The required minimal module can be calculated as:

$$m \geq 2.22 \sqrt[3]{\frac{M_1}{Z_1 \Psi \sigma_{adm}} Y}$$

Whilst the Hertzian pressure is expressed as:

$$m \geq \sqrt[3]{\frac{8 * 0.418^2 M_1 E}{\sigma_{adm}^2 Z_1^2 \Psi \sin(2\alpha)} \left(\frac{1+i}{i}\right)}$$

Hence, the number of teeth must first be calculated since the transmission coefficient can be expressed as:

$$i = \frac{Z_1}{Z_2}$$

The minimum number of teeth to avoid interference can be expressed as:

$$\sqrt{Z_1^2 + 4\frac{1+Z_1}{\sin^2(\alpha)}} - Z_1 = Z_{2min} \leq Z_2 \leq Z_{2max} = \frac{\left(\frac{Z_1}{2}\sin(\alpha)\right)^2 - 1}{1 - \frac{Z_1 \sin^2(\alpha)}{2}}$$

With a moment equal a force of 30g for a mass of 0.5Kg applied at 4mm from the centre (primitive radius of the worm gear), fixing Ψ to minimize the gear thickness the following table can be developed:

module	Z_1 max	Z_1	Y	m	Check	Z_2 min	Z_2 max	Z_2 geom	Z_2	i	Hertz
0.25	38	38	0.565	0.282	Not OK	-	-	-	-	-	-
0.5	18	18	0.458	0.404	OK	0.900	9.358	9	9	2	1.031
1	8	8	0.355	0.486	OK	1.521	0.004	-	-	-	-
2	3	too little	-	-	-	-	-	-	-	-	-

Table 30 | Wheel check

Since the Hertzian pressure is too high, the gears won't touch but rather have a chain linking them, which serves also to respect the maximum number of teeth for the main gear (since if they touched it would have needed 62 teeth to respect the geometrical constraints, way too many).

Thus, the motor wheel will have 9 teeth with a module of 0.5 whilst the wheels attached to the worm gears.

The worm gears themselves will be driven by a trapezoidal belt.

The friction coefficient of the trapezoidal belt can be obtained solving (where N stands for the equivalent force of the contact pressure):

$$\begin{cases} F = 2Nsin\left(\frac{\beta}{2}\right) \\ F_r = 2N\mu \end{cases} \rightarrow \mu' = \frac{\mu}{sin\left(\frac{\beta}{2}\right)}$$

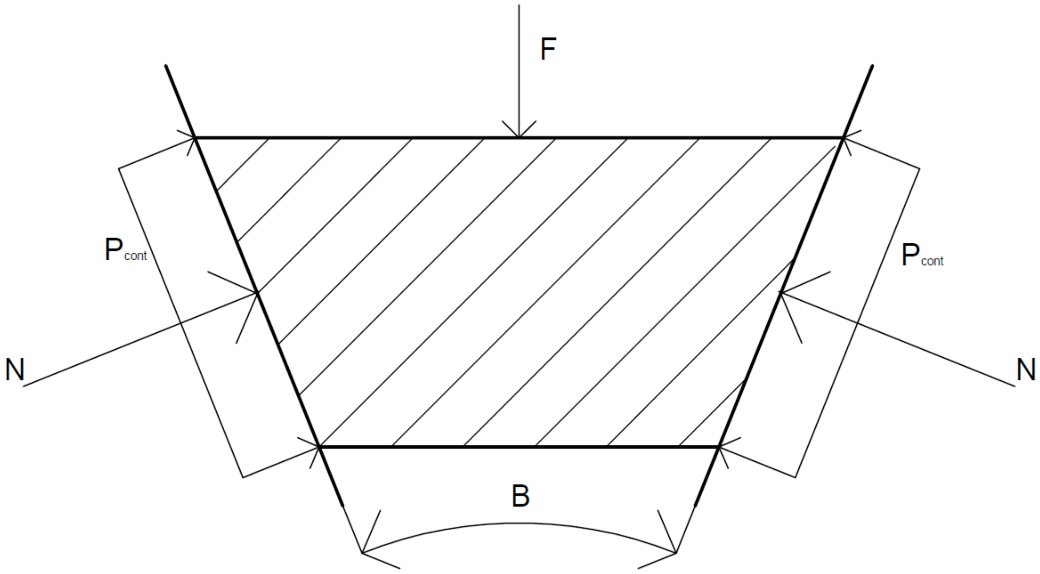

Figure 78 | Trapezoidal belt cross-section

The angle is not standardized; however, it tends to range from 34º to 40º, alas, the angle selected for this application (to maximize the equivalent friction coefficient):

$$\beta = 40º \rightarrow \mu' = 3.4\mu$$

Furthermore, the total length of the belt can also be calculated as:

$$L = (\pi - \delta)\frac{d_1}{2} + (\pi + \delta)\frac{d_2}{2} + 2a\sqrt{1 - \left(\frac{d_2 - d_1}{2a}\right)^2}$$

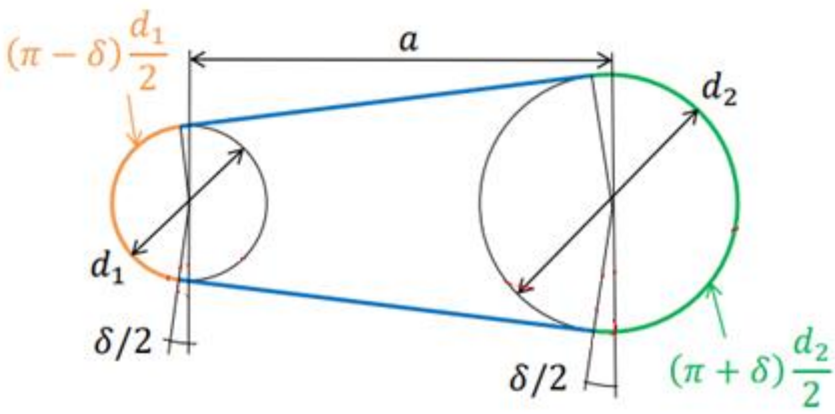

Figure 79 | Belt length scheme (Soubielle, Transmissions à courroies III, 2020)

The normal force which originates from the tension of the belt and the belt itself pressing against the pulley.

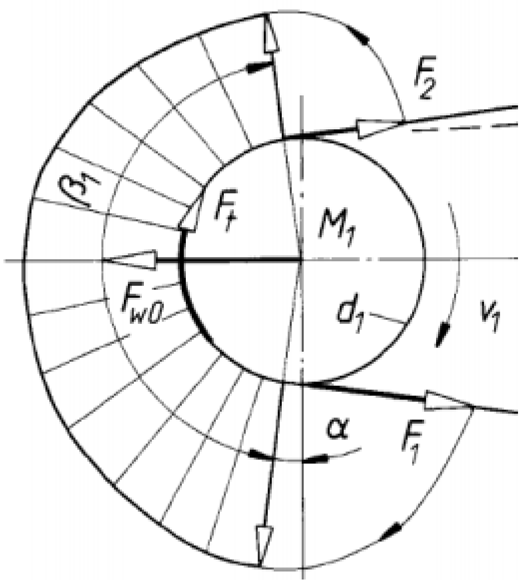

Figure 80 | Belt-Puller induced stress (Soubielle, Transmission à courroies I, 2020)

Where β represents the angle of contact between the pulley and the belt.

The useful traction force can be obtained from a dynamic equilibrium between the inertial force, Fw_o, and the tension in both sides of the belt (F_1, F_2):

$$\begin{cases} \sum \vec{F} \rightarrow \overrightarrow{F_{wo}} = -(\overrightarrow{F_1} + \overrightarrow{F_2}) \\ \sum \vec{M} \rightarrow M_1 = \dfrac{d_1 + e}{2}(F_1 - F_2) \end{cases}$$

Where e is the thickness of the belt.

The useful traction force is:

$$F_U = F_1 - F_2 = \frac{2M_i}{d_i + e}$$

And the power can be calculated as:

$$P_i = w_i M_i = F_u \frac{d_i + e}{2} w_1$$

Considering the equations for the deformation of a cable (longitudinally and perpendicularly):

$$\varepsilon_l = \frac{\Delta L}{L_o} \rightarrow L = L_o(1 + \varepsilon_l)$$

$$\varepsilon_t = -\nu\varepsilon_l \rightarrow A = A_o(1 - \nu\varepsilon_l)^2$$

Which, when paired with the conservation of mass, yields:

$$\rho = \frac{\rho_o}{(1 + \varepsilon_l)(1 - \nu\varepsilon_l)^2}$$

Therefore,

$$\frac{V_1}{1 + \varepsilon_1} = \frac{V_2}{1 + \varepsilon_2}$$

In turn, it generates 2 sections upon contact with the pulley one where there is a perfect contact between the pulley and the belt and another where there is an elastic gliding in between the 2.

The input pulley shares its speed with the leading section of the belt whilst the trailing part has the same speed as the output pulley.

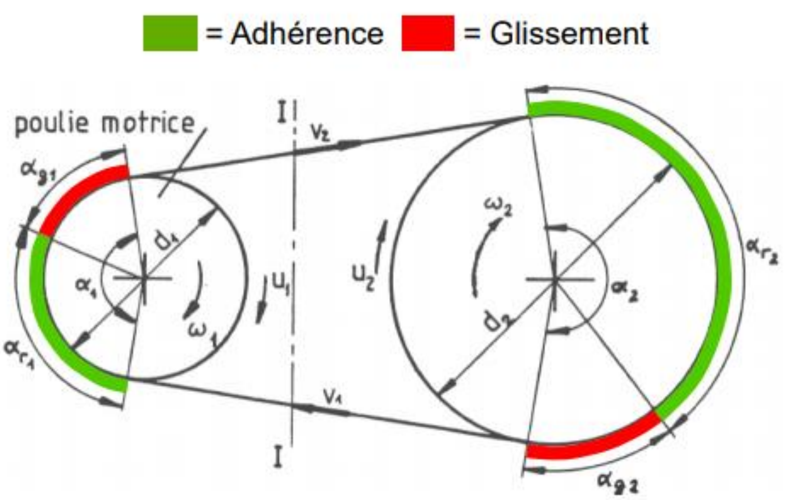

Figure 81 | Sections of a belt-assembly (Soubielle, Transmission à courroies I, 2020)

Since they share speed, it can be calculated as:

$$V_i = \frac{d_i + e}{d_i} w_1$$

If the pressure the belt exerts on the pulley is approximated as a uniform distribution along the entirety of the arc the initial tension can be calculated (Soubielle, Transmission à courroies I, 2020):

$$\overrightarrow{N_c} + \overrightarrow{T_{1o}} + \overrightarrow{T_{2o}} = \vec{0}$$

$$\int_{-\frac{\alpha_1}{2}}^{\frac{\alpha_1}{2}} br_1 p cos(\theta) d\theta + (T_{1o} + T_{2o}) \sin\left(\frac{\alpha_1}{2}\right) = 0 \rightarrow T_o = br_1 p$$

Where b is the contact length between the pulley and the belt with a pressure p.

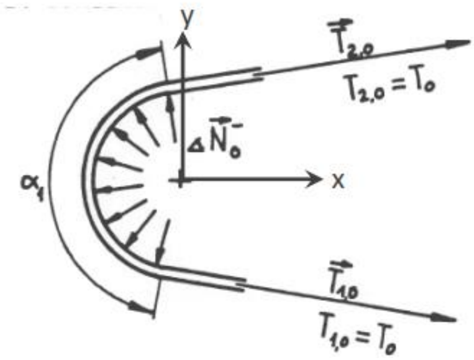

Figure 82 | Initial tension schema (Soubielle, Transmission à courroies I, 2020)

Therefore, the transmitted tension in the belt is:

$$\begin{matrix} T_1 = T_o - \Delta T \\ T_2 = T_o + \Delta T \end{matrix} \mid \Delta T = \frac{F_U}{2}$$

Which in turn yields Poncelet's equation:

$$T_o = T_1 + T_2$$

The power and moment transferred is thus:

$$M_1 = (T_1 - T_2)\frac{d_1 + e}{2}$$

$$P_1 = (T_1 - T_2)\frac{d_1 + e}{2} w_1$$

The reduced friction tension of the belt can also be calculated as:

$$\int_{-\frac{\alpha_1}{2}}^{\frac{\alpha_1}{2}} br_1(p - p_c)\cos\theta \, d\theta = T_{f1} \sin\frac{\alpha_1}{2} - T_{f2} \sin\frac{\alpha_1}{2} \; |p_c = \frac{\rho A_o r W^2}{b}$$

Where T_{f1} and T_{f2} represent the forces transferred by the belt and p_c stands for the centrifugal pressure (a representation of the reduction of the contact pressure between the belt and the pulley).

This results in (by analogy):

$$2(T_o - T_c)\sin\frac{\alpha_1}{2} = \left(T_{f1} + T_{f2}\right)\sin\frac{\alpha_1}{2} \rightarrow\ T_{f1} = T_{f2} = T_o - T_c \mid T_c = \rho A_o V^2$$

Therefore, the centrifugal tension reduces the forces transferred by the belt-pulley system.

The effective tensions, when plotted in a differential section yield:

$$\overrightarrow{e_r} \rightarrow dN - \left(T_f(\theta) + T_f(\theta + d\theta)\right)\sin\left(\frac{d\theta}{2}\right) = 0$$
$$\overrightarrow{e_\theta} \rightarrow \mu dN + \left(T_f(\theta + d\theta) - T_f(\theta)\right)\cos\left(\frac{d\theta}{2}\right) = 0$$

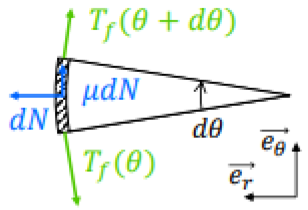

Figure 83 | Differential Section-Belt (Soubielle, Transmission à courroies I, 2020)

Alas Euler's equation is obtained,

$$T_{f1} = T_{f2}e^{\mu\alpha_{g1}}$$
$$T_1 - T_c = (T_2 - T_c)e^{\mu\alpha_{g1}}$$

And,

$$T_1 - T_2 = T_{f1} - T_{f2} = F_U$$

With a transmission coefficient of (with g as the gliding coefficient):

$$i = \frac{w_1}{w_2} = \frac{d_{p2}}{d_{P1}}\frac{1}{1-g} \mid g = \frac{V_1 - V_2}{V_1} \cong \frac{F_U}{A_o E} \cong \frac{T_1}{A_1 E} - \frac{T_2}{A_2 E}$$

The condition for the belt to glide on the pulleys is therefore:

$$\alpha_1 + \alpha_2 = 2\pi \mid \alpha_i = \alpha_{gi}$$

Alas, the maximum values are:

$$\begin{matrix} T_{f1-MAX} = \frac{e^{\alpha_1\mu}}{e^{\alpha_1\mu} - 1}F_{U-MAX} \\ T_{f2-min} = \frac{1}{e^{\alpha_1\mu} - 1}F_{U-MAX} \end{matrix} \rightarrow \begin{matrix} T_{1-MAX} = T_C + \frac{e^{\alpha_1\mu}}{e^{\alpha_1\mu} - 1}F_{U-MAX} \\ T_{2-min} = T_C + \frac{1}{e^{\alpha_1\mu} - 1}F_{U-MAX} \end{matrix}$$

Which, results in the diagram:

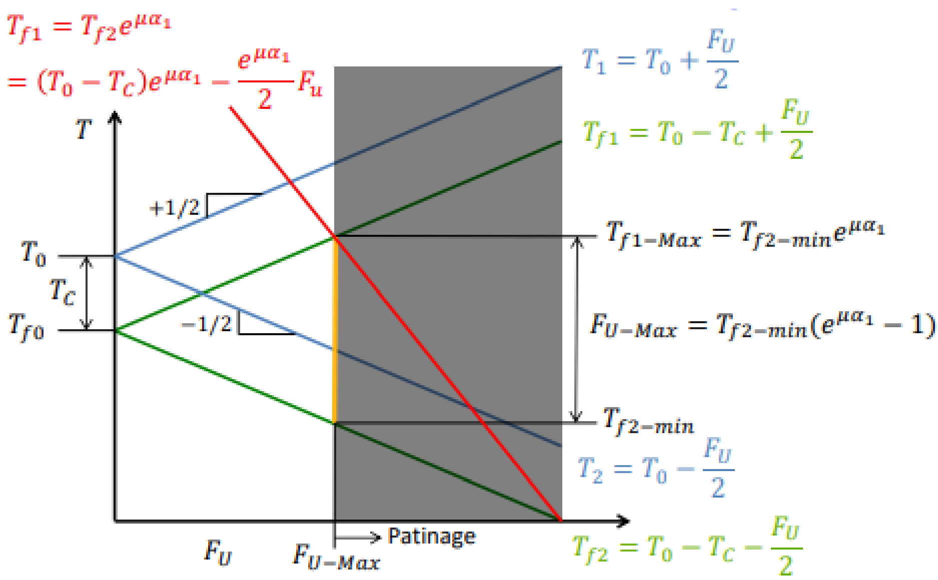

Figure 84 | Operation limits Belt (Soubielle, Transmission à courroies I, 2020)

The belt ought to withstand 3 different types of internal stresses (centrifugal, friction and incurvation):

$$\sigma_c = \frac{T_C}{A_o}$$

$$\sigma_{adm} \geq \sigma_c + \sigma_F + \sigma_{In} \rightarrow \sigma_F = \frac{e^{\alpha_1 \mu}}{e^{\alpha_1 \mu} - 1}\frac{F_{U-MAX}}{A_o}$$

$$\sigma_{In} = E\frac{e}{d_1} = \frac{M_F}{I}\frac{e}{2}$$

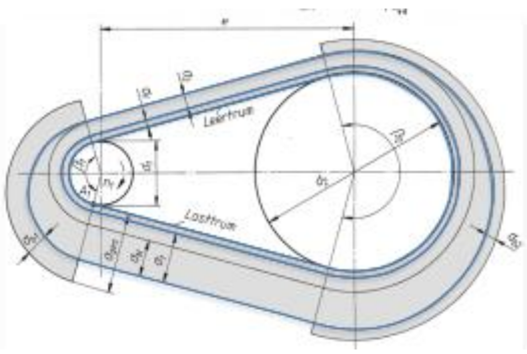

Figure 85 | Stress distribution in the belt (Soubielle, Transmission par courroies, 2020)

Therefore, re-writing the equation:

$$F_{U-MAX} = (\sigma_{adm} - \sigma_{In} - \rho V^2)A_o\frac{e^{\alpha_1 \mu} - 1}{e^{\alpha_1 \mu}}$$

Where the increase in speed greatly reduces the force which can be transmitted by the belt, alas, the maximum speed is.

$$V_{MAX} = \sqrt{\frac{\sigma_{adm} - \sigma_{In}}{\rho}}$$

The power can be defined as:

$$P = F_{U-MAX}V$$

Therefore, to find the optimal speed of the belt:

$$\frac{dP}{dV} = 0 \rightarrow V_{opt} = \sqrt{\frac{\sigma_{adm} - \sigma_{In}}{3\rho}} = \frac{V_{MAX}}{\sqrt{3}}$$

Thus, the maximum power output is:

$$P_{MAX} = \frac{2}{3}\sqrt{\frac{1}{3\rho}}\left(\sigma_{adm} - E\,\frac{e}{d_1}\right)^{\frac{3}{2}} A_o\,\frac{e^{\alpha_1\mu} - 1}{e^{\alpha_1\mu}}$$

Returning to Pocelet's equation it's possible to determine the minimum values required to transmit a given force:

$$T_o \geq T_c + \frac{1}{2}\frac{e^{\alpha_g\mu} + 1}{e^{\alpha_g\mu} - 1}F_U$$

$$F_U \leq 2(T_o - T_c)\frac{e^{\alpha_g\mu} - 1}{e^{\alpha_g\mu} + 1} = 2[(\sigma_{Adm} - \sigma_{In})A_o - T_o]$$

Hence, optimizing the initial stress:

When considering the space limitations within the rocket, the driven wheel ought to have a radius of 7.5mm to leave enough clearance for the I-beams that support the module, this means the driving wheel can have a much bigger diameter than the wheels attached to the worm gears, however, the bigger it is, the smaller the contact angle is, thus reducing the maximum power which can be transmitted by the assembly, therefore, the driving wheel will have a diameter twice the driven pulley (15mm) with intermediary pulleys with a diameter of 5mm to adjust the belt's positioning relative to the 4 main pulleys so they have the same angle (the angle they would have if they were a simple pulley belt assembly of a 7.5mm radius and 15mm radius separated by 40mm).

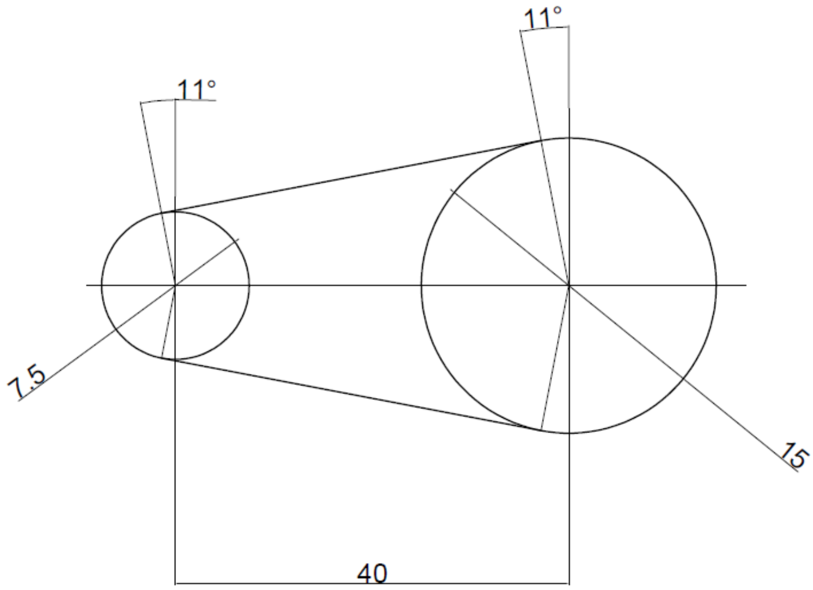

Figure 86 | Simple 2 pulley system

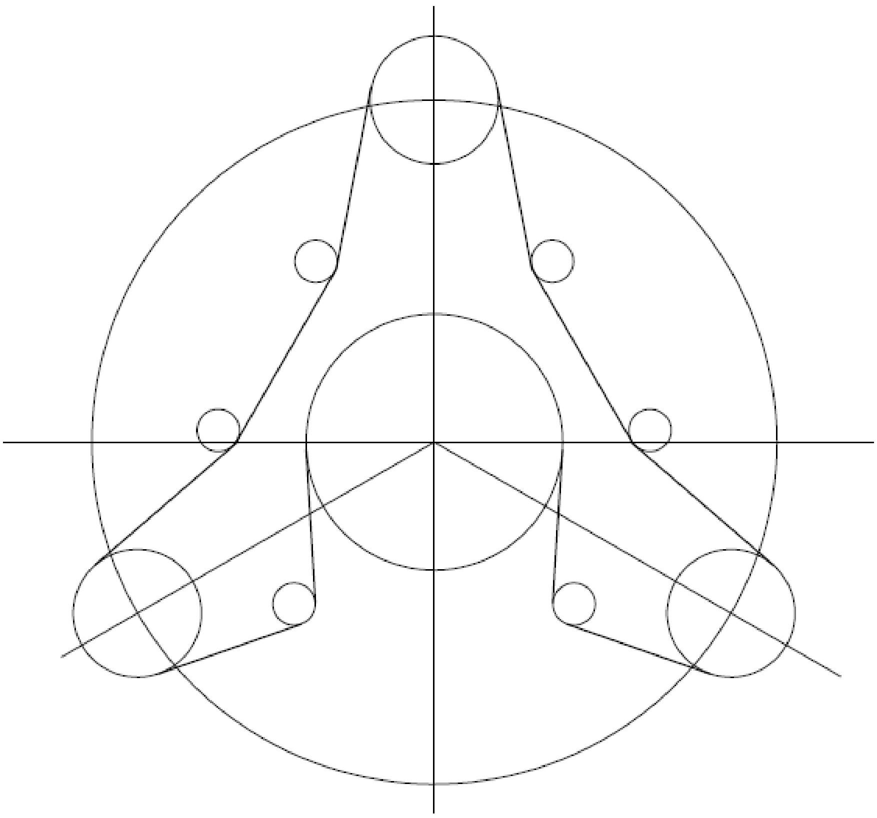

Figure 87 | Pulley-Belt assembly

From the design of the worm gear the vertical speed of the slide can be calculated from the axial pass:

$$p_z = \pi d tan(\gamma) \rightarrow p_z = \pi 8 \tan(7.1808^{\text{º}}) = 3.167 \frac{mm}{rev}$$

Alas, wanting the slide to travel 5cm in 1 second:

$$w_1 = \frac{50}{p_z} \rightarrow w_1 = \frac{50}{3.167} = 15.791\frac{rev}{s} = 99.215\frac{rad}{s}$$

Furthermore, the vertical force exerted by the slide assembly (slide the 3 pins and the 3 gears) when it moves upwards is $260.61*10^{-3}$g, to ensure a security coefficient of 3, the force which the worm gears will experience upon functioning will be considered to the mass of the slide assembly times gravity (for each), therefore:

$$F = 260.61 * 10^{-3}g = 2.557N$$

Alas, the power and moment can both be calculated as well (for each driving wheel):

$$P = F * V_{up} = 0.05 * 2.557 = 1.048W$$

$$M = \frac{P}{w} = \frac{1.048}{99.215} = 0.0106Nm$$

Considering the system of equations (considering $d_1 + e = dp_1$ to maximize the force in the calculations):

$$\begin{cases} M = (T1 - T_2)\frac{d_1 + e}{2} \\ F_U = T_1 - T_2 \end{cases} \rightarrow F_U = \frac{0.0106}{7.5 * 10^{-3}} = 1.413N$$

The speed of the belt can be calculated as:

$$V_1 = w_1 r \rightarrow V_1 = 99.215 * 7.5 * 10^{-3} = 0.744\frac{m}{s}$$

Assuming the belt will be made of polyamide ($e = 5mm; \sigma = 70MPa;\ \rho = 1.14\frac{kg}{m^3};\ \mu = 0.8\ and\ E = 3GPa$), the initial tension ought to be:

$$T_o \geq T_c + \frac{1}{2}\frac{e^{\alpha_g \mu} + 1}{e^{\alpha_g \mu} - 1}F_U |\ T_c = \rho A_o V^2$$

$$T_o = 1.14 * 19.86 * 10^{-6} * 0.744^2 + \frac{1}{2}\frac{e^{\frac{11}{180}*\pi*0.8*3.4} + 1}{e^{\frac{11}{180}*\pi*0.8*3.4} - 1}1.413 = 1.384N$$

To check the useful force is within the safety parameters:

$$F_U = 1.413N \leq 2(1.384 - 1.14 * 19.86 * 10^{-6} * 0.744^2)\frac{e^{\frac{11}{180}*\pi*0.8*3.4} + 1}{e^{\frac{11}{180}*\pi*0.8*3.4} - 1} = 10.837N$$

To allow the payload to be deployed a slide ought to push it horizontally to launch it from the rocket and a separate mechanism must open the doors on the tube wall.

The simplest and lightest option is to embed slightly charged metal sheet on the cover and install on top of the structural beams 2 electromagnets which can change polarity to either maintain the cover in place or push it out.

The cover is connected to the rest of the rocket via a cable.

As such, the electromagnets can be considered to have a net dipolar moment equal to:

$$\overrightarrow{m_{elec-beams}} = \pm 240 * 10^{-6} * 2 * \frac{\sqrt{3}}{2} ni\overrightarrow{e_1}$$

Since, they are opposite to each other all the other components cancel out, leaving the radial component.

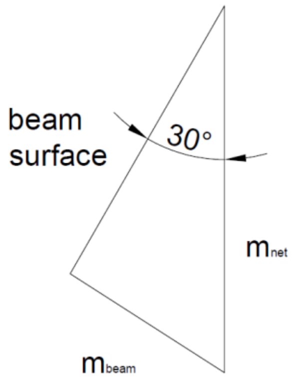

Figure 88 | Net magnetic dipole beams

Similarly, the pushers to deploy the CanSat are mounted with a 90º offset, alas, the electromagnetic structure will only have a net component in the radial direction, pushing the CanSat outwards for it's deployment, with a magnetic dipolar moment of:

$$\overrightarrow{m_{elec-push}} = \pm 3420.85 * 10^{-6} ni * 2 * \frac{\sqrt{2}}{2}\overrightarrow{e_1}$$

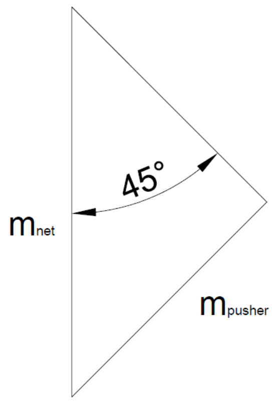

Figure 89 | Net electromagnetic dipole pusher

Payload system assembly

Figure 90 | Payload deployment system assembly

Motor Characterization

A brief summary of the motors selected for each level:

	Level 1	Level 2	Level 3
Model	I218R	L1100	M650W
Manufacturer	Aerotech	AMW	Aerotech
Motor casing diameter (mm)	38	54	75
Motor casing length (mm)	191	728	801
Total Impulse (Ns)	319.63	2576.19	5964
Average Thrust (N)	226.51	1132	656
Maximum Thrust (N)	289.04	1340.23	1475
Time to burn out (s)	1.41	2.35	9.13
Total mass (g)	358.4	2588.1	5125
Casing mass (g)	199.23	1242	1774
Propellant mass (g)	172.7	1346	3351
Mass after firing	177.7	1381	2232
Source	(National Association of Rocketry, 2001)	(NAR Official Certification Laboratory, 2006)	(National Association of Rockertry, 2007)

Table 31 | Motor characteristics

Each motor has been selected with a criterion based on 4 conditions:

- The static motor testing data must be available to build the characteristic curve.
- The engine must have a NAR/Tripoli certificate
- The rocket motor must fulfil each Level requirements:
  - Level 1: A single class H or I motor with a total maximum impulse of 640Ns.
  - Level 2: A single class J, K or L motor with a total maximum impulse of 5120Ns.
  - Level 3: A single class M or larger motor with a total maximum impulse greater than 5120Ns.
- The outer diameter must adhere to standard European dimensions (for rocket engines):
  - Level 1: Outer diameter equal to 18 or 29mm.
  - Level 2: The outer diameter must be equal to 54mm.
  - Level 3: Outer diameter of 75mm.

Level 1 motor characterization

For the Level 1 certification flight Aerotech's I class motor, I218R has been deemed the most suitable, due to it adhering to the above mentioned specifications and having a static test data with sufficient points (32 time-thrust measurements in total) although not many, which can lead to not a very exact characterization.

Furthermore, the casing's temperature does not exceed 200ºC at any point of the static tests.

From the available data (National Association of Rocketry, 2001), the motor's characteristic impulse curve can be drawn:

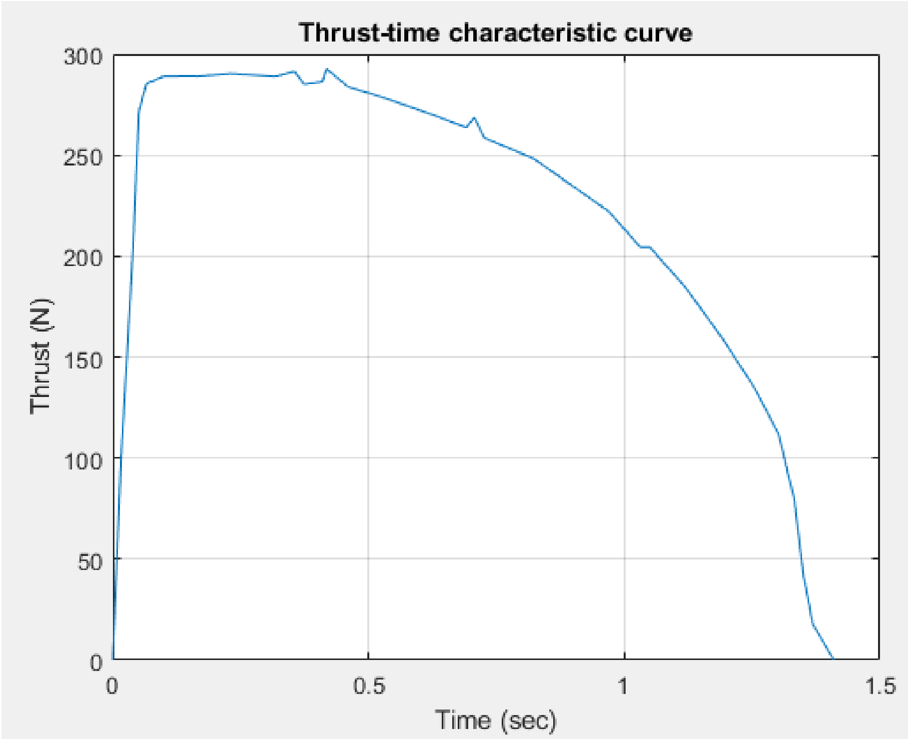

Figure 91 | I218R characteristic curve

Hence the decision was made to split the curve into 2 functions, one for the ascending branch (from 0.000 sec, 0.000N to 0.099 sec, 288.906 N), and a second one for the descending arm (from 0.099 sec, 288.906 N to 1.410 sec, 0.000 N), repeating the break point in both to ensure a better continuity.

For the ascending arm the resulting non-linear regression was:

$$F = 7191.8t - 43023t^2$$

```
Estimated Coefficients:
               Estimate      SE        tStat       pValue
               ________    ______    _______    __________

    T_1         7191.8     282.58      25.45    1.4155e-05
    T_1^2       -43023     3452.4    -12.462    0.00023845


Number of observations: 6, Error degrees of freedom: 4
Root Mean Squared Error: 11
```

Figure 92 | Non-linear regression ascending arm Level 1 results

Its a high RMSE, but there are very few observations (6 in total), however, both p-values suggest these coefficients should be kept.

Upon the analysis of the residuals:

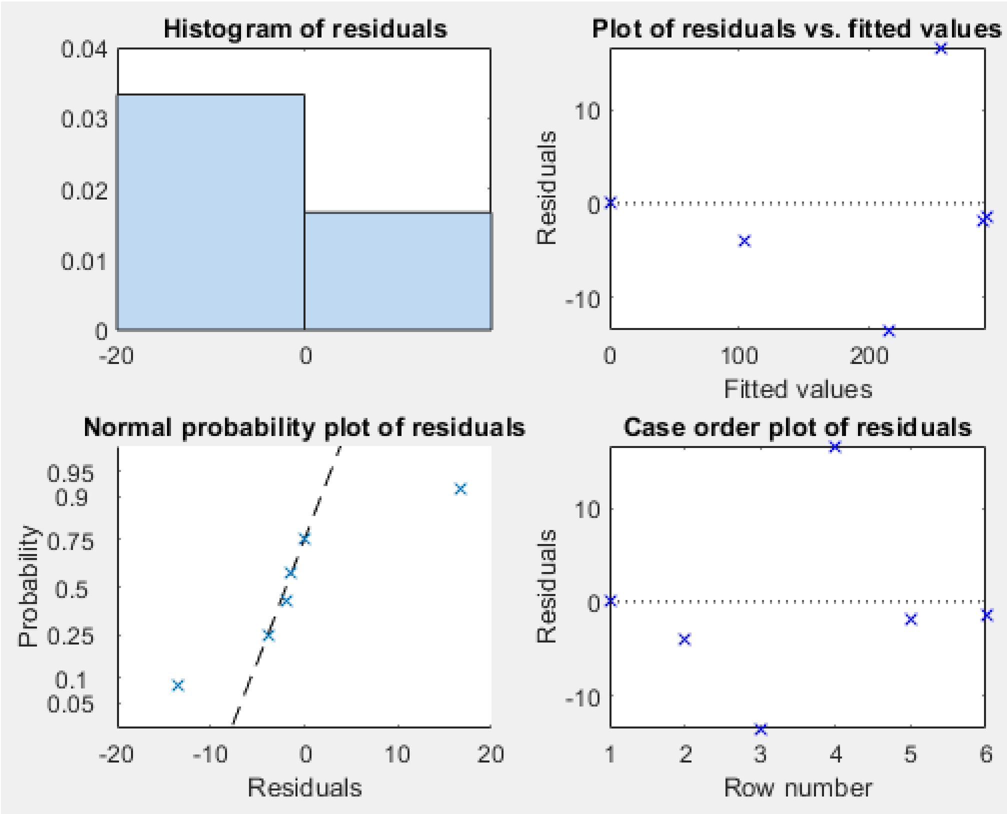

Figure 93 | Residual analysis ascending arm Level 1

There are not enough observations to judge the distribution, their normality or if there are any structure in the residuals, but its easy to see it the model adjusts fairly well to the recorded data graphically.

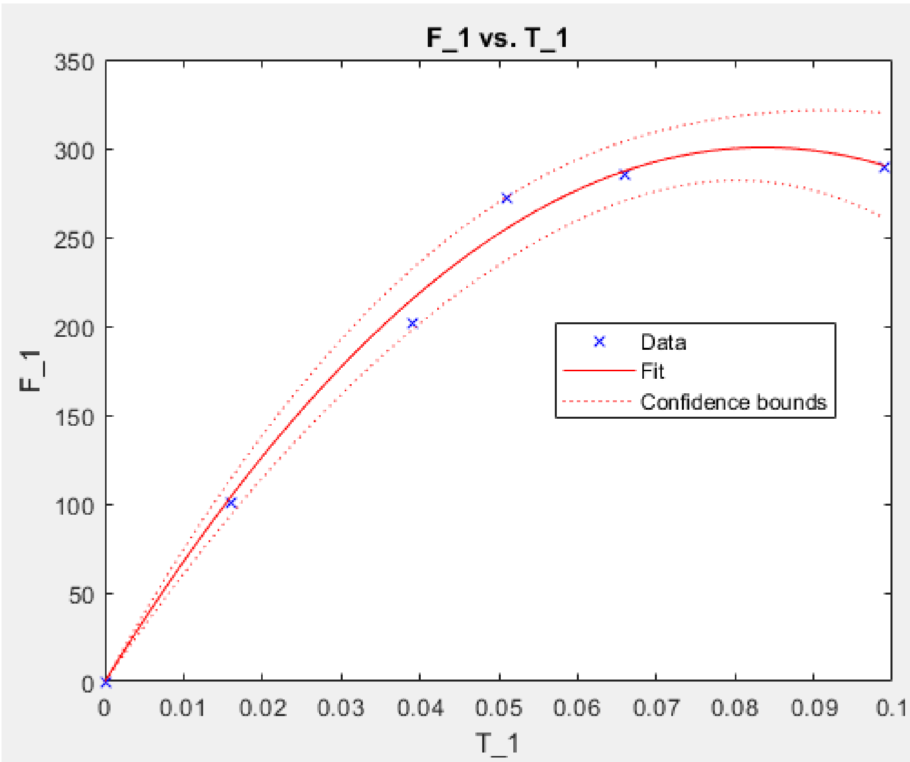

Figure 94 | Level 1 ascending arm model

The descending arm non-linear regression output:

$$F = 282.31 + 96.705t^2 - 163.17t^3$$

```
Estimated Coefficients:
                   Estimate     SE       tStat       pValue
                   ________   ______    _______    __________

    (Intercept)     282.31    4.9692     56.812    4.2278e-27
    T_2^2           96.705    24.984     3.8706    0.00073021
    T_2^3          -163.17    17.815    -9.1593    2.6538e-09


Number of observations: 27, Error degrees of freedom: 24
Root Mean Squared Error: 12.3
R-squared: 0.984,  Adjusted R-Squared: 0.982
F-statistic vs. constant model: 729, p-value = 3.24e-22
```

Figure 95 | Non-linear regression descending arm Level 1 results

Although the RMSE is still high the p-value of each coefficient as well as that of the model show they must be kept, even though its still a small number of points to analyse.

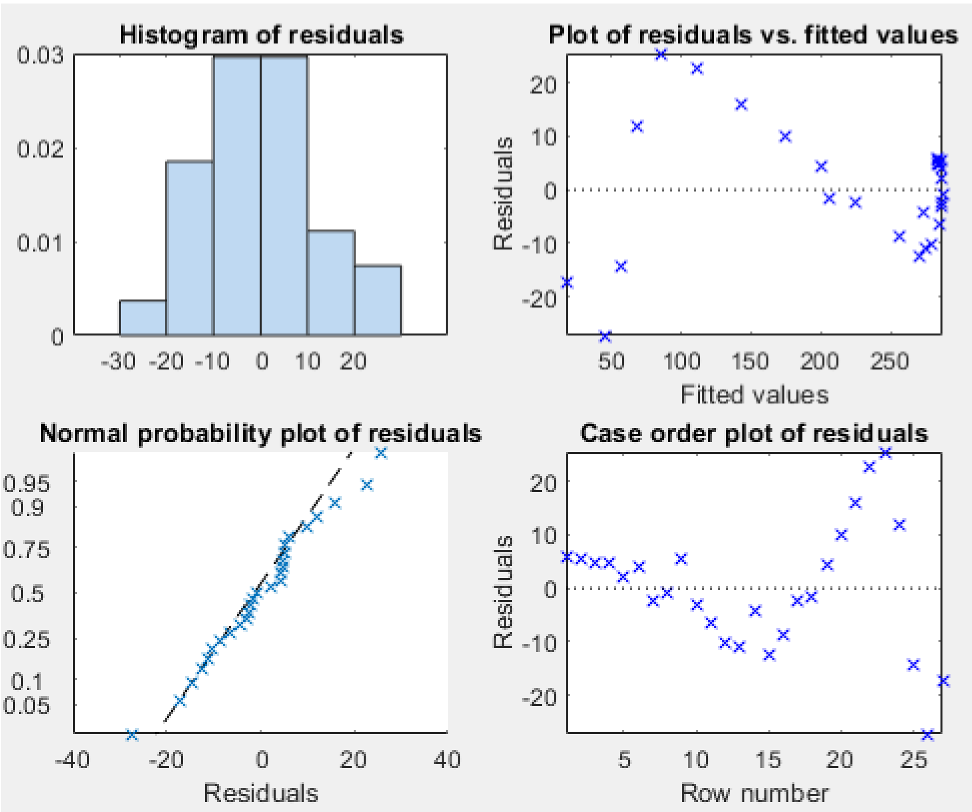

Figure 96 | Residual analysis descending arm Level 1

The residual analysis does resemble a normal distribution more closely as shown in the histogram and the normality plot, however due to the small amount of data there seems to be a structure when taking into account the residues are plotted against the fitted values and in the case order, but this is most likely due to the lack of redundancy in the data, since there is only 1 observation for each unit of time.

When plotted, however, it is easy to see it does resemble the model, although it overestimates somewhat at the shoulder and the ending points but it underestimates the start and just after the shoulder:

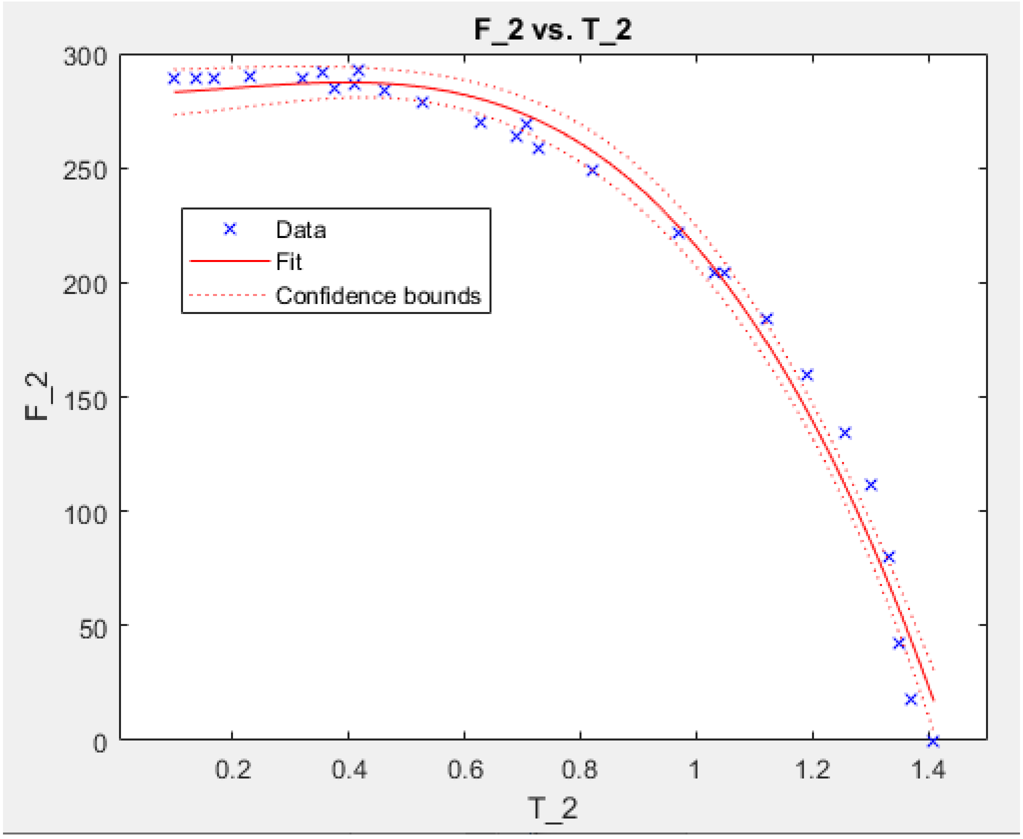

Figure 97 | Level 1 ascending arm model

Therefore, the final model for the Level 1 motor is:

$$F(t) = \begin{cases} 7191.8t - 43023t^2 \; if \; t \leq 0.099 \\ 282.31 + 96.705t^2 - 163.17t^3 \; if \; t > 0.099 \end{cases}$$

Thus obtaining:

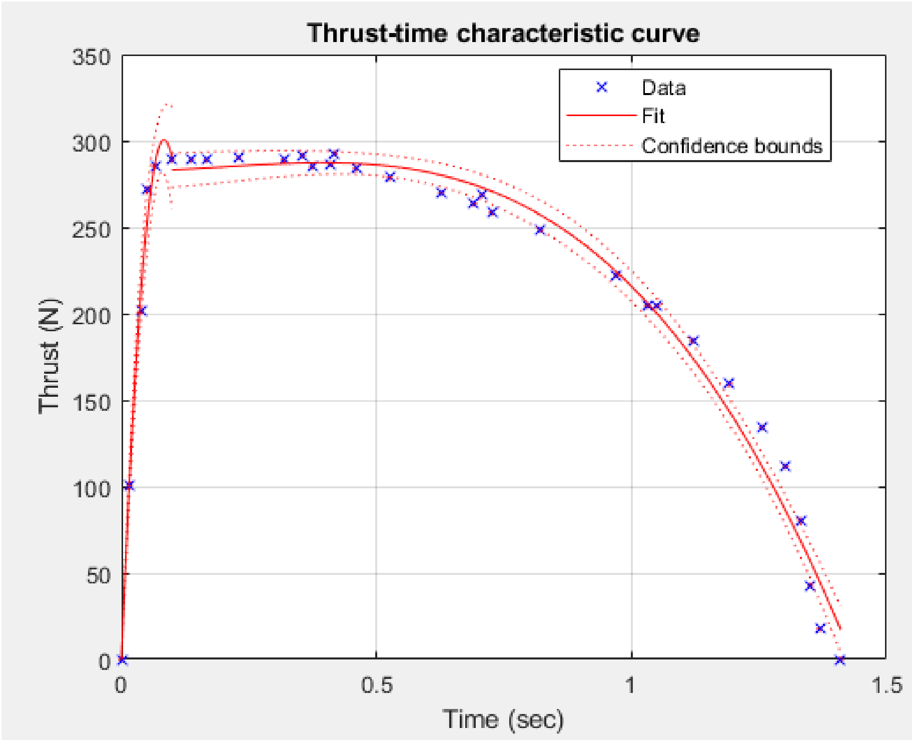

Figure 98 | Level 1 motor characterization

There is a small discontinuity between the graphs which, therefore, the limit between the 2 is taken to the left, so that it overestimates the force at that moment.

Level 2 motor characterization

For the Level 2 certification the best candidate seems to be AMW L1100, since it has a consistent thrust of 1200N throughout most of the burn time and a motor casing with a diameter of 54mm and a maximum casing temperature below 200ºC.

As with previous regressions, the data is rather limited (only 32 measurements), hence it might lead to inexact results.

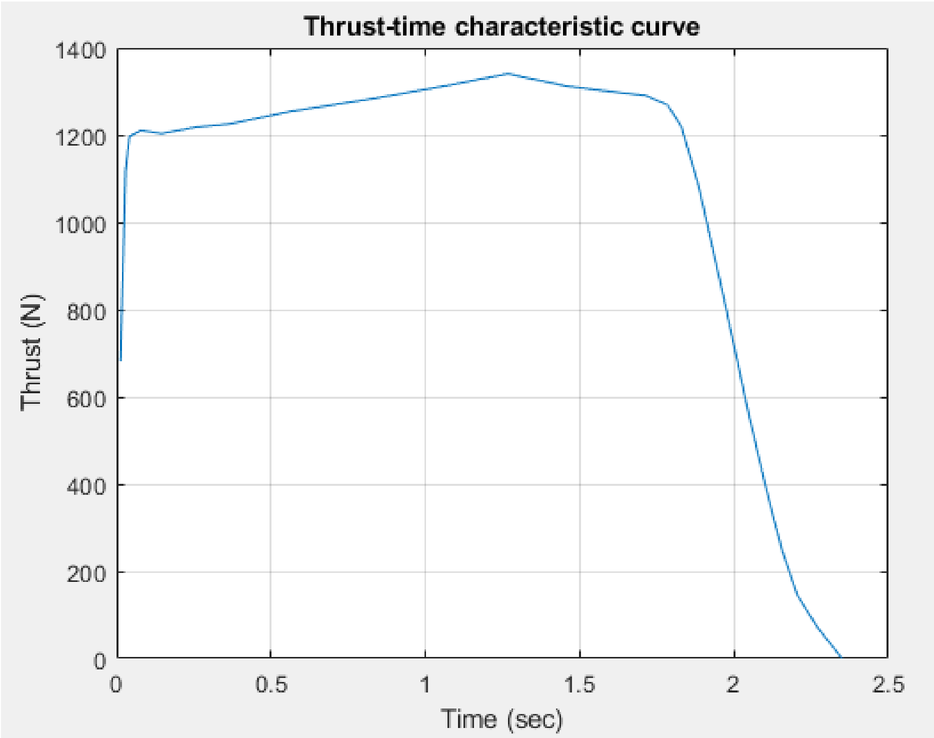

Figure 99 | L1100 characteristic curve (National Association of Rocketry, 2004)

Upon inspecting the data, it will be split into 3 separate regressions to minimize the error replicating the last measurement of a regression as the first of the following to guarantee a better time-continuity.

The first section's characteristic equation is:

$$F = 62312t - 8.1025 * 10^5 t^2$$

```
Estimated Coefficients:
                  Estimate        SE       tStat       pValue
               ___________    ______    ________    _________

    T_1              62312    1106.3      56.326     0.011301
    T_1^2      -8.1025e+05     30409     -26.645     0.023881


Number of observations: 3, Error degrees of freedom: 1
Root Mean Squared Error: 12.6
```

Figure 100 | Non-linear regression ascending section Level 2 results

The first part, although the p-values are relatively high (at 1.1 and 2.3%) they do show a fairly low RMSE (12.6 N) when compared to the scale of the Thrust (up to 1200N).

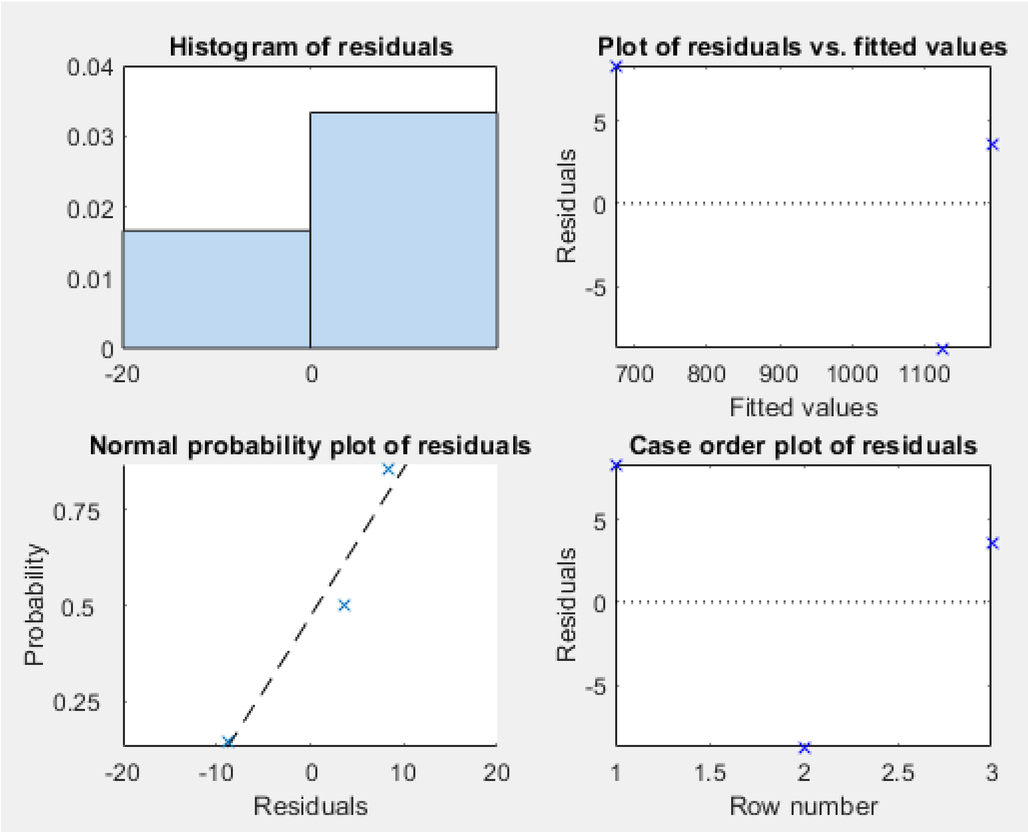

Figure 101 | Residual analysis ascending arm Level 2

Since the dataset is so small a structure of the residuals and their normality cannot be evaluated.

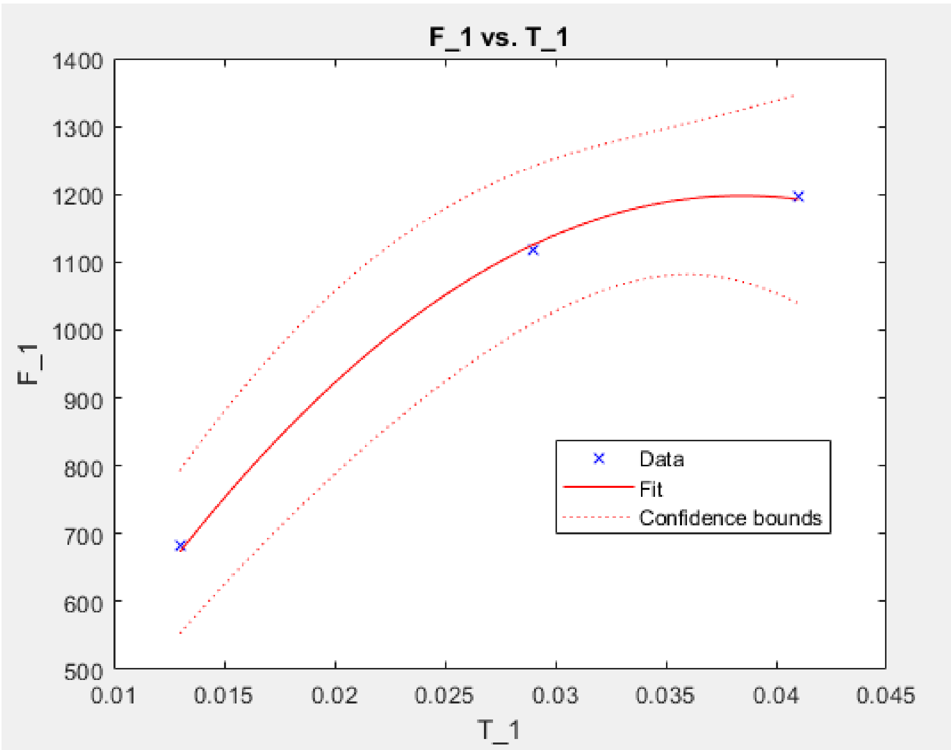

Figure 102 | Level 2 ascending arm model

Upon visual inspection of the data, the model seems to be slightly overfitted, however, as explained, the lack of data limits greatly the regression, therefore, considering the low RMSE it will be accepted.

The second part of the thrust curve will be taken to be the plateau seen in the Static Fire Test Data.

The characteristic equation is

$$F = 1202.1 + 229.64t^2 - 119.26t^3$$

```
Estimated Coefficients:
                   Estimate      SE       tStat       pValue
                   ________    ______    ______    __________

    (Intercept)     1202.1     5.7347    209.63    1.5002e-19
    T_2^2           229.64     17.582    13.061    1.3119e-07
    T_2^3          -119.26     9.6667   -12.337    2.2499e-07


Number of observations: 13, Error degrees of freedom: 10
Root Mean Squared Error: 11.2
R-squared: 0.95,  Adjusted R-Squared: 0.939
F-statistic vs. constant model: 94.1, p-value = 3.27e-07
```

Figure 103 | Non-linear regression plateau Level 2 results

All 3 coefficients show a minimal p-value, suggesting they should be accepted, paired with the RMSE (11.2 N) and the low p-value of the model as a whole it should be accepted, given that the residuals show likewise.

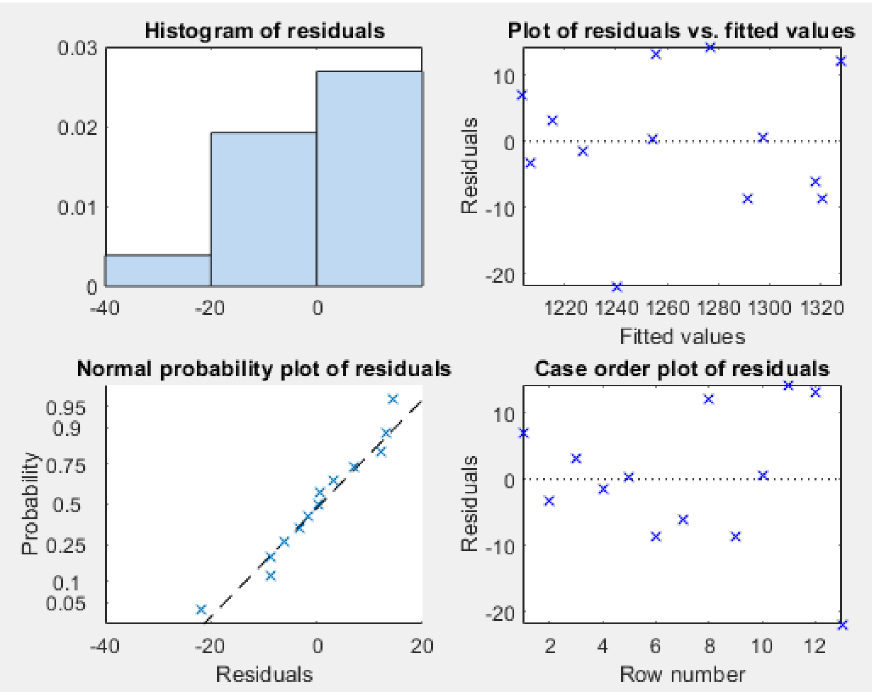

Figure 104 | Residual analysis plateau Level 2

Although the histogram does not show a bar plot resembling a normal distribution, the normal probability plot of the residuals does show that it can be considered to be normal, with only the tail value diverging from the normality line ever so slightly. When plotted against their fitted values the residuals do not show any structure nor a variance change (the residuals do not scatter more as the fitted values change).

Hence the model should be accepted.

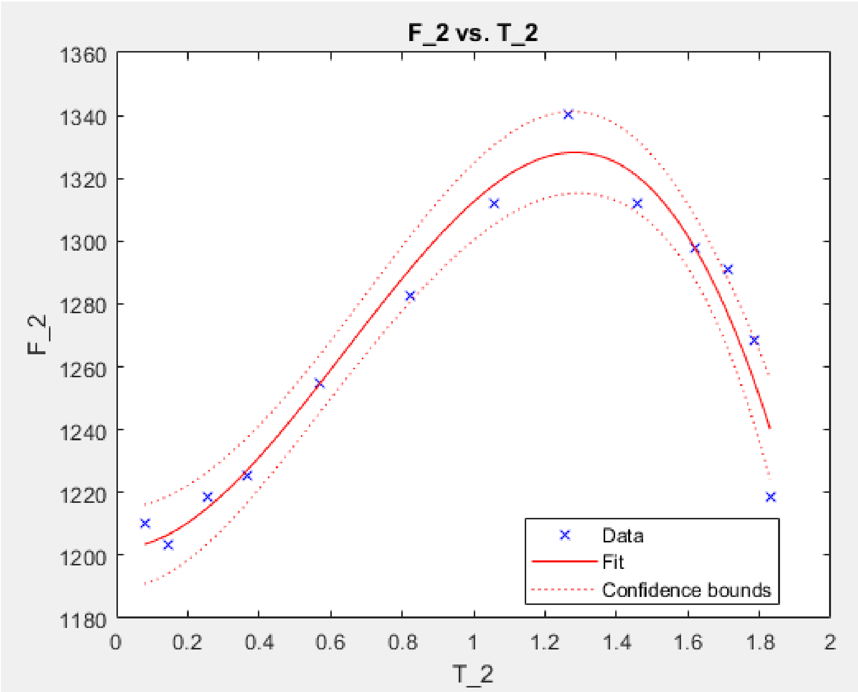

Figure 105 | Level 2 plateau arm

The model slightly underestimates the peak value, although it is within confidence bounds still, although it shows a discontinuity with regards to the ascending arm model.

The third part of the model is the descending arm, with the following coefficients:

$$F = -60099 + 98392t - 51183t^2 + 8595.1t^3$$

```
Estimated Coefficients:
                   Estimate      SE       tStat       pValue
                   ________    ______    _______    _________

    (Intercept)     -60099      12962    -4.6366    0.0056501
    T_3              98392      18701     5.2614     0.003295
    T_3^2           -51183     8961.9    -5.7112    0.0022995
    T_3^3           8595.1     1426.7     6.0244    0.0018129


Number of observations: 9, Error degrees of freedom: 5
Root Mean Squared Error: 14.5
R-squared: 0.999,  Adjusted R-Squared: 0.999
F-statistic vs. constant model: 2.53e+03, p-value = 2.27e-08
```

Figure 106 | Non-linear regression descending arm Level 2 results

Although none of the p-values are as low as the previous model, all are below 1%, thus suggesting they should be all kept, this is further reinforced the RMSE (14.5 N) is taken into account. Finally, the model's p-value supports all previously discussed results and thus the model must be accepted, pending the residual analysis.

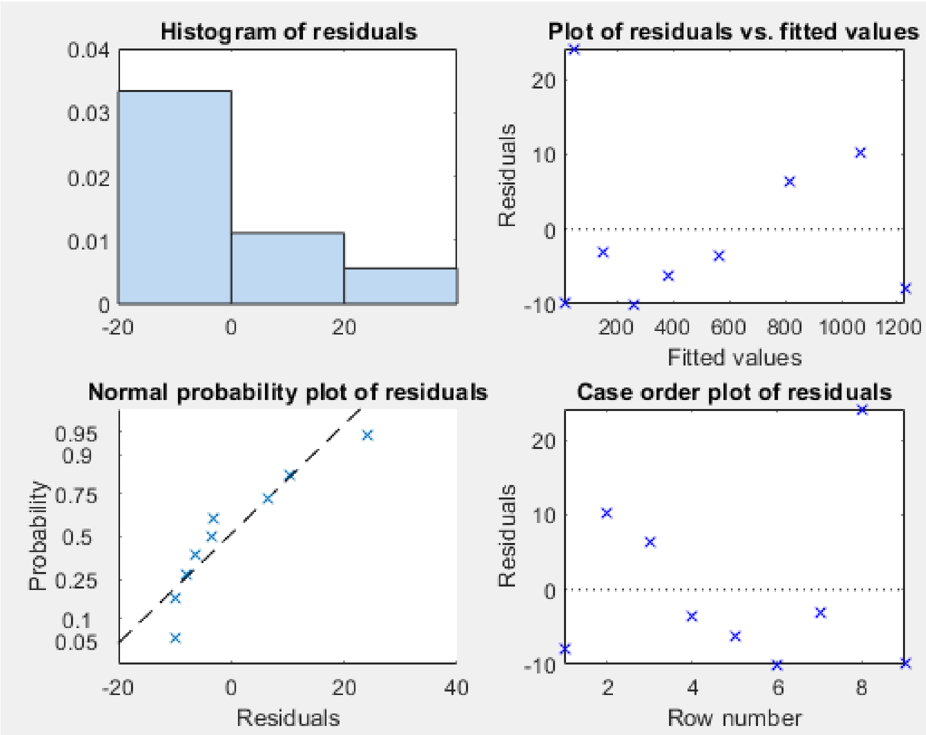

Figure 107 | Residual analysis descending arm Level 2

The histogram does not show a normal distribution nor does the probability plot, and the residuals seem to be rather symmetrical, however, there does seem to be a wide margin. This is most likely caused by the small amount of data available for the regression, since the p-values show promising results.

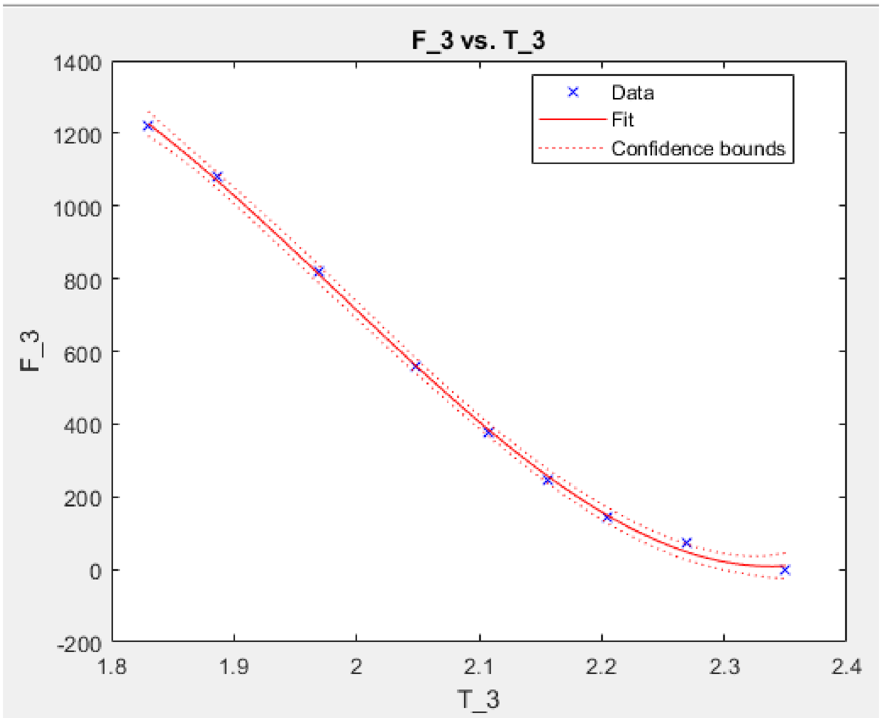

Figure 108 | Level 2 descending arm model

The model does resemble closely the data, which suggests it might be over-fitted, even though it does slight underestimate the shoulder at the base of the thrust curve.

The final model is thus:

$$F = \begin{cases} 62312t - 8.1025 * 10^5 t^2 \ if \ t < 0.041s \\ 1202.1 + 229.64t^2 - 119.26t^3 \ if \ 0.041 \leq t < 1.803s \\ -60099 + 98392t - 51183t^2 + 8595.1t^3 \ if \ t > 1.803s \end{cases}$$

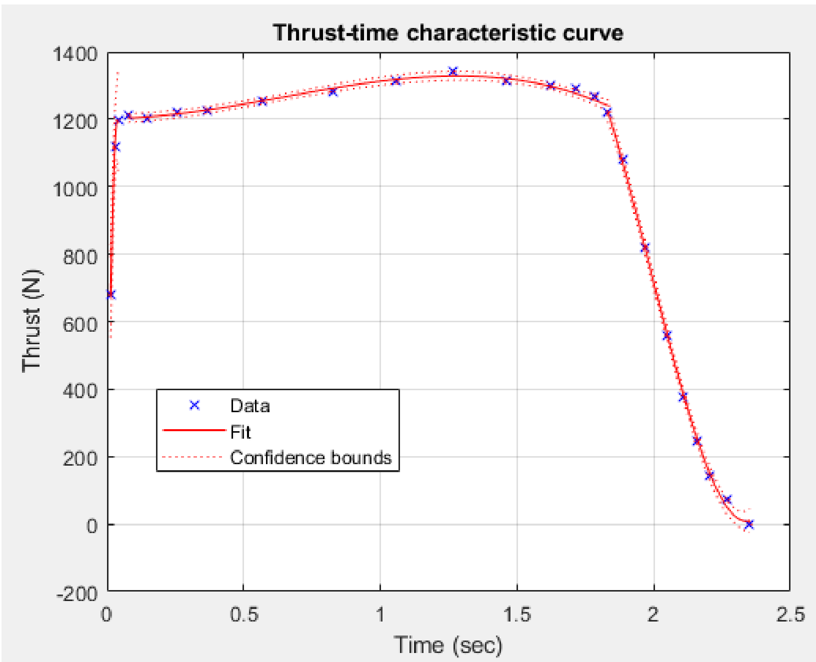

Figure 109 | Level 2 motor characterization

Level 3 motor characterization

The motor chosen for the Level 3 certification flight is Aerotech's M650W, with an external diameter of 75mm and a total impulse of 5964 Ns.

The characteristic thrust curve from the tests is:

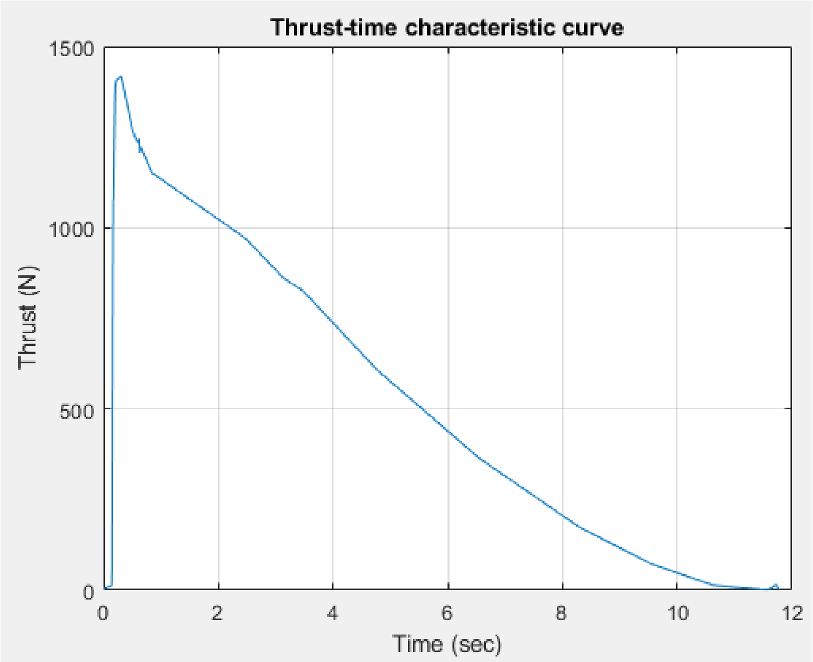

Figure 110 | M650W characteristic curve (National Association of Rockertry, 2007)

As shown in the figure, the curve has a sudden increase and then a progressive decrease over time thus it can be broken down into 2 parts, for better accuracy, one for the increase and another for the decrease.

For the ascending arm, the initial point (0.0, 3.92403) must be considered an outlier from the rest of the data:

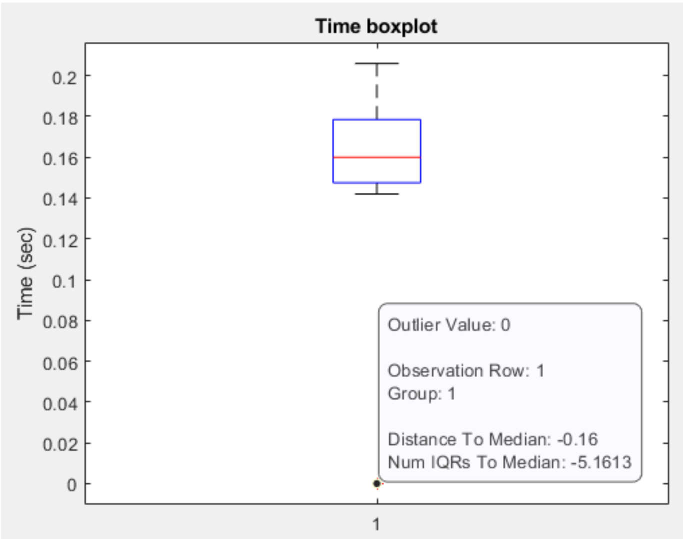

Figure 111 | Level 3 ascending arm boxplot

Furthermore, considering all other test started with a thrust of 0 N and this test shows an initial thrust of 3.92N suggest it might be a miscalibration of the sensors. Furthermore, the time difference is such that it can be considered a delay following the ignition sequence, therefore, the resulting model for the ascending arm is:

$$F = -16654 + 1.8093 * 10^5 t - 4.5393 * 10^5 t^2$$

```
Estimated Coefficients:
                    Estimate        SE        tStat       pValue
                   __________    ______    _______    __________

    (Intercept)        -16654    2043.8    -8.1486    1.9103e-05
    T_1            1.8093e+05     23773     7.6108    3.2895e-05
    T_1^2         -4.5393e+05     68314    -6.6448    9.4301e-05


Number of observations: 12, Error degrees of freedom: 9
Root Mean Squared Error: 86.5
R-squared: 0.977,  Adjusted R-Squared: 0.972
F-statistic vs. constant model: 194, p-value = 4e-08
```

Figure 112 | Non-linear regression descending arm Level 3 results

Although the RMSE is relatively big, at 86.5 N, it's diminished when compared to the maximum power the model gets to (1388.02 N).

When looking at the p-value of the model it suggests it should be accepted and the coefficients' all have very low p-values hence they should be accepted as well.

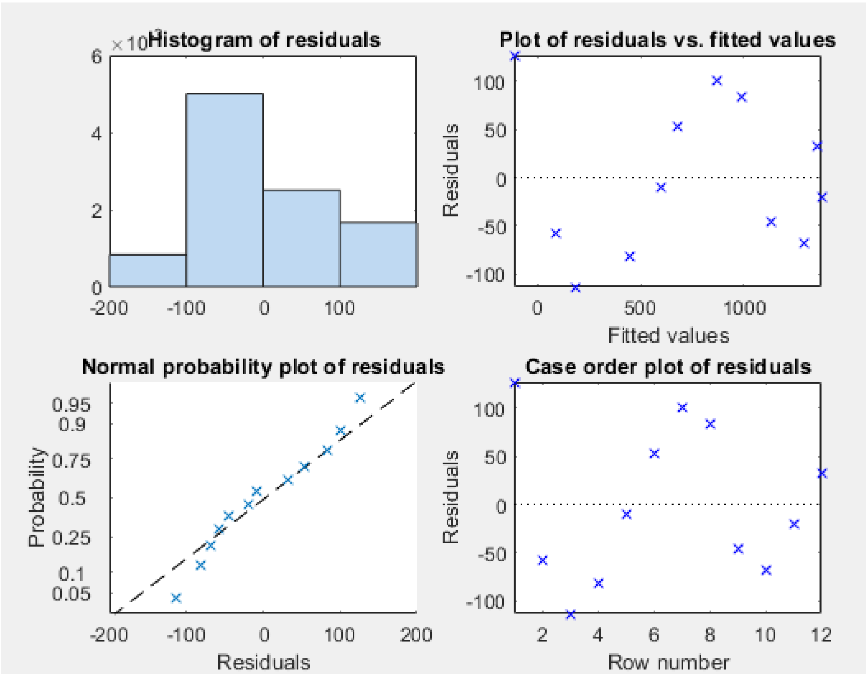

Figure 113 | Residual analysis ascending arm Level 3

The histogram of the residuals does not resemble a normal distribution and the residuals do not seem to adjust to the normal probability plot, mainly the tails, however, when they are plotted against their fitted values and against their case order they do not show a structure and the variance seems to be constant, therefore, the model must be accepted.

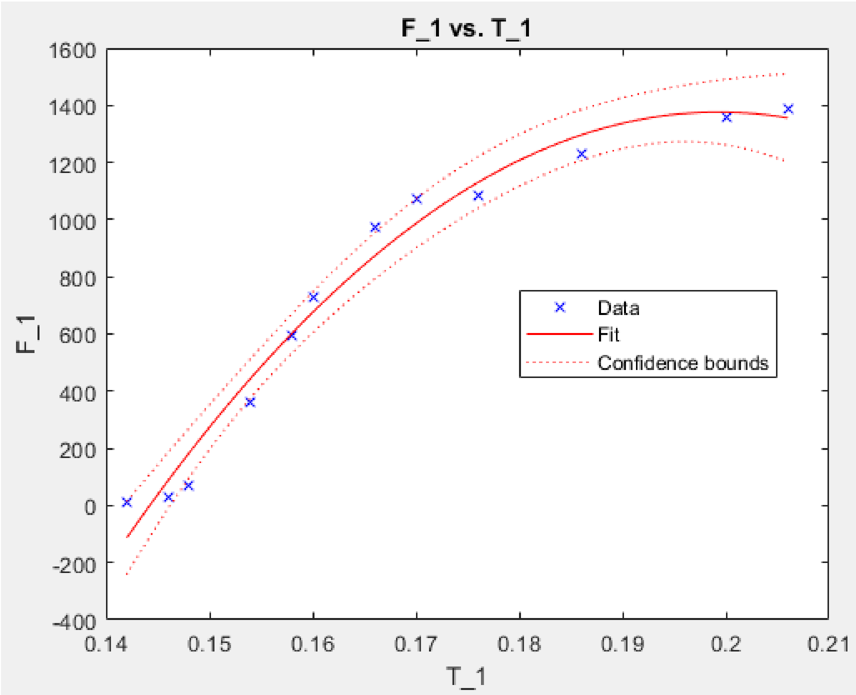

Figure 114 | Level 3 ascending arm model

It's easy to see the model does represent the data and by eliminating the outlier at (0.0,3.92) the regression is strictly positive and increasing for the entirety of the domain.

Having accepted the model, the delay can be calculated:

$$0 = -16654 + 1.8093 * 10^5 t - 4.5393 * 10^5 t^2 \rightarrow t = 0.2543\ s$$

The descending arm's regression resulted in:

$$F = 1260 - 36.112t^2 + 2.3225t^3$$

Estimated Coefficients:

	Estimate	SE	tStat	pValue
(Intercept)	1260	27.355	46.061	2.7197e-19
T_2^2	-36.112	2.8626	-12.615	4.6663e-10
T_2^3	2.3225	0.24892	9.3301	4.2357e-08

```
Number of observations: 20, Error degrees of freedom: 17
Root Mean Squared Error: 88
R-squared: 0.977,  Adjusted R-Squared: 0.975
F-statistic vs. constant model: 369, p-value = 9.91e-15
```

Figure 115 | Non-linear regression descending arm Level 3 results

Pending on the residual analysis, the p-value of the model does suggest it should be kept, even though the RMSE is somewhat high (88N). The coefficient's p-values should also be kept.

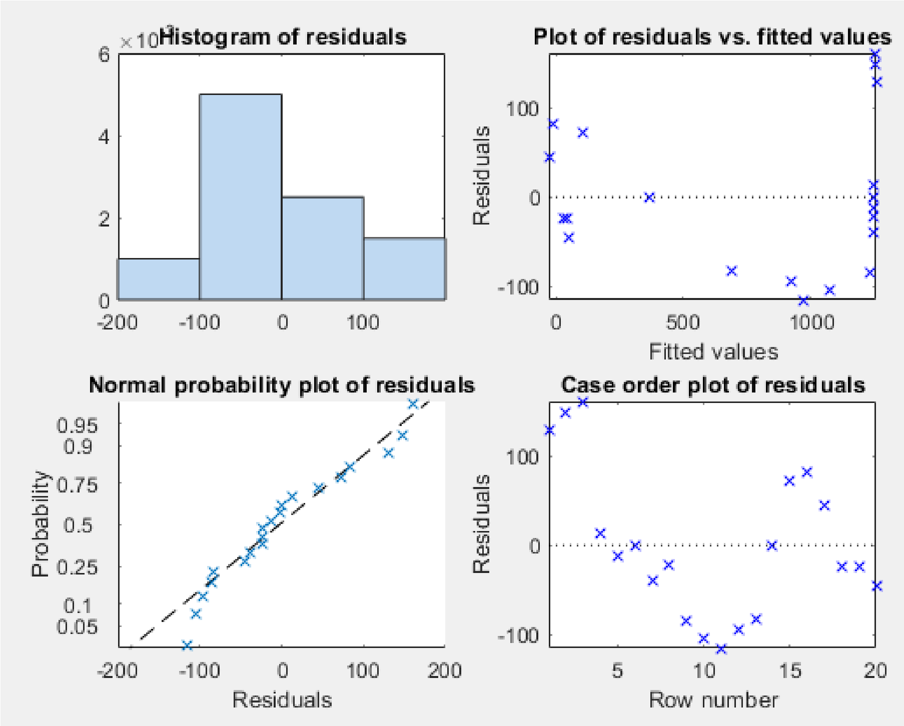

Figure 116 | Residual analysis descending arm Level 3

The residuals do not follow a strict normal distribution in the histogram although they do seem to adhere to the normal probability plot. They do not show any structure when plotted against their fitted values nor in the case order and the variance seems to remain fairly constant. Therefore, the model will be accepted.

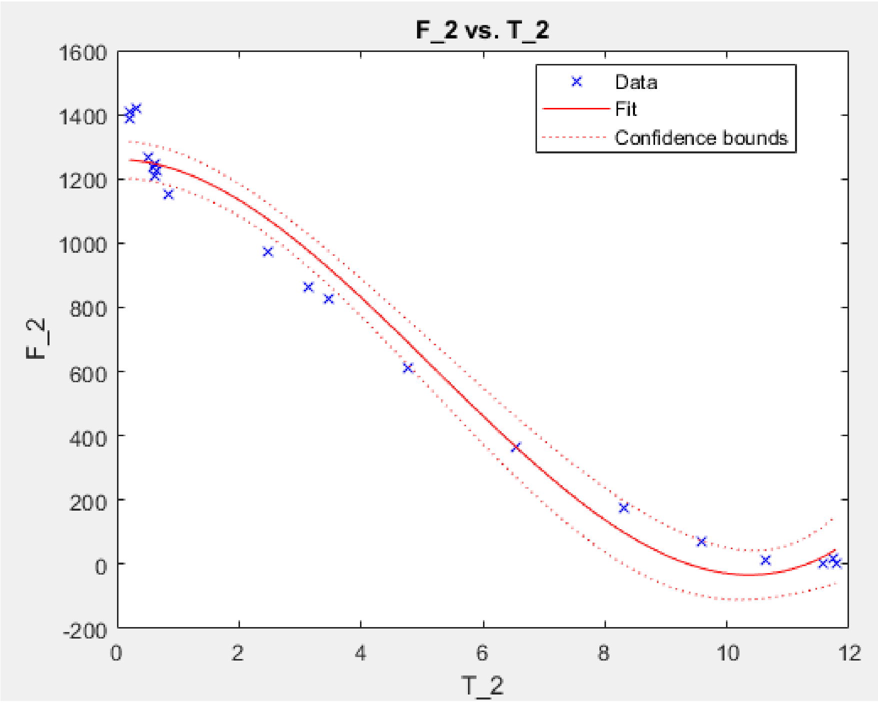

Figure 117 | Level 3 descending arm model

Although at first it does not adhere to the maximum (which will cause a discontinuity in the final model) it does adhere to the data afterwards, overestimating the thrust therefore, it's more useful for dimensioning all structural elements, since, it will grant a bigger margin of safety.

The final model for the Level 3 motor is:

$$F = \begin{cases} 0 \; if \; t < 0.254s \\ -16654 + 1.8093 * 10^5 t - 4.5393 * 10^5 t^2 \; if \; 0.254 \leq t < 0.206s \\ 1260 - 36.112t^2 + 2.3225t^3 \; if \; t > 0.206s \end{cases}$$

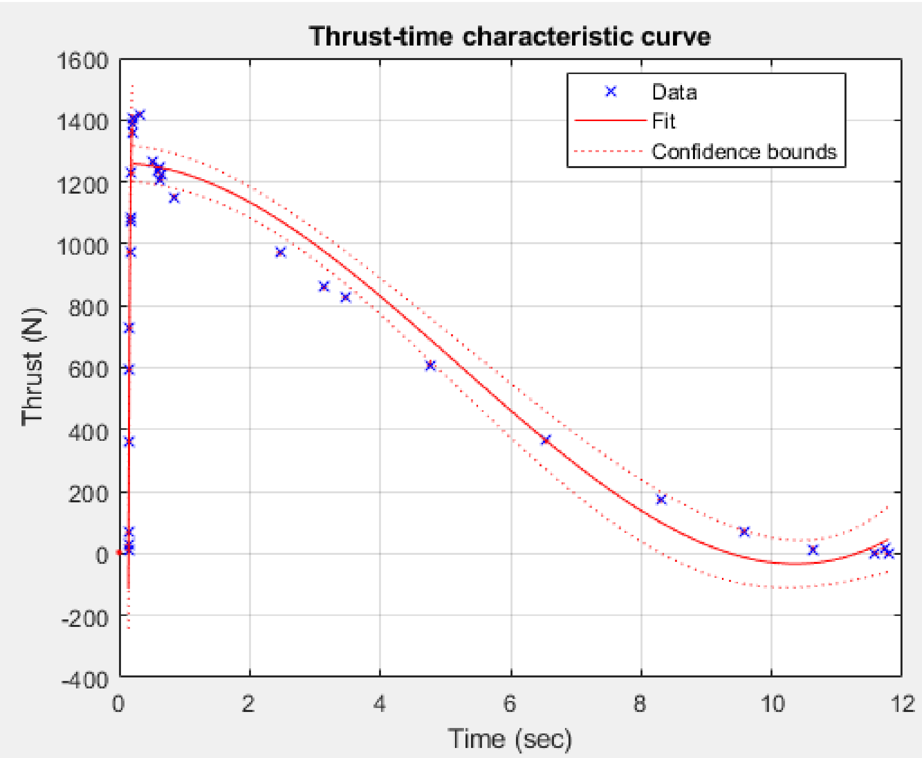

Figure 118 | Level 3 motor characterization

Knowing the propellant mass burnt and the equation driving the motor the proportions of each component found in the mixture can be calculated combining it with the findings in the reference paper for a De Laval Nozzle:

$$F_{Thrust} = F_{flux} + F_{pressure} = v_e \dot{m} + \Delta P A_e$$

Where F_{Thrust} is the average thrust, F_{flux} is the force due to the mass flux and $F_{pressure}$ is due to the pressure variation in the nozzle.

Due to the specifications of the motors not being available, the equivalent mass flux (and therefore the burnt propellant mass) can be calculated as per the reference **Fuente especificada no válida.**:

$$\frac{I_{total}}{t_{burn}} = F_{Thrust} = g_o t_{burn} \dot{m} \rightarrow m_{burnt} = \frac{F_{Thrust}}{g_o}$$

Therefore, for each motor:

	Engine		
	I218R	L1100	M650W
Manufacturer	Aerotech	AMW	Aerotech
Total Impulse (Ns)	319.63	2576.19	5964
Time to burn out (s)	1.41	2.35	9.13
Equivalent mass (g)	23107.844	111748.325	66588.288

Table 32 | Engine impulse

Multivariate adaptative regression splines

Another modelling attempt to achieve a more accurate model was tested with multivariate adaptative regression splines.

It's a regression method which models variables calculating interactions and non-linear relationships employing hinge functions, which have the following definition (Rudy, 2013):

$$h(x-t) = [x-t]_+ = \begin{cases} x - t \; if \; x > t \\ 0 \; if \; x \leq t \end{cases}$$

To evaluate the results of the regressions 5 main statists will be employed:

- Generalized Cross-Validation (GCV): An evaluation technique employed to guarantee the results are independent from the train/test samples input (Devijver, 1982).
- Mean Square Error: Measures the average of the square of the errors, measures the quality of the estimator.
- Root Mean Square Error: Another way of measuring the quality of the estimator but in the units of the output variable.
- Generalized R squared of the model (RSQ): Proportion of the variance in the output variable that is explained by the input variables.
- Generalized R squared based on the GCV (GRSQ).

The coefficients were then presented as a graph dependant on the complexity of the model:

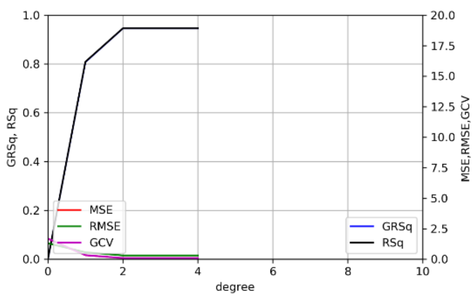

Figure 119 | Good modelling output tests

To determine the validity of a model, 2 main factors were taken into account:

- An ever-decreasing RMSE, MSE and GCV at low values as a method for measuring the quality of the fitting.
- A strictly increasing RSQ and GRSQ (with a convergence amongst themselves) at high values.

The appropriate model complexity was then chosen at a compromise between an elbow in the RMSE and MSE functions (which coincide due to their definition) and a high percentage value for the RSQ and GRSQ.

However, the results were far from relevant.

The Level 2 engine could not be characterized due to a lack of data to represent such a complex graph, and both level and and level 3, showed underwhelming complexity graphs.

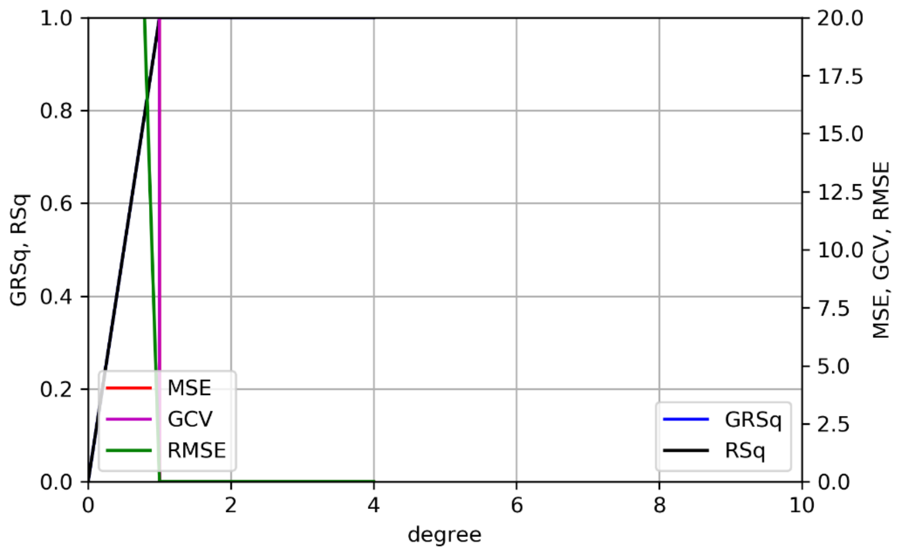

Figure 120 | Level 1 model complexity graph

Clearly, the characterization for the Level 1 rocket is not relevant at all, with all the estimators suggesting these hinge function splines are not an appropriate way of modelling said data, which is further reinforced if the model is compared to the data:

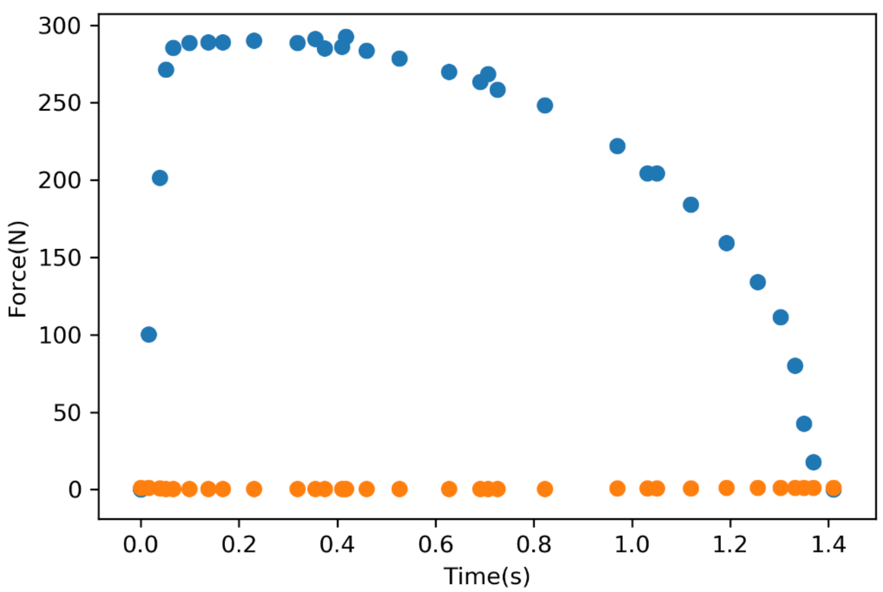

Figure 121 | Level 1 modelling results vs data

Likewise, the Level 3 engine's model complexity graph yields the same results:

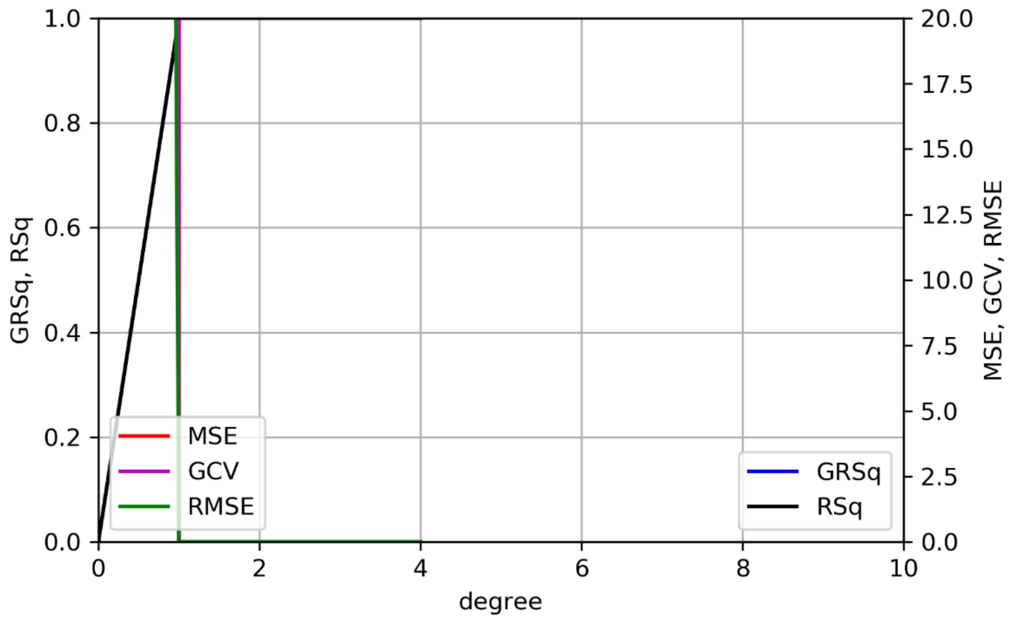

Figure 122 | Level 3 Model Complexity Graph

Which are once again corroborated if the data is compared to the model:

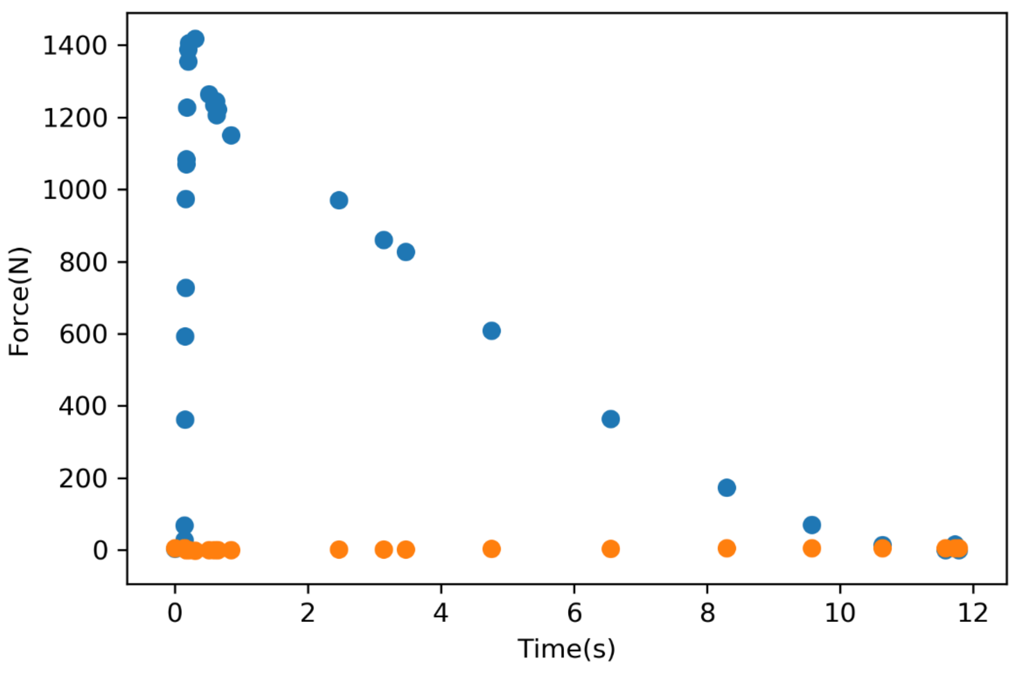

Figure 123 | Level 3 model vs data

Engine Bay

Mis-fire safety system

Amongst amateur rocketry there exist 3 main types of solid propellant:

- Sugar-based fuels: commonly referred to as “Rocket Candy”, they consist of a mixture of different types of sugars and an oxidizer and it is most found in home-made fuel mixtures, generally consisting of 65% potassium nitrate and 35% sucrose per mass (Nakka, Richard Nakka's Experimental Rocketry Web Site, 2017).
- Black powder-based propellant: Based on the mixture of potassium nitrate, sulphur and charcoal which have slowly been falling into oblivion due to their low performance and the black powder’s high volatility (Rocketry, 2020).
- Ammonium perchlorate-based mixtures: They are found mainly in commercially available engines and certified motors. They generally consist of a rubber matrix containing a mixture of ammonium perchlorate and an oxidizer, generally aluminium due to its high reactivity and high concentration in the earth’s crust (baperry3, 2016).

Upon a misfire a safety system should be in place to extinguish the ignition and avoid the propellant exploding and damaging the rest of the launch vehicle.

The driving equation for the burning of aluminium-ammonium perchlorate engines is:

$$10Al + 6NH_4ClO_4 \rightarrow 4Al_2O_3 + 2AlCl_3 + 3N_2 + 12H_2O$$

Thus, generating high amounts of gasses (nitrogen and water vapour) which then escape the casing through the nozzle and propel the rocket upwards. Furthermore, the reaction is highly exothermic (comprised in the 100ºC-200ºC, alas, vaporizing the water), however the ammonium perchlorate decomposes in the 200-300ºC range (F.Siegmund, 1969), thus why none of the manufacturer’s casing surpasses said temperature.

Prior to ignition the fuel tends to be rather safe since it’s activation energy is rather high at

Thus, in the event of a misfire, another reaction needs to take place to avoid the designed reaction which releases huge amounts of gasses which might cause a deflagration.

The main problem lies in the aluminium’s high reactivity; thus, a more reactive metal is required, which according to literature (EdPlace, 2020) are the following:

- Potassium.
- Sodium.
- Calcium.
- Magnesium.

The main aim is to reduce the ammonium perchlorate with a hydroxide group to avoid generating any gases and thus avoid a lift-off after the launch is compromised.

Potassium hydroxide is highly toxic if inhaled and very corrosive according to the literature (New Jersey Department of Health, 2010).

Sodium hydroxide is extremely corrosive and irritating and as per the literature's description (Agency for Toxic Substances and Disease Registry, 2014) it can cause severe burns when it comes into contact with the skin.

Calcium hydroxide is commonly used in skin care and industrially and entails few risks (other than poisoning if eaten), thus it seems to be a safer option.

Finally, magnesium hydroxide is commonly used in fire retardants and a number of studies have not found it to be significantly toxic (National Research Council (US) Subcommittee on Flame-Retardant Chemicals., 2000).

Since, if there isn't a misfire the substance will take flight, the element with the best reactivity to weight correlation should be selected, and since both non-toxic options belong to the alkaline earth metals, with the lightest being magnesium, it will be employed (which has the added benefit of being a fire retardant, alas, if the kill system fails it will grant by-standers more time to evacuate the vicinity), therefore the neutralization reaction is:

$$Mg(OH)_2 + 2NH_4ClO_4 \rightarrow 2NH_3 + 2H_2O + MgCl_2O_8$$

Hence, avoiding the release of any gases other than ammonia.

Considering their molecular mass (having to assume a perfect reaction and no left-overs, whilst assuming the entire propellant to be the aluminium-ammonium perchlorate mixture) an over-estimation of each component can be calculated to later size the amount of magnesium hydroxide required:

$$X[10 * 26.9815 + 6 * (4 * 1.0079 + 14.0067 + 35.453 + 4 * 15.9994)] = m_{propellant}$$

All molecular masses were extracted from lenntech.com (Lenntech B.V., 2020)

For each motor:

	Engine		
	I218R	L1100	M650W
Propellant mass (g)	172.7	1346	3351
Aluminium mass (g)	47.804	372.579	927.573
ammonium perchlorate mass(g)	124.896	973.421	2423.427

Table 33 | Engine composition

The approximation is not too far off since typically, the propellant mixtures contain about 30% aluminium (slightly higher to the results obtained above).

Knowing the magnesium hydroxide reaction to be:

$$Mg[OH]_2 + 2NH_4ClO_4 \rightarrow 2NH_3 + Ca[ClO_4]_2 + 2H_2O$$

The available volume for the magnesium hydroxide container is:

$$V = \pi R^2 L \rightarrow V = \pi \left(100 * \frac{10^{-3}}{2}\right)^2 * 100 * 10^{-3} = 0.000785398 m^3 = 0.7854 dm^3$$

Alas, per 2 mols of ammonium perchlorate one mol of magnesium hydroxide will be needed:

	Engine		
	I218R	L1100	M650W
Ammonium perchlorate mass(g)	124.896	973.421	2423.427
Ammonium perchlorate mols (mol)	0.5315	4.1426	10.3134
Magnesium hydroxide concentration (mol/L)	0.6767	5.2745	13.1314

Table 34 | Magnesium hydroxide calculations

Therefore, the density of each solution can be calculated as well (from a volume of 1 m^3):

$$V_{Mg(OH)_2} = N \frac{mol}{dm^3} * \frac{10^3 dm^3}{1m^3} * 1m^3 * \frac{58.3197 * 10^{-3} kg}{1\ mol} * \frac{10^3 g}{1^3 kg} * \frac{1\ cm^3}{2.34 g} * \frac{1m^3}{10^6 cm^3}$$

$$V_{H_2O} = 1m^3 - V_{Mg(OH)_2}$$

$$\rho_{sol} = \frac{\rho_{H_2O} * V_{H_2O} + N \frac{mol}{dm^3} * \frac{10^3 dm^3}{1m^3} * 1m^3 * \frac{58.3197 * 10^{-3} kg}{1\ mol}}{1m^3}$$

	Engine		
	I218R	L1100	M650W
Magnesium hydroxide concentration (mol/L)	0.6767	5.2745	13.1314
Density solution (kg/m^3)	1020.924	1231.596	1437.405

Table 35 | Magnesium hydroxide concentration and density

Having characterized the fire-extinguishing fluid, now the hydraulic system can be sized accordingly.

The reservoir will implement 2 one-way (or stop check valve) valve to fill in the gap left by the magnesium hydroxide with air once the tank begins to empty so it can remain at atmospheric pressure and thus avoid the pressure in the tank dropping below the magnesium hydroxide's vapour pressure, which would not only damage the entire system but also release a potentially hazardous material for the rest of the launch vehicle.

Below the reservoir there will be 2 separate electronically controlled normally-closed valves which will implement an OR gate with redundancy (one at the outlet of each pump) since both will lead to a T-junction. Finally, after both stream coming from the pumps merge, they will be split into 3 nozzles to spray the interior of the engine and prevent the faulty reaction from taking place.

Hydrodynamic circuit

The pipes connecting the nozzles to the pumps can be modelled as (Avellan, 2017):

$$gH_{rv} = K_v \frac{C^2}{2} = \frac{\lambda L}{D} \frac{8Q^2}{\pi^2 D^4}$$

With:

$$\lambda = 8 \left[\left(\frac{8}{Re}\right)^{12} + \frac{1}{\left(\left(2.457 \ln \left(\frac{1}{\left(\frac{7}{Re}\right)^{0.9} + 0.27 \frac{k_s}{D}} \right) \right)^{16} + \left(\frac{37530}{Re}\right)^{16} \right)^{\frac{3}{2}}} \right]^{\frac{1}{12}}$$

Considering the information explained in the reference (EvanAndKatelyn, 2018) for a controlled, far reaching water jet is preferable to have a laminar flow, alas the maximum Reynold number in the system will be set at the laminar-fluent transition Re=2300.

Furthermore, the piper can be considered to be made out of PVC pipes (completely unreactive with the highly concentrated alkali), thus according to the literature (PipeFlow, 2020), it presents a roughness of $k_s = e = 0.0015mm$.

There are 2 main types of valves to consider, a butterfly valve or a spherical valve, in the literature (Avellan, 2017) however, the spherical valve is shown to have consistently lower loss coefficients (for small deviation angles):

Loss coefficient for a spherical valve										
Θ (º)	5	10	15	25	35	45	55	65		
K_v	0.05	0.29	0.75	3.1	9.7	31	110	490		
Loss coefficient for a butterfly valve										
Θ (º)	5	10	15	20	30	40	45	50	60	70
K_v	0.24	0.52	0.9	1.5	3.9	11	19	33	120	750

Table 36 | Valve Loss Coefficient

Alas, considering a perfect alignment is almost unattainable, for the calculations a K_v of 0.05 will be considered (spherical valve with Θ=5º), obtaining:

$$gH_{rv} = K_v \frac{C^2}{2} = 0.05 \frac{8Q^2}{\pi^2 D^4}$$

The Y-junction can be modelled following the version of Gardel's equation given in the literature (Vasava, 2007)for combining or dividing flow:

$$gH_{rv} = K_v \frac{C^2}{2} = K_{0,1} \frac{8Q^2}{\pi^2 D^4}$$

Such that:

$$K_{0,1} = \lambda_1 + (2\lambda_2 - \lambda_1)\left(\frac{V_1}{V_0}\right)^2 - 2\lambda_2\left(\frac{V_1}{V_0}\right)\cos\alpha'$$

Such that,

$$\lambda_1 = \begin{cases} 0.0712\alpha^{0.7141} + 0.37\ for\ \alpha < 22.5º \\ 1\ for\ \alpha \geq 22.5º \end{cases}$$

$$\lambda_2 = \begin{cases} 0.0592\alpha^{0.7029} + 0.37\ for\ \alpha < 22.5º \\ 0.9\ for\ \alpha \geq 22.5º \end{cases}$$

Where,

$$\alpha' = 1.41\alpha + 0.00594\alpha^2$$

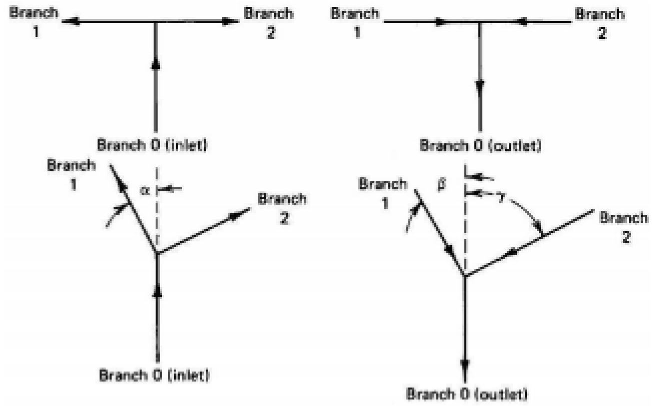

Figure 124 | Converging and diverging flows (Vasava, 2007)

As such, both junctions can be modelled with this formula, the merger coming from the pumps at an angle α=45º degrees and the 3-way-split with angles of 60º.

The energy loss at the elbows can be calculated as:

$$gH_{rv} = K_v\frac{C^2}{2} = \left[0.131 + 1.847\left(\frac{D}{2r}\right)^{3.5}\right]\frac{\theta}{90}\frac{8Q^2}{\pi^2 D^4}$$

Where, r stands for the elbow's radius.

Since the reservoir cannot be considered as an infinite body of water which's height never changes, the inlet into the pumps can be considered as a sudden contraction, hence, the charge loss can be calculated as (Avellan, 2017):

$$gH_{rv} = K_v\frac{C^2}{2} = \frac{1}{2}\left[1 - \frac{A_1}{A_2}\right]\frac{8Q^2}{\pi^2 D^4}$$

According to the literature, the energy loss at the nozzle is generally disregarded since K_v varies from 0.02 to 0.04, alas, for the calculations of the circuit the equation for the energy loss at any nozzle should be:

$$gH_{rv} = K_v\frac{C^2}{2} = 0.04\frac{8Q^2}{\pi^2 D^4}$$

However, since the system would only come into operation when there is a real possibility of the fuel damaging the rest of the vehicle, the systems needs to be over-dimensioned to ensure it will function, alas, following the explanations laid out in the reference (Avellan, 2017), the nozzle should be considered a sudden contraction to increase the calculated energy loss and thus ensure in reality the system will be able to perform up to standard, therefore, the formula describing the sudden contraction (as a stand in for the nozzle) as per the literature (Avellan, 2017):

$$gH_{rv} = K_v \frac{C^2}{2} = \frac{1}{2}\left[1 - \frac{A_1}{A_2}\right]\frac{8Q^2}{\pi^2 D^4}$$

Therefore, the equation governing the hydrodynamic circuit is (based on Bernoulli's equation), accounting for the height given by the pump:

$$\frac{Q^2}{2A_1^2} + gz_1 + \frac{P_1}{\rho} + H = \frac{Q^2}{2A_2^2} + gz_2 + \frac{P_2}{\rho} + E_r(Q)$$

Considering the base nozzle to be the reference height ($z_2 = 0$) and both the reservoir and the exit of the nozzle ought to be at atmospheric pressure ($P_1 = P_2$), the equation can be rewritten as:

$$\frac{Q^2}{2A_1^2} + gz_1 + H = \frac{Q^2}{2A_2^2} + E_r(Q)$$

Since the output velocity ought to be enough to reach the top of the biggest case, allowing for a casing wall of 10mm all around, thus needing to reach height of at least 791mm when exiting the nozzle at an angle tight enough to allow for the jet to reach the apex, alas:

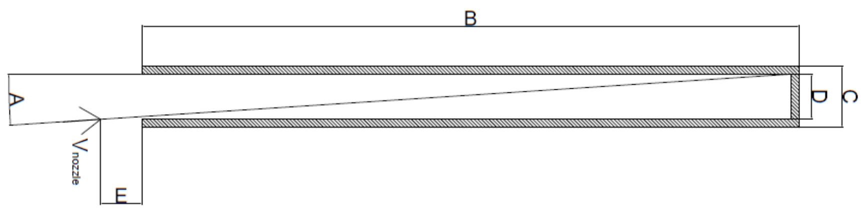

Figure 125 | Nozzle-fuel tube interaction

Dimension	Value
A	4.204º
B	801mm
C	75mm
D	55mm
E	50mm

Table 37| Casing nozzle values

Accepting the traditional equation for the displacement extracted from the speed and acceleration for a parabolic shot:

$$h = v_{nozzle\ vertical} t - \frac{1}{2} g t^2 | \ v_{nozzle\ vertical}$$
$$= v_{nozzle} \cos(4.204) = \frac{Q}{A_{nozzle}} cos(4.204)$$

Which can be re-written as:

$$0.751 = \frac{Q_{nozzle}}{A_{nozzle}} t * cos(4.204) - \frac{1}{2} g t^2$$

Ideally, the water should reach the top within a half a second of having left the nozzle, alas:

$$Q_{nozzle} = \left(0.751 + \frac{1}{2} g * 0.5^2\right) \frac{A_{nozzle}}{0.5 * \cos{(4.204)}}$$

Alas, to ensure the fluid reaches the top of the fuel compartment with ease a security factor ought to be in place, therefore:

$$Q_{nozzle} = 1.1Q = 1.1 \left(0.751 + \frac{1}{2} g * 0.5^2\right) \frac{A_{nozzle}}{0.5 * \cos{(4.204)}}$$

The nozzle will have an opening of 5mm in diameter, alas, the discharge of the system can be numerically determined:

$$Q_{nozzle} = 1.1 \left(0.751 + \frac{1}{2} g * 0.5^2\right) \frac{\pi * \frac{(5 * 10^{-3})^2}{4}}{0.5 * \cos{(4.204)}} = 8.56415 * 10^{-5} \frac{m^3}{s}$$

Since this is the discharge required by 1 nozzle, aiming for a redundancy of 3, the total discharge of the system will be:

$$Q_{system} = 3Q_{nozzle} \rightarrow Q_{system} = Q = 0.002567 \frac{m^3}{s} = 2.567 \frac{litres}{s}$$

Since the nozzle will have an inner diameter of of 5mm, the pipes will need to have a diameter of 10mm.

The losses in the system can thus be calculated:

Location	characteristics	K_v	Flow rate (m^3/s)	Energy loss (J)
Reservoir exit	$D_1 = 10mm$ $D_2 = 100mm$	0.495	$2.567 * 10^{-3}$	264.391
Valve	$\Theta = 5º$	0.05	$2.567 * 10^{-3}$	26.706
Y-junction	$\alpha = 45º$ $V_o = V_1$	1.349	$2.567 * 10^{-3}$	720.533
Triple-Split	$\alpha = 60º$ $V_o = 3V_1$ Present 3 times in the system	$3K_v = 3 * 1.254$	$\frac{2.567 * 10^{-3}}{3}$	223.264
Elbow	$\theta = 60º$ $D = 10mm$ $r = 20mm$ Present 3 times in the system	$3K_v = 3 * 0.0969$	$\frac{2.567 * 10^{-3}}{3}$	17.252
Pipe	$L = 0.9m$ $Re = 2300$ $K_s = 1.5E - 6m$ Present 3 times in the system	$3K_v = 3 * 2.776$	$\frac{2.567 * 10^{-3}}{3}$	494.243
Elbow	$\theta = 85.796º$ $D = 10mm$ $r = 20mm$ Present 3 times in the system	$3K_v = 3 * 0.1386$	$\frac{2.567 * 10^{-3}}{3}$	24.677
nozzle	$D_1 = 5mm$ $D_2 = 10mm$	$3K_v = 3 * 0.75$	$\frac{2.567 * 10^{-3}}{3}$	133.531
Total Energy loss				1904.597

Table 38| Energy loss calculations

Alas, the pump will need to add a power of:

$$\frac{Q^2}{2A_1^2} + gz_1 = 3\frac{Q^2/9}{2A_2^2} + E_r(Q) + H$$

Which, with numerical application:

$$\frac{(2.567 * 10^{-3})^2}{2 * \left(\frac{0.1^2\pi}{4}\right)^2} + g0.9 + H = 3\frac{(2.567 * 10^{-3})^2/9}{2 * \left(\frac{0.005^2\pi}{4}\right)^2} + 1904.597 \rightarrow H = 4.7444KJ$$

Finally, the pipe walls will need to have a thickness which will withstand the maximum pressure in the system (right after the pump), thus, assuming the entirety of the pump's energy was transformed into pressure:

$$\frac{P}{\rho} = H \rightarrow P = 4744.4 * 1437.405 = 6.82MPa$$

Applying the general formula to calculate the wall thickness (Vagnoni, 2019):

$$\frac{2e}{D} = \frac{P}{\sigma} \rightarrow e = \frac{PD}{2\sigma}$$

Knowing the elastic limit of the pipe PVC to be 90MPa (Vinidex by Aliaxis, 2020), and with a security coefficient of 1.1:

$$e_{min} = \frac{PD}{\frac{2\sigma}{1.1}} \rightarrow e_{min} = 0.417mm \rightarrow e_{pipe} = 1mm$$

Thrust plate design

They are meant to absorb the upwards force coming from the engine and distribute it along the rocket, therefore, they ought to withstand some of the biggest loads in the rocket.

To maintain the theme of the rocket, there are 3 thrust plates mounted on the motor retainer which is in turn glued to the engine bay tube.

They themselves ought to take the thrust of the engine, therefore, unlike the rest of the vehicle, only need to withstand a force of 20gm (with m being the rocket's 30kg) and as a security measure, 2 out of the 3 need to be able to withstand said force.

Sizing them so that 1 could take the entirety of the load would greatly increase the weight and therefore reduce both the maximum speed of the rocket and altitude whilst also lowering the centre of gravity and reducing the stability of the launch vehicle.

Alas, they were simulated (since due to their complex geometry they could not be accurately calculated) twice:

- Stand-Alone simulation (1 thrust plate taking a force of 3000N).
- Service simulation (3 thrust plates under a total force of 6000N).

The stand-alone simulations yielded:

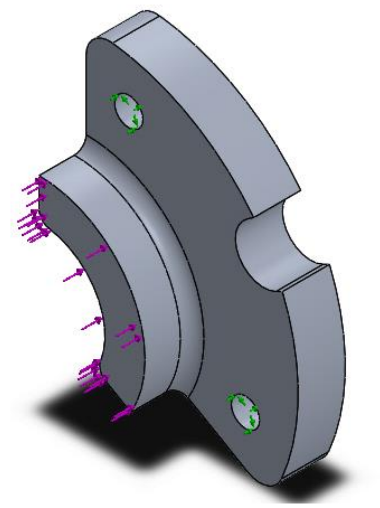

Figure 126 | Forces distribution stand-alone simulation

The force was applied along the lower part of the thrust plate and it had a total value of 3000N (evenly distributed along the surface), with 2 fixed cylinders where the M6 screws pass through to the coupler's thread.

The thrust plate, like most of the rocket’s disassemble parts was considered to be made out of Al 6063 T6 with a mesh consisting of 4 Jacobian points, 11320 nodes with 7067 individual cuves and a maximum aspect ratio of 3.6925 (with 99.8% of the cubes having an aspect ratio bigger than 3).

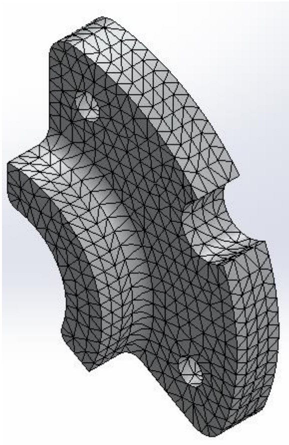

Figure 127 | Thrust plate mesh stand-alone simulation

The simulation showed the maximum stress did not surpass 15MPa, and it could be found in the live edges of the screw holes.

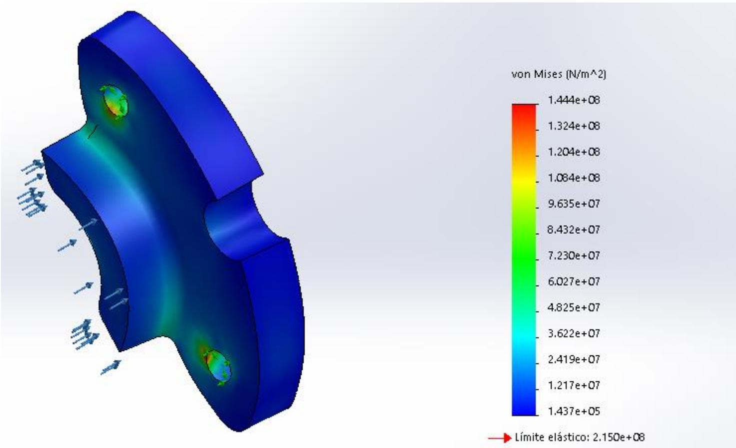

Figure 128 | Thrust plate stress distribution stand-alone simulation

Which paired with the equivalent unitary deformation analysis (with a maximum at 0.0012), which, was in turn used to validate the simulations:

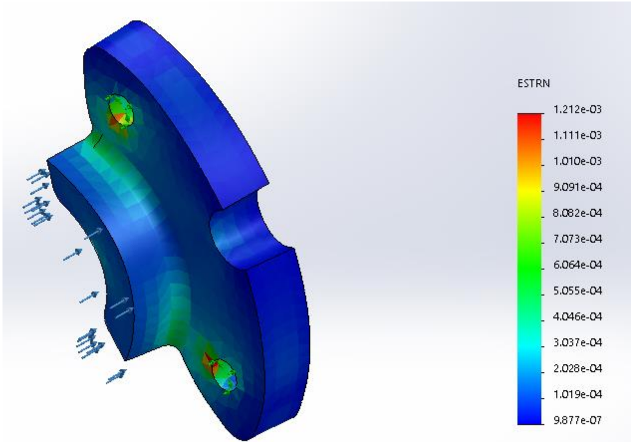

Figure 129 | Thrust plate unitary deformation stand-alone simulation

The real deformations could then be processed (with a maximum of 0.03mm):

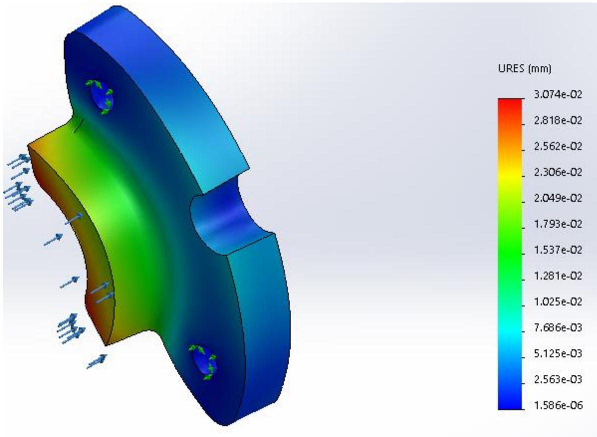

Figure 130 | Thrust plate deformations stand-alone simulation

To simulate the stress they will endure when flying 3 thrust plates have been assemble together in the same configuration as in flying procedures and a load of 6000N was applied distributed amongst all 3 surfaces which will be in contact with the engines.

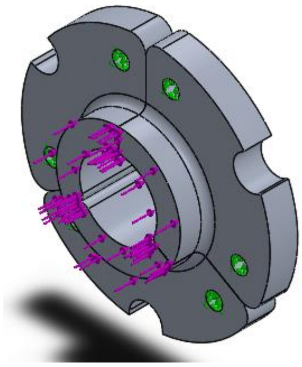

Figure 131 | Load distribution thrust plate service simulation

The force was applied along the lower part of the thrust plate and it had a total value of 6000N (evenly distributed along the surface), with 6 fixed cylinders where the M6 screws pass through to the coupler's thread.

The thrust plates, like most of the rocket's disassemble parts was considered to be made out of Al 6063 T6 with a mesh consisting of 4 Jacobian points, 13659 nodes with 8196 individual cuves and a maximum aspect ratio of 4.8942 (with 98.9% of the cubes having an aspect ratio bigger than 3).

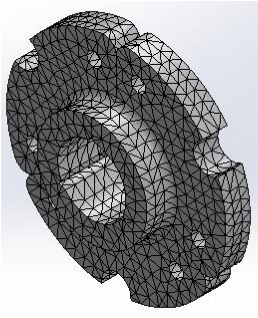

Figure 132 | Thrust plate mesh service simulation

The simulation showed the maximum stress did not surpass 5MPa, and it could be found in the live edges of the screw holes.

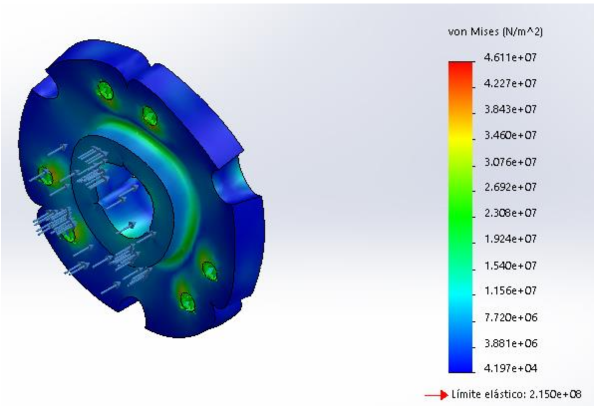

Figure 133 | Thrust plate stress distribution service simulation

Which paired with the equivalent unitary deformation analysis (with a maximum at 0.0004), which, was in turn used to validate the simulations:

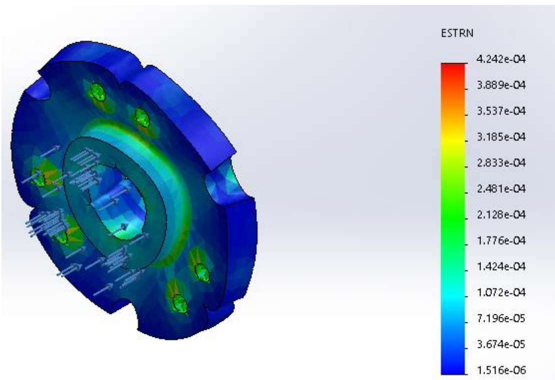

Figure 134 | Thrust plate unitary deformation service simulation

The real deformations could then be processed (with a maximum of 0.009mm):

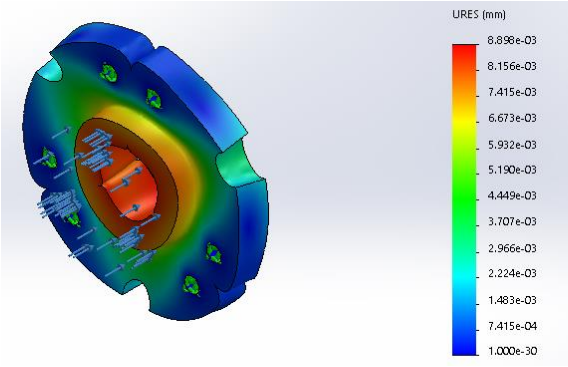

Figure 135 | Thrust plate deformations service simulation

Engine bay configuration

Right underneath the connectors the reservoir containing the magnesium hydroxide will be placed, to raise as much as possible the centre of gravity and thus augment the stability of the launch vehicle.

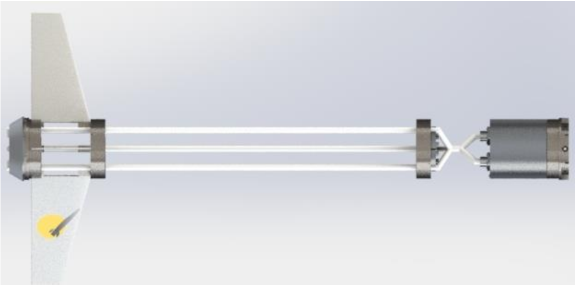

Figure 136 | Engine bay configuration

Since it'll have an external diameter of 120mm it can be directly glued into the tube and thanks to its height (much more than the coupler's gluing length) the load can be considered to be transferred safely to the structural part of the tubes.

Underneath, after having left enough space for the joints of the hydraulic system to merge and split again the thrust plates and their supporting structure can be found.

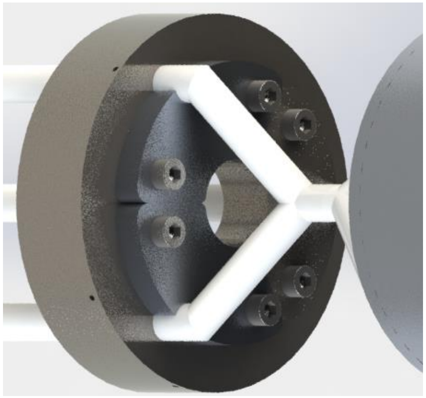

Figure 137 | Thrust Plate assembly details

The supporting structure is but an iteration of the couplers, alas, it's safe to assume that by maintaining the gluing length (24mm of height) the thrust from the engine will be safely transferred to the tube.

A similar technique is employed for the fin's supporting structure, where they are glued into an iteration of the coupleurs (maintaining the gluing length) which is in turn glued to the inside of the tube.

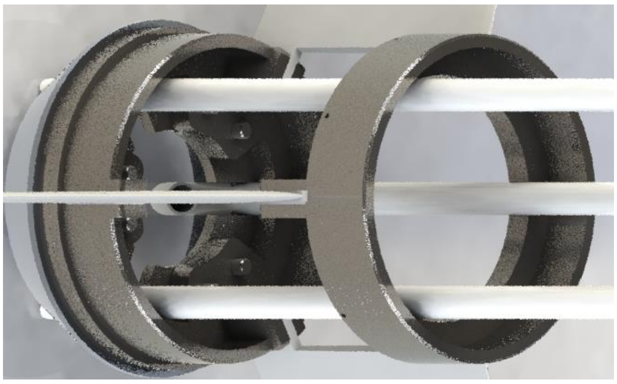

Figure 138 | Fins retainer assembly

Below the lower connector the tube cannot be considered to be structural since the tube is cut into 3 separate sections by the fin slots.

Boat tail

The boat tail can be optimized to reduce drag and guide the fluid lines around the rocket following the same geometrical or mathematical principles as the nosecone, however, it is a purely sacrificial piece hence it would not be reasonable to demand certain properties from a piece which will only fly once.

It would not be cost-effective to optimize said piece.

Similarly, since it's purely sacrificial (it's job is to absorb the impact upon landing) it's better to attach it with a glue than with any type of screws since there is a risk of them breaking and the thread getting stuck in the retainer.

Alas, it will be constructed out of a sheet of aluminium folded to resemble the section of a cone, welded to a flat aluminium ring.

Considering the welding principle which states that the maximum size of a weld ought to be:

$$a_{max} \leq 0.7t_{min}$$

And aiming for a weld of 2mm:

$$2 \leq 0.7t_{min} \rightarrow t_{min} \geq 2.85mm \rightarrow t = 3mm$$

Figure 139 | Boat tail assembly detail

Fins

The rockets normally only have 1 form of passive control, the fins.

When the rocket deviates from a perfectly vertical trajectory the wind acts on the exposed fin area, generating a torque on the rocket and re-aligning it vertically.

The fin size is directly related to the position of the centre of gravity, since they are the key component which determines the position of the centre of pressures, and as any object moving through a fluid, the centre of pressure (CP) ought to be below the centre of gravity (CG) to ensure a stable equilibrium (alas, ensuring the body will return to its default stage, flying vertically upwards for this particular case).

The standardized measure to characterize the resistance of a rocket to deviations during the flight which can be corrected by the fins is known as it's stability:

$$S = \frac{X}{D_{ext}} \; [-]$$

Where S is the distance between the centre of gravity and the centre of pressure (X in mm) normalized by the internal diameter (D_{int} in mm). The stability margins for rockets should be anywhere between 3 and 5, where anything below is too little (therefore the rocket will not be able to align itself after a disturbance) and anything above is too much (which implies the rockets impervious to the disturbance or resists it too much, alas loosing flight capability).

Furthermore, to lower the centre of pressures and therefore increase the stability, the fin size ought to increase, which in turn, increases drag and thus the effective range of the launch vehicle is reduced.

A first widely accepted approximation for the total fin area is (FxSolver, 2020):

$$A_{fins} = \frac{(d + 12.7)L}{6}$$

Where d stands for the external diameter in mm and L represents the length of the rocket.

Since the rocket is a 3-dimensional body in a 3-dimensional flow, although mostly uniaxial forces, disturbances can come from any angle, therefore the minimum number of fins required by any rocket is 3.

Generally, scratch built amateur rockets tend to have from 4 to 6 (mainly for aesthetics reasons) but the higher the fin number the bigger the drag, since, although the total cross section remains largely unchanged, the interactions outboard edge-fluid are largely disregarded since they are very complex to properly model, thus reducing the efficiency of the launch vehicle.

Therefore, following the recommendations listed in the literature (Nakka, Fins, 2001), the rocket will have 3 fins.

Therefore, a first approximation of the fins size for the rocket would be:

	Level 1	Level 2	Level 3
Length (mm)	2000	2500	3000
External Diameter (mm)	125		
$A_{fins}\ (mm^2)$	45900	57375	68850
$A_{fin}\ (mm^2)$	15300	19125	22950
Base height (mm)	120		
End Height (mm)	60		

Table 39|Fin size approximation

Knowing the fins will have a height equal to 120mm at the base (the internal diameter), the length can be characterized as a function of the height at the end of the fin (obtained from rewriting the formula for a trapezoidal area):

$$L_{fin} = \frac{D_{ext} + 12.7}{9(120 + h_{end})} L$$

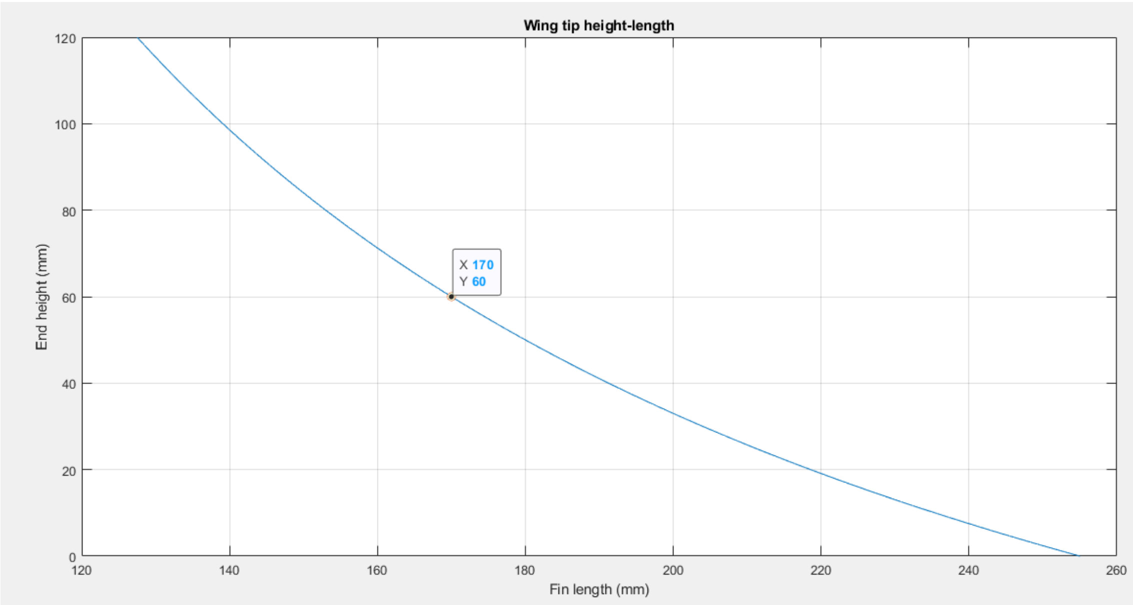

Figure 140 | End height-Fin length plot Level ·1

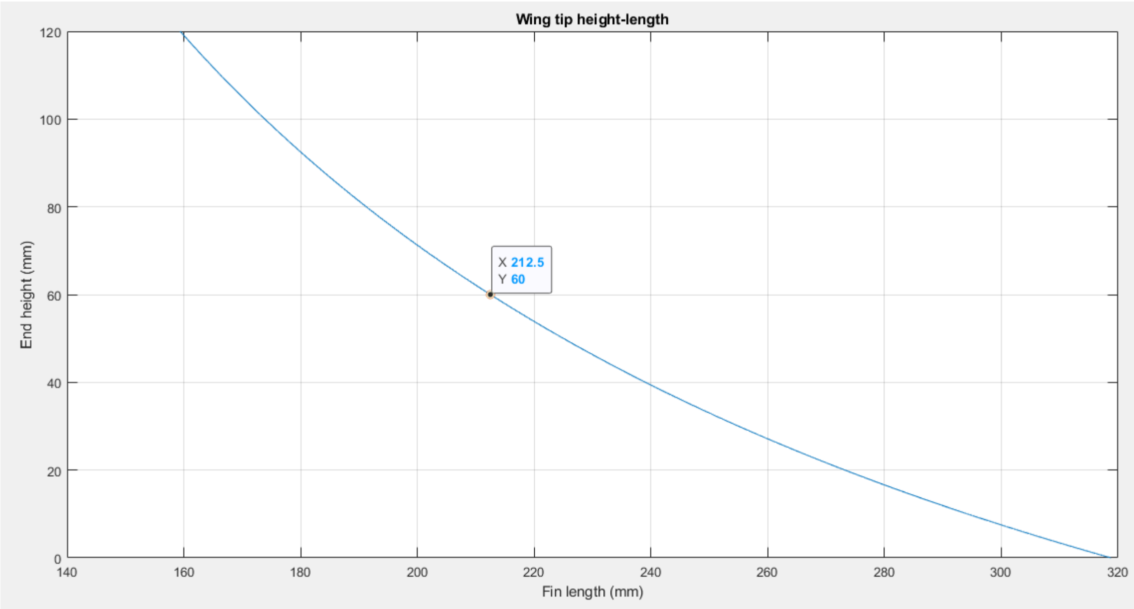

Figure 141 | End height-Fin length plot Level ·2

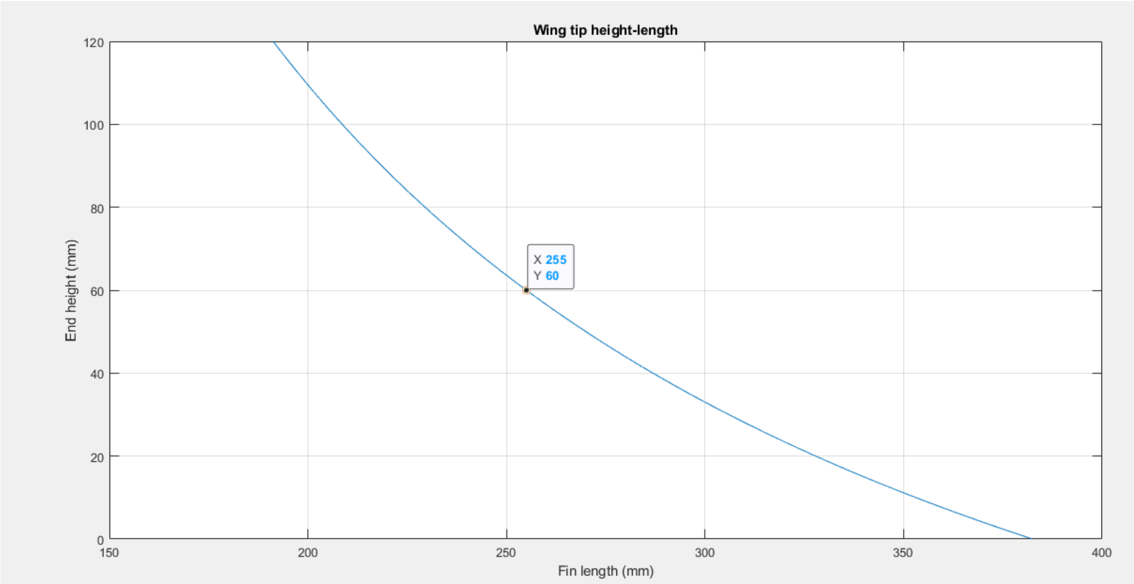

Figure 142 | End height-Fin length plot Level ·3

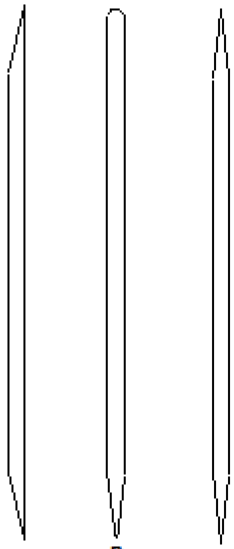

Figure 143|Fin cross-section (Nakka, Fins, 2001)

As seen in the figure above, there are largely 3 types of cross sections:

- A) Asymmetrical fins
- B) Subsonic fins
- C) Supersonic fins

Asymmetrical fins add a torsional moment to the rocket along it's main axis and cause it to rotate as it flies upwards, which not only does it add needless stress to the body of the rocket but it also reduces the effective height it can reach, since a significant portion of the energy outputted by the fuel mixture is diverted towards the rotation of the rocket.

Subsonic fins tend to be the most commonly used since most amateur rockets cannot overcome a Match number greater than 0.6. The generally consist of a rounded leading edge (to prevent flow separation) and a sharp trailing edge to reduce the drag coefficient, since a blunt trailing edge, although it allows for a good lift-weight ratio (hence why it's present in wings across the aeronautical industry) it greatly increases the drag coefficient, since, it generates an area of low pressures in the wake of the air foil which act on the rounded edge (Johnson, 2012).

However, since there is no need for lift in the rocket airfoil, a sharp trailing edge is preferred.

Subsonic flights can also have sharp leading edges but they are greatly affected by the inclusion of vortices in their calculations or not, as seen in the literature (Darden, 1987).

Supersonic flights have both a sharp leading and trailing edge since for Match numbers greater than 1 the behaviour of the fluid (air in this case) largely changes. A Sharp leading edge prevents the creation of a detached bow flow in front of the airfoil (Zucker, 2002).

To reduce drag the fins often present an airfoil shape, most commonly a NACA 4-digit airfoils, since they are already standardized:

$$NACA - XYZ$$

Where X (1 digit number, from 0 to 9%) stands for the maximum camber as a percentage of the cord length, Y (1 digit number, from 0 to 9), represents where the camber is located as a percentage of the cord length from the leading edge ($location = Y * 10\%$), finally Z (2 digit number, from 10 to 99) indicates the maximum thickness as a percentage of the cord length.

Since the rocket does not require any lift from the airfoils (it would cause a moment along the axis of the rocket and thus cause it to spin and lose effective height), the series NACA-00XX series will be employed (0 camber and the maximum camber, said camber being 0, can be found in the leading edge).

The formula for a NACA-00XX series profile is (Moran, 2003):

$$y_t = 5t\left[0.2969\sqrt{x} - 0.1260x - 0.3516x^2 + 0.2843x^3 - 0.1015x^4\right]$$

Where x is the position along the chord (from 0 to 100%), y_t is the half thickness at any given point x and t is the maximum thickness as a fraction of the chord.

It's worth noting that symmetrical 4-digit series have their maximum thickness at 30% of the cord from the leading edge and the trailing edge's thickness is not 0 (Moran, 2003):

$$y_t(x = 1) = 0.0105t$$

Furthermore, the leading edge can be approximated to a cylinder with a radius (Leishman, 2000):

$$r = \frac{1.1019t^2}{c}$$

Where c is the cord (position on the x-axis, from 0 to 100%).

Likewise, the trailing edge can be defined as either a straight edge or any other geometry, for simplicity, it will be considered a semi-circle (also to add some stiffness to the cross-section as previously described), therefore, the formula for the cross-section is:

$$y\begin{cases} 5t\left[0.2969\sqrt{\frac{x}{L}} - \frac{0.1260}{L}x - 0.3516\left(\frac{x}{L}\right)^2 + 0.2843\left(\frac{x}{L}\right)^3 - 0.1015\left(\frac{x}{L}\right)^4\right] & if\ x \le L \\ \sqrt{(0.0105t)^2 - (x-L)^2}\ if\ L \le x \le L + 0.0105t \end{cases}$$

The thickness will need to be determined by the resistance of the material selected (carbon fibre).

By considering a symmetrical thin NACA profile it is safe to assume the 2 main conclusions derived from the thin airfoil theory (Clancy, Aerodynamics, 1975):

- On a symmetrical thin airfoil the centre of pressures and the aerodynamic centre coincide at 25% of the cord from the leading edge (as a result, the centre of pressures does not change with the angle of attack).
- The lift coefficient for a symmetrical airfoil can be calculated as:

$$C_L = 2\pi\alpha$$

Where α is the angle of attack from the leading edge in radians.

The centre of gravity of the section can be calculated with the integral definition along the x axis, since it's symmetrical for y the coordinate y_G=0. Considering the formula:

$$x_G = \frac{\iint_A \; xdA}{\iint_A \; dA}$$

Where,

$$dA = 2y_t(x)dx$$

Thus, for the x coordinate:

$$x_G = \frac{\int_0^1 x * 2 * 5t\left[0.2969\sqrt{x} - 0.126x - 0.3516x^2 + 0.2843x^3 - 0.1015x^4\right]dx}{\int_0^1 2 * 5t\left[0.2969\sqrt{x} - 0.126x - 0.3516x^2 + 0.2843x^3 - 0.1015x^4\right]dx}$$

$$x_G = \frac{10t\left[\frac{0.2969 * 2}{5}x^{\frac{5}{2}} - \frac{0.126}{3}x^3 - \frac{0.3516}{4}x^4 + \frac{0.2843}{5}x^5 - \frac{0.1015}{6}x^6\right]_0^1}{10t\left[\frac{0.2969 * 2}{3}x^{\frac{3}{2}} - \frac{0.126}{2}x^2 - \frac{0.3516}{3}x^3 + \frac{0.2843}{4}\;x^4 - \frac{0.1015}{5}\;x^5\right]_0^1}$$
$$= 0.4204$$

Hence the centre of gravity of the section will be at:

$$\begin{pmatrix} x_G \\ y_G \end{pmatrix} = \begin{pmatrix} 0.4204 \\ 0 \end{pmatrix}$$

Its possible to calculate the moment of inertia of a section as well as a function of the thickness:

$$I_y^o = \iint_A x^2 dA = \int_0^L x^2 * 2 * y_t(x)dx = 10t * 1.58919 * 10^{-2} = t * 0.158919$$

$$I_x^o = \iint_A y^2 dA = \int_0^L x * 2 * [y_t(x)]^3\; dx = 250t^3 * 173037 * 10^{-4}$$
$$= t^3 * 4.32594 * 10^{-2}$$

Since when the rocket is skewed there will be a lift force generated in the fins, they will cause a wingtip vortex, which, in managed incorrectly could generate induced drag (Clancy, Aerodynamics, 1975), it is in essence unavoidable as the high pressure air from one side makes its way down the wing (or fin) and eventually mixes with the low pressure coming from the other side of the wing, but it can be managed.

A common practice is to employ wingtips (folding the trailing edge of the wing upwards or downwards) to prevent both flows from mixing so close to the airfoil, this is not applicable in this stance however since a wingtip would induce a spin in the rocket and thus reduce its efficiency whilst also subjecting the entirety of the structure to a centrifugal force.

In fighter planes and delta-shaped-wing planes attempt to reduce the pressure differential at the wingtip by reducing the cord length and thus the cross section of the wing as it increases in length (radially from the body of the vehicle).

Therefore, considering the cross-section of the fin to reduce linearly with the length of the fin:

$$t = t_o - z\frac{t_o - t_f}{L_{fin}} \rightarrow t = 4 - z\frac{3}{L_{fin}}$$

Implementing the equation found in the literature to calculate the aspect ratio in cylindrical coordinates (Spera, 2008):

$$\pi(R_t^2 - R_m^2) = \pi(R_m^2 - R_h^2)$$

Where R_t stand for the tip radius (in mm), R_m represents the mean radius (in mm) and R_h (in mm) represents the inner end of the airfoil (the external radius of the launch vehicle).

Therefore, the aspect ratio can be calculated as:

$$AR = \frac{2(R_t - R_h)}{cm}$$

Where cm stans for the cord length at the mean radius.

	Level 1	Level 2	Level 3
$R_t(mm)$	232.5	275	317.5
$R_h(mm)$	62.5		
$R_m\ (mm)$	170.238	199.413	228.815
cm	2.096	2.067	2.043
AR	162.196	205.601	249.590

Table 40 | Aspect Ratio per Level

Therefore, it is safe to accept the thin airfoil hypothesis.

Similarly the length of each section can be calculated as:

$$L = 120 - \frac{60}{L_{fin}}z$$

All fins will be considered to have an initial thickness of 4mm and a final thickness of 1mm, therefore, the centre of gravity of each fin will be:

	Level 1	Level 2	Level 3
X coordinate (mm)	71.82		
Y coordinate (mm)	0		
Z coordinate (mm)	68.73	85.92	103.1

Table 41 | Centre of gravity of each fin type

Therefore, the moment of inertia of each cross-section can be re-calculated as:

$$y\begin{cases} 5t(z)\left[0.2969\sqrt{\frac{x}{L(z)}}-\frac{0.1260}{L(z)}x-0.3516\left(\frac{x}{L(z)}\right)^2+0.2843\left(\frac{x}{L(z)}\right)^3-0.1015\left(\frac{x}{L(z)}\right)^4\right] \\ \quad if\ x\leq L(z) \\ \sqrt{(0.0105t(z))^2-(x-L(z))^2}\ if\ L(z)\leq x\leq L(z)+0.0105t(z) \end{cases}$$

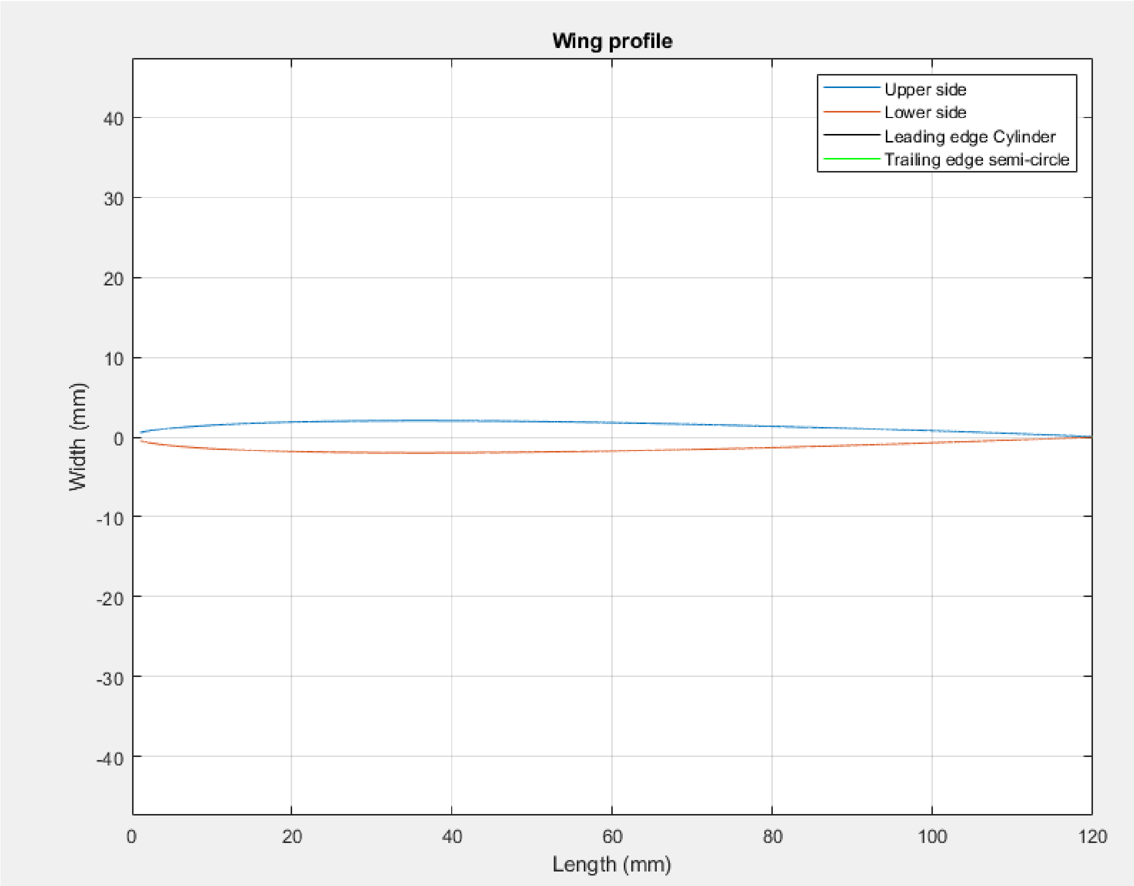

Figure 144 | Fin NACA cross-section

$$I_y^o=\iint_A x^2dA=\int_0^{L(z)}x^2*2*y_t(x,z)dx=0.4489190476*t(z)*[L(z)]^3mm^4$$

$$I_x^o=\iint_A y^2dA=\int_0^{L(z)}x*2*[y_t(x,z)]^3\,dx$$
$$=0.0432584113291[L(z)]^2*[t(z)]^3mm^4$$

Therefore, considering a distributed pressure (90g, 3mg) along the main axes, the stress distribution can be calculated:

$$\sigma\,(x,y)=-\frac{M_x}{W_x}+\frac{M_y}{W_y}\mid W_x=\frac{I_x}{\frac{t(z)}{2}},W_y=\frac{I_y}{\frac{L(z)}{2}},M_i=3mgz-\frac{3mgz^2}{2L_{fin}}$$

Hence, the distribution when the force is applied on each axis:

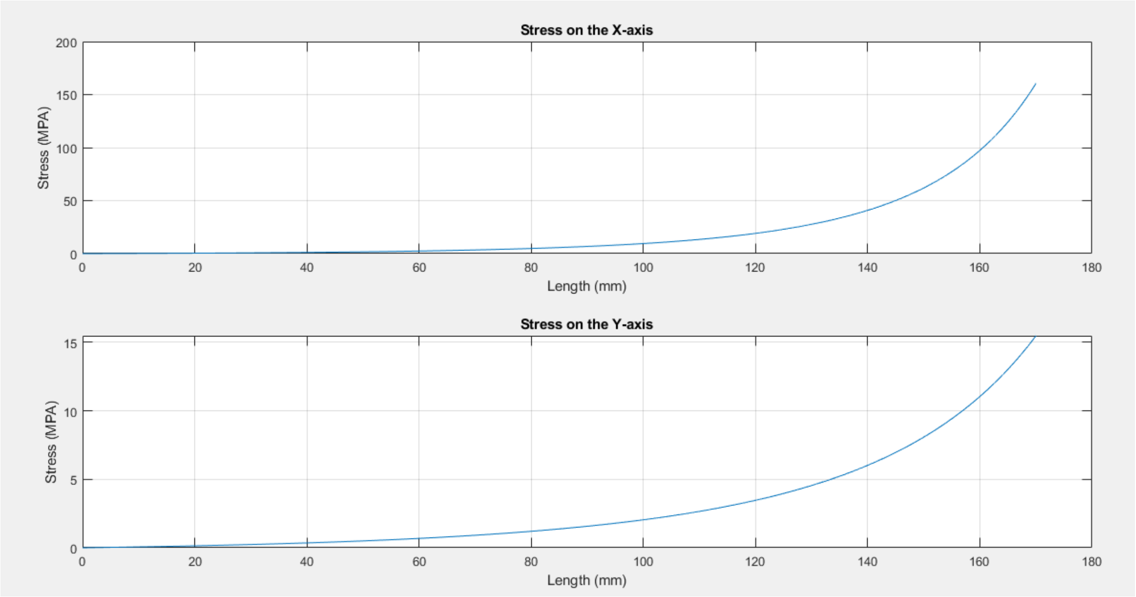

Figure 145 | Stress distribution on a Level 1 fin

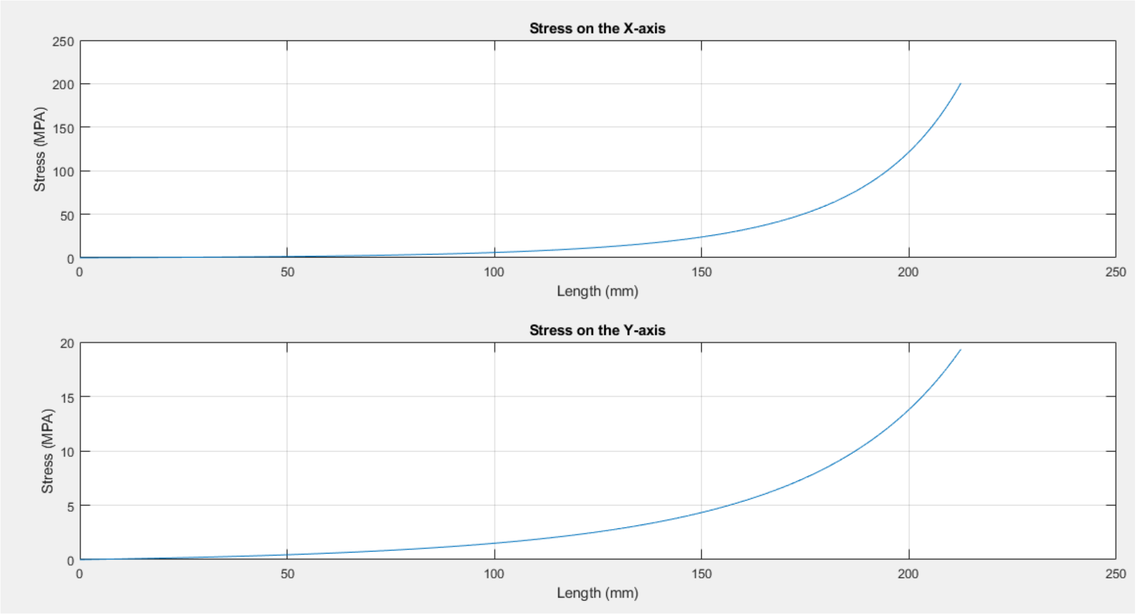

Figure 146 | Stress distribution in a Level 2 fin

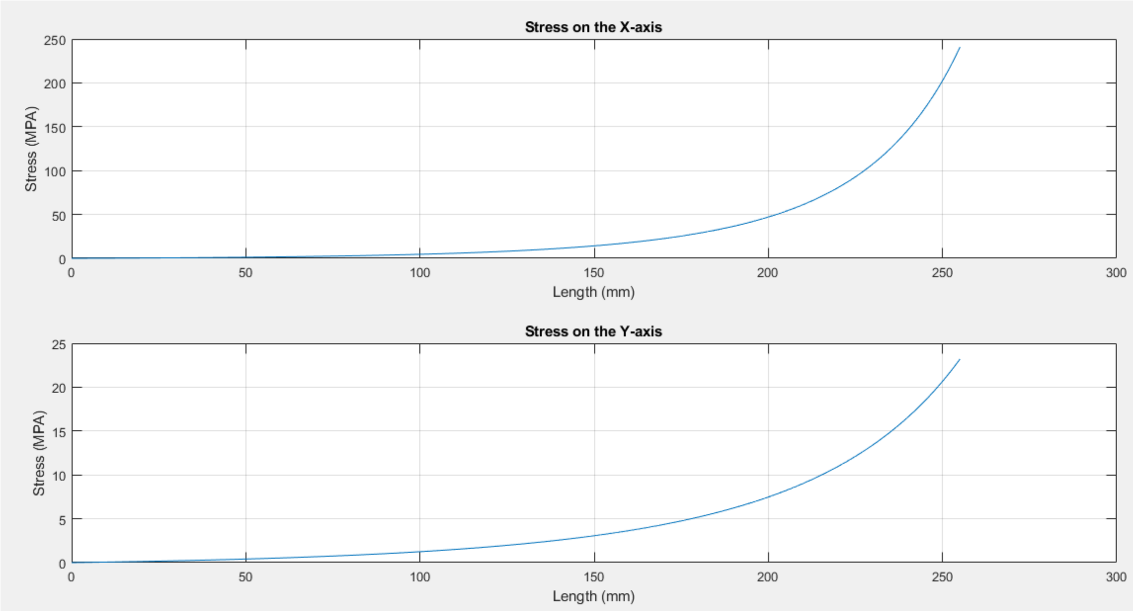

Figure 147 | Stress distribution on a Level 3 fin

All were considered to be under a distributed force of 90g, since it ensures the lower level fins are over-sized, which adds safety since they are smaller rockets and thus more sensible to perturbations, which implies the fins will always hold for all 3 levels.

	$\sigma_{x-MAX}\ (MPa)$	$\sigma_{y-MAX}\ (MPa)$
Level 1	160.5513	15.4711
Level 2	200.6892	19.3389
Level 3	240.8270	23.2067

Table 42 | Maximum Stress on the fins per axise

Composite materials must always be at a stress below it's proportionality limit, which can be described as (Princeton University, 2020):

$$\sigma_{yC} = \left[1 + \frac{V_f E_f}{V_m E_m}\right] V_m \sigma_{ym}$$

Where σ_{yC} represents the proportionality limit (in MPa); V_f stands for the percentage of reinforcement by weight (dimensionless); E_f is Young's modulus of the reinforcement (in GPa), V_m is the percentage of matrix by weight (dimensionless), E_m is Young's modulus of the matrix (in GPa) and σ_{ym} is the yield limit of the matrix (in GPa).

Following the data provided for glass fibre (AZO Materials, 2020) it can be characterized as:

$$E = 72 - 85\ GPa$$
$$Re = 2750 - 2850\ MPa$$
$$\rho = 2550 - 2600\,\frac{kg}{m^3}$$
$$\nu = 0.21 - 0.23$$

Likewise, the epoxy resin (Simmons ltd, 2020):

$$E = 10.5\ GPa$$

$$Ru = 85\ MPa$$

$\rho = 1100 - 1400\ kg/m^3$ (NetComposites, 2020)

$$\nu = 0.3 - 0.35$$

Since the limit obtained from the literature is the rupture limit, the elastic limit will be considered at 80% of the rupture, alas: $Re = 0.8 * 85 = 68MPa$

Therefore, the proportionality limit can be used (at 110% of the maximum service tension) to determine the percentages of each component required:

$$1.1 * \sigma_{MAX} = \left[1 + \frac{V_f * 72}{V_m 10.5}\right] V_m 68 \mid V_m + V_f = 1$$

Resulting in 6 different calculations (one for each stress present):

	$\sigma_{MAX}\ (MPa)$	V_m	V_f	Density (kg/m^3)
Level 1	15.4711	1	0	1400
	160.5513	0.811	0.189	1626.8
Level 2	19.3389	1	0	1400
	200.6892	0.753	0.247	1696.4
Level 3	23.2067	1	0	1400
	240.8270	0.703	0.297	1756.4

Table 43 | Composition percentages of each fin

As previously discussed, the wing tip vortices are inevitable, even though they are greatly reduced by reducing the cord, as such, the exit velocity of said vortex can be computed as (Larson, 1972):

$$w = \frac{\Gamma_o}{2\pi y}\left[0.16 + 0.16 \ln\left(3.91 \frac{\pi^2 b}{S} \frac{y}{\sqrt{\frac{0.0065Vbt}{S}}}\right)\right] \mid \Gamma_o = \frac{2C_L VS}{\pi b}$$

Where w is the vortex vertical velocity (m/s); Γ_o is the initial midspan vortex circulation (m^2/s); y is the width of the vortex (m); b represents the wingspan; S is the wing area (m^2), t is the vortex' age (s); V is the true air speed (m/s) and C_L is the lift coefficient.

Applying thin airfoil theory, the lift coefficient should be 0 since when the rocket is aligned with the flow the theory states it must be 0, however, for any other angle:

$$V = V_{rocket} \cos(\alpha)$$

$$C_L = 2\pi\alpha$$

Where α is the angle of attack (rad).

Therefore, the speed of the vortex at any given time is:

$$w = \frac{\alpha}{y}\frac{2V_{rocket}\cos(\alpha)\,A_{fins}}{\pi\left(2*L_{fin}+125\right)*10^{-3}}\left[0.16 + 0.16\ln\left(3.91\frac{\pi^2\left(2*L_{fin}+125\right)*10^{-3}}{A_{fins}}\frac{y}{\sqrt{\frac{0.0065V_{rocket}\cos(\alpha)\left(2*L_{fin}+125\right)*10^{-3}t}{A_{fins}}}}\right)\right]$$

For and angle of attack of up to 145 degrees, as per the literature (Sogukpinar, 2018)

The width of the vortex can be approximated as:

$$y = \frac{V_{rocket}\cos(\alpha)}{\tan(\beta)}t$$

Where β stands tor the equivalent cone angle of the vortex.

Considering a conservative approximation of said angle to be up to 30º, the main issue the vortex could present is if they collided with the boat tail of the launch vehicle, causing induced drag and unpredictable tilting in the rocket, thus enducing internal stresses for which the structure is not sized for, alas, the simplest solution is to ensure the vortex never come into contact with the rocket.

To guarantee this, the opening of the vortex should never meet at low speeds, where they are most likely to interact with the rocket and cause induced drag:, however, due to the length of the fins (minimum 170mm) it's completely avoided since by construction the lowest point of the rocket is less than 10cm from the end of the fins, alas, require a minimum cone angle of 60º, far greater than any vortex cone.

The 3D interactions of the fins with the fluid could not be computed due to computational limitations, alas, the constructions of the rocket is determined to avoid said vortex, however, it could be further optimized.

Finally, it's vital to avoid fluttering in the fins, since not only does it irreparably damage the control surfaces but it also renders them useless during flight, thus leaving the rocket without any means of control at all.

Figure 148 | Hydra Fins flutter

According to reference the fin's fluttering speed can be calculated as (Apogee components, 2011):

$$V_{flutter} = a\sqrt{\frac{G}{\frac{1.337AR^3P(1+\lambda)}{2(AR+2)\left(\frac{t_r}{c_r}\right)^3}}} \mid AR = \frac{L_{fin}^2}{A_{fin}}; \lambda = \frac{c_t}{c_r}$$

Where a is the speed of sound, G is the shear modulus in Pa, AR is the aspect ratio, c_t is the cord at the tip and c_r is the cord at the root and finally, t is the thickness at the root (since a higher thickness means a lower fluttering speed), therefore, for each in composition (with the cord at the root being 2mm and at the tip 0.5mm, along with a pressure of 101325Pa and the speed of sound at 330m/s):

	V_m, V_f	A_{fin} (mm^2)	L_{fin} (mm)	Shear Modulus(GPa)	Flutter Speed (m/s)	Avoided
Level 1	0.811;0.189	15300	170	8.334	22244.75	Yes
Level 2	0.753;0.247	19125	212.5	9.728	182108.67	Yes
Level 3	0.703;0.297	22950	255	10.943	154682.07	Yes

Table 44 | fins fluttering results

Alas, the fluttering is avoided since the rockets will never reach those speeds.

To the determine the gluing strength of the fins, the same commercially available glue (shear stress of 15MPa) will be considered, applied on all 4 face of the fins inserts into the tube:

$$F_{max} = 15 * 2 * [2 * 15 * 25] = 22500N > 30mg = 8899N$$

Considering that there is no axial contact between the fins and their supports, which would greatly reduce the efforts the glue joint would suffer, thus, adding structural security.

Rocket Overview

Level 1

The Level 1 Rocket is composed of:

Bay	Length (mm)	Weight (g)
Nosecone	625	1018
Recovery Single Event	250	5622
Avionics module	200	781
Payload bay	200	2064
Engine Bay	800	5535.03

Table 45 | Level 1 modules

Overall, the rocket has the following characteristics:

Weight (g)	Length (mm)	Internal Diameter (mm)	External Diameter (mm)	Centre of Gravity from the tip (mm)	Centre of pressures from the tip (mm)
15020.03	1875	120	125	1003	1069

Table 46 | Level 1 characteristics

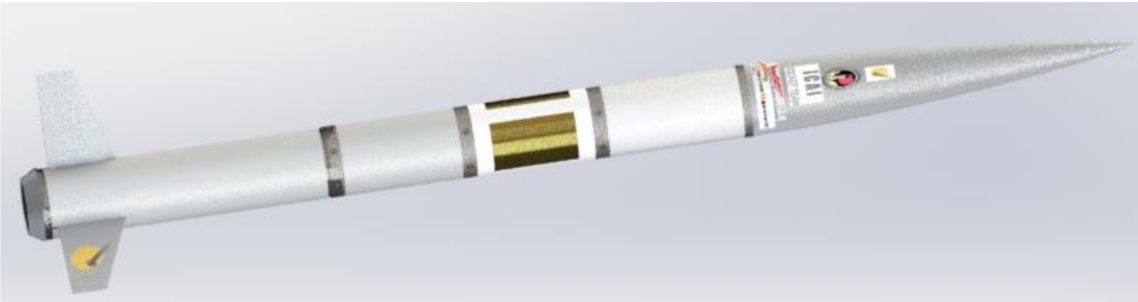

Figure 149 | Level 1 rocket assembly

Level 2

The Level 2 Rocket is composed of:

Bay	Length (mm)	Weight (g)
Nosecone	625	1018
Recovery Double Event	500	11729
Avionics module	200	781
Payload bay	200	2064
Engine Bay	1039.33	6612.84

Table 47 | Level 2 modules

Overall, the rocket has the following characteristics:

Weight (g)	Length (mm)	Internal Diameter (mm)	External Diameter (mm)	Centre of Gravity from the tip (mm)	Centre of pressures from the tip (mm)
22204.84	2114.33	120	125	13330	1690

Table 48 | Level 2 characteristics

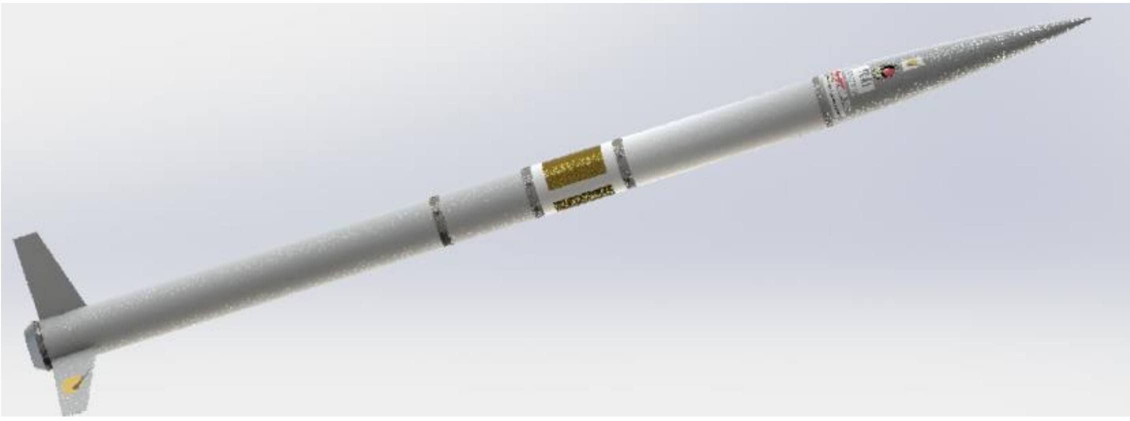

Figure 150 | Level 2 rocket assembly

Level 3

The Level 3 Rocket is composed of:

Bay	Length (mm)	Weight (g)
Nosecone	625	1018
Recovery Double Event	500	11729
Back up Single Event Recovery	250	5622
Avionics module	200	781
Payload bay	200	2064
Engine Bay	1109	7704.74

Table 49 | Level 3 modules

Overall, the rocket has the following characteristics:

Weight (g)	Length (mm)	Internal Diameter (mm)	External Diameter (mm)	Centre of Gravity from the tip (mm)	Centre of pressures from the tip (mm)
28918.74	2884	120	125	1530	2030

Table 50 | Level 3 characteristics

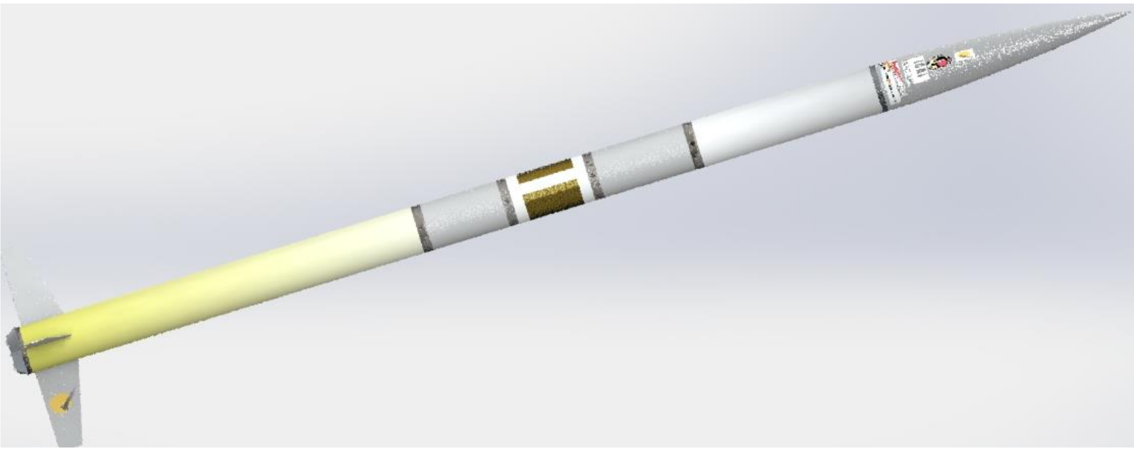

Figure 151 | Level 3 rocket assembly

Flight Simulations

For all simulations the recovery system was considered to be the Single Event (Even though both Level 2 and Level 3 mounted the Double Event as well) to maximize the acceleration suffered by the rocket upon the parachute's deployment.

Furthermore, it was considered to be a fuse burning recovery, rather than electronically driven since they are much slower to react and thus the rocket gains more speed as it's free falling for a longer period of time.

Moreover, it also resembles the worst-case scenario for all 3 levels, a slow to act recovery with a single parachute after free falling for longer than needed.

Level 1 rocket

With the Level 1 flight, the configuration was (with each module having it's appropriate length, centre of mass and moments of inertia):

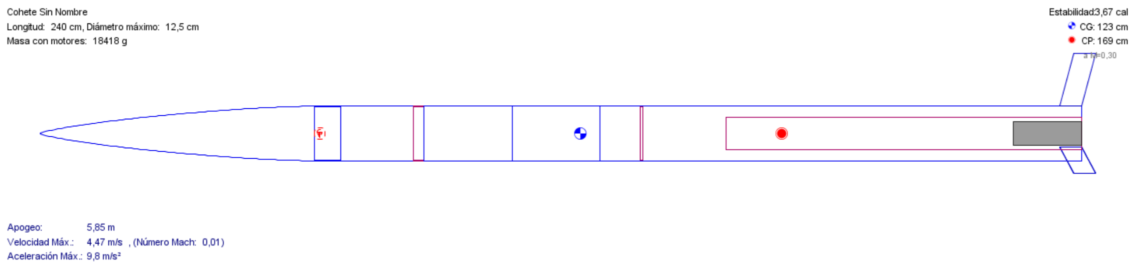

Figure 152 | Level 1 simulation configuration

It is easy to see the stability of the rocket is (as specified by the simulator):

$$S = 3.67$$

Which is rather within the acceptable range.

The flight simulations show:

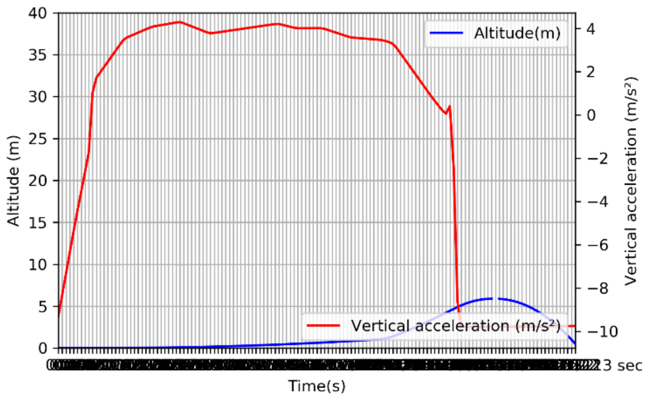

Figure 153 | Level 1 simulation results

The rocket barely lifts off (the apogee is at 5.85 m), clearly not enough to be considered a maiden flight and be awarded the Certification, this is due to the mass of the rocket, since Level 1 engines are targeted to 5kg, 1 meter long vehicles, if a lighter version is simulated (removing the avionics and payload modules, since at Level 1 only add dead weight):

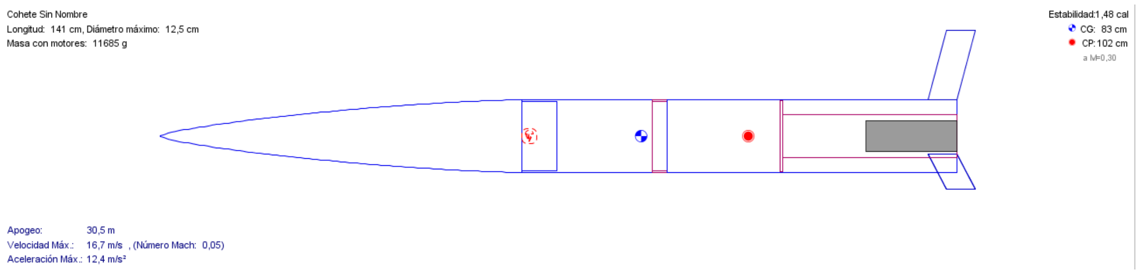

Figure 154 | Alternative Level 1 configuration

Where the stability is much smaller, at only 1.48, which is outside of what's considered safe, however, since the apogee is so low (30.5m) it's safe to fly, as corroborated by the simulation results:

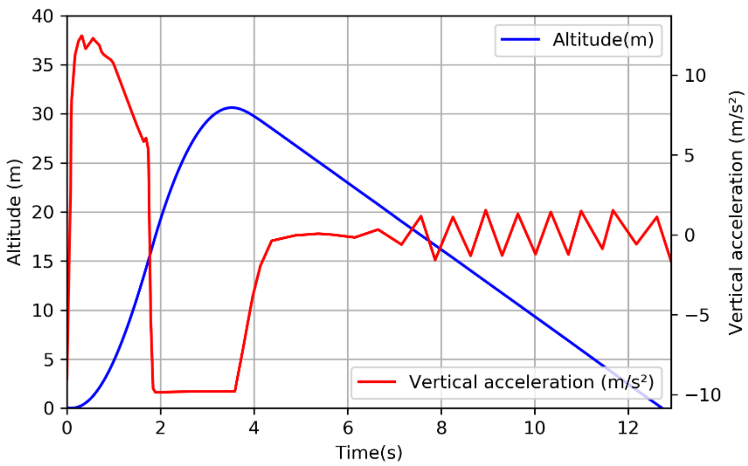

Figure 155 | Alternative Level 1 simulation

Where the apogee is high eneought to be considered an acceptable flight and thus be awarded the certificate. Furthermore, the maximum acceleration barely surmounts 1g, hence it's safely within the safety parameters and the lading speed is 3.97m/s, below the 5-4m/s which is considered to be a safe landing, overall it can be considered a successful flight.

Level 2 Rocket

The Level 2 flight required a different set-up:

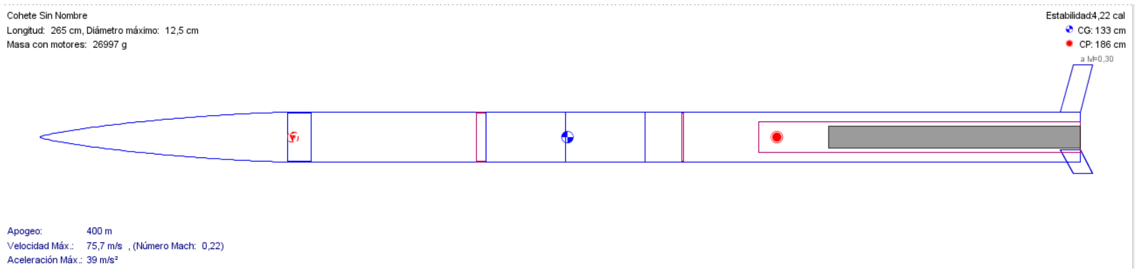

Figure 156 | Level 2 simulation configuration

As seen in the set up, the stability is 4.22, on the upper end of the acceptable range and the apogee is at 400m, with a maximum speed of 75.7m/s (Ma 0.22) and a maximum upwards acceleration of $39m/s^2$ (4g approximately, within design parameters). The flight development:

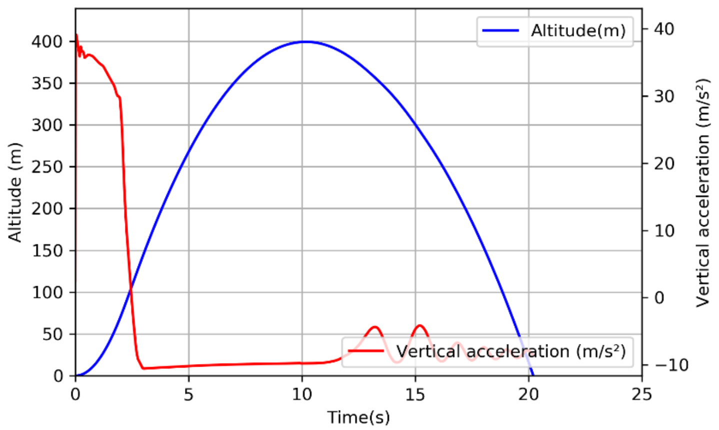

Figure 157 | Level 2 simulation results

With maximum acceleration between 4g and -1g, safely within the design parameters, and a touchdown speed of 4.4m/s (safe landing).

Level 3 Rocket

Finally, for the Level 3 flight, the set-up was:

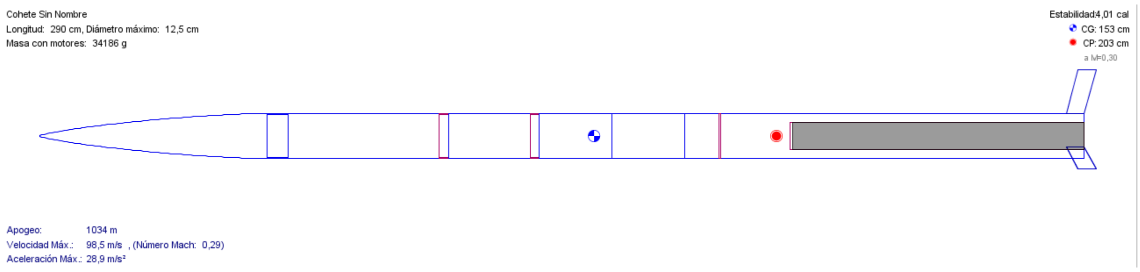

Figure 158 | Level 3 simulation configuration

With a stability of 4, safely within the acceptable parameters and an apogee at 1004m with a maximum upwards speed of 98.5m/s (Ma 0.29) and an upwards acceleration of $30m/s^2$ (3g approximately).

The flight resulted in:

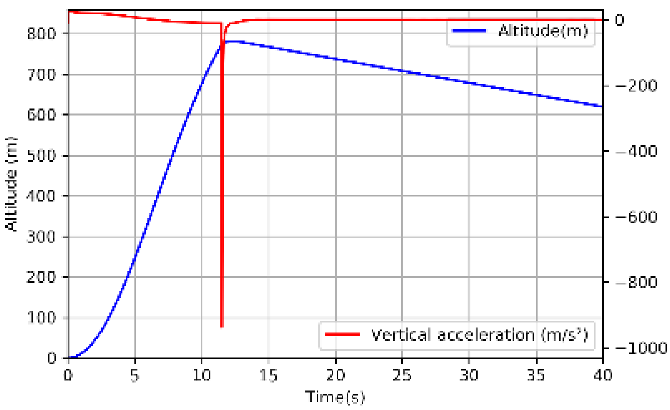

Figure 159 | Level 3 simulation results

Clearly, it's not a safe simulation since the maximum negative acceleration upon the parachute's deployment is 100g, far above the design limits.

Upon further study, it is not an outlier, but the genuine result from the simulation however, it cannot be considered to be the reality of the flight because, as previously explained, this considers a completely analogue recovery, far slower than an electronically driven one, such as the ones the rocket will have, however, the simulation does preserve a safe landing speed of 4.4m/s.

If the rocket is re-simulated, with an electronic recovery which is set to deploy the parachute after the apogee the results are:

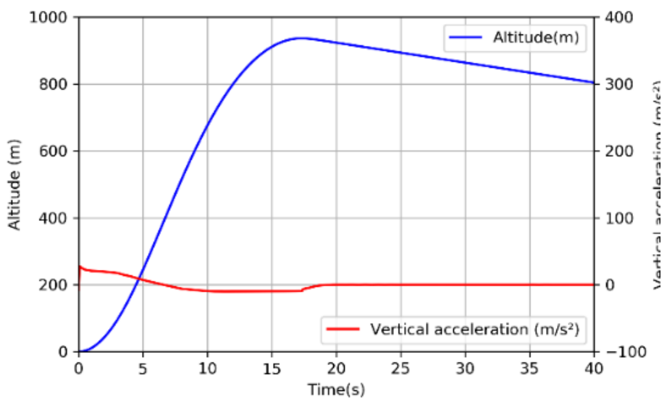

Figure 160 | Level 3 alternative simulation results

The forces experienced not only are they within safety margins, but the landing speed is maintained at 5.5m/s, thus bringing the rocket down safely.

Naming

The project name will be:

Home-built Miniaturized Jinxed Nautical Compartment Ship – Ohana

Or

HMJNCS-Ohana (for short)

Since all the components ought to perform together to bring the launch to fruition.

Millennium developments goals

The main sustainable development goal of this project is Objective 9: Industry, innovation and infrastructure, belonging to the economic area of said objectives.

Rocket science has pushed science forward ever since the Space Race started with the dawn of the 1950s, adding in the development of new technologies which we use nowadays such as LEDs and cochlear implants.

Hence, by contributing to this field we'll be indirectly promoting new technologies forward which in the near-future might improve the quality of living of the general population.

Furthermore, learning about the use of composite materials in a complex structure could aid in the development of better, stronger and lighter infrastructure for future projects, as transferable skills.

The promotion of amateur rocketry also indirectly aids the transportation sector and therefore promotes industry since it helps educate engineers whom may later go into said industries.

Furthermore, rocketry not only requires a heavy designing stage but a manufacturing stage which directly links into industry and infrastructure since quite often "jigs" need to be created to create certain piece which then turn out to be mock trials for definitive machinery whilst also teaching all those involved manufacturing techniques for a new set of materials which they may otherwise never experience.

Moreover, a sizable quantity of products which are commonly used today stem from rocketry such as the implementation of the gimbal in flight and the development of ogives which are nowadays even implemented in hydraulics turbomachinery.

A secondary motivation for this project is also Objective 13: Climate Action (Biosphere section), since air traffic released flights produced 915 million tonnes of CO_2 in 2019 (Air Transport Action Group, 2020), therefore any minor improvement in air transport could have a high turnover, greatly ameliorating the air's quality and reducing the emission of greenhouse gasses.

Rocketry also indirectly promotes space exploration which sorely needs the development of new eco-friendly technologies and improving waste management whilst also reducing the overall carbon footprint.

Finally Objective 4: Quality Education (under the Society section) could also be implemented, since, challenging students to design and build vehicles as complex as rockets could greatly encourage them to pursue further knowledge in STEM-related fields (Science, Technology, Engineering and Mathematics).

Modern education is also moving towards teaching more transferable skills such as problem solving and logical and stepped reasoning, which a building a rocket requires of, in unmeasurable quantities.

Outlook

Some of the possible projects which may stem from this one are:

- Full study and characterization of the adimensional numbers technique to deduce drag in the nosecones.
- Re-simulation of the tangent cross-section nosecone to determine the drag and whether or not it would be appropriate to mount it in the rocket.
- Design of a paraglider controlled by servos to obtain a controlled descent.
- Design of the electrical and electronic components of the rocket.
- Design of a scientific experiment to be mounted in the CanSat payload.
- Design and optimization of the lauch lugs and a supporting structure to present the rocket and carry out the launch.
- Integration in a ground structure of the mis-fire safety assembly to lighten the rockets and raise the centre of gravity, thus augmenting the stability of the vehicle.
- Development of the rocket's own fuel mixture (liquid or solid).
- To deploy the CanSat sometime mid ascension rather than at the apogee an airbrake system capable of correcting the trajectory of the rocket ought to be designed to counter act the fluid-structure interactions which might occur when the payload bay is opened.
- Refinement and full study of the composite material beams.
- Perform the external flow simulations on the rocket which could not be carried out in this project due to computational limitations.
- Refinement of the fins to cause condensation on the main axis of the wingtip vortex to later record it's trajectory and further study it.

References

Agency for Toxic Substances and Disease Registry. (2014). *Sodium Hydroxide.* Atlanta: CDC.

Aimmanee, S. (2017). *A Unified Analysis of Adhesive-Bonded Cylindrical Coupler Joints.* IntechOpen.

Air Transport Action Group. (2020). *Air Transport Action Group*. Retrieved from https://www.atag.org/facts-figures.html

Alen Space. (2020). *Alen Space*. Retrieved from ¿Qué es un nanosatélite?: https://alen.space/es/guia-basica-nanosatelites/

Apogee components. (2011). How to Calculate Fin Flutter Speed. *Peak of Flight Newsletter*, 6.

Apogee Rockets. (2011). *Peak of Flight Newsletter: issue 291.*

Avellan, P. F. (2017). Singular Specific Energy Losses. In P. F. Avellan, *MECHANICAL ENGINEERING MASTER COURSE HYDRAULIC TURBOMACHINES HANDOUT* (pp. 35-38). Lausanne: LMH.

AZO Materials. (2020). *E-glass fibre mechanical properties*. Retrieved from Azo Materials: https://www.azom.com/properties.aspx?ArticleID=764

baperry3. (2016, 04 21). *NASA*. Retrieved from Rocketology: NASA's Space Launch System: https://blogs.nasa.gov/Rocketology/tag/ammonium-perchlorate/

Brohm, J. (2009). *The Mathematics of Flat Parachutes.* National Association of Rocketry.

California Polytechnic State University. (2014). *CubeSat Design Specification REV13.*

Castro Composites. (2020). *Fibra de vidrio unidireccional*. Retrieved from Castro Composites: https://www.castrocompositesshop.com/es/79-unidireccionales-ud

Clancy, L. (1975). Aerodynamics. In L. Clancy, *Aerodynamics* (p. Section 8). London: Pitman Publishing Limited.

Clancy, L. (1975). *Aerodynamics.* London: Ptman Publishing Limited.

Culp, R. (2008). *Parachute Descent Calculations*. Retrieved from http://www.rocketmime.com/rockets/descent.html

Darden, H. W. (1987). *NASA Technical Paper 2653: Applicability of Linearized-Theory Attached Flow Methods to Design and Analysis of Flap Systems at Low Speeds for Thin Swept Wings with Sharp Leading Edges.* Hampton: NASA.

Department of Defence, United States of America. (1996). *Design of Erodynamically Stabilized Free Rockets MIL-HDBK-762(MI).*

Devijver, P. A. (1982). *Pattern Recognition: A Statistical Approach.* London: Prentice-Hall.

EdPlace. (2020). *Reactivity Series*. Retrieved from EdPlace: https://www.edplace.com/worksheet_info/science/keystage3/year9/topic/955/3102/reactivity-series

European Space Agency. (2020). *European Space Agency-Education*. Retrieved from What is a CanSat?: https://www.esa.int/Education/CanSat/What_is_a_CanSat

European Space Agency. (n.d.). *Teach with space- Design your own parachute | T10.*

EvanAndKatelyn. (2018, 07 2). *EvanAndKatelyn.* Retrieved from DIY Super Soaker vs. Store Bought (& How We Made It!): https://www.youtube.com/watch?v=w1PFRmOCiDU

F.Siegmund, A. a. (1969). Thermal decomposition of ammonium perchlorate. *Chemical Society Quaterly Reviews, Issue 3*, 430-452.

Fastenings. (2020). *Thread Geometry-Metric Coarse*. Retrieved from Fastenings: https://www.trfastenings.com/products/knowledgebase/thread-geometry/metric-coarse-standard

Filho, L. d. (2019). CFD analysis of drag force for different nose cone design. *CFD analysis of drag force for different nose cone design* (p. 4). Lagoa Nova: Universidade Federal do Rio Grande do Norte.

Fruity Chutes Inc. (2019). *Fruity Chutes*. Retrieved from How we make our parachutes: https://fruitychutes.com/help_for_parachutes/how_to_make_a_parachute.htm

FxSolver. (2020). *FxSolver*. Retrieved from Fin area on a rocket: https://www.fxsolver.com/browse/formulas/Fin+Area+on+a+Rocket

Haack, W. (1941). *Geschoßformen kleinsten Wellenwiderstandes.* Bericht 139 der Lilienthal-Gesellschaft.

International Standard Atmosphere. (n.d.). *Air pressure as a function of altitude, considering the universal gas constant.*

Ira H. Abbott, A. E. (1945). *report No. 824: Summary of Airfoil Data.* National Advisory Commitee for Aeronautics.

Johnson, A. C. (2012, 08 5). *Rounded or sharp trailing edge?* Retrieved from http://claesjohnson.blogspot.com/: http://claesjohnson.blogspot.com/2012/08/rounded-or-sharp-trailing-edge.html#:~:text=Blunt%20trailing%20edge%20airfoils%20are,lift%20to%20structural%20weight%20ratio.

KHK Gears. (n.d.). *khkgears*. Retrieved from Gear Design: https://khkgears.net/new/gear_knowledge/gear_technical_reference/calculation_gear_dimensions.html

Larson, G. H. (1972). *A flight evaluation of methods for predicting vortex wake effects on trailing aircraft.* California: Flight Research Centre, National Aeronautics and Space Administration.

Leishman, G. J. (2000). Principles of Helicopter Aerodynamics. In G. J. Leishman, *Principles of Helicopter Aerodynamics* (p. 361). Maryland.

Lenntech B.V. (2020). *Chemical elements listed by atomic mass*. Retrieved from Lenntech: https://www.lenntech.com/periodic/mass/atomic-mass.htm

Moran, J. (2003). *An Introduction to Theoretical and Computational Aerodynamics.* Chemsford: WileyCourier Corporation.

Nakka, R. (2001, 08 01). *Fins*. Retrieved from Richard Nakka's Experimental Rocketry Web Site: https://www.nakka-rocketry.net/fins.html

Nakka, R. (2017, 10 25). *Richard Nakka's Experimental Rocketry Web Site*. Retrieved from Potassium Nitrate/Sucrose Propellant (KNSU): https://www.nakka-rocketry.net/sucrose.html

NAR Official Certification Laboratory. (2006). *High Power Rocket Engine Testing Report: AMW L1100.* National Association of Rocketry.

National Aeronautics and Space Administration. (2017). *CubeSat 101: Basic Concepts and processes for first-time CubeSat developers.*

National Association of Rockertry. (2007). *High Power Rocket Motor.* National Association of Rockertry .

National Association of Rocketry. (2001). *Aerotech I218 Certificate.* National Association of Rocketry.

National Association of Rocketry. (2004). *HIGH POWER ROCKET ENGINE TESTING REPORT AMW L1100.* NAR OFFICIAL CERTIFICATION LABORATORY.

National Fire Protection Association 1122: Code for Model Rocketry. (2018). United States of America.

National Research Council (US) Subcommittee on Flame-Retardant Chemicals. (2000). *Toxicological Risk of Selected Flame-Retardant Chemicals.* Washington D.C.: National Academic Press.

NetComposites. (2020). *Resin Formula Calculator*. Retrieved from Net Composites: https://netcomposites.com/calculator/resin-formula-calculator/

New Jersey Department of Health. (2010). *Hazardous Substance Fact Sheet: Potassium hydroxide.*

Nussbaumer, A. (2015). Torsion Uniforme. In R. B. Manfred A. Hirt, *Génie Civil de l'Ecole polytechnique fédérale de Lausanne Volume 10: Construction Métallique* (pp. 109-117). Lausanne: Presse polytechniques et universitaires romandes.

Parneix, M. G. (2010). High electromagnetic shielding effectiveness of hybrid glass/carbon composite laminate. *International Symposium on Electromagnetic Compatibility* (p. 6). Fort Lauderdale: IEEE.

PipeFlow. (2020). *PipeFlow.com*. Retrieved from Pipe Roughness: https://www.pipeflow.com/pipe-pressure-drop-calculations/pipe-roughness#:~:text=The%20roughness%20of%20a%20pipe,mm%20for%20rough%20concrete%20pipes.

Princeton University. (2020). *Princeton University*. Retrieved from Princeton University: https://www.princeton.edu/~maelabs/mae324/11/11mae_21.htm

Rocketry, A. (2020). *AeroTech Rocketry*. Retrieved from FAQ: http://www.aerotech-rocketry.com/faq.aspx

Rudy, J. (2013). *py-earth*. Retrieved from scikit-learn.org: https://contrib.scikit-learn.org/py-earth/content.html

Senthiil, A. Y. (2018). Nose Cone Design and Analysis of an Avion. *International Journal of Applied Mathematics Volume 119*.

Simmons ltd. (2020). Retrieved from Material Properties: https://epoxyworktops.com/epoxy-resin/material-properties/

Small Business Innovation Research. (2020). *Small Business Innovation Research-Small Business Technology Transfer*. Retrieved from Lightweight Material for Full-Scale Parachutes: https://www.sbir.gov/content/lightweight-material-full-scale-parachutes

Sogukpinar, H. (2018). Numerical Calculation of Wind Tip Vortex Formation for Different Wingtip devices. *Aerospace Europe CEAS 2017 Conference* (pp. 167-176). Bucharest: Aerospace Europe CEAS 2017 Conference.

Soubielle, D. S. (2020). Transmission à courroies I. *ME-202 Systèmes Mécaniques* (p. 38). Lausanne: EPFL.

Soubielle, D. S. (2020). Transmission par courroies. *ME-202 Systèmes Mécaniques* (p. 20). Lausanne: EPFL.

Soubielle, D. S. (2020). Transmissions à courroies III. *ME-202 Systèmes Mécaniques* (p. 31). Lausanne: EPFL.

Spera, D. A. (2008). *NASA/CR-2008-215434 Models of Lift and Drag Coefficients of Stalled and Unstalled Airfoils in Wind Turbines and Wind Tunnels.* Cleveland: Jacobs Engineering Group.

Sr., G. A. (1996). *The Descriptive Geometry of Nose Cones.*

Stroick, G. (2011). *Nose Cone and Fin Optimization.* Minnesota: Tripoli Minnesota.

Stroick, G. (2011). *Nose Cone and Fin Optimization.* Minessota: Tripoli Minessota.

Tribonet. (2020). *Frictions coefficient table of solid lubricants, metals, plastics and anti-friction materials*. Retrieved from Tribonet: https://www.tribonet.org/wiki/friction-coefficients-in-atmosphere-and-vacuum/

Tripoli Rocketry Association. (2020). *Tripoli Rocketry Association*. Retrieved from Level 1 Certification: http://www.tripoli.org/Level1

Tripoli Rocketry Association. (2020). *Tripoli Rocketry Association*. Retrieved from Level 2 Certification: http://www.tripoli.org/Level2

Tripoli Rocketry Association. (2020). *Tripoli Rocketry Association*. Retrieved from Level 3 Certification: http://www.tripoli.org/Level3

Vagnoni, F. A. (2019). *Specific Energy Losses Exercises.* Lausanne: Laboratoire de machines hydrauliques.

Vasava, P. R. (2007). 5.1 Dividing Flows. In P. R. Vasava, *Fluid Flow in T-Junction of Pipes* (pp. 45-50). Lappeenranta: LAPPEENRANTA UNIVERSITY OF TECHNOLOGY.

Vinidex by Aliaxis. (2020). *PVC properties*. Retrieved from Vinidex by Aliaxis: https://www.vinidex.com.au/technical-resources/material-properties/pvc-properties/

Westra, L. (2020). *Sizing a Parachute*. Retrieved from Sizing a Parachute: https://www.webpages.uidaho.edu/dl2/on_target/tv.htm

Zucker, R. &. (2002). Fundamentals of Gas Dynamics. In R. &. Zucker, *Fundamentals of Gas Dynamics* (pp. 226-229). John Wiley & Sons, Inc.

DOCUMENT 2: BLUEPRINTS

Note

Since ICAI Rocket Team does not yet have their own template for blueprints and this document will form the basis for their rocket at the SpacePort America Cup all the blueprints have been done following the ISO requirements

Rundown

This document contains the blueprints for:

- Overall Level 1 Rocket
- Overall Level 2 Rocket
- Overall Level 3 Rocket
- Modular connector
- Nosecone assembly
    - Respective pieces
- Recovery bay assembly
    - Both Single and Double event with their respective pieces
- Avionics/Payload bay assembly
    - Respective pieces
- Engine bay assembly
    - All 3 levels and their respective pieces

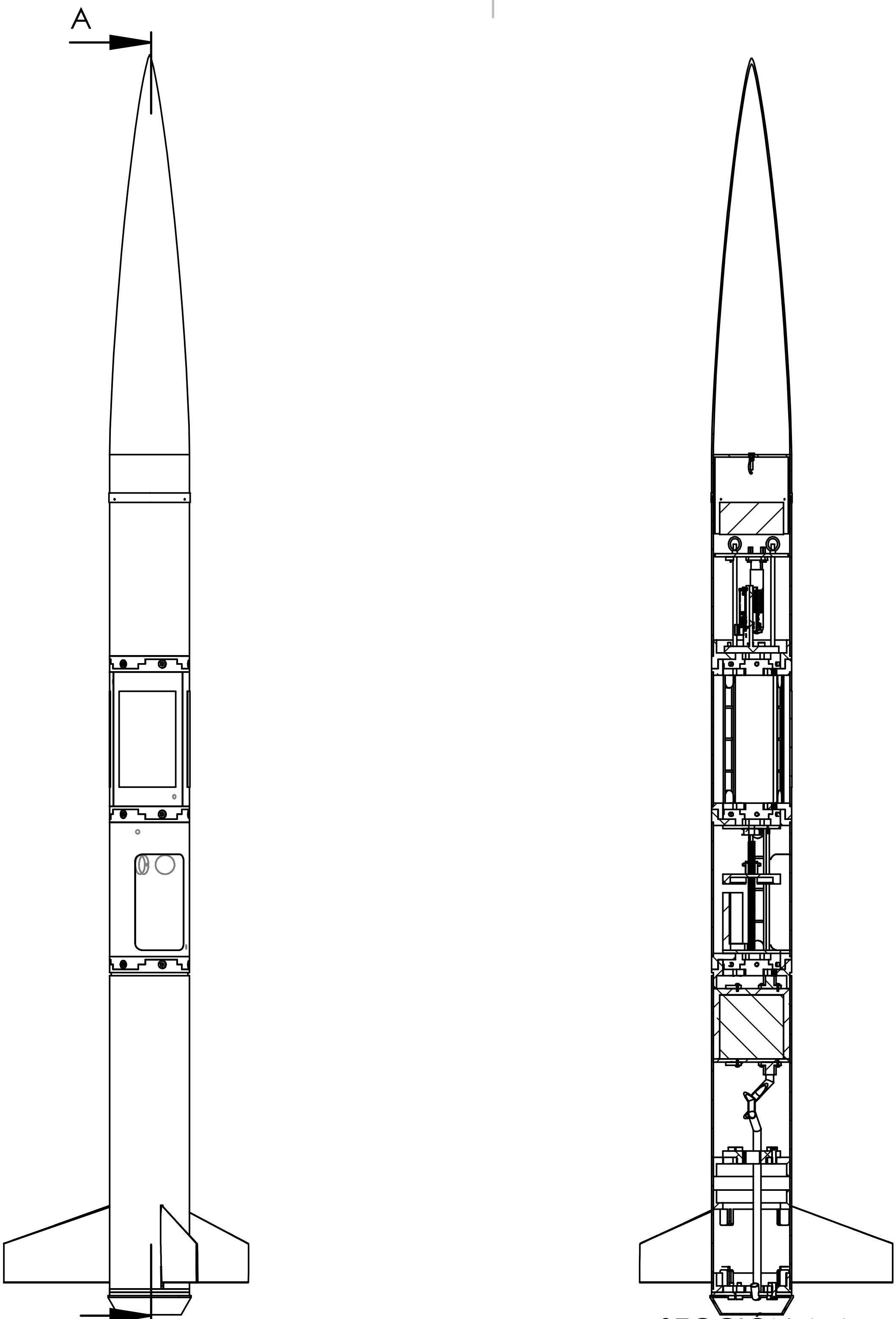

SECCIÓN A-A
ESCALA 1 : 10

SI NO SE INDICA LO CONTRARIO:
LAS COTAS SE EXPRESAN EN MM
ACABADO SUPERFICIAL:
TOLERANCIAS:
LINEAL:
ANGULAR:

ACABADO:

REBARBAR Y ROMPER ARISTAS VIVAS

NO CAMBIE LA ESCALA

REVISIÓN

	NOMBRE	FIRMA	FECHA
DIBUJ.	I.V.R.		05/07
VERIF.			
APROB.			
FABR.			
CALID.			

TÍTULO:

HMJNCS-Ohana

MATERIAL:

N.º DE DIBUJO

ST_Assembly Lv1

A4

PESO: 15020.03g

ESCALA:1:20

HOJA 1 DE 1

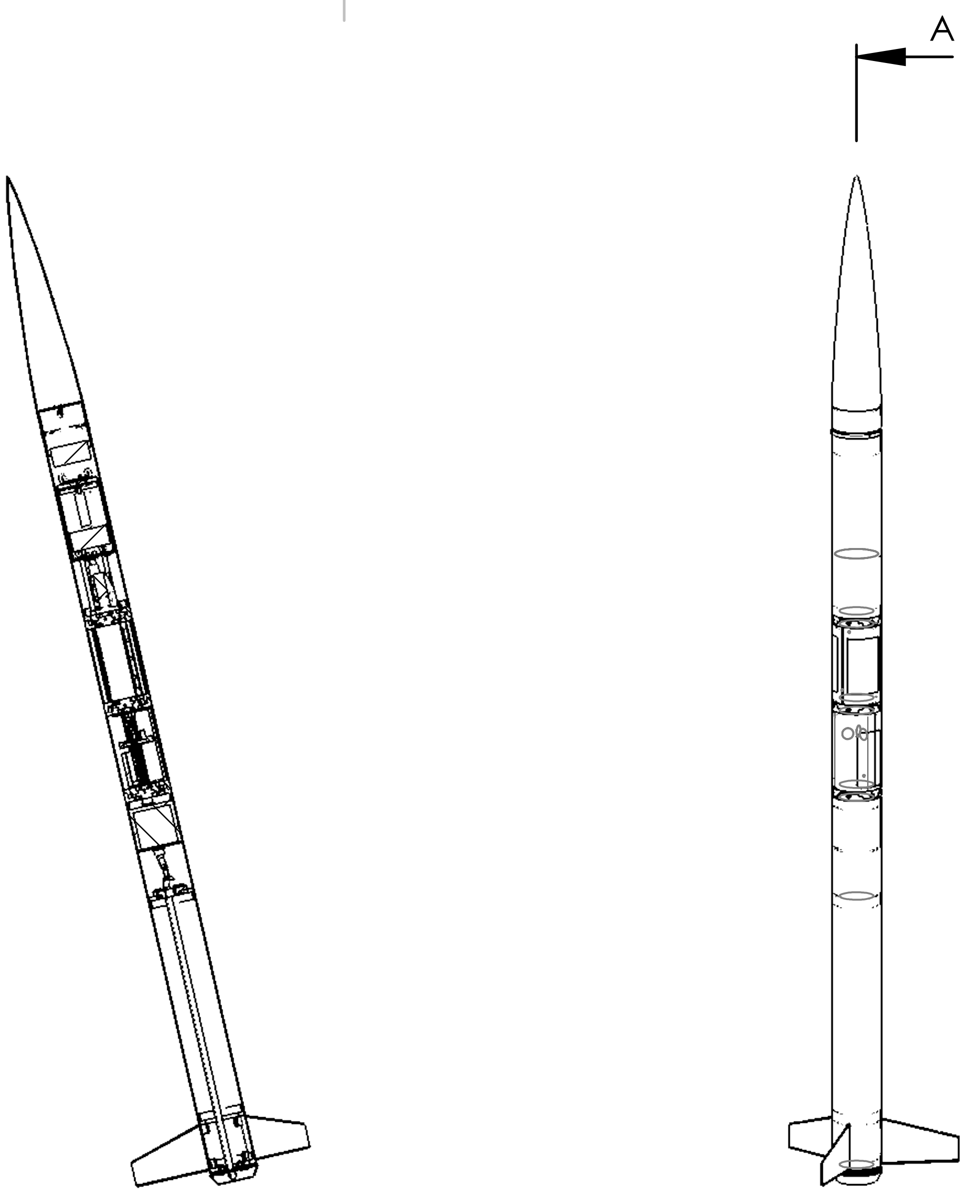

SECCIÓN A-A
ESCALA 1 : 20

SI NO SE INDICA LO CONTRARIO: LAS COTAS SE EXPRESAN EN MM ACABADO SUPERFICIAL: TOLERANCIAS: LINEAL: ANGULAR:	ACABADO:	REBARBAR Y ROMPER ARISTAS VIVAS	NO CAMBIE LA ESCALA	REVISIÓN	

	NOMBRE	FIRMA	FECHA
DIBUJ.	I.V.R.		05/07
VERIF.			
APROB.			
FABR.			
CALID.			

TÍTULO:

HMJNCS-Ohana

MATERIAL:

N.º DE DIBUJO

ST_Assembly Lv2

A4

PESO: 22501.65g

ESCALA: 1:20

HOJA 1 DE 1

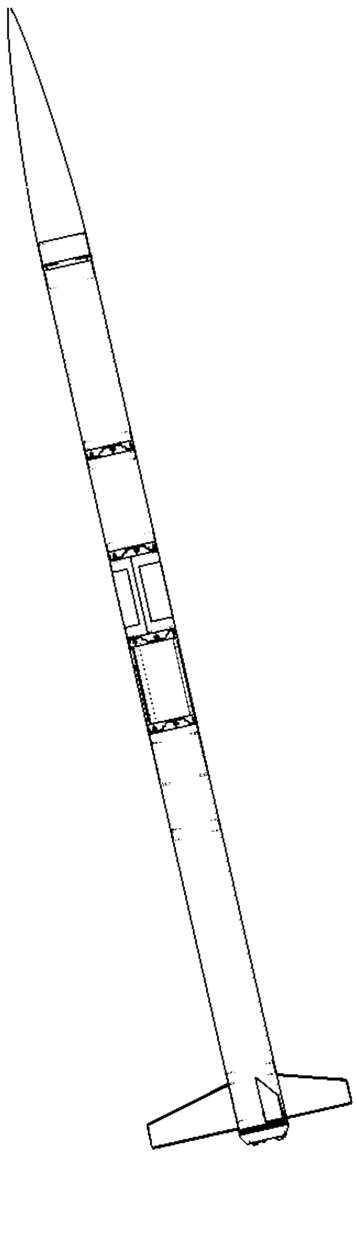

SI NO SE INDICA LO CONTRARIO: LAS COTAS SE EXPRESAN EN MM ACABADO SUPERFICIAL: TOLERANCIAS: LINEAL: ANGULAR:	ACABADO:	REBARBAR Y ROMPER ARISTAS VIVAS	NO CAMBIE LA ESCALA	REVISIÓN

	NOMBRE	FIRMA	FECHA
DIBUJ.	I.V.R.		05/07
VERIF.			
APROB.			
FABR.			
CALID.			

MATERIAL:

PESO: 28918.74g

TÍTULO:

HMJNCS-Ohana

N.º DE DIBUJO

ST_Assembly Lv3

A4

ESCALA: 1:20

HOJA 1 DE 1

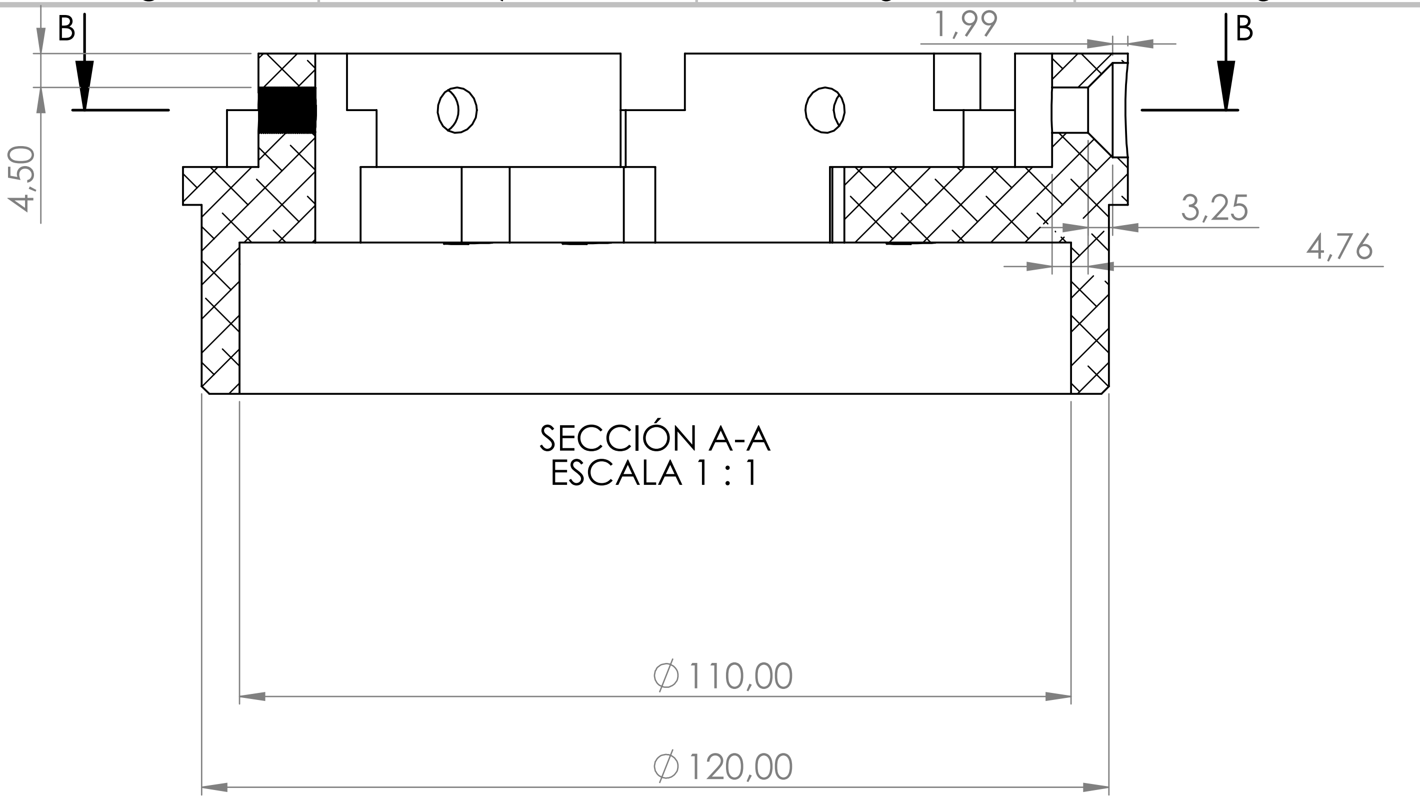

SECCIÓN A-A
ESCALA 1 : 1

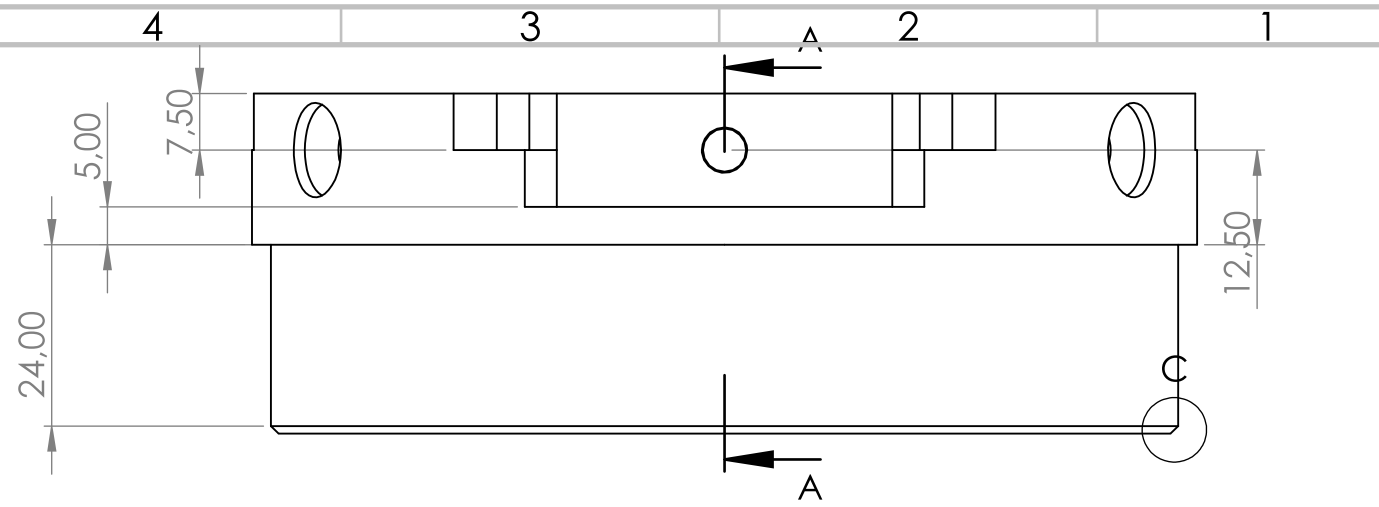

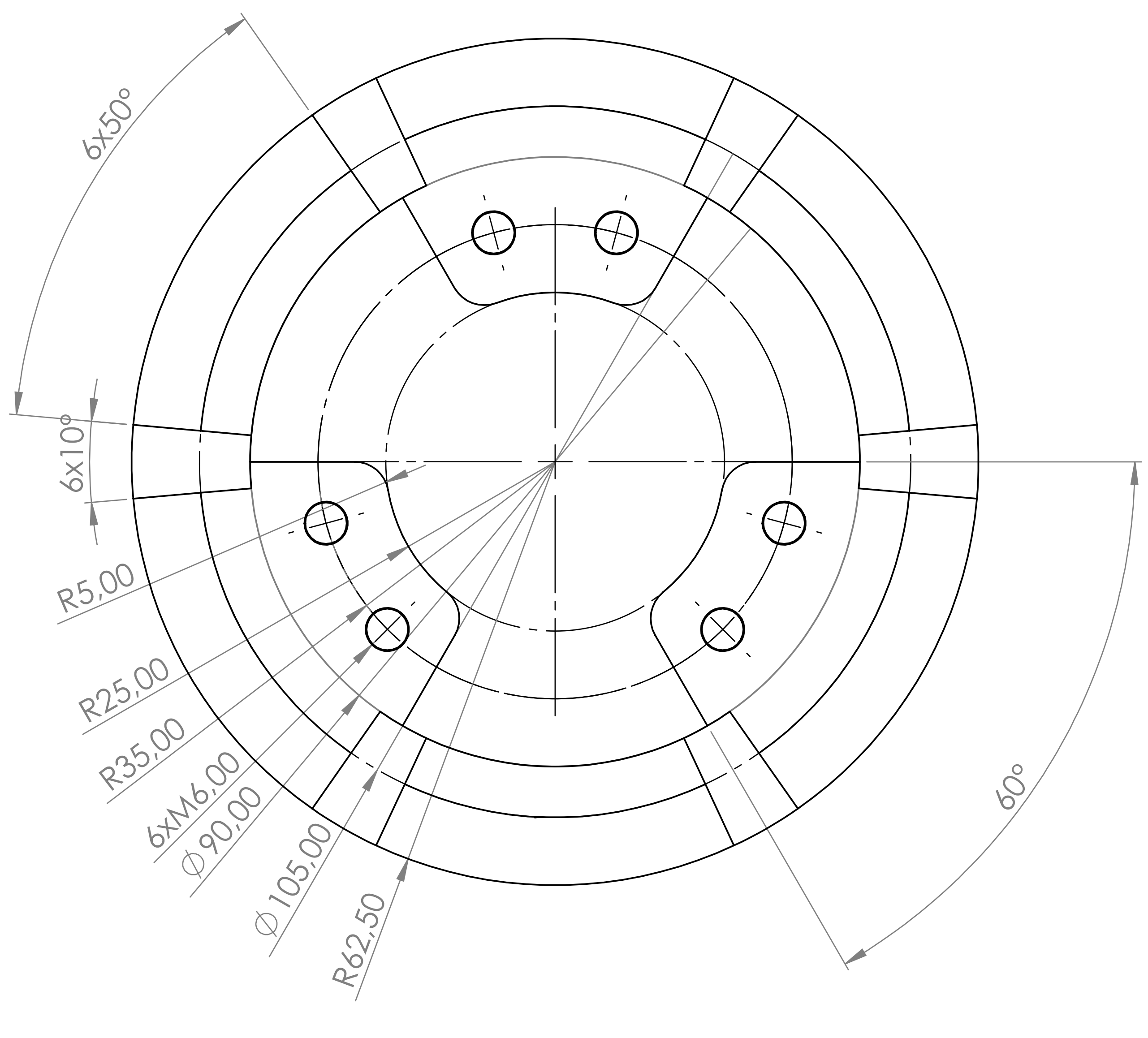

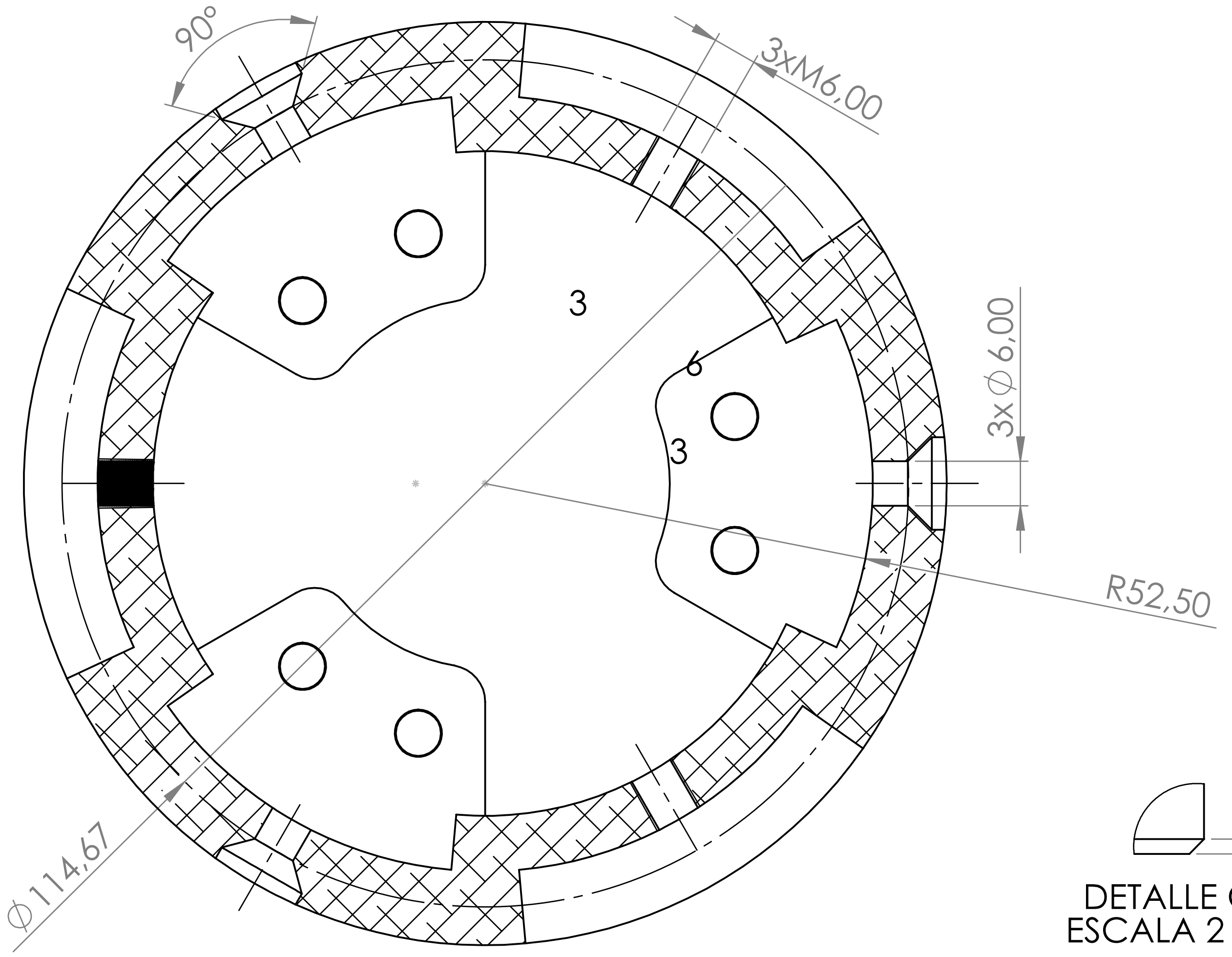

SECCIÓN B-B
ESCALA 1 : 1

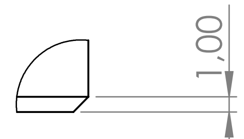

DETALLE C
ESCALA 2 : 1

SI NO SE INDICA LO CONTRARIO: LAS COTAS SE EXPRESAN EN MM ACABADO SUPERFICIAL: TOLERANCIAS: LINEAL: ANGULAR:	ACABADO:		REBARBAR Y ROMPER ARISTAS VIVAS	NO CAMBIE LA ESCALA	REVISIÓN
	NOMBRE	FIRMA	FECHA	TÍTULO: HMJNCS-Ohana	
DIBUJ.	I.V.R.		02/07		
VERIF.					
APROB.					
FABR.					
CALID.			MATERIAL: Al 6063-T6	N.º DE DIBUJO CONNECTOR	A3
			PESO: 410.53g	ESCALA:1:1	HOJA 1 DE 1

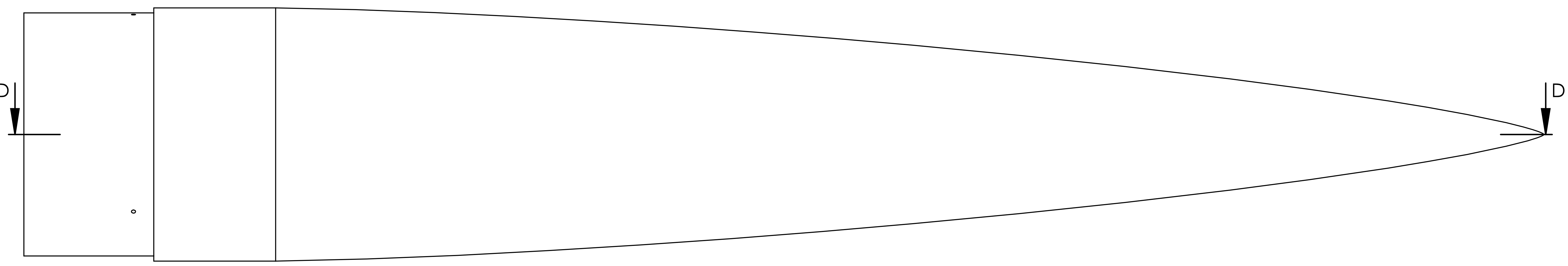

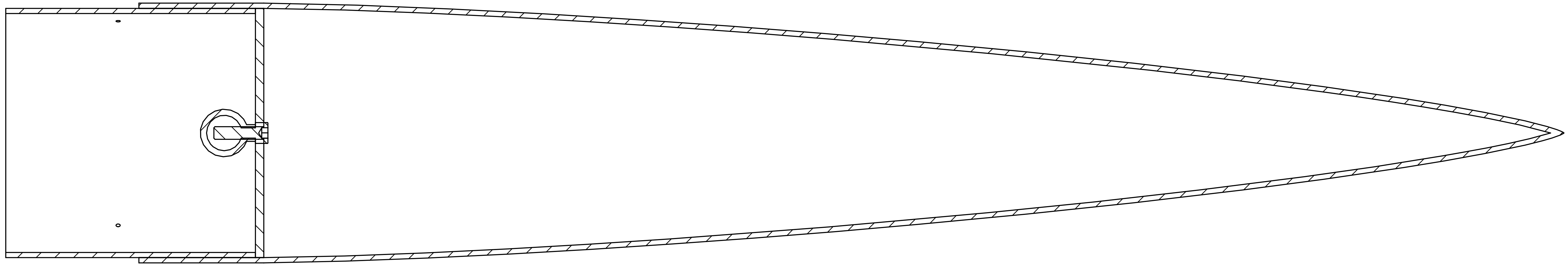

SECCIÓN D-D
ESCALA 1 : 2

N.º DE ELEMENTO	N.º DE PIEZA	DESCRIPCIÓN	CANTIDAD
1	haack_c0_nose_cone		1
2	Chute_plate		1
3	EYE_BOLT_RE		1
4	ISO 4762 M6 x 20 - 20N		1
5	Slide_in		1

SI NO SE INDICA LO CONTRARIO: LAS COTAS SE EXPRESAN EN MM
ACABADO SUPERFICIAL:
TOLERANCIAS:
LINEAL:
ANGULAR:

ACABADO:

REBARBAR Y ROMPER ARISTAS VIVAS

NO CAMBIE LA ESCALA

REVISIÓN

	NOMBRE	FIRMA	FECHA
DIBUJ.	I.V.R.		02/07
VERIF.			
APROB.			
FABR.			
CALID.			

MATERIAL:

PESO: 1078.39g

TÍTULO:

HMJNCS-Ohana

N.º DE DIBUJO

Nosecone

A3

ESCALA 1:5

HOJA 1 DE 1

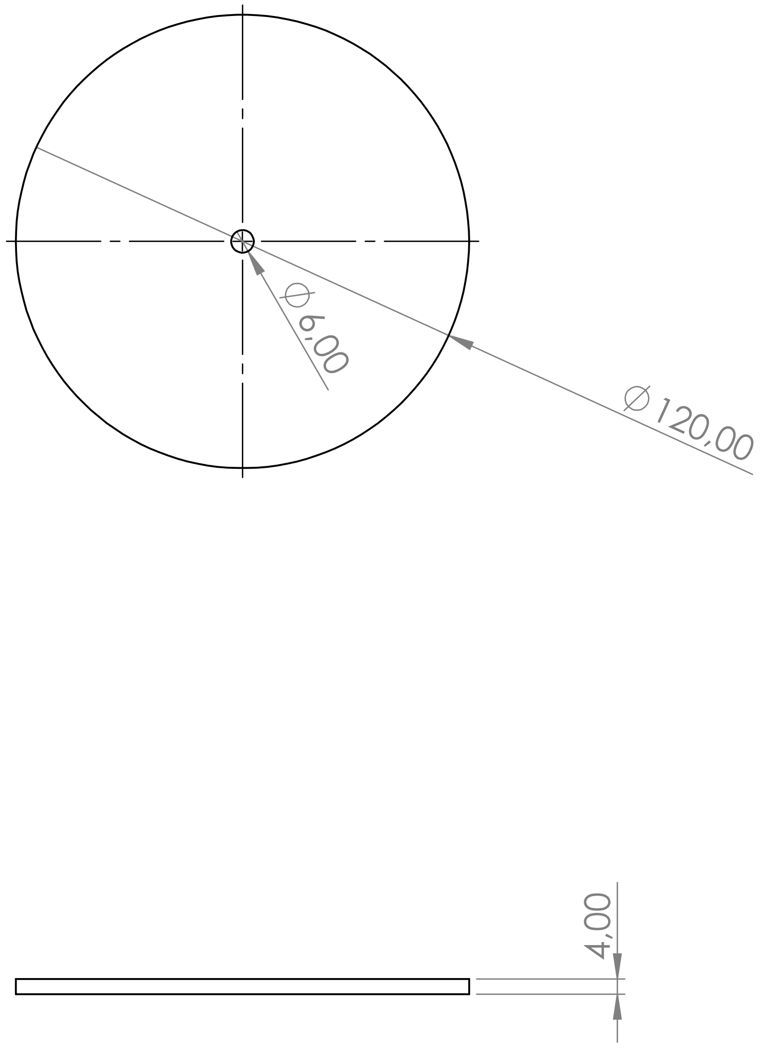

SI NO SE INDICA LO CONTRARIO:
LAS COTAS SE EXPRESAN EN MM
ACABADO SUPERFICIAL:
TOLERANCIAS:
LINEAL:
ANGULAR:

ACABADO:

REBARBAR Y ROMPER ARISTAS VIVAS

NO CAMBIE LA ESCALA

REVISIÓN

	NOMBRE	FIRMA	FECHA
DIBUJ.	I.V.R		02/07
VERIF.			
APROB.			
FABR.			
CALID.			

TÍTULO:

HMJNCS-Ohana

MATERIAL:

Epoxy Resin: 50%
E-glass Fiber: 50%

N.º DE DIBUJO

Chute_plate

A4

PESO: 80.32g

ESCALA:1:2

HOJA 1 DE 1

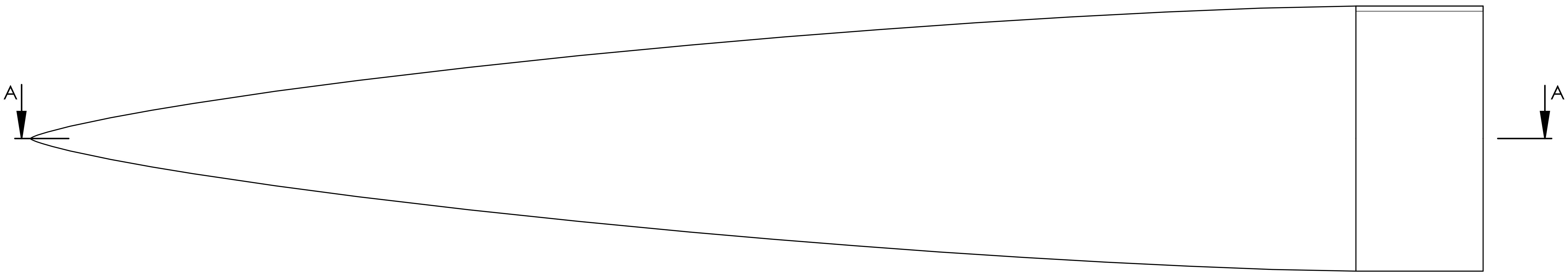

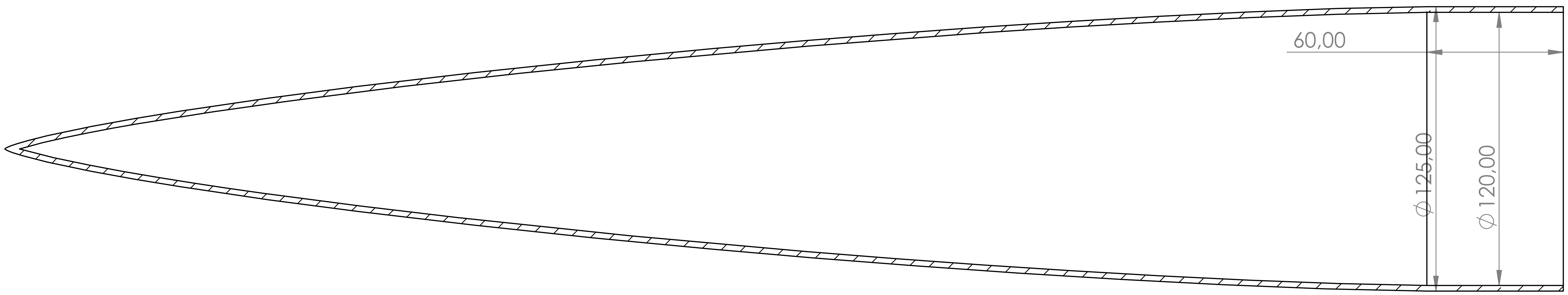

SECCIÓN A-A
ESCALA 1 : 2

The nosecone follows the function (where C=0):

$$y = \frac{R}{\sqrt{\pi}}\sqrt{\theta - \frac{\sin(2\theta)}{2} + C\sin^3(\theta)}$$

$$\theta = \arccos\left(1 - \frac{2x}{L}\right)$$

SI NO SE INDICA LO CONTRARIO: LAS COTAS SE EXPRESAN EN MM ACABADO SUPERFICIAL: TOLERANCIAS: LINEAL: ANGULAR:	ACABADO:		REBARBAR Y ROMPER ARISTAS VIVAS	NO CAMBIE LA ESCALA	REVISIÓN	
	NOMBRE	FIRMA	FECHA	TÍTULO: HMJNCS-Ohana		
DIBUJ.	I.V.R.		2/07			
VERIF.						
APROB.						
FABR.						
CALID.				MATERIAL: Epoxy Resin: 50% Glass Fibre E: 50%	N.º DE DIBUJO Haack Nosecone	A3
				PESO: 795.54g	ESCALA:1:5	HOJA 1 DE 1

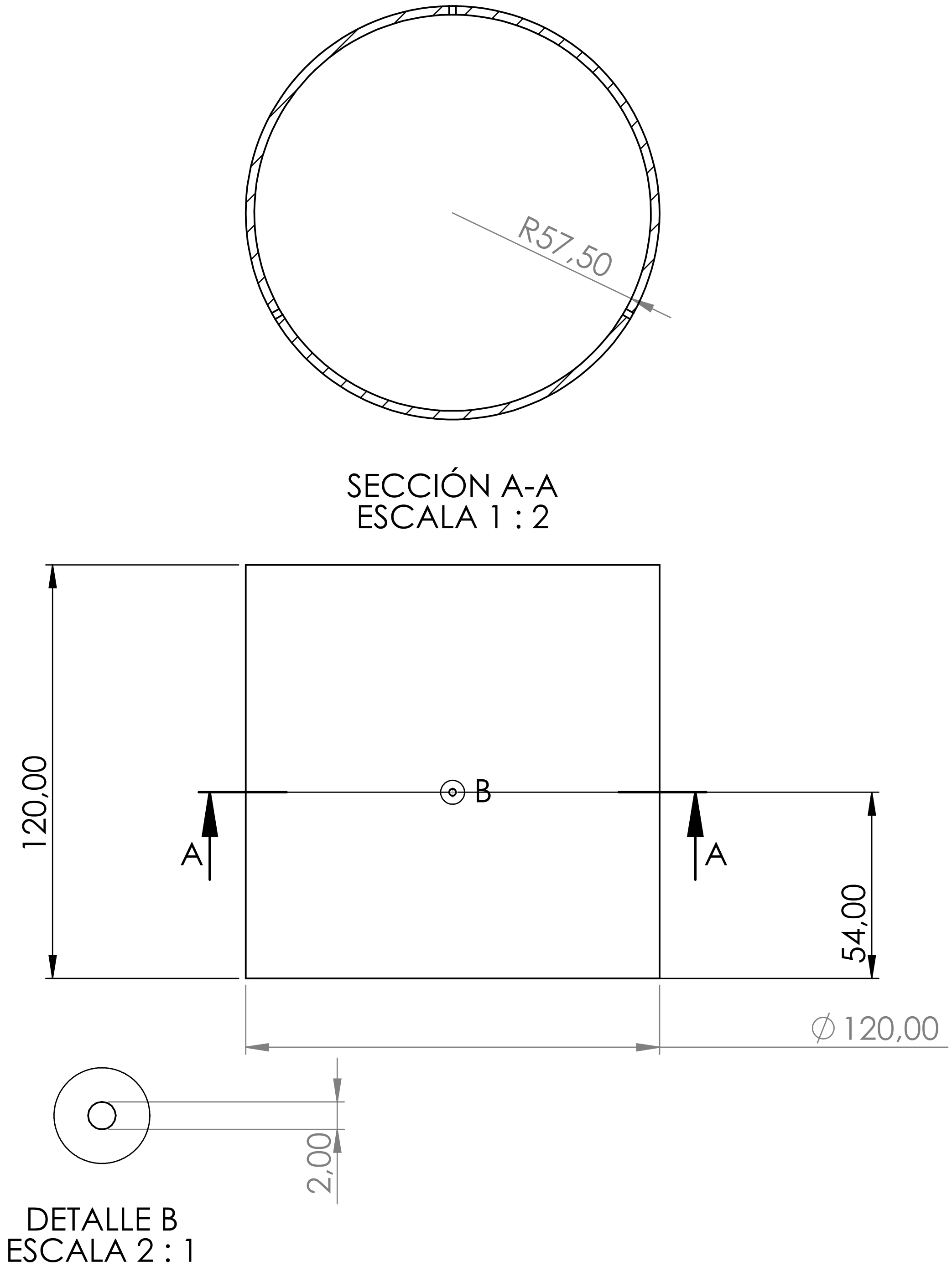

SI NO SE INDICA LO CONTRARIO:
LAS COTAS SE EXPRESAN EN MM
ACABADO SUPERFICIAL:
TOLERANCIAS:
LINEAL:
ANGULAR:

ACABADO:

REBARBAR Y ROMPER ARISTAS VIVAS

NO CAMBIE LA ESCALA

REVISIÓN

	NOMBRE	FIRMA	FECHA
DIBUJ.	I.V.R		02/07
VERIF.			
APROB.			
FABR.			
CALID.			

TÍTULO:

HMJNCS-Ohana

MATERIAL:

Epoxy Resin: 50%
E-glass Fiber: 50%

N.º DE DIBUJO

Slide_in

A4

PESO: 197.08g

ESCALA:1:5

HOJA 1 DE 1

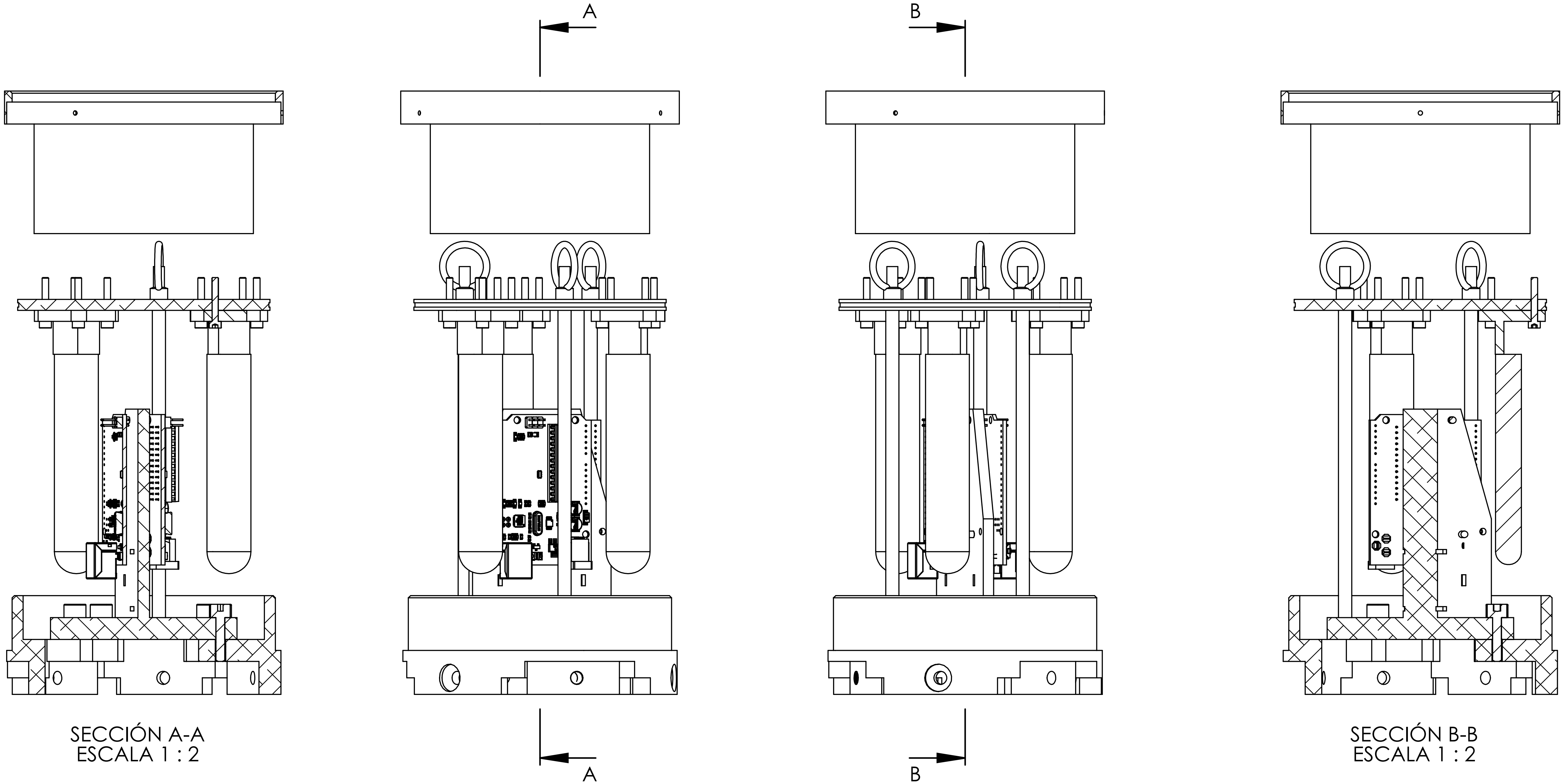

SECCIÓN A-A
ESCALA 1 : 2

SECCIÓN B-B
ESCALA 1 : 2

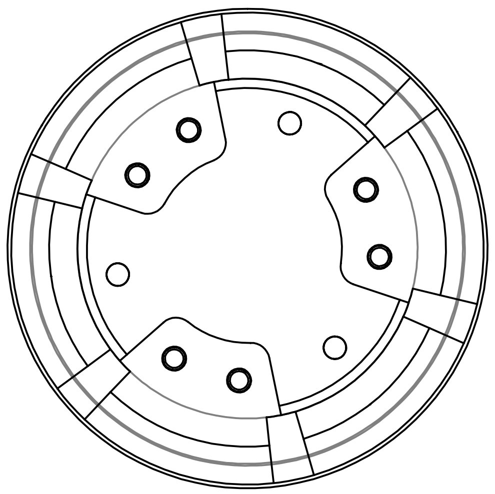

SI NO SE INDICA LO CONTRARIO: LAS COTAS SE EXPRESAN EN MM ACABADO SUPERFICIAL: TOLERANCIAS: LINEAL: ANGULAR:	ACABADO:	REBARBAR Y ROMPER ARISTAS VIVAS	NO CAMBIE LA ESCALA	REVISIÓN

	NOMBRE	FIRMA	FECHA
DIBUJ.	I.V.R.		02/07
VERIF.			
APROB.			
FABR.			
CALID.			

TÍTULO:
HMJNCS-Ohana

MATERIAL:

N.º DE DIBUJO
Single Event

A3

PESO: 5293.82g

ESCALA:1:5

HOJA 1 DE 2

N.º DE ELEMENTO	N.º DE PIEZA	DESCRIPCIÓN	CANTIDAD
1	TUBE_RE_BAY		1
2	PROTECTION_RING_RE_BAY		1
3	CONNECTOR_RE_BAY		1
4	RE_BASE		1
5	USB SHELL.STEP		2
6	USB core.STEP		2
7	usb top contact.STEP		4
8	usb btm contact.STEP		4
9	dip28-0.STEP		2
10	dip socket pin.STEP		56
11	RESET CORE.STEP		2
12	RESET.STEP		2
13	unoboard blue.STEP		2
14	47uf CAP Dcase.STEP		4
15	power jack.STEP		2
16	crystal.STEP		2
17	2pin_header__02.STEP		6
18	nano - reg.STEP		2
19	led.STEP		8
20	atmega16u2.STEP		2
21	ATMEL328P.STEP		2
22	102 RESISTOR PACK.STEP		4
23	103 RESISTOR PACK.STEP		2
24	220 RESISTOR PACK.STEP		2
25	16mhz crystal - measured.STEP		2
26	PADS001.STEP		2
27	603 cap on pad.STEP		16

N.º DE ELEMENTO	N.º DE PIEZA	DESCRIPCIÓN	CANTIDAD
28	ssot3.STEP		2
29	mf-msmf050-2.STEP		2
30	lmv358.STEP		2
31	lp2985dgkr.STEP		2
32	cd1206 diode.STEP		4
33	603 resistor.STEP		2
34	blm21.STEP		2
35	m7 diode.STEP		2
36	MLC0603.STEP		4
37	spacer_RE		4
38	PILAR_RE		3
39	RE_TOP		1
40	EYE_BOLT_RE		3
41	VALVE_RE		3
42	CO2_CARTRIGE		3
43	ISO 4762 M3 x 20 - 20N		12
44	ISO 4762 M6 x 20 - 20N		6
45	single_event		1

SI NO SE INDICA LO CONTRARIO: LAS COTAS SE EXPRESAN EN MM ACABADO SUPERFICIAL: TOLERANCIAS: LINEAL: ANGULAR:

ACABADO:

REBARBAR Y ROMPER ARISTAS VIVAS

NO CAMBIE LA ESCALA

REVISIÓN

	NOMBRE	FIRMA	FECHA
DIBUJ.	I.V.R.		02/07
VERIF.			
APROB.			
FABR.			
CALID.			

TÍTULO: HMJNCS-Ohana

MATERIAL:

N.º DE DIBUJO: Single Event

A3

PESO: 5293.82g

ESCALA:1:5

HOJA 2 DE 2

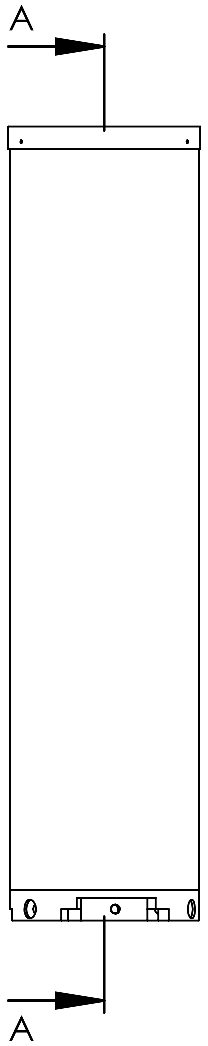

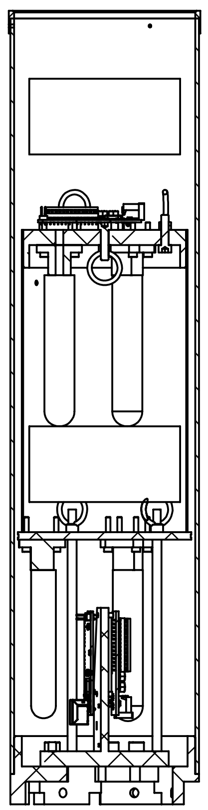

SECCIÓN A-A

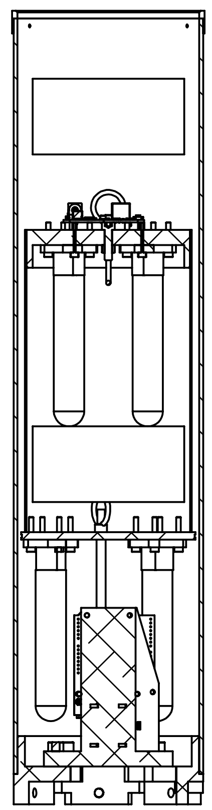

SECCIÓN B-B

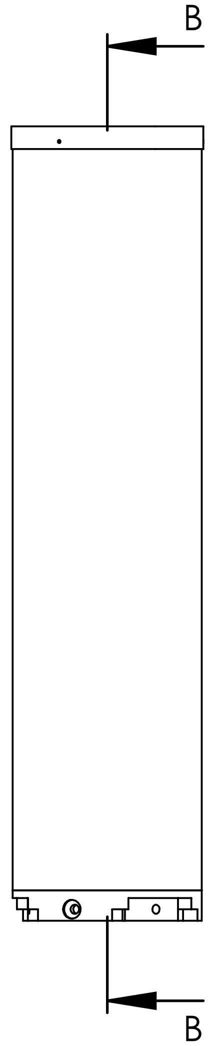

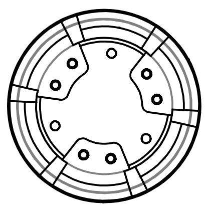

SI NO SE INDICA LO CONTRARIO: LAS COTAS SE EXPRESAN EN MM ACABADO SUPERFICIAL: TOLERANCIAS: LINEAL: ANGULAR:	ACABADO:		REBARBAR Y ROMPER ARISTAS VIVAS	NO CAMBIE LA ESCALA	REVISIÓN
	NOMBRE	FIRMA	FECHA	TÍTULO: HMJNCS-Ohana	
DIBUJ.	I.V.R.		02/07		
VERIF.					
APROB.					
FABR.					
CALID.			MATERIAL:	N.º DE DIBUJO Double_event	A3
			PESO: 11729.19g	ESCALA:1:5	HOJA 1 DE 2

N.º DE ELEMENTO	N.º DE PIEZA	DESCRIPCIÓN	CANTIDAD
1	PROTECTION_RING_RE_BAY		1
2	CONNECTOR_RE_BAY		1
3	RE_BASE		1
4	USB SHELL.STEP		3
5	USB core.STEP		3
6	usb top contact.STEP		6
7	usb btm contact.STEP		6
8	dip28-0.STEP		3
9	dip socket pin.STEP		84
10	RESET CORE.STEP		3
11	RESET.STEP		3
12	unoboard blue.STEP		3
13	47uf CAP Dcase.STEP		6
14	power jack.STEP		3
15	crystal.STEP		3
16	2pin_header__02.STEP		9
17	nano - reg.STEP		3
18	led.STEP		12
19	atmega16u2.STEP		3
20	ATMEL328P.STEP		3
21	102 RESISTOR PACK.STEP		6
22	103 RESISTOR PACK.STEP		3
23	220 RESISTOR PACK.STEP		3
24	16mhz crystal - measured.STEP		3
25	PADS001.STEP		3
26	603 cap on pad.STEP		24
27	ssot3.STEP		3

N.º DE ELEMENTO	N.º DE PIEZA	DESCRIPCIÓN	CANTIDAD
28	mf-msmf050-2.STEP		3
29	lmv358.STEP		3
30	lp2985dgkr.STEP		3
31	cd1206 diode.STEP		6
32	603 resistor.STEP		3
33	blm21.STEP		3
34	m7 diode.STEP		3
35	MLC0603.STEP		6
36	spacer_RE		8
37	PILAR_RE		3
38	RE_TOP		1
39	EYE_BOLT_RE		7
40	VALVE_RE		6
41	CO2_CARTRIGE		6
42	ISO 4762 M3 x 20 - 20N		24
43	ISO 4762 M6 x 20 - 20N		6
44	TOP_COVER_Phenolic		1
45	ISO 4762 M5 x 20 - 20N		4
46	Phenolic_TUBE_RE		1
47	TUBE_RE_BAY_Bouble_event		1
48	Double_event_drogue		1
49	Double_event_1		1

SI NO SE INDICA LO CONTRARIO:
LAS COTAS SE EXPRESAN EN MM
ACABADO SUPERFICIAL:
TOLERANCIAS:
LINEAL:
ANGULAR:

ACABADO:

REBARBAR Y ROMPER ARISTAS VIVAS

NO CAMBIE LA ESCALA

REVISIÓN

	NOMBRE	FIRMA	FECHA
DIBUJ.	I.V.R.		02/07
VERIF.			
APROB.			
FABR.			
CALID.			

MATERIAL:

TÍTULO:

HMJNCS-Ohana

N.º DE DIBUJO

Double_event

A3

PESO: 11729.19g

ESCALA:1:5

HOJA 2 DE 2

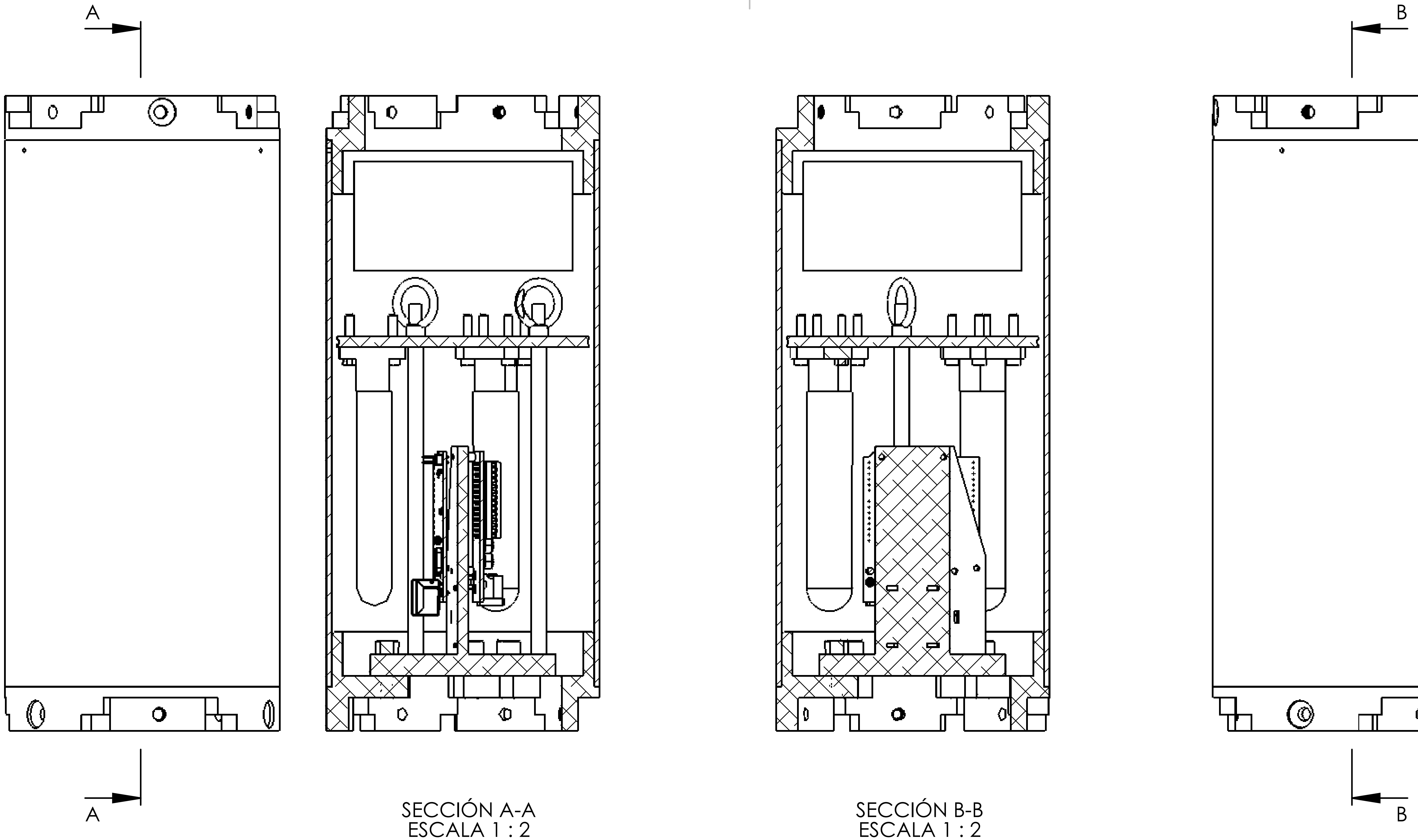

SECCIÓN A-A
ESCALA 1 : 2

SECCIÓN B-B
ESCALA 1 : 2

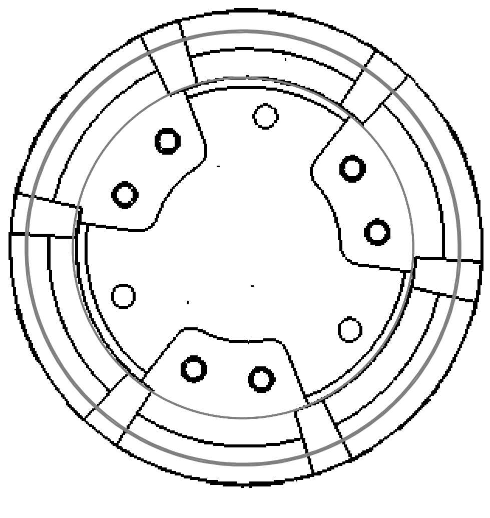

SI NO SE INDICA LO CONTRARIO: LAS COTAS SE EXPRESAN EN MM ACABADO SUPERFICIAL: TOLERANCIAS: LINEAL: ANGULAR:	ACABADO:	REBARBAR Y ROMPER ARISTAS VIVAS	NO CAMBIE LA ESCALA	REVISIÓN

	NOMBRE	FIRMA	FECHA
DIBUJ.	I.V.R.		02/07
VERIF.			
APROB.			
FABR.			
CALID.			

MATERIAL:

PESO: 5704.35g

TÍTULO:

HMJNCS-Ohana

N.º DE DIBUJO

RE-back up Bay

A3

ESCALA: 1:2

HOJA 1 DE 2

N.º DE ELEMENTO	N.º DE PIEZA	DESCRIPCIÓN	CANTIDAD
1	TUBE_RE_BAY		1
2	CONNECTOR_RE_BAY		1
3	RE_BASE		1
4	USB SHELL.STEP		2
5	USB core.STEP		2
6	usb top contact.STEP		4
7	usb btm contact.STEP		4
8	dip28-0.STEP		2
9	dip socket pin.STEP		56
10	RESET CORE.STEP		2
11	RESET.STEP		2
12	unoboard blue.STEP		2
13	47uf CAP Dcase.STEP		4
14	power jack.STEP		2
15	crystal.STEP		2
16	2pin_header__02.STEP		6
17	nano - reg.STEP		2
18	led.STEP		8
19	atmega16u2.STEP		2
20	ATMEL328P.STEP		2
21	102 RESISTOR PACK.STEP		4
22	103 RESISTOR PACK.STEP		2
23	220 RESISTOR PACK.STEP		2
24	16mhz crystal - measured.STEP		2
25	PADS001.STEP		2
26	603 cap on pad.STEP		16
27	ssot3.STEP		2
28	mf-msmf050-2.STEP		2
29	lmv358.STEP		2
30	lp2985dgkr.STEP		2
31	cd1206 diode.STEP		4
32	603 resistor.STEP		2
33	blm21.STEP		2
34	m7 diode.STEP		2
35	MLC0603.STEP		4
36	spacer_RE		4
37	PILAR_RE		3
38	RE_TOP		1
39	EYE_BOLT_RE		3
40	VALVE_RE		3
41	CO2_CARTRIGE		3
42	ISO 4762 M3 x 20 - 20N		12
43	ISO 4762 M6 x 20 - 20N		6
44	single_event		1
45	CONNECTOR_RE_BAY LV3_BACK up		1

SI NO SE INDICA LO CONTRARIO: LAS COTAS SE EXPRESAN EN MM ACABADO SUPERFICIAL: TOLERANCIAS: LINEAL: ANGULAR:	ACABADO:	REBARBAR Y ROMPER ARISTAS VIVAS	NO CAMBIE LA ESCALA	REVISIÓN
	NOMBRE	FIRMA	FECHA	TÍTULO: HMJNCS-Ohana
DIBUJ.	I.V.R		02/07	
VERIF.				
APROB.				
FABR.				
CALID.			MATERIAL:	N.º DE DIBUJO RE-back up Bay A3
			PESO: 5704.35g	ESCALA: 1:2 HOJA 2 DE 2

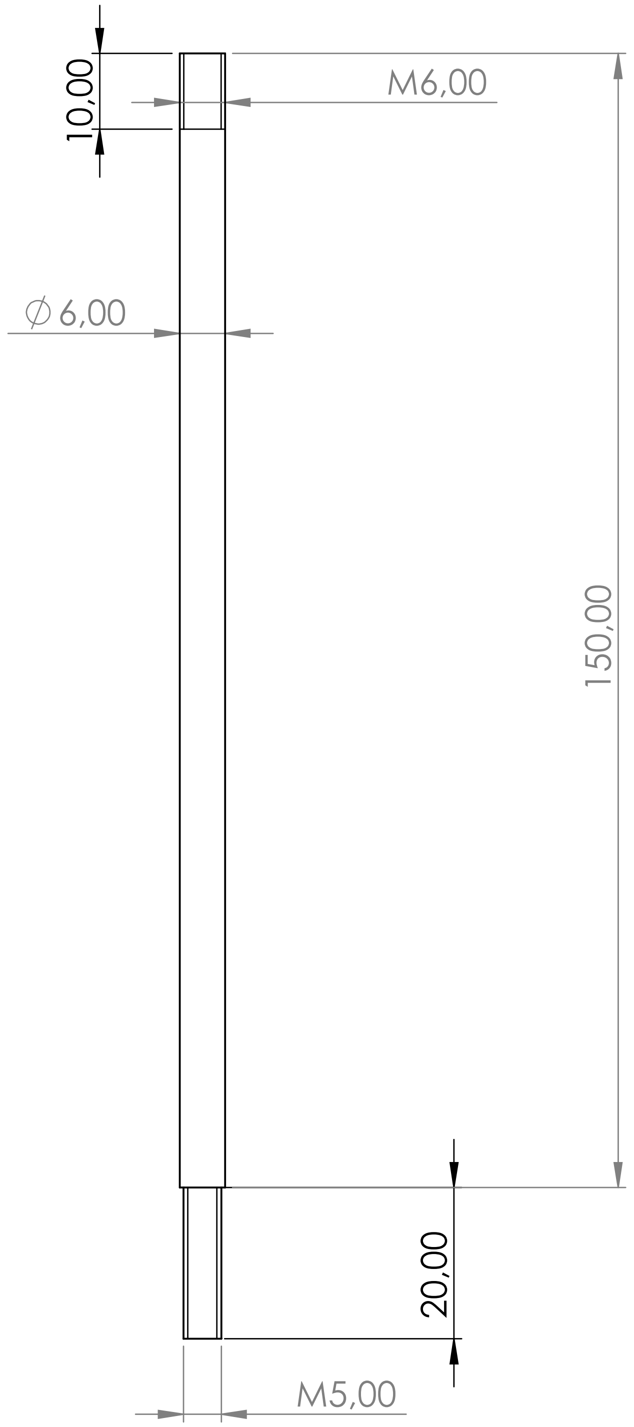

SI NO SE INDICA LO CONTRARIO: LAS COTAS SE EXPRESAN EN MM ACABADO SUPERFICIAL: TOLERANCIAS: LINEAL: ANGULAR:	ACABADO:	REBARBAR Y ROMPER ARISTAS VIVAS	NO CAMBIE LA ESCALA	REVISIÓN

	NOMBRE	FIRMA	FECHA
DIBUJ.	I.V.R.		02/07
VERIF.			
APROB.			
FABR.			
CALID.			

TÍTULO: HMJNCS-Ohana

MATERIAL: S275

N.º DE DIBUJO: PILAR_RE

A4

PESO: 52.15g

ESCALA 1:1

HOJA 1 DE 1

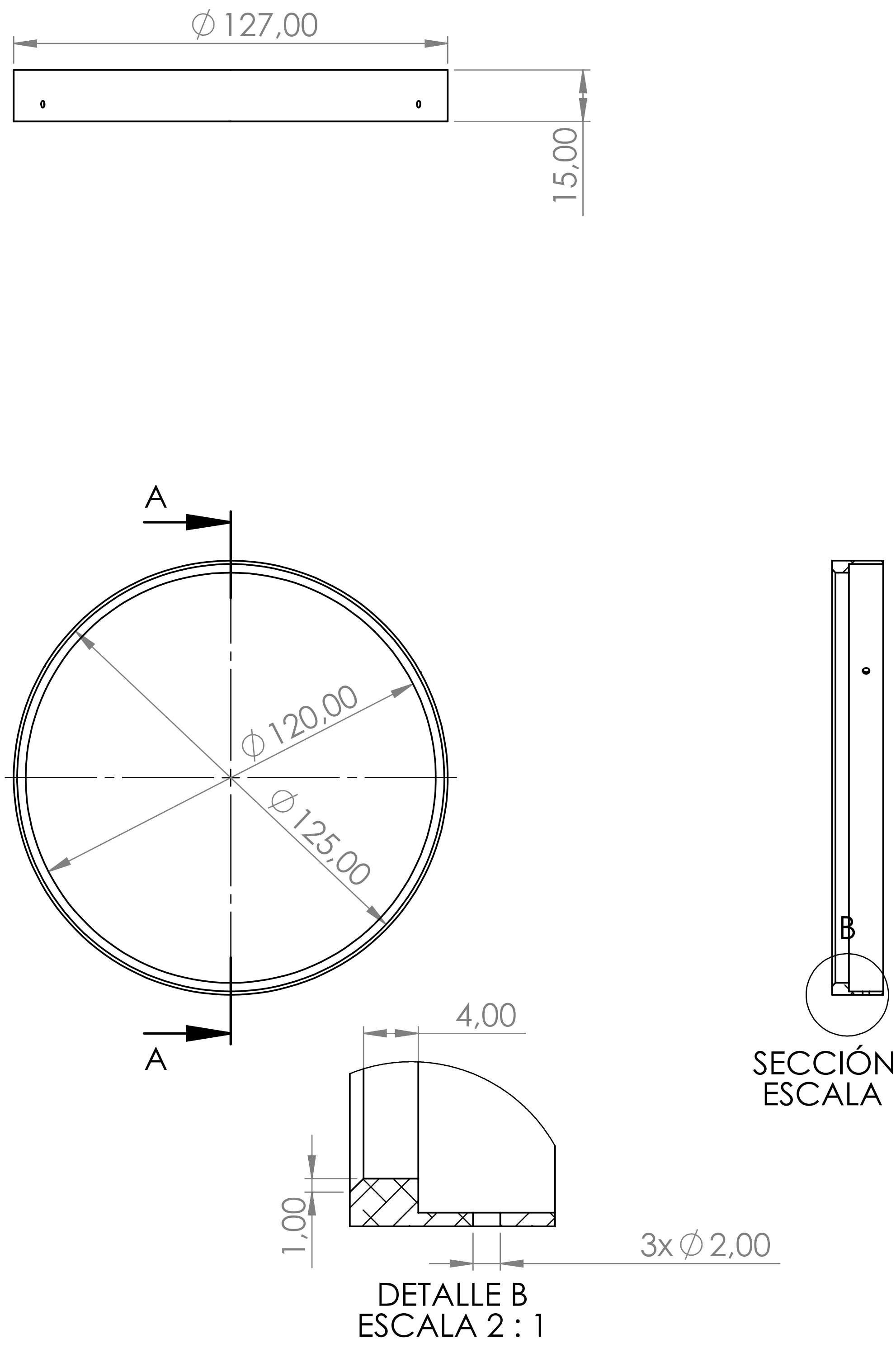

SI NO SE INDICA LO CONTRARIO: LAS COTAS SE EXPRESAN EN MM ACABADO SUPERFICIAL: TOLERANCIAS: LINEAL: ANGULAR:	ACABADO:	REBARBAR Y ROMPER ARISTAS VIVAS	NO CAMBIE LA ESCALA	REVISIÓN

	NOMBRE	FIRMA	FECHA
DIBUJ.	I.V.R.		02/07
VERIF.			
APROB.			
FABR.			
CALID.			

TÍTULO:

HMJNCS-Ohana

MATERIAL: Al 6063-T6

N.º DE DIBUJO: PROTECTION_RING

A4

PESO: 28.48g

ESCALA:1:5

HOJA 1 DE 1

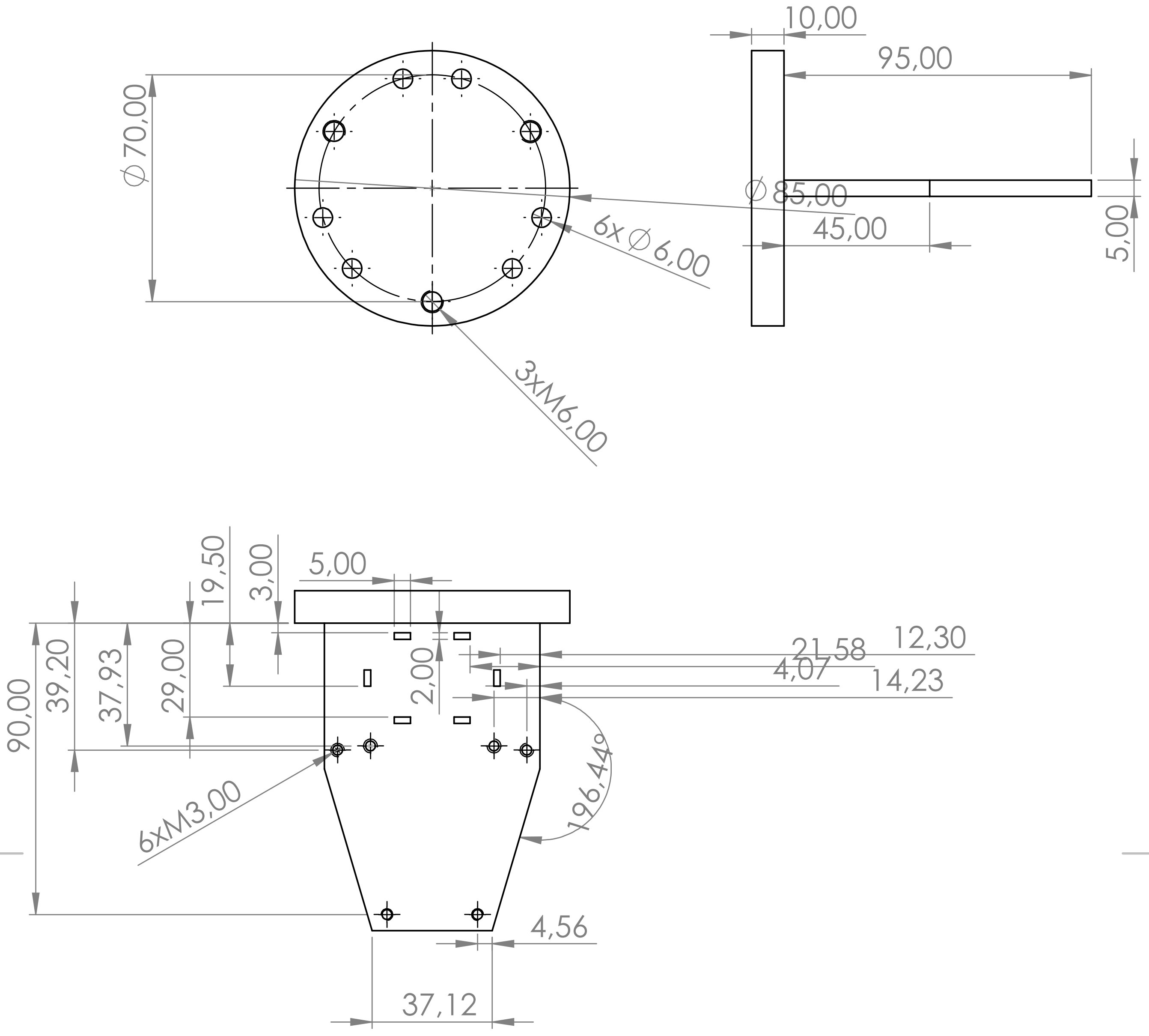

SI NO SE INDICA LO CONTRARIO:
LAS COTAS SE EXPRESAN EN MM
ACABADO SUPERFICIAL:
TOLERANCIAS:
LINEAL:
ANGULAR:

ACABADO:

REBARBAR Y ROMPER ARISTAS VIVAS

NO CAMBIE LA ESCALA

REVISIÓN

	NOMBRE	FIRMA	FECHA
DIBUJ.	I.V.R.		02/07
VERIF.			
APROB.			
FABR.			
CALID.			

TÍTULO:

HMJNCS-Ohana

MATERIAL: Al 6063-T6

N.º DE DIBUJO

RE_BASE

A4

PESO: 220.44g

ESCALA:1:2

HOJA 1 DE 1

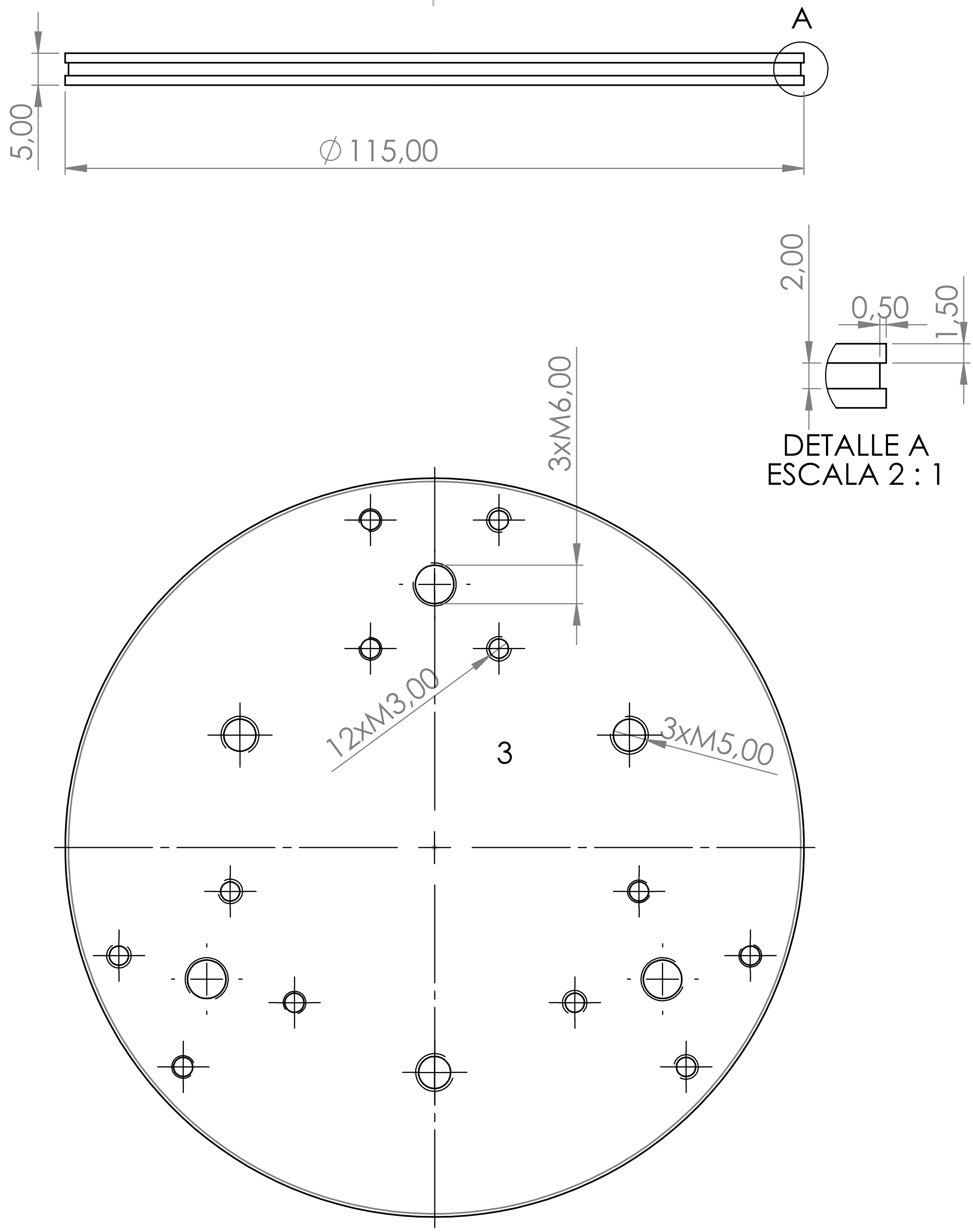

SI NO SE INDICA LO CONTRARIO:
LAS COTAS SE EXPRESAN EN MM
ACABADO SUPERFICIAL:
TOLERANCIAS:
LINEAL:
ANGULAR:

ACABADO:

REBARBAR Y ROMPER ARISTAS VIVAS

NO CAMBIE LA ESCALA

REVISIÓN

	NOMBRE	FIRMA	FECHA
DIBUJ.	I.V.R.		02/07
VERIF.			
APROB.			
FABR.			
CALID.			

TÍTULO:

HMJNCS-Ohana

MATERIAL:

Al 6063-T6

N.º DE DIBUJO

RE_TOP

A4

PESO: 136.17g

ESCALA: 1:1

HOJA 1 DE 1

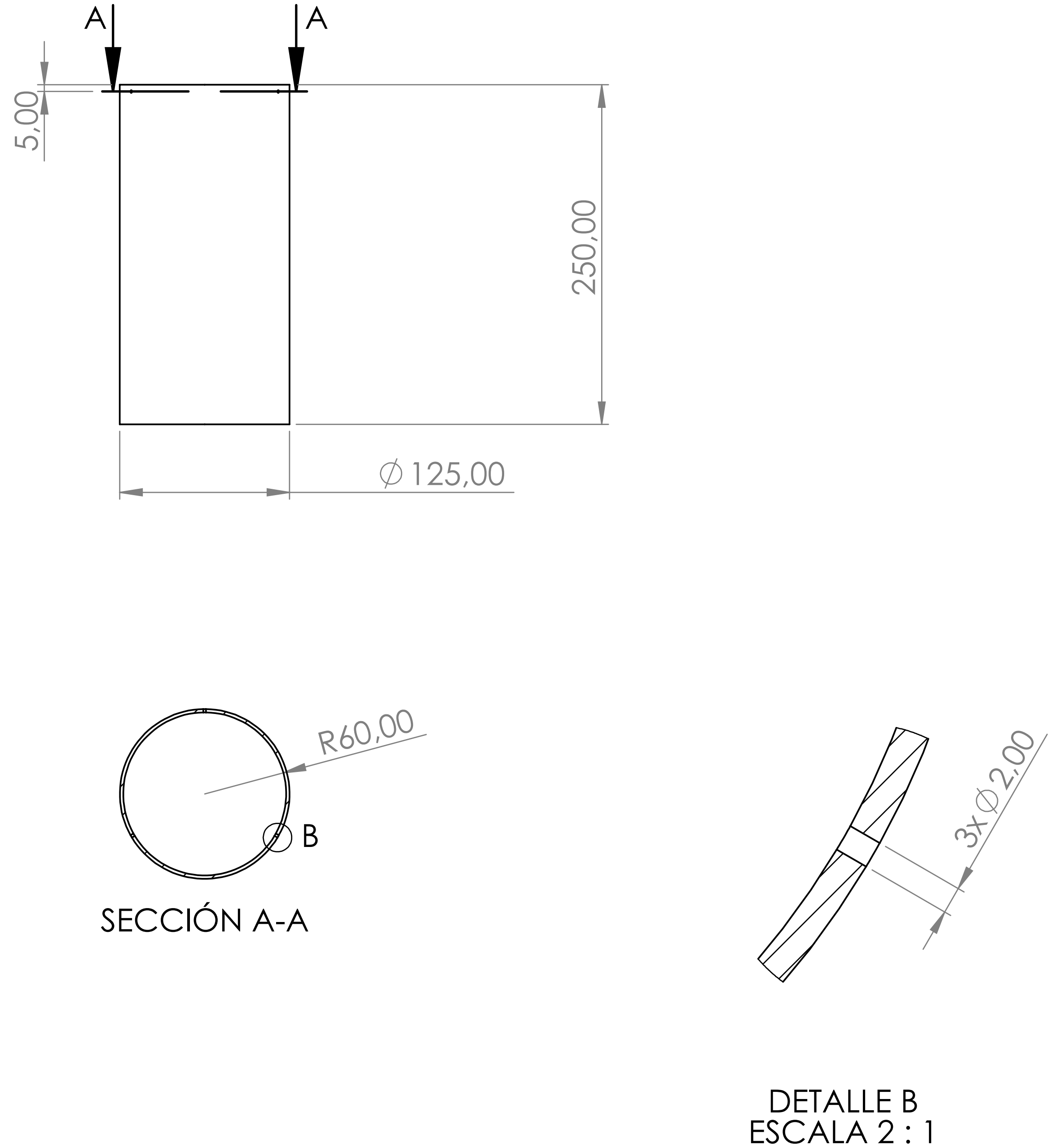

SI NO SE INDICA LO CONTRARIO: LAS COTAS SE EXPRESAN EN MM ACABADO SUPERFICIAL: TOLERANCIAS: LINEAL: ANGULAR:	ACABADO:	REBARBAR Y ROMPER ARISTAS VIVAS	NO CAMBIE LA ESCALA	REVISIÓN

	NOMBRE	FIRMA	FECHA
DIBUJ.	I.V.R.		02/07
VERIF.			
APROB.			
FABR.			
CALID.			

TÍTULO:

HMJNCS-Ohana

MATERIAL:

Epoxy Resin: 18.72%
E Glass Fiber: 81.28%

N.º DE DIBUJO

TUBE_RE_BAY

A4

PESO: 571.325g

ESCALA:1:5

HOJA 1 DE 1

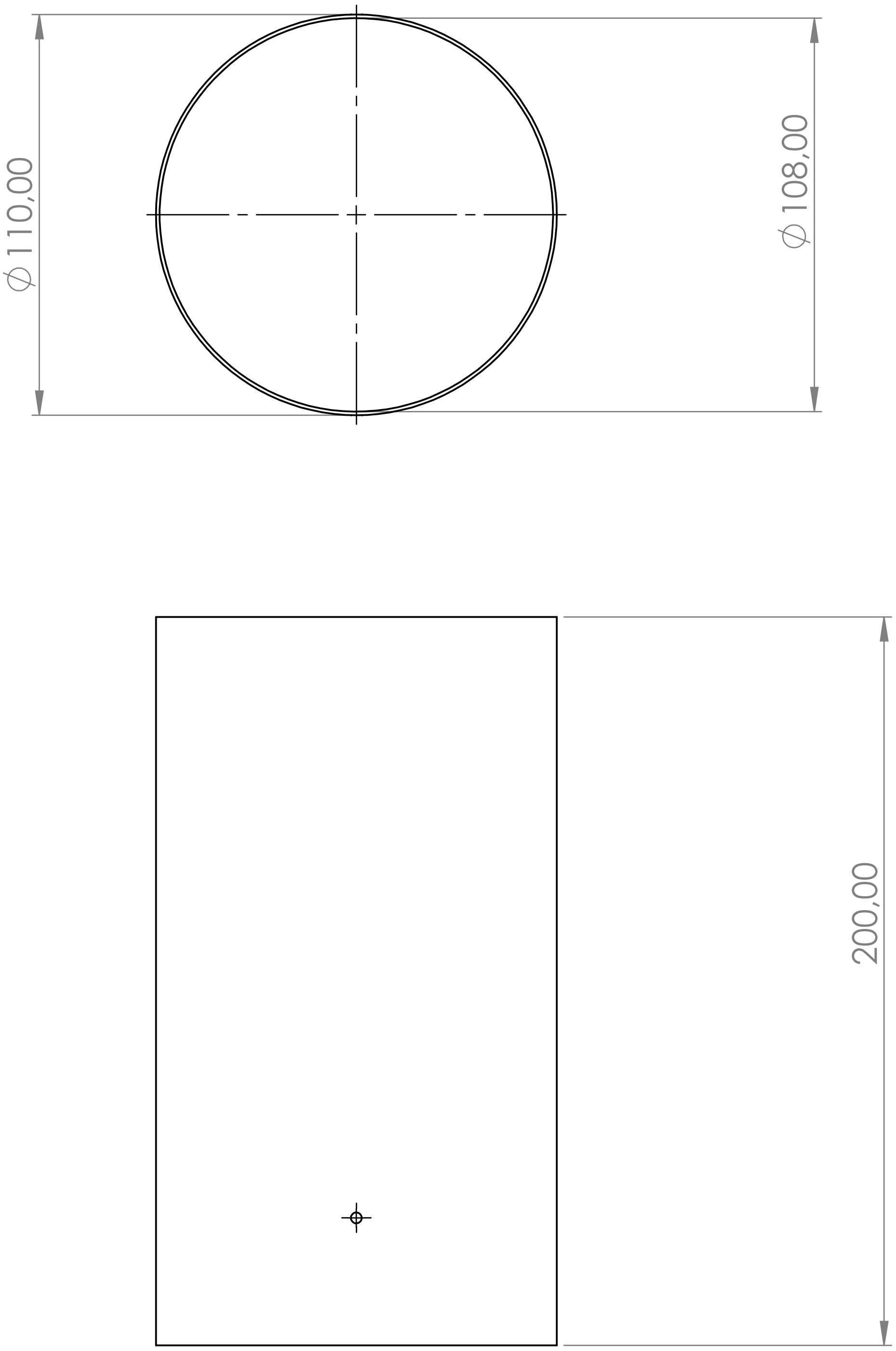

SI NO SE INDICA LO CONTRARIO:
LAS COTAS SE EXPRESAN EN MM
ACABADO SUPERFICIAL:
TOLERANCIAS:
LINEAL:
ANGULAR:

ACABADO:

REBARBAR Y ROMPER ARISTAS VIVAS

NO CAMBIE LA ESCALA

REVISIÓN

	NOMBRE	FIRMA	FECHA
DIBUJ.	I.V.R.		02/07
VERIF.			
APROB.			
FABR.			
CALID.			

TÍTULO:

HMJNCS-Ohana

MATERIAL:
Phenolique

N.º DE DIBUJO
Phenolique Tube

A4

PESO: 141.08g

ESCALA: 1:2

HOJA 1 DE 1

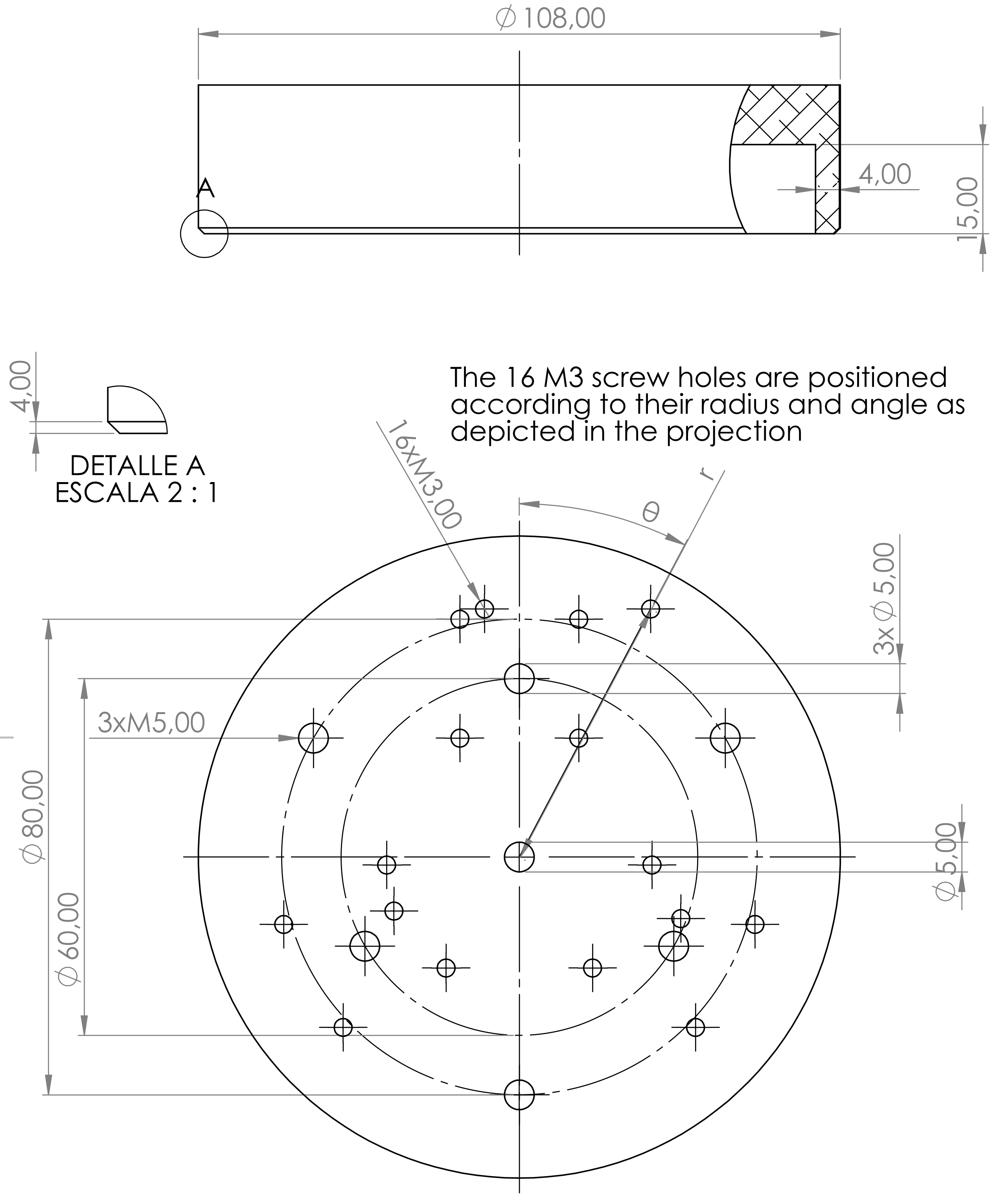

SI NO SE INDICA LO CONTRARIO:
LAS COTAS SE EXPRESAN EN MM
ACABADO SUPERFICIAL:
TOLERANCIAS:
LINEAL:
ANGULAR:

ACABADO:

REBARBAR Y ROMPER ARISTAS VIVAS

NO CAMBIE LA ESCALA

REVISIÓN

	NOMBRE	FIRMA	FECHA
DIBUJ.	I.V.R.		02/07
VERIF.			
APROB.			
FABR.			
CALID.			

TÍTULO:

MATERIAL:
Al 6063-T6

N.º DE DIBUJO
Cover Phenolique

A4

PESO: 293.05g

ESCALA: 1:1

HOJA 1 DE 2

Number	Radiua (mm)	Angle (°)
1	41.23	14.04
2	22.36	26.57
3	47.20	27.9
4	22.36	93.43
5	41.23	10596
6	29.7	110.87
7	41.23	134.04
8	22.36	146.57
9	22.36	213.43
10	41.23	225.96
11	22.97	246.69
12	41.23	254.04
13	22.36	266.57
14	22.36	333.43
15	39.73	345.96
16	42.12	352.01

SI NO SE INDICA LO CONTRARIO:
LAS COTAS SE EXPRESAN EN MM
ACABADO SUPERFICIAL:
TOLERANCIAS:
LINEAL:
ANGULAR:

ACABADO:

REBARBAR Y ROMPER ARISTAS VIVAS

NO CAMBIE LA ESCALA

REVISIÓN

	NOMBRE	FIRMA	FECHA
DIBUJ.	I.V.R.		02/07
VERIF.			
APROB.			
FABR.			
CALID.			

TÍTULO:

MATERIAL:
Al 6063-T6

N.º DE DIBUJO
Cover Phenolique

A4

PESO: 293.05g

ESCALA: 1:1

HOJA 2 DE 2

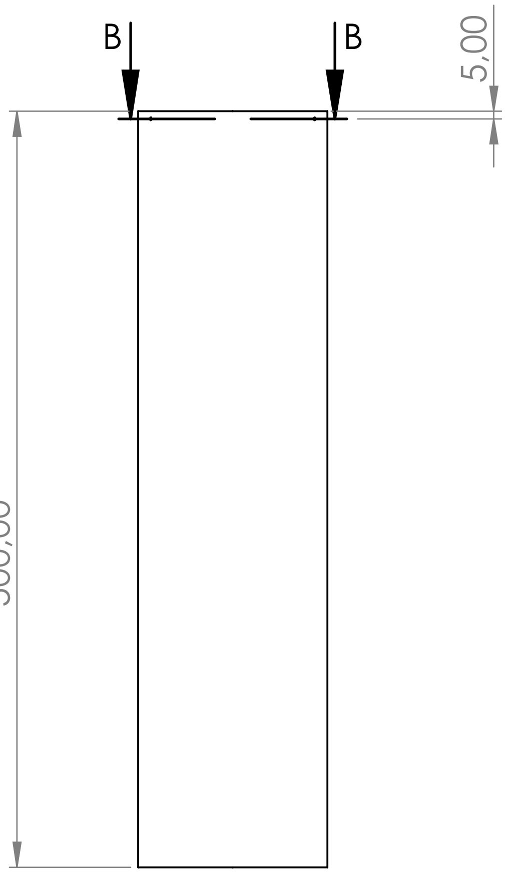

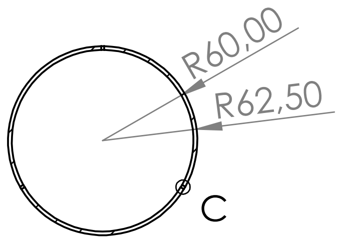

SECCIÓN B-B

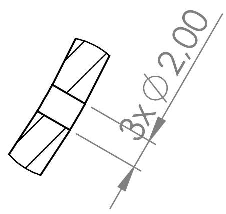

DETALLE C
ESCALA 2 : 1

SI NO SE INDICA LO CONTRARIO: LAS COTAS SE EXPRESAN EN MM ACABADO SUPERFICIAL: TOLERANCIAS: LINEAL: ANGULAR:	ACABADO:	REBARBAR Y ROMPER ARISTAS VIVAS	NO CAMBIE LA ESCALA	REVISIÓN

	NOMBRE	FIRMA	FECHA
DIBUJ.	I.V.R.		02/07
VERIF.			
APROB.			
FABR.			
CALID.			

TÍTULO:

HMJNCS-Ohana

MATERIAL:

Epoxy Resin: 18.72%
E Glass Fiber: 81.28%

N.º DE DIBUJO

Double event tube

A4

PESO: 1142.65g

ESCALA:1:5

HOJA 1 DE 1

N.º DE ELEMENTO	N.º DE PIEZA	DESCRIPCIÓN	CANTIDAD
1	CONNECTOR_AV_PL_BAY		2
2	I_beam		3
3	Base_PIS		1
4	worm		3
5	Slide_PIS		1
6	ISO - RH Helical gear 1M 24T 30HA 20PA 6.4468FW --- 24A75H50L4.0N		3
7	ISO 2340 - B - 4 x 28 x 1 - St		3
8	Top_PIS		1
9	ISO 15 ABB - 272.5 - 12,SI,NC,12_68		24
10	driven_wheel		3
11	driving_wheel		1
12	electro_magnet_push		2
13	push_over		2
14	tube_AV		1
15	AV_cover		1
16	beam_magnet		2

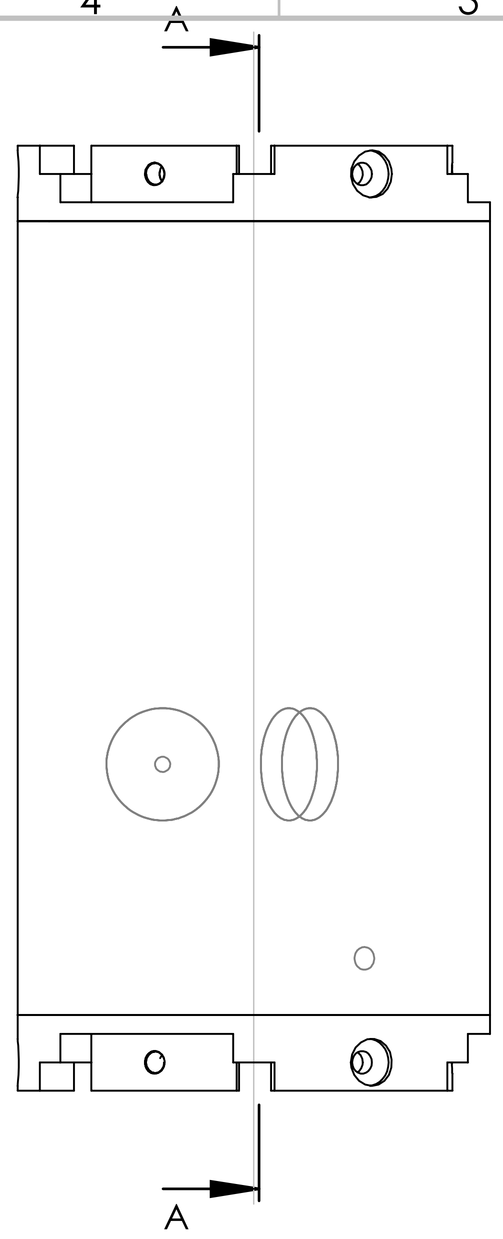

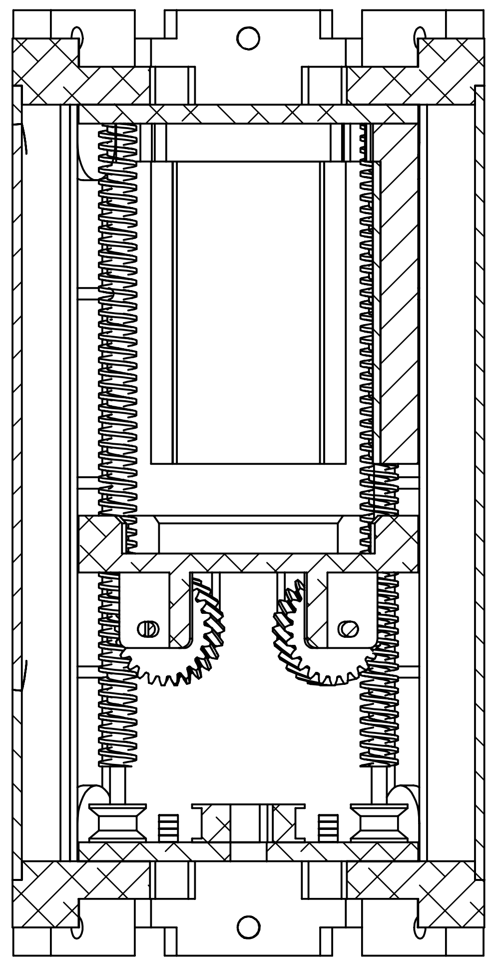

SECCIÓN A-A
ESCALA 1 : 2

SI NO SE INDICA LO CONTRARIO: LAS COTAS SE EXPRESAN EN MM ACABADO SUPERFICIAL: TOLERANCIAS: LINEAL: ANGULAR:

ACABADO:

REBARBAR Y ROMPER ARISTAS VIVAS

NO CAMBIE LA ESCALA

REVISIÓN

	NOMBRE	FIRMA	FECHA
DIBUJ.	I.V.R.		05/07
VERIF.			
APROB.			
FABR.			
CALID.			

TÍTULO:

HMJNCS-Ohana

MATERIAL:

N.º DE DIBUJO

PL Bay

A3

PESO: 2051.79g

ESCALA: 1:2

HOJA 1 DE 1

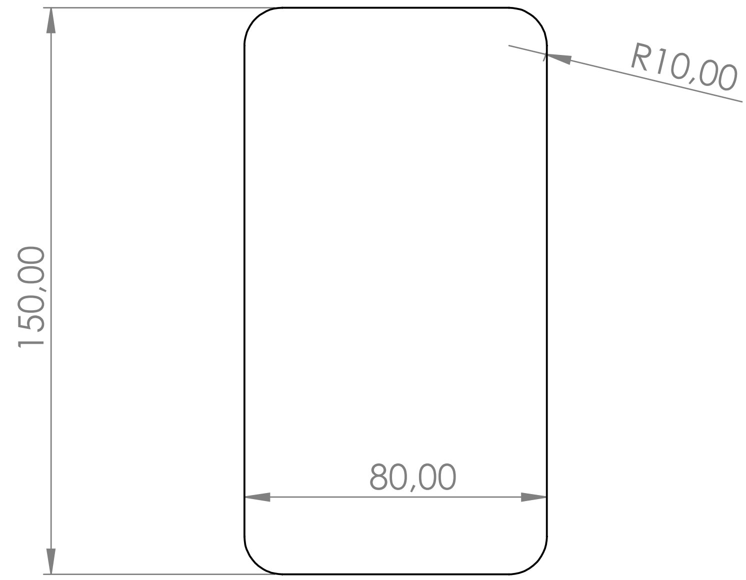

material to be determined from a range of light weight composited based on availability

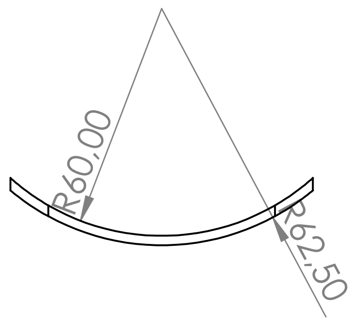

SI NO SE INDICA LO CONTRARIO:
LAS COTAS SE EXPRESAN EN MM
ACABADO SUPERFICIAL:
TOLERANCIAS:
LINEAL:
ANGULAR:

ACABADO:

REBARBAR Y ROMPER ARISTAS VIVAS

NO CAMBIE LA ESCALA

REVISIÓN

	NOMBRE	FIRMA	FECHA
DIBUJ.	I.V.R.		05/07
VERIF.			
APROB.			
FABR.			
CALID.			

TÍTULO:

HMJNCS-Ohana

MATERIAL:

N.º DE DIBUJO

PL_cover

A4

PESO:

ESCALA:1:2

HOJA 1 DE 1

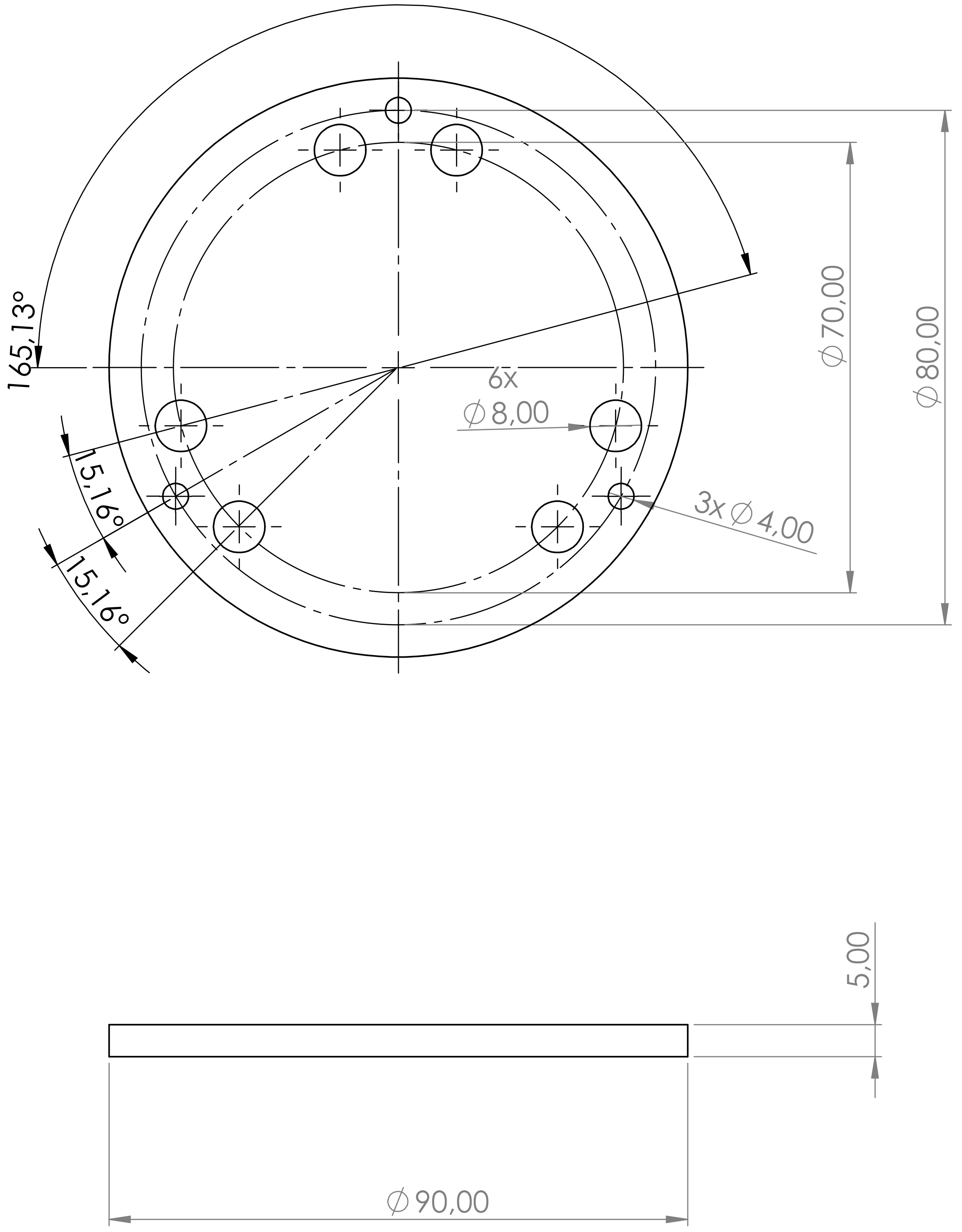

SI NO SE INDICA LO CONTRARIO: LAS COTAS SE EXPRESAN EN MM ACABADO SUPERFICIAL: TOLERANCIAS: LINEAL: ANGULAR:	ACABADO:		REBARBAR Y ROMPER ARISTAS VIVAS		NO CAMBIE LA ESCALA	REVISIÓN
	NOMBRE	FIRMA	FECHA		TÍTULO:	
DIBUJ.						
VERIF.						
APROB.						
FABR.						
CALID.				MATERIAL:	N.º DE DIBUJO Base_PIS	A4
				PESO:	ESCALA:1:1	HOJA 1 DE 1

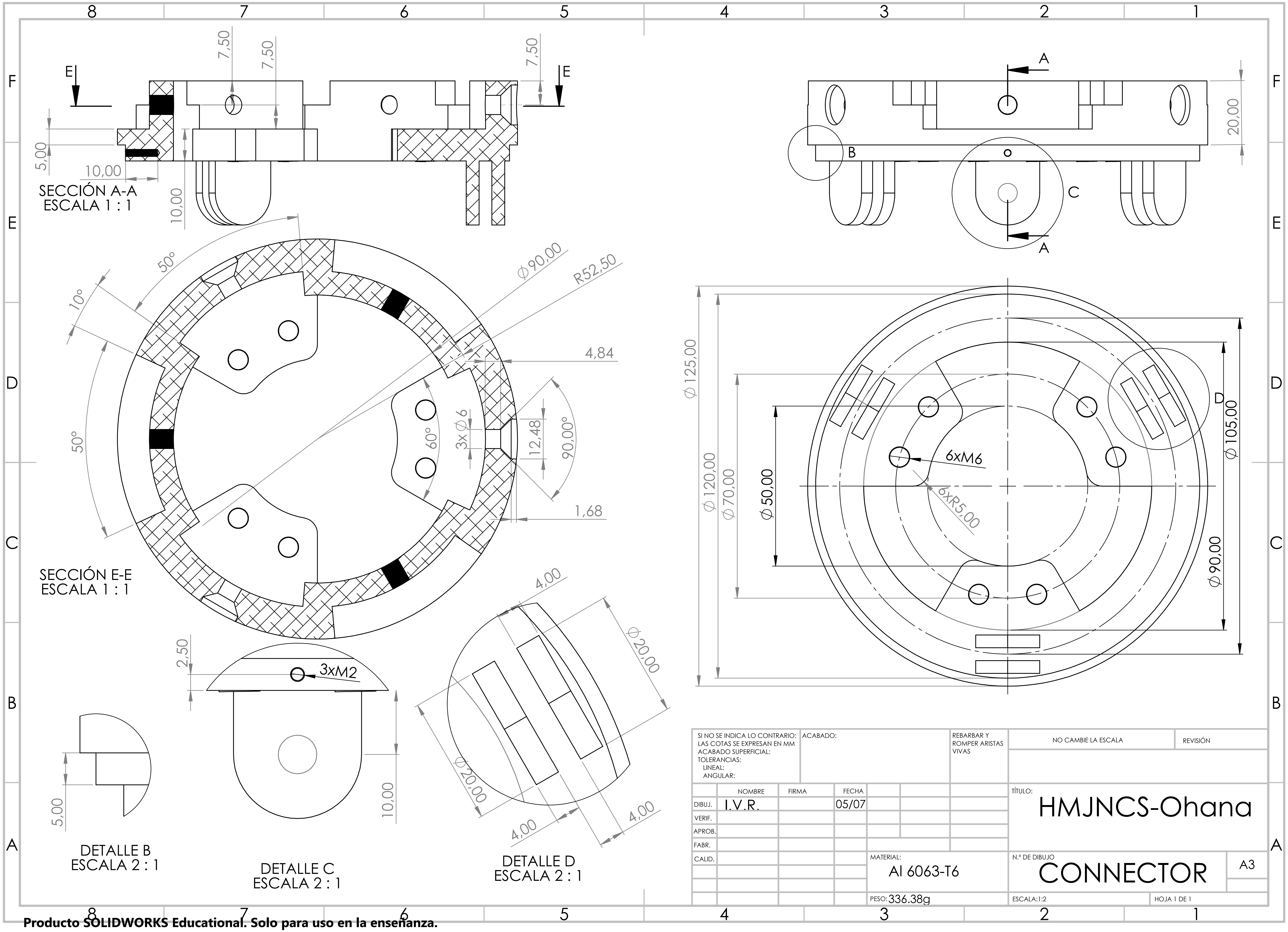
SECCIÓN A-A
ESCALA 1 : 1
SECCIÓN E-E
ESCALA 1 : 1
DETALLE B
ESCALA 2 : 1
DETALLE C
ESCALA 2 : 1
DETALLE D
ESCALA 2 : 1
7,50
5,00
10,00
50°
10°
Ø90,00
R52,50
4,84
3x Ø6
60°
12,48
90,00°
1,68
2,50
3xM2
4,00
Ø20,00
Ø125,00
Ø120,00
Ø70,00
Ø50,00
Ø105,00
Ø90,00
20,00
6xM6
6xR5,00
SI NO SE INDICA LO CONTRARIO:
LAS COTAS SE EXPRESAN EN MM
ACABADO SUPERFICIAL:
TOLERANCIAS:
LINEAL:
ANGULAR:
ACABADO:
REBARBAR Y ROMPER ARISTAS VIVAS
NO CAMBIE LA ESCALA
REVISIÓN
NOMBRE
FIRMA
FECHA
DIBUJ. I.V.R. 05/07
VERIF.
APROB.
FABR.
CALID.
TÍTULO:
HMJNCS-Ohana
MATERIAL:
Al 6063-T6
N.º DE DIBUJO
CONNECTOR
A3
PESO: 336.38g
ESCALA:1:2
HOJA 1 DE 1

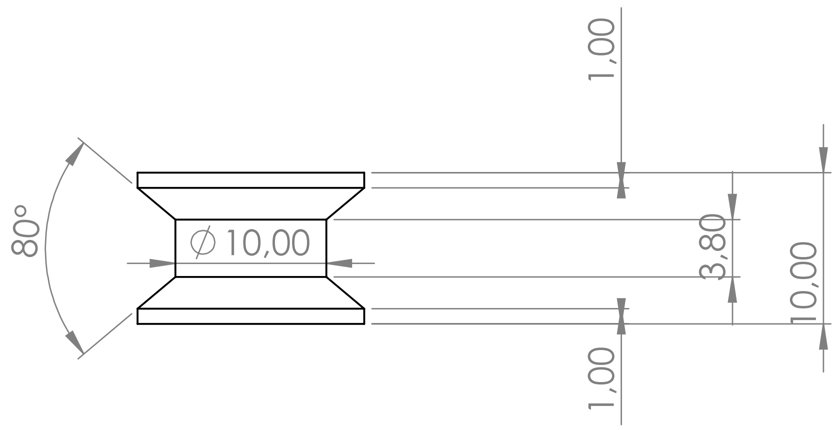

The tolerance in the inner 5mm hole needs to be calculated to ressemble a pressure fit after a study of said connection types

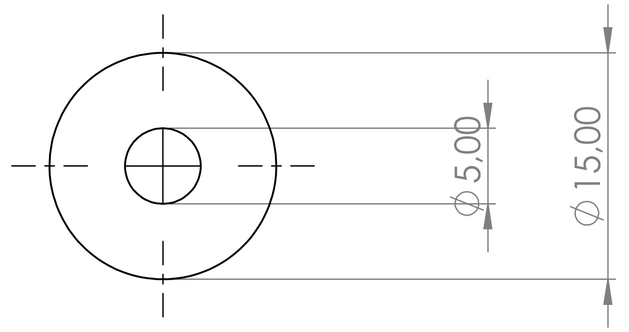

SI NO SE INDICA LO CONTRARIO: LAS COTAS SE EXPRESAN EN MM ACABADO SUPERFICIAL: TOLERANCIAS: LINEAL: ANGULAR:	ACABADO:		REBARBAR Y ROMPER ARISTAS VIVAS	NO CAMBIE LA ESCALA		REVISIÓN
	NOMBRE	FIRMA	FECHA	TÍTULO:		
DIBUJ.	I.V.R.		05/07	HMJNCS-Ohana		
VERIF.						
APROB.						
FABR.						
CALID.				MATERIAL: Al 6063-T6	N.º DE DIBUJO driven_wheel	A4
				PESO: 2.64g	ESCALA:2:1	HOJA 1 DE 1

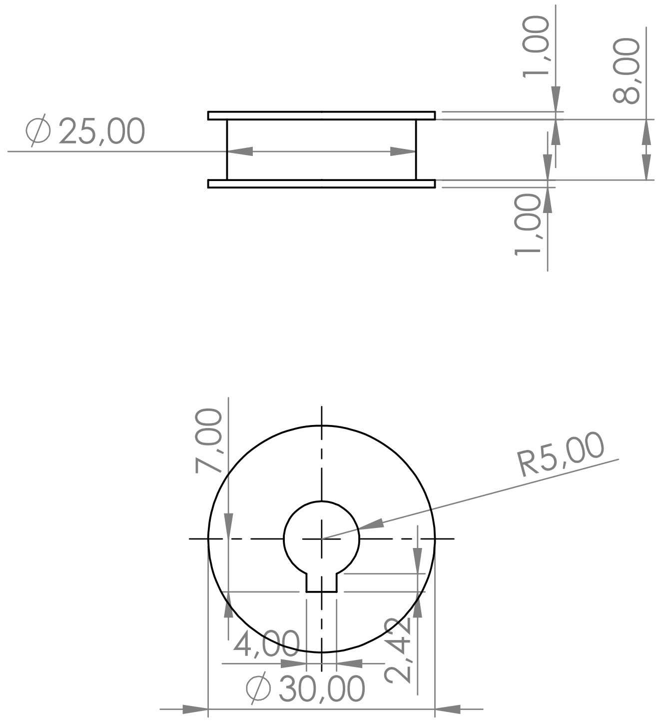

SI NO SE INDICA LO CONTRARIO:
LAS COTAS SE EXPRESAN EN MM
ACABADO SUPERFICIAL:
TOLERANCIAS:
LINEAL:
ANGULAR:

ACABADO:

REBARBAR Y ROMPER ARISTAS VIVAS

NO CAMBIE LA ESCALA

REVISIÓN

	NOMBRE	FIRMA	FECHA
DIBUJ.	I.V.R.		05/07
VERIF.			
APROB.			
FABR.			
CALID.			

TÍTULO:

HMJNCS-Ohana

MATERIAL:
Al 6063-T6

N.º DE DIBUJO
driving_wheel

A4

PESO: 12.07g

ESCALA:1:1

HOJA 1 DE 1

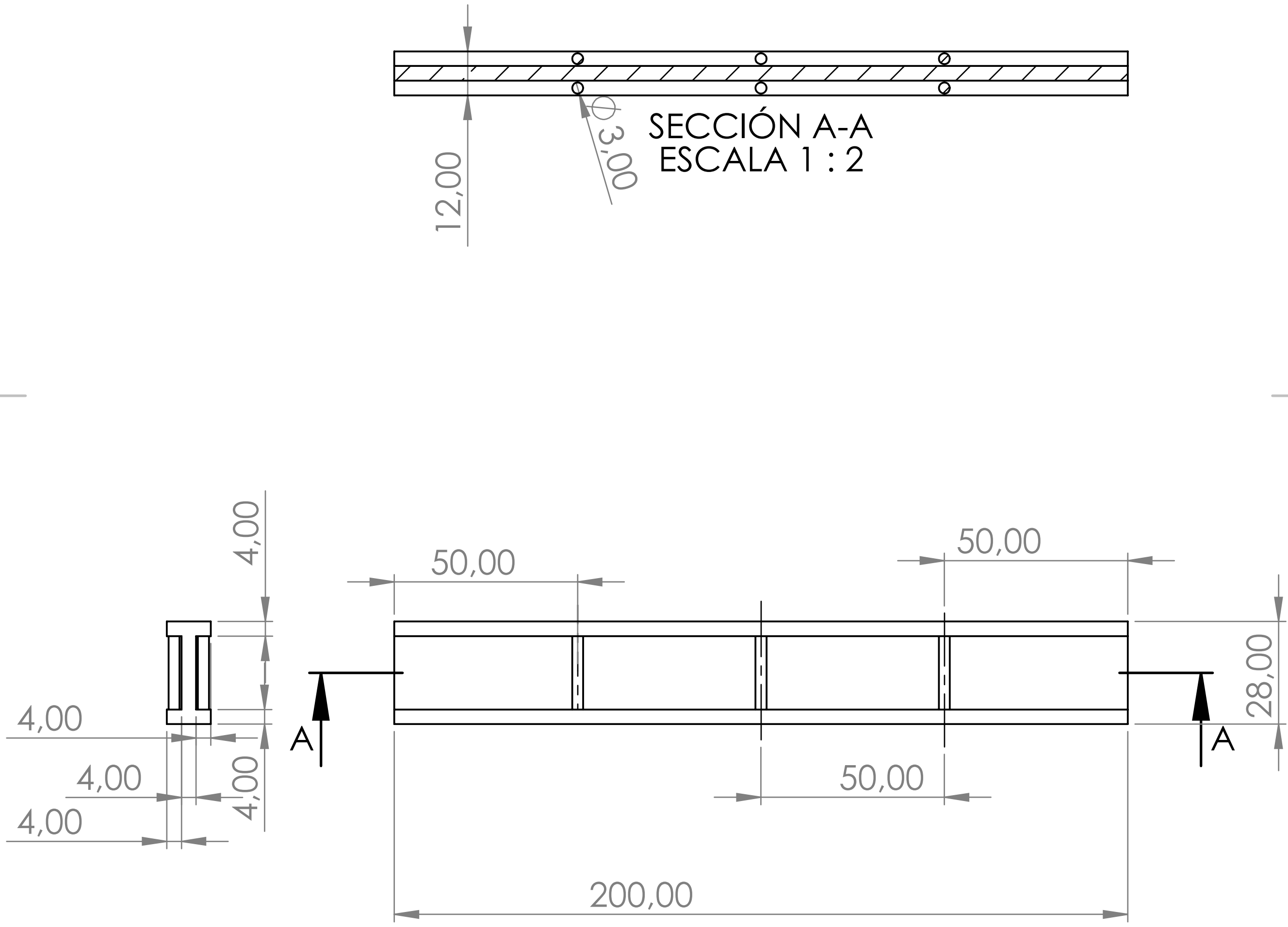

SI NO SE INDICA LO CONTRARIO:
LAS COTAS SE EXPRESAN EN MM
ACABADO SUPERFICIAL:
TOLERANCIAS:
LINEAL:
ANGULAR:

ACABADO:

REBARBAR Y ROMPER ARISTAS VIVAS

NO CAMBIE LA ESCALA

REVISIÓN

	NOMBRE	FIRMA	FECHA
DIBUJ.	I.V.R.		05/07
VERIF.			
APROB.			
FABR.			
CALID.			

TÍTULO:

HMJNCS-Ohana

MATERIAL:

Epoxy Resin: 55.1%
E Glass Fiber: 44.9%

N.º DE DIBUJO

I_beam

A4

PESO: 68.24g

ESCALA:1:5

HOJA 1 DE 1

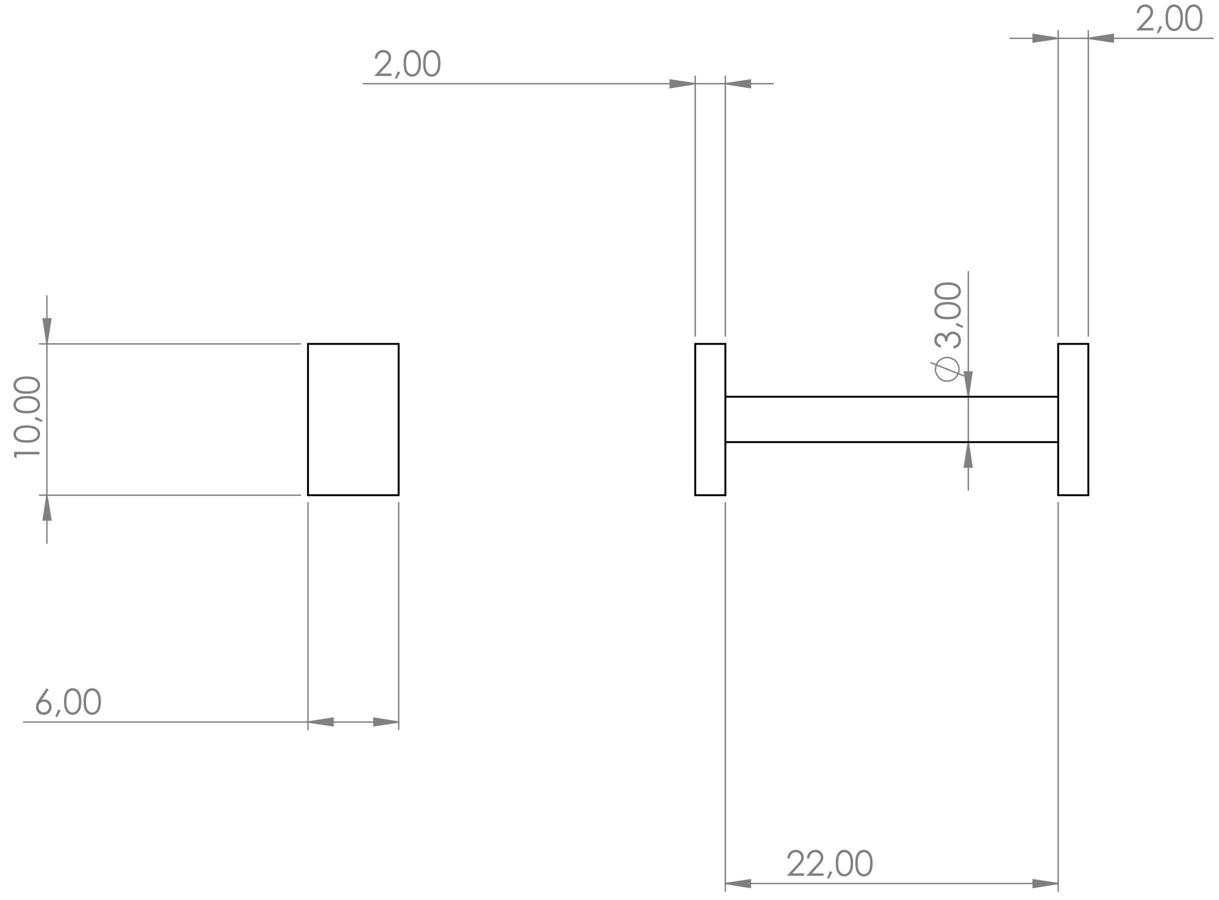

SI NO SE INDICA LO CONTRARIO:
LAS COTAS SE EXPRESAN EN MM
ACABADO SUPERFICIAL:
TOLERANCIAS:
LINEAL:
ANGULAR:

ACABADO:

REBARBAR Y ROMPER ARISTAS VIVAS

NO CAMBIE LA ESCALA

REVISIÓN

	NOMBRE	FIRMA	FECHA
DIBUJ.	I.V.R.		05/07
VERIF.			
APROB.			
FABR.			
CALID.			

TÍTULO:

HMJNCS-Ohana

MATERIAL:
AlsI 316L

N.º DE DIBUJO
radisseur

A4

PESO: 3.17g

ESCALA:2:1

HOJA 1 DE 1

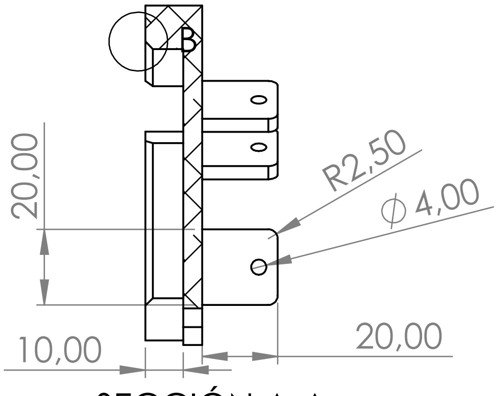

SECCIÓN A-A

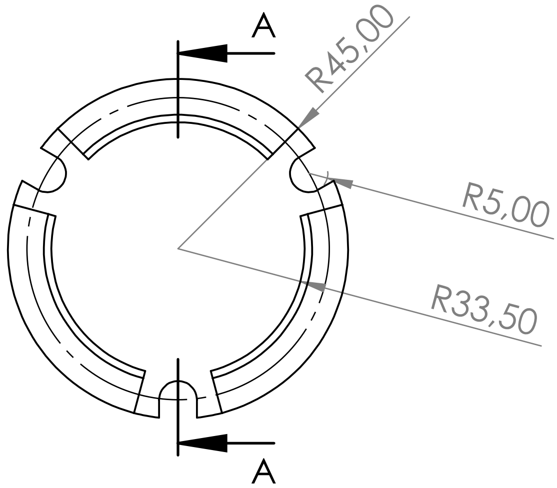

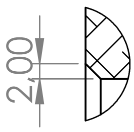

DETALLE B
ESCALA 1 : 1

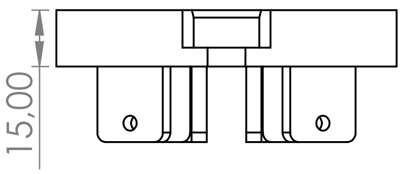

SI NO SE INDICA LO CONTRARIO:
LAS COTAS SE EXPRESAN EN MM
ACABADO SUPERFICIAL:
TOLERANCIAS:
LINEAL:
ANGULAR:

ACABADO:

REBARBAR Y ROMPER ARISTAS VIVAS

NO CAMBIE LA ESCALA

REVISIÓN

	NOMBRE	FIRMA	FECHA
DIBUJ.	I.V.R.		05/07
VERIF.			
APROB.			
FABR.			
CALID.			

TÍTULO:

HMJNCS-Ohana

MATERIAL: Al 6063-T6

N.º DE DIBUJO: Slide_PIS

A4

PESO: 163.08g

ESCALA:1:2

HOJA 1 DE 1

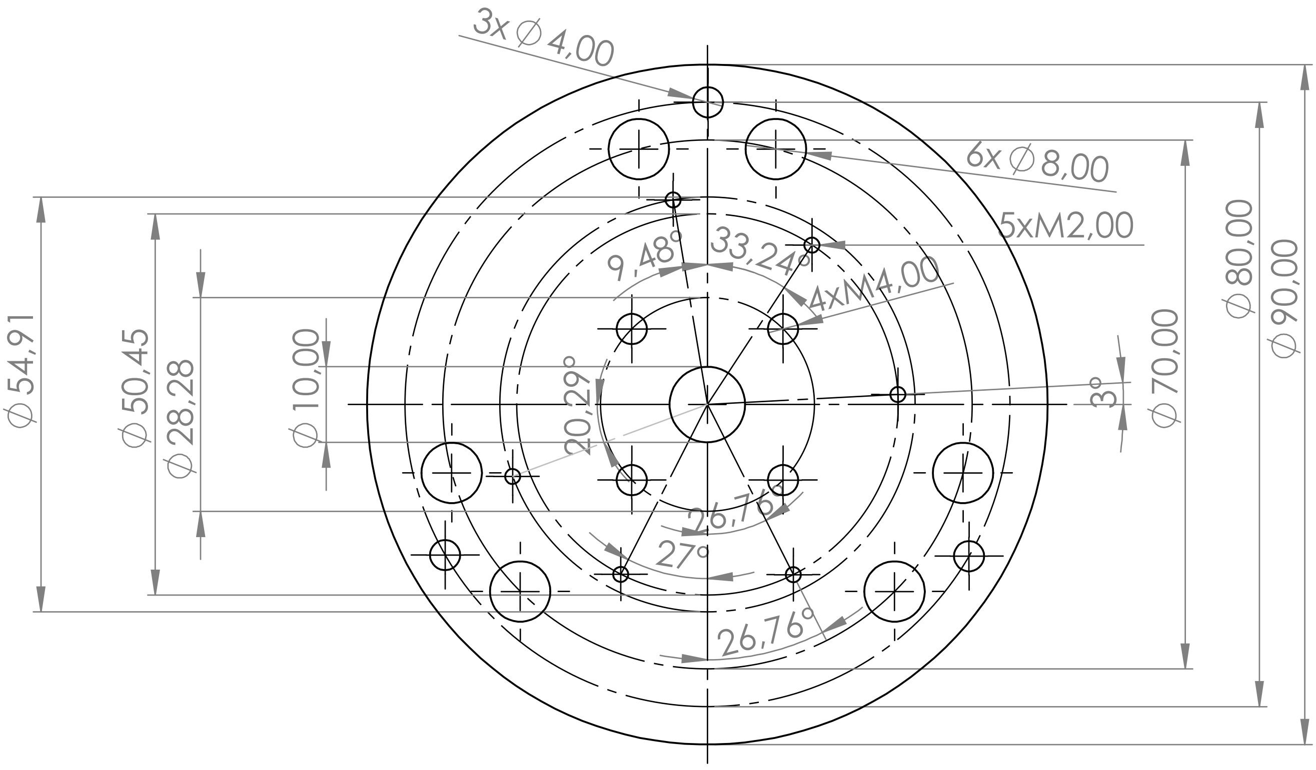

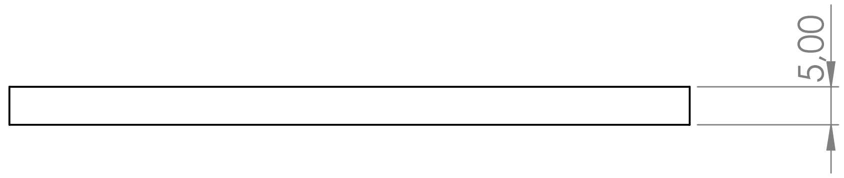

SI NO SE INDICA LO CONTRARIO: LAS COTAS SE EXPRESAN EN MM ACABADO SUPERFICIAL: TOLERANCIAS: LINEAL: ANGULAR:	ACABADO:	REBARBAR Y ROMPER ARISTAS VIVAS	NO CAMBIE LA ESCALA | REVISIÓN

	NOMBRE	FIRMA	FECHA
DIBUJ.	I.V.R.		05/07
VERIF.			
APROB.			
FABR.			
CALID.			

TÍTULO:

HMJNCS-Ohana

MATERIAL: Al 6063-T6

N.º DE DIBUJO: Top_PIS

A4

PESO: 79.31g

ESCALA:1:1

HOJA 1 DE 1

material to be determined
from a range of light weight
composited based on
availability

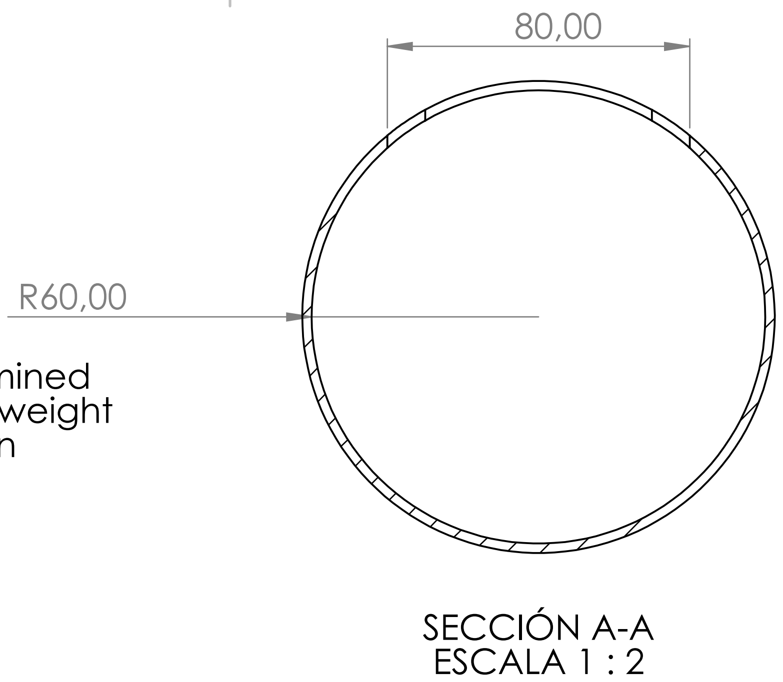

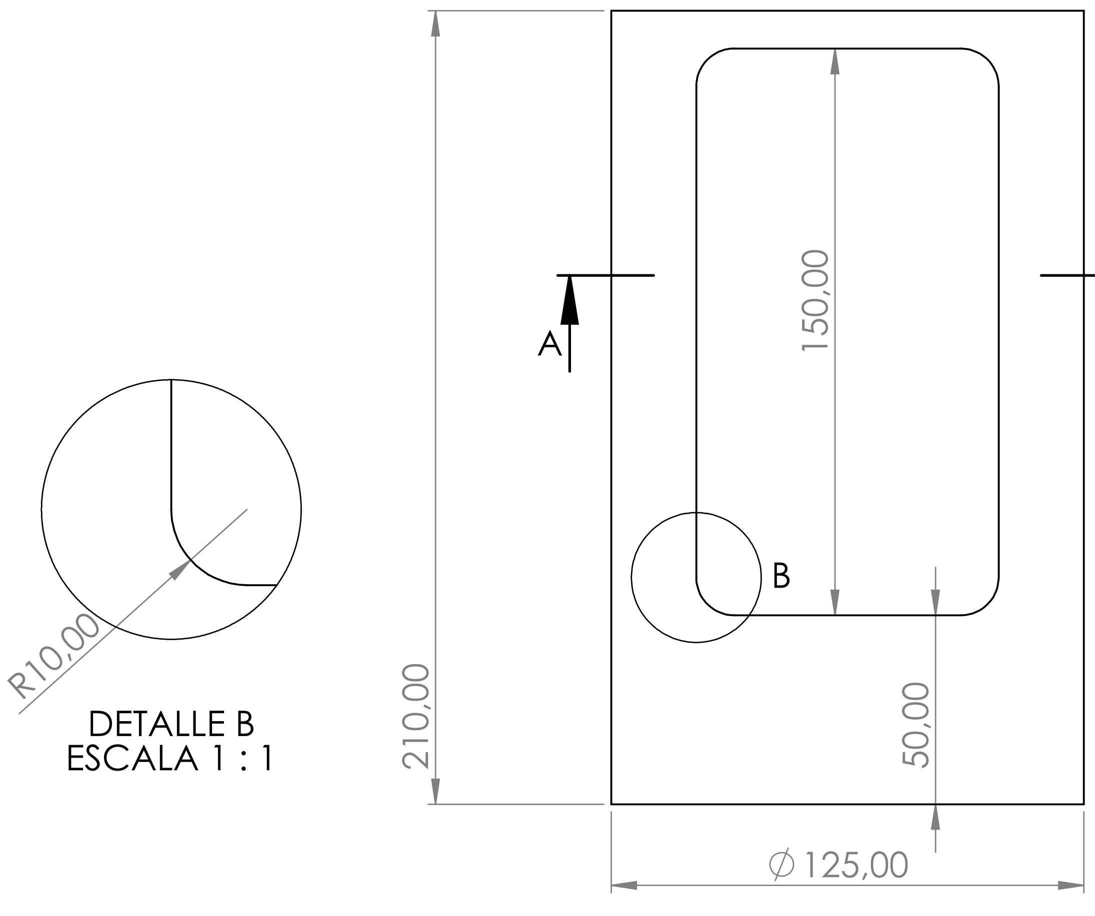

SI NO SE INDICA LO CONTRARIO: LAS COTAS SE EXPRESAN EN MM ACABADO SUPERFICIAL: TOLERANCIAS: LINEAL: ANGULAR:	ACABADO:	REBARBAR Y ROMPER ARISTAS VIVAS	NO CAMBIE LA ESCALA	REVISIÓN

	NOMBRE	FIRMA	FECHA
DIBUJ.	I.V.R.		05/07
VERIF.			
APROB.			
FABR.			
CALID.			

TÍTULO: HMJNCS-Ohana

MATERIAL:

N.º DE DIBUJO: tube_AV

A4

PESO:

ESCALA:1:2

HOJA 1 DE 1

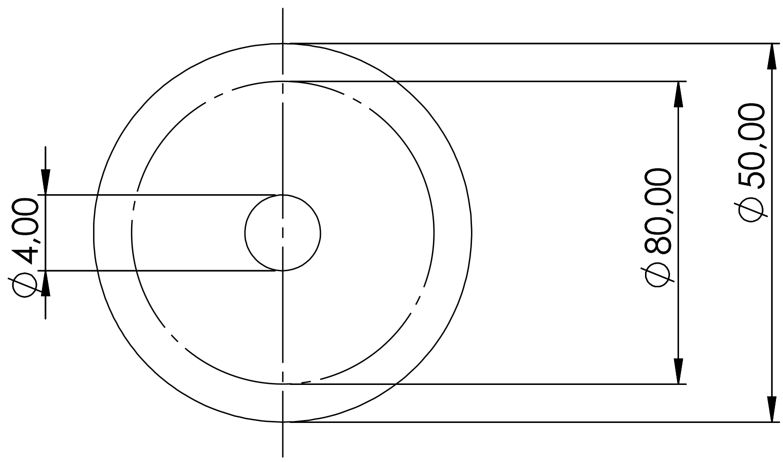

ESCALA: 5:1

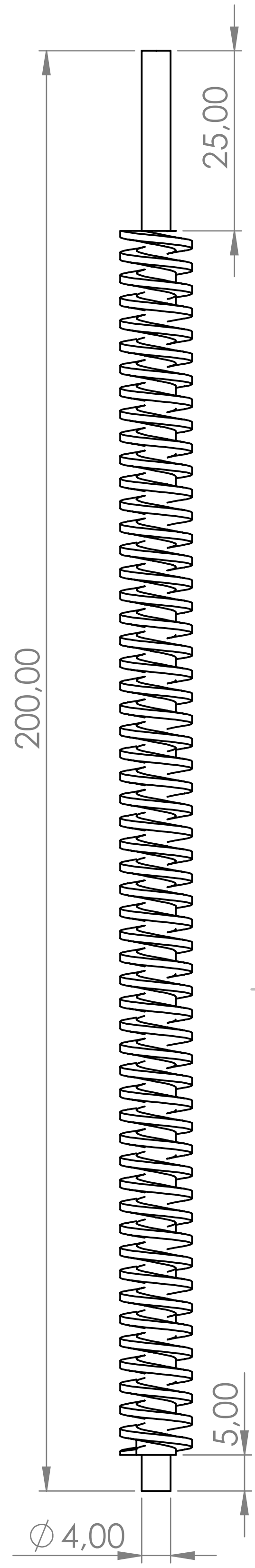

Item	Symbol	Worm (1)
Normal module (mm)	m_n	1
Nomall pressure angle (º)	α_n	20
Number of threads/teeth	Z	1
Primitive Diameter (mm)	d_1	8
Reference Cylinder lead angle (º)	Y	7.1808
Addendum (mm)	h_{a1} h_{a2}	1
Tooth depth (mm)	h	2.25
Tip diameter (mm)	d_{a1}	10
Root diameter (mm)	d_{f1}	5.5

SI NO SE INDICA LO CONTRARIO:
LAS COTAS SE EXPRESAN EN MM
ACABADO SUPERFICIAL:
TOLERANCIAS:
LINEAL:
ANGULAR:

ACABADO:

REBARBAR Y ROMPER ARISTAS VIVAS

NO CAMBIE LA ESCALA

REVISIÓN

	NOMBRE	FIRMA	FECHA
DIBUJ.	I.V.R.		05/07
VERIF.			
APROB.			
FABR.			
CALID.			

TÍTULO:

HMJNCS-Ohana

MATERIAL:

S275 steel

N.º DE DIBUJO

worm

A4

PESO: 64.93g

ESCALA:1:1

HOJA 1 DE 1

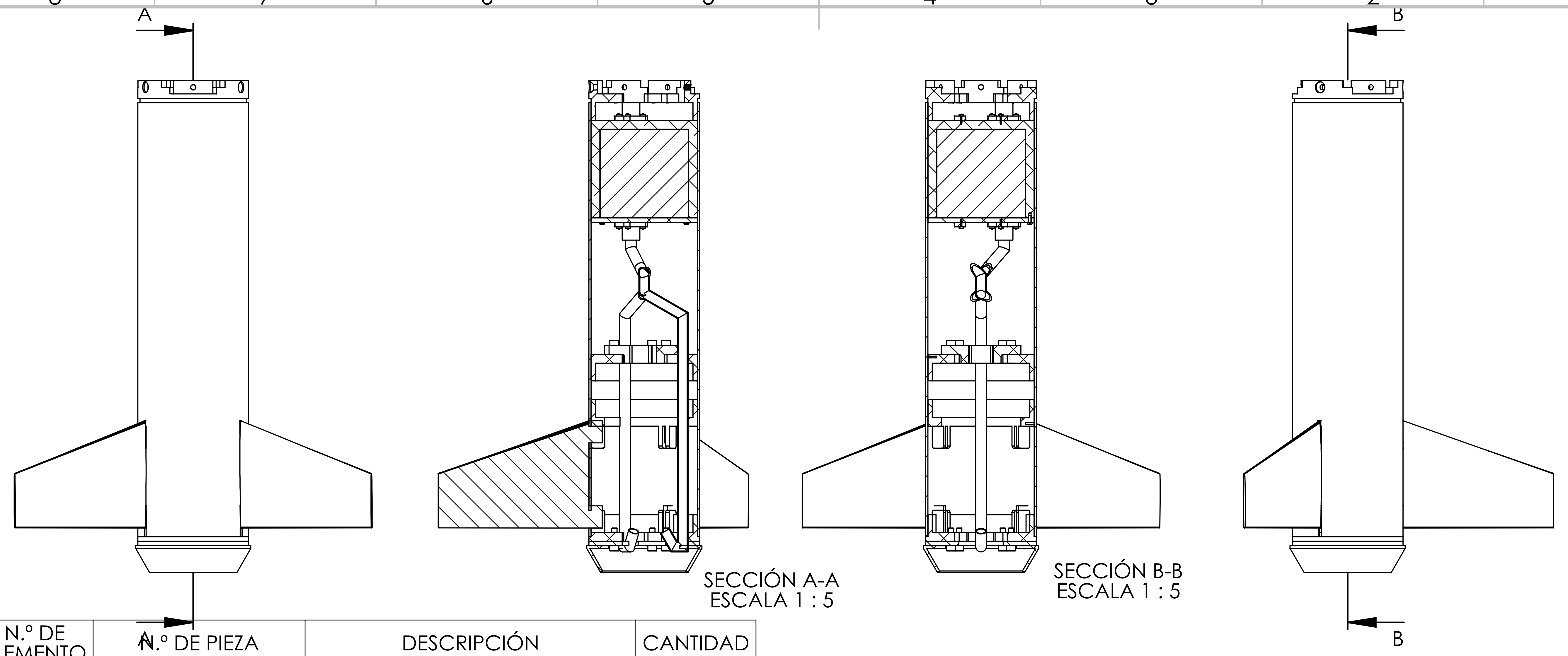

SECCIÓN A-A
ESCALA 1 : 5

SECCIÓN B-B
ESCALA 1 : 5

N.º DE ELEMENTO	N.º DE PIEZA	DESCRIPCIÓN	CANTIDAD
1	Boat_tail_coupling		1
2	Fins_retainer_LV2		1
3	motor_retinaer LV2		1
4	Thirst_plate_Lv1		3
5	CONNECTOR_ENGINE_BAY		1
6	ISO 4762 M6 x 20 - 20N		12
7	boat_tail_connector_lv3		1
8	Reservoir_main		1
9	MgO2H2		1
10	Reservoir_cover		1
11	valve_pump		4
12	ISO 7045 - M3 x 8 - Z - 8N		19
13	pipesLV1		1
14	LV1_Tube		1
15	FIN_LV1		3
16	BOAT_TAIL		1

SI NO SE INDICA LO CONTRARIO:
LAS COTAS SE EXPRESAN EN MM
ACABADO SUPERFICIAL:
TOLERANCIAS:
LINEAL:
ANGULAR:

ACABADO:

REBARBAR Y ROMPER ARISTAS VIVAS

NO CAMBIE LA ESCALA

REVISIÓN

	NOMBRE	FIRMA	FECHA
DIBUJ.	I.V.R.		05/07
VERIF.			
APROB.			
FABR.			
CALID.			

MATERIAL:

PESO: 5566.58g

TÍTULO:

HMJNCS-Ohana

N.º DE DIBUJO

LV1_Engine Bay

A3

ESCALA:1:10

HOJA 1 DE 1

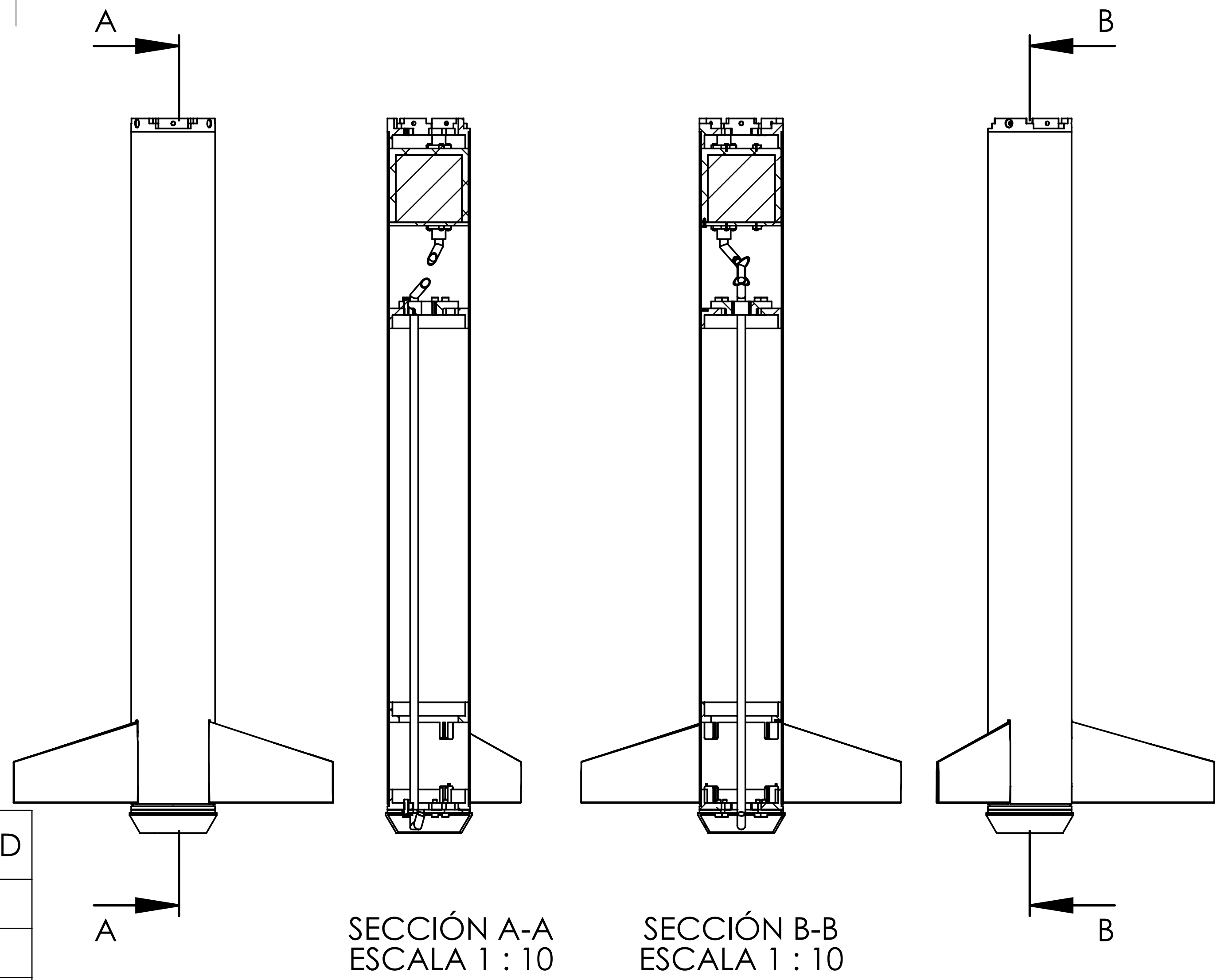

N.º DE ELEMENTO	N.º DE PIEZA	DESCRIPCIÓN	CANTIDAD
1	Boat_tail_coupling		1
2	Fins_retainer_LV2		1
3	motor_retinaer LV2		1
4	Thirst_plate_Lv1		3
5	CONNECTOR_ENGINE_BAY		1
6	ISO 4762 M6 x 20 - 20N		12
7	boat_tail_connector_lv3		1
8	LV3_Tube		1
9	Reservoir_main		1
10	MgO2H2		1
11	Reservoir_cover		1
12	valve_pump		4
13	ISO 7045 - M3 x 8 - Z - 8N		19
14	pipesLV2		1
15	BOAT_TAIL		1
16	LV2_Tube		1
17	FIN_LV2		3

SI NO SE INDICA LO CONTRARIO:
LAS COTAS SE EXPRESAN EN MM
ACABADO SUPERFICIAL:
TOLERANCIAS:
LINEAL:
ANGULAR:

ACABADO:

REBARBAR Y ROMPER ARISTAS VIVAS

NO CAMBIE LA ESCALA

REVISIÓN

	NOMBRE	FIRMA	FECHA
DIBUJ.	I.V.R.		05/07
VERIF.			
APROB.			
FABR.			
CALID.			

TÍTULO:

HMJNCS-Ohana

MATERIAL:

N.º DE DIBUJO

Engine Bay LV2

A3

PESO: 6612.84g

ESCALA: 1:10

HOJA 1 DE 1

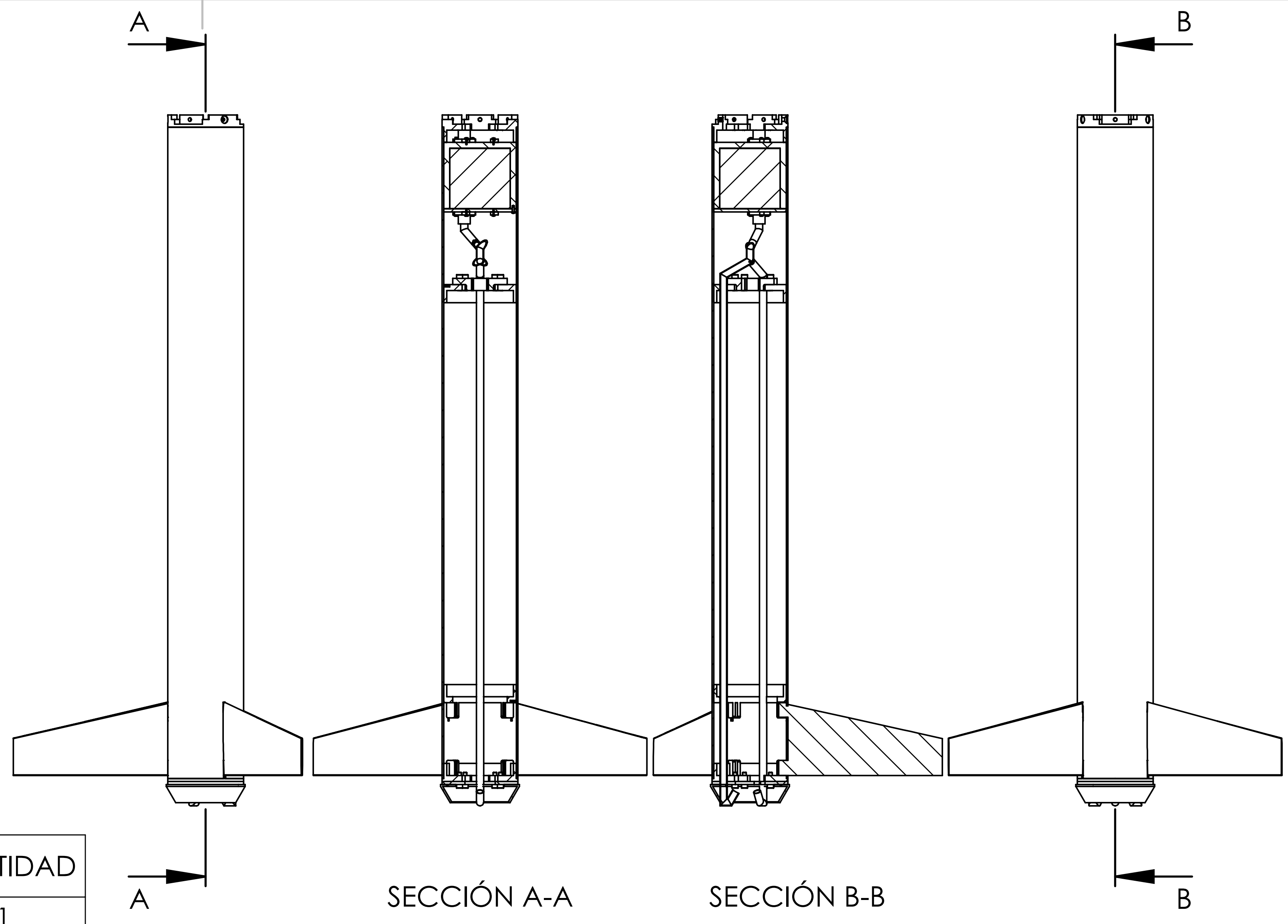

N.º DE ELEMENTO	N.º DE PIEZA	DESCRIPCIÓN	CANTIDAD
1	Boat_tail_coupling		1
2	Fins_retainer_LV2		1
3	motor_retinaer LV2		1
4	Thirst_plate_Lv1		3
5	CONNECTOR_ENGINE_BAY		1
6	ISO 4762 M6 x 20 - 20N		12
7	boat_tail_connector_lv3		1
8	Reservoir_main		1
9	MgO2H2		1
10	Reservoir_cover		1
11	valve_pump		4
12	pipes		1
13	ISO 7045 - M3 x 8 - Z - 8N		19
14	LV3_Tube		1
15	BOAT_TAIL		1
16	FIN_LV3		3

SI NO SE INDICA LO CONTRARIO:
LAS COTAS SE EXPRESAN EN MM
ACABADO SUPERFICIAL:
TOLERANCIAS:
LINEAL:
ANGULAR:

ACABADO:

REBARBAR Y ROMPER ARISTAS VIVAS

NO CAMBIE LA ESCALA

REVISIÓN

	NOMBRE	FIRMA	FECHA
DIBUJ.	I.V.R.		05/07
VERIF.			
APROB.			
FABR.			
CALID.			

TÍTULO:

HMJNCS-Ohana

MATERIAL:

N.º DE DIBUJO

LV_3_Engine_Bay

A3

PESO: 6847.64g

ESCALA:1:10

HOJA 1 DE 1

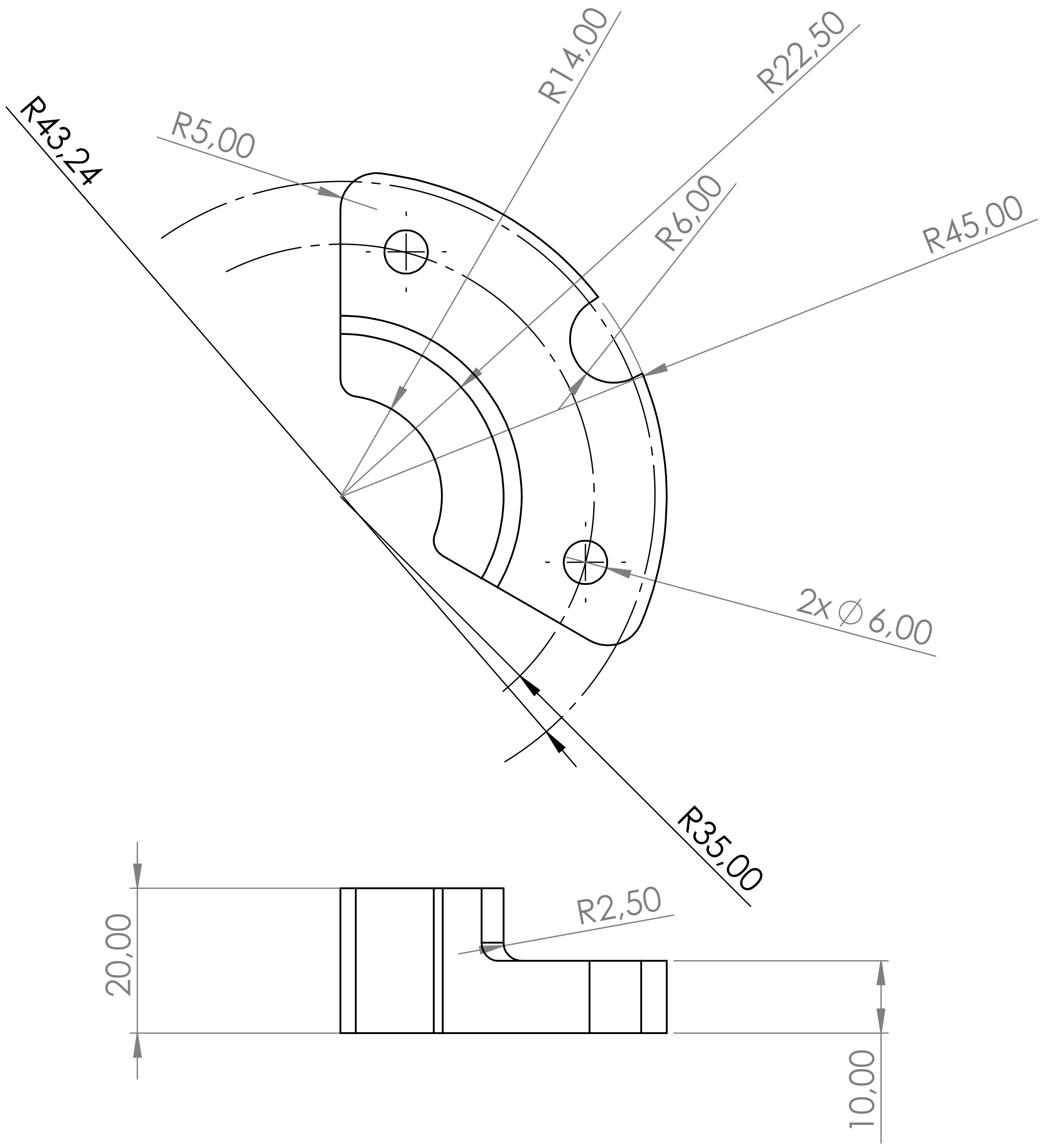

SI NO SE INDICA LO CONTRARIO: LAS COTAS SE EXPRESAN EN MM ACABADO SUPERFICIAL: TOLERANCIAS: LINEAL: ANGULAR:	ACABADO:	REBARBAR Y ROMPER ARISTAS VIVAS	NO CAMBIE LA ESCALA	REVISIÓN	
	NOMBRE	FIRMA	FECHA	TÍTULO: HMJNCS-Ohana	
DIBUJ.	I.V.R.		05/07		
VERIF.					
APROB.					
FABR.					
CALID.				MATERIAL: Al 6063-T6	N.º DE DIBUJO Thirst_plate_V2	A4
				PESO: 56.7g	ESCALA:1:1	HOJA 1 DE 1

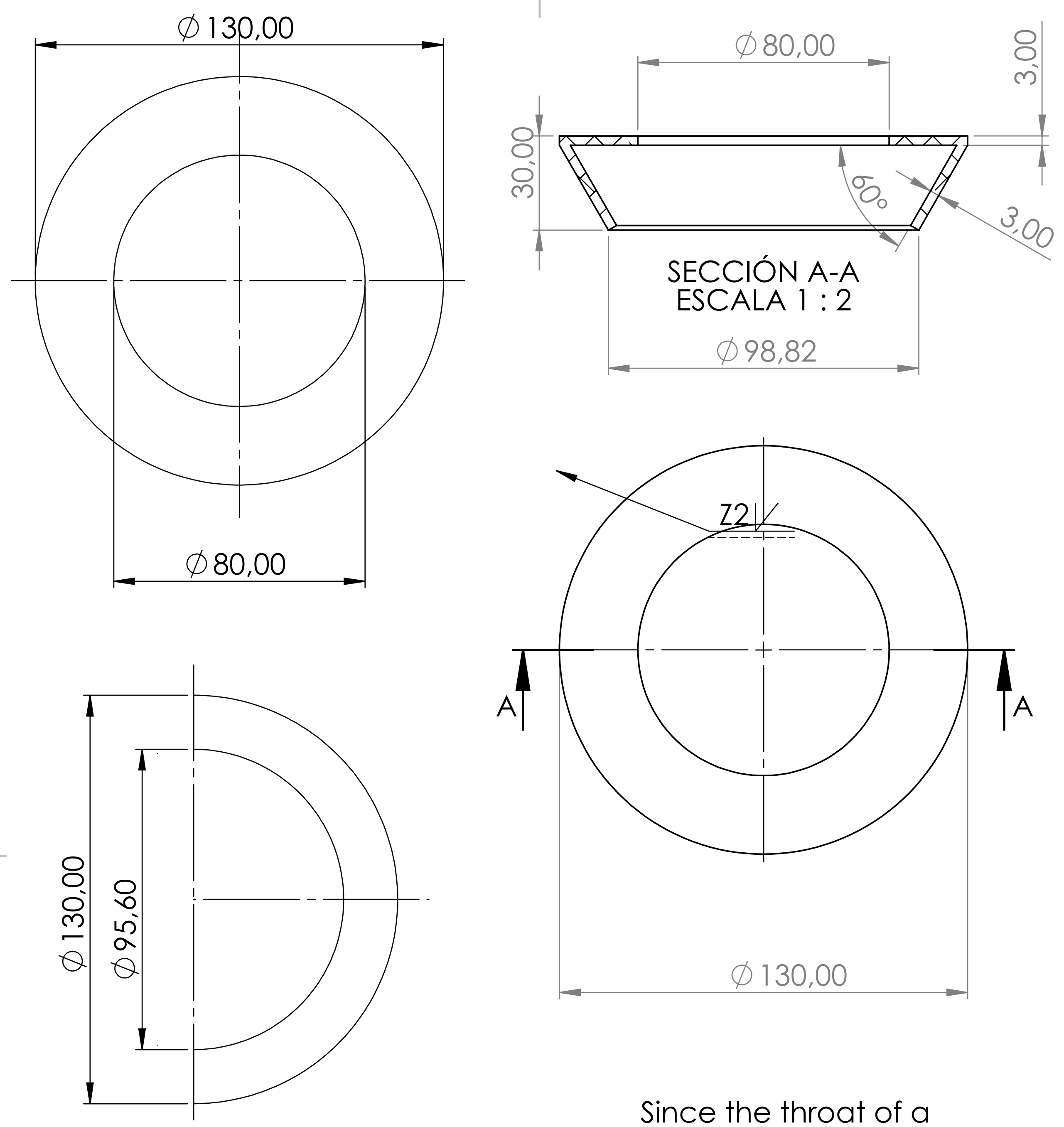

Both parts of the boat tail are to be cut from a 3mm piece of aluminium as per the dimensions stipulated above

Since the throat of a weld shoudl not exceed 0.7t=3*0.7=2.1mm, a=2mm

SI NO SE INDICA LO CONTRARIO: LAS COTAS SE EXPRESAN EN MM ACABADO SUPERFICIAL: TOLERANCIAS: LINEAL: ANGULAR:	ACABADO:	REBARBAR Y ROMPER ARISTAS VIVAS	NO CAMBIE LA ESCALA	REVISIÓN

	NOMBRE	FIRMA	FECHA
DIBUJ.	I.V.R.		06/07
VERIF.			
APROB.			
FABR.			
CALID.			

TÍTULO: HMJNCS-Ohana

MATERIAL: Al 6063-T6

N.º DE DIBUJO: BOAT_TAIL

A4

PESO: 152.73g

ESCALA:1:5

HOJA 1 DE 1

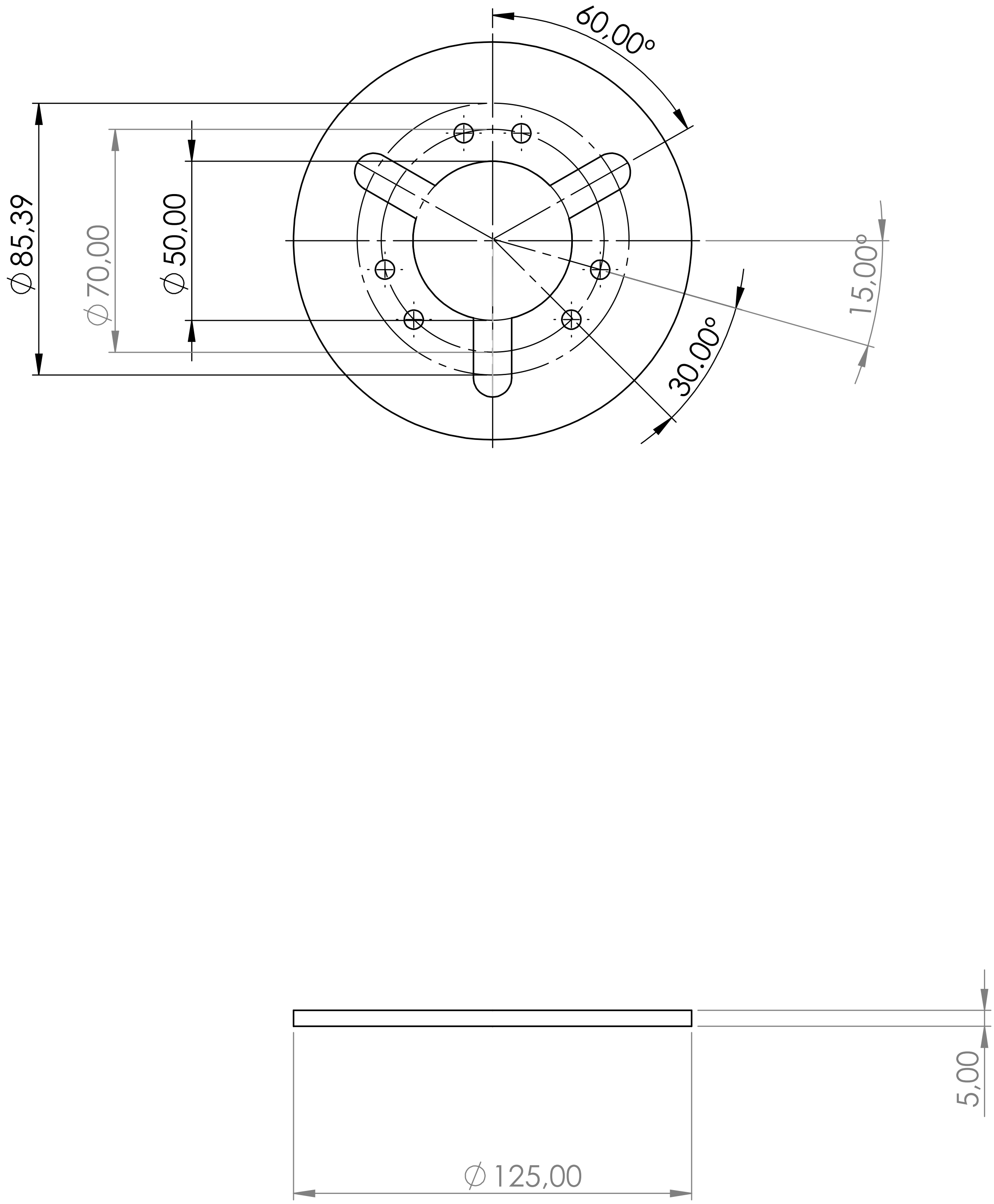

SI NO SE INDICA LO CONTRARIO: LAS COTAS SE EXPRESAN EN MM ACABADO SUPERFICIAL: TOLERANCIAS: LINEAL: ANGULAR:	ACABADO:	REBARBAR Y ROMPER ARISTAS VIVAS	NO CAMBIE LA ESCALA / REVISIÓN

	NOMBRE	FIRMA	FECHA
DIBUJ.	I.V.R.		05/07
VERIF.			
APROB.			
FABR.			
CALID.			

TÍTULO:

HMJNCS-Ohana

MATERIAL: Al 6063-T6

N.º DE DIBUJO: Boat_tail_connector

A4

PESO: 125.68g

ESCALA:1:2

HOJA 1 DE 1

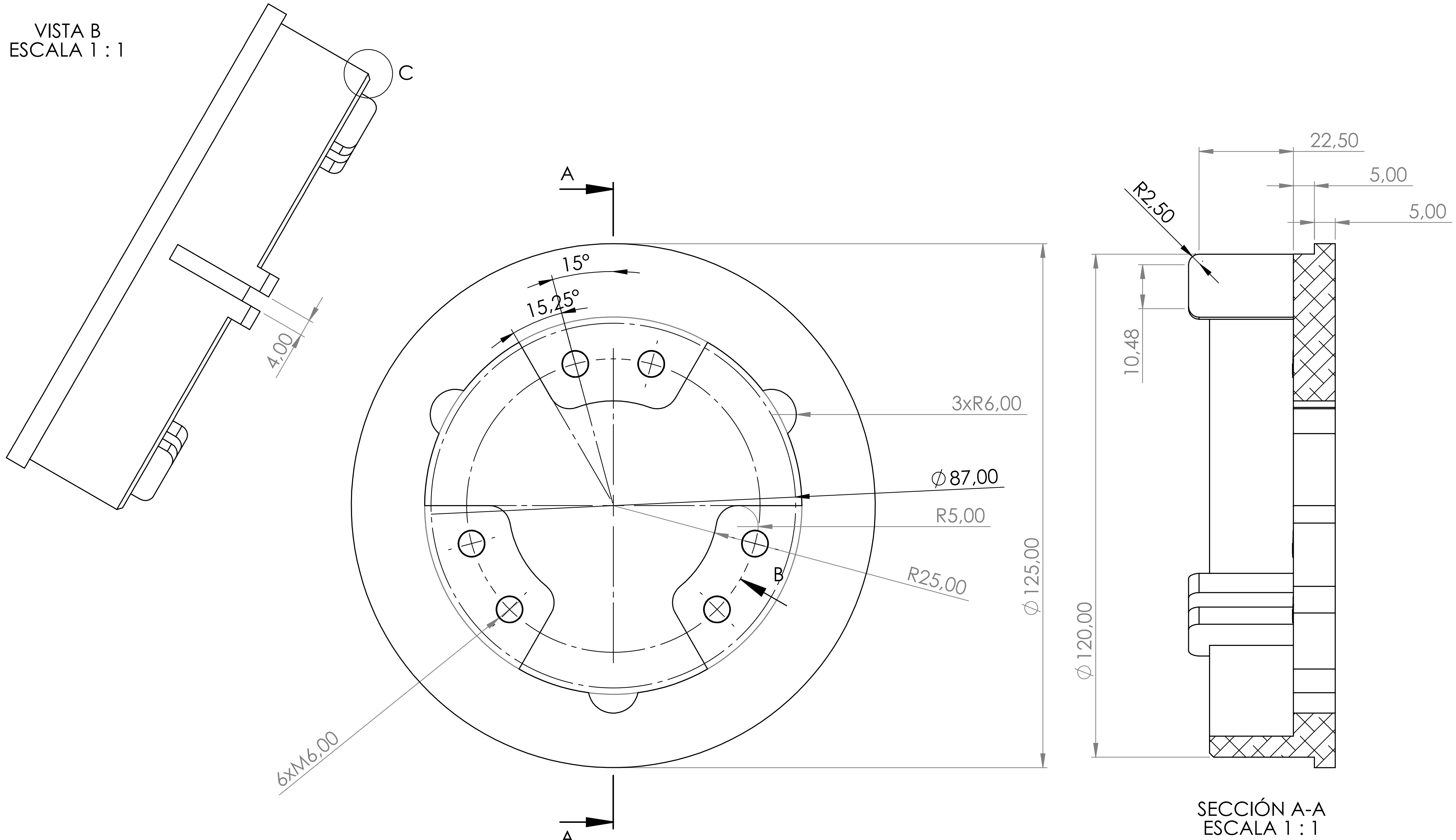

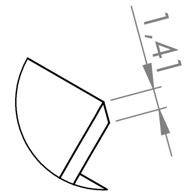

DETALLE C
ESCALA 2 : 1

SI NO SE INDICA LO CONTRARIO:
LAS COTAS SE EXPRESAN EN MM
ACABADO SUPERFICIAL:
TOLERANCIAS:
LINEAL:
ANGULAR:

ACABADO:

REBARBAR Y ROMPER ARISTAS VIVAS

NO CAMBIE LA ESCALA

REVISIÓN

	NOMBRE	FIRMA	FECHA
DIBUJ.	I.V.R.		05/07
VERIF.			
APROB.			
FABR.			
CALID.			

TÍTULO:

HMJNCS-Ohana

MATERIAL:

Al 6063-T6

N.º DE DIBUJO

Boat_tail_coupling

A3

PESO: 313.09g

ESCALA: 1:1

HOJA 1 DE 1

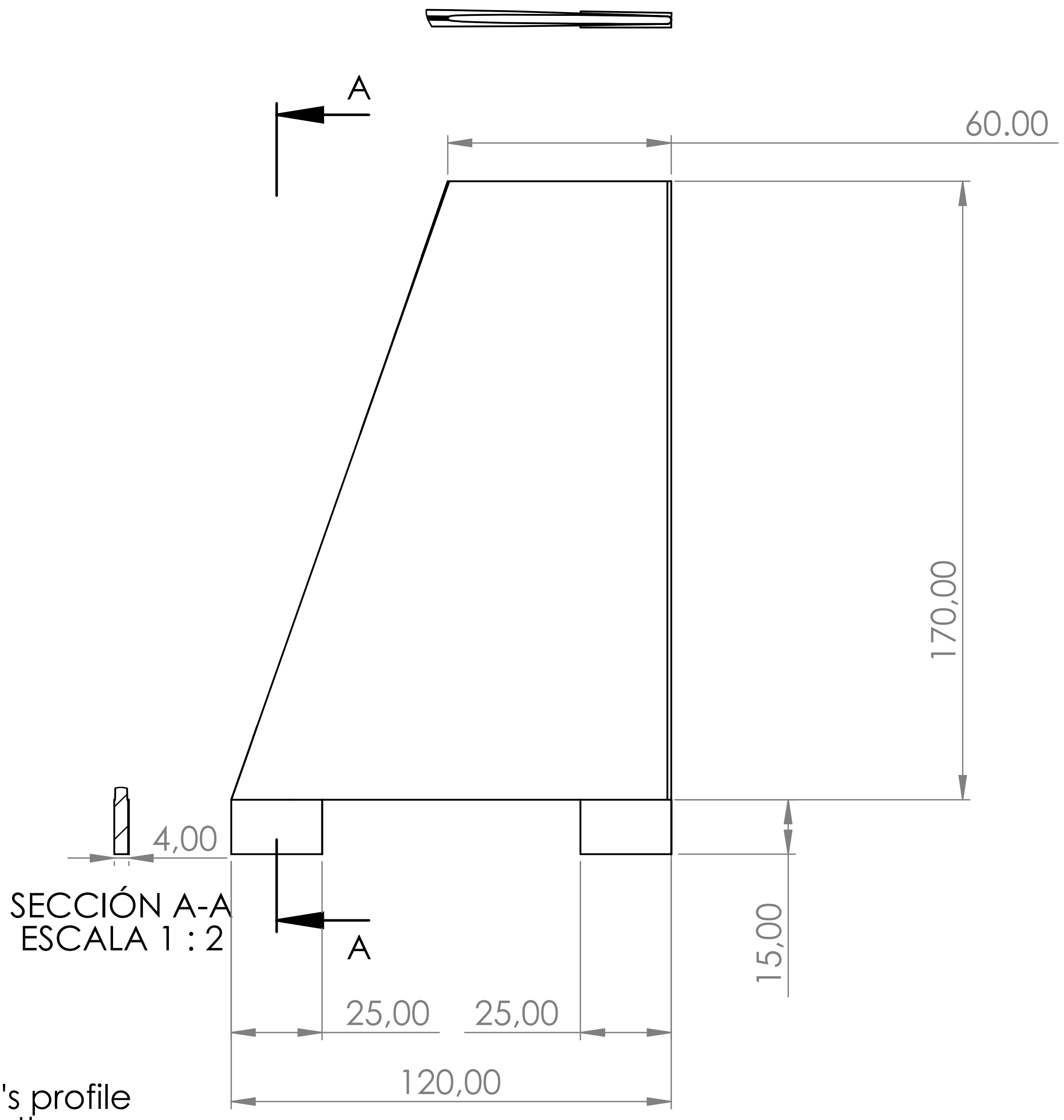

The fin's profile follows the equations:

$$L = 120 - \frac{60}{L_{fin}} z$$

$$y \begin{cases} 5t(z)\left[0.2969\sqrt{\frac{x}{L(z)}} - \frac{0.1260}{L(z)}x - 0.3516\left(\frac{x}{L(z)}\right)^2 + 0.2843\left(\frac{x}{L(z)}\right)^3 - 0.1015\left(\frac{x}{L(z)}\right)^4\right] & if\ x \leq L(z) \\ \sqrt{(0.0105t(z))^2 - (x - L(z))^2} & if\ L(z) \leq x \leq L(z) + 0.0105t(z) \end{cases}$$

SI NO SE INDICA LO CONTRARIO: LAS COTAS SE EXPRESAN EN MM ACABADO SUPERFICIAL: TOLERANCIAS: LINEAL: ANGULAR:	ACABADO:	REBARBAR Y ROMPER ARISTAS VIVAS	NO CAMBIE LA ESCALA / REVISIÓN

	NOMBRE	FIRMA	FECHA
DIBUJ.	I.V.R.		05/07
VERIF.			
APROB.			
FABR.			
CALID.			

TÍTULO: HMJNCS-Ohana

MATERIAL: Epoxy Resin: 81.1% E Glass Fibeer: 18.9%

N.º DE DIBUJO: FIN_LV1

A4

PESO: 81.39g

ESCALA:1:5

HOJA 1 DE 1

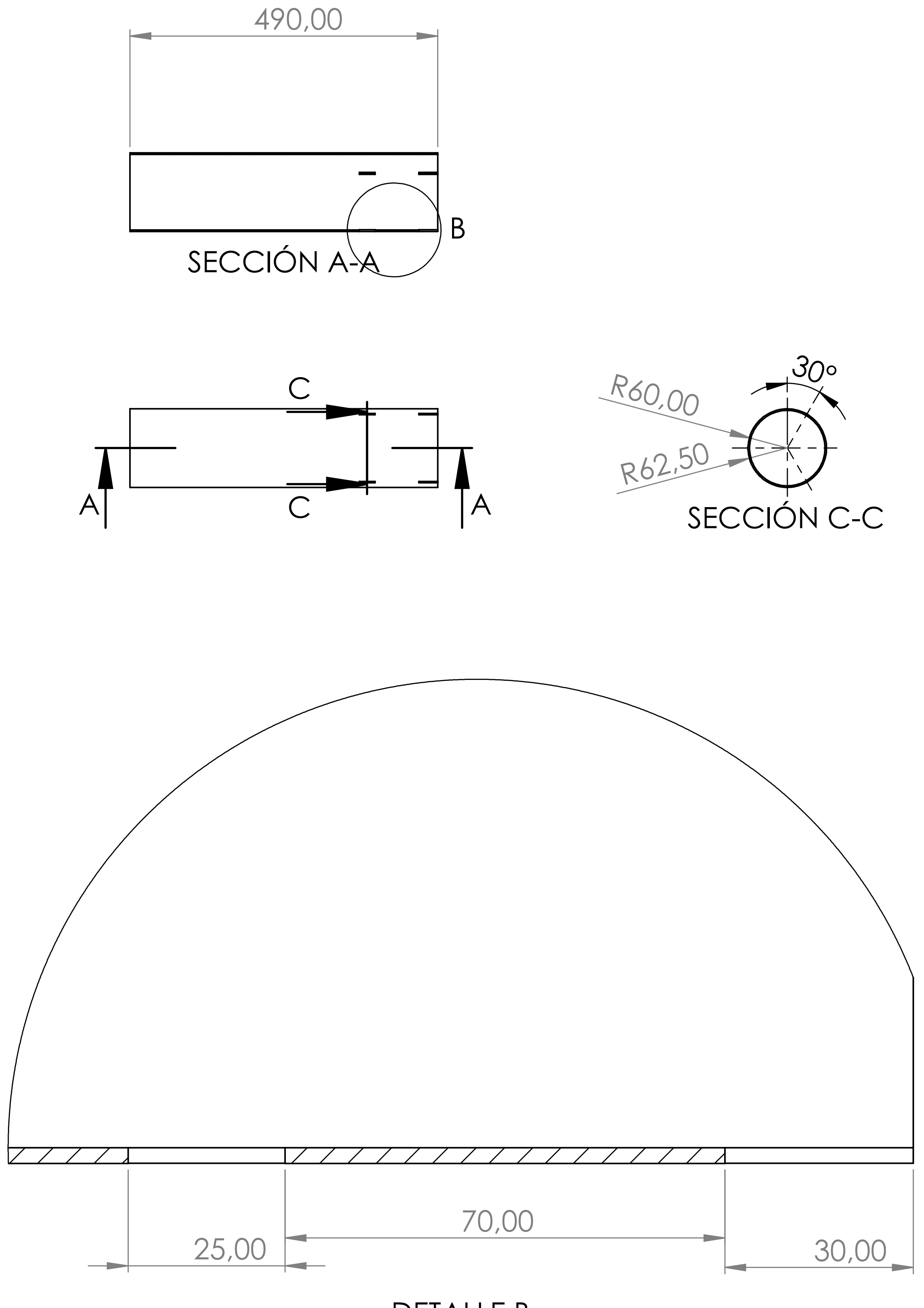

SI NO SE INDICA LO CONTRARIO: LAS COTAS SE EXPRESAN EN MM ACABADO SUPERFICIAL: TOLERANCIAS: LINEAL: ANGULAR:	ACABADO:	REBARBAR Y ROMPER ARISTAS VIVAS	NO CAMBIE LA ESCALA / REVISIÓN

	NOMBRE	FIRMA	FECHA
DIBUJ.	I.V.R.		05/07
VERIF.			
APROB.			
FABR.			
CALID.			

TÍTULO:

HMJNCS-Ohana

MATERIAL:

Epoxy Resin: 18.72%
E Glas Fiber: 81.285

N.º DE DIBUJO

LV1_Tube

A4

PESO: 1119.80g

ESCALA:1:10

HOJA 1 DE 1

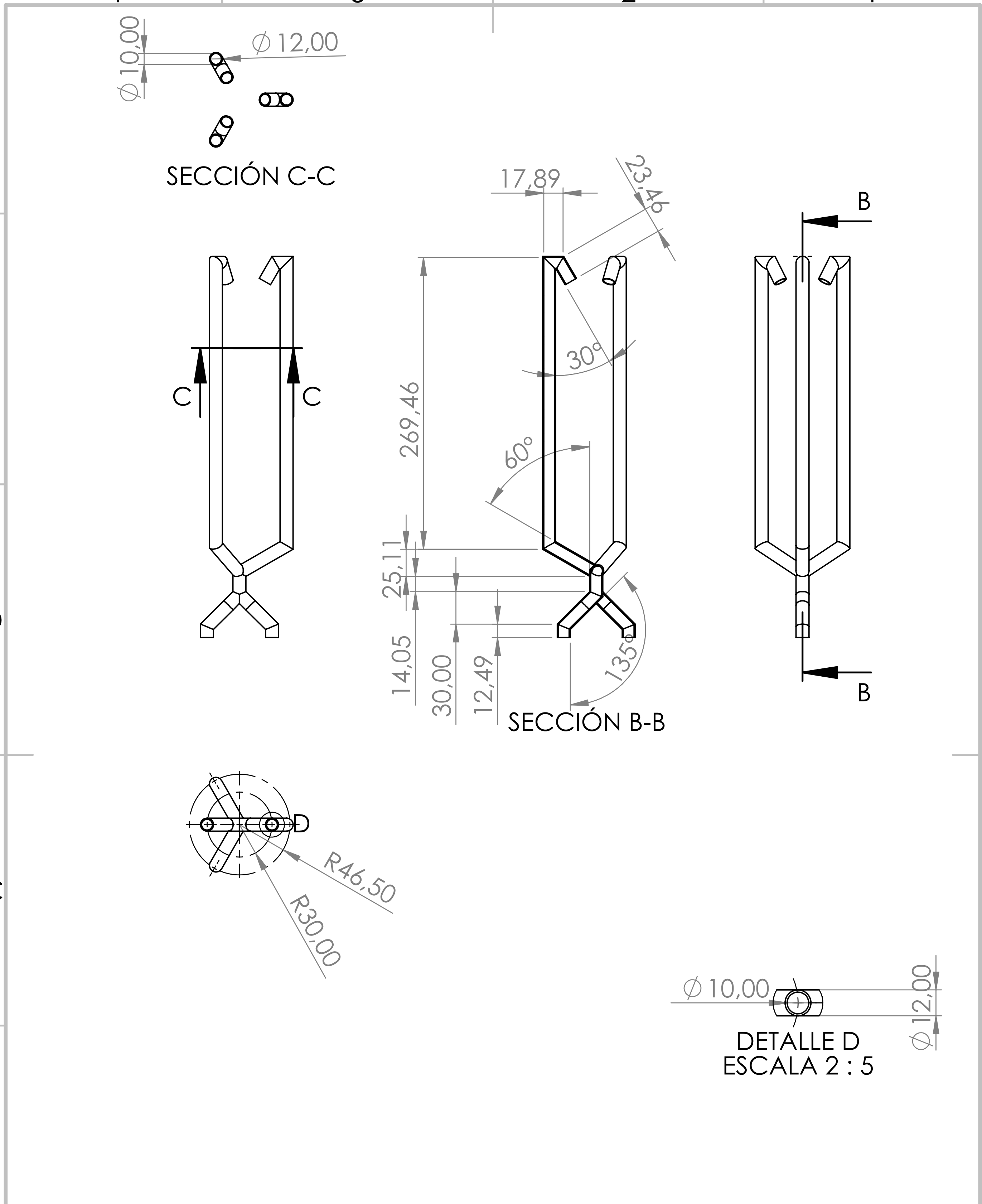

SI NO SE INDICA LO CONTRARIO: LAS COTAS SE EXPRESAN EN MM ACABADO SUPERFICIAL: TOLERANCIAS: LINEAL: ANGULAR:	ACABADO:	REBARBAR Y ROMPER ARISTAS VIVAS	NO CAMBIE LA ESCALA	REVISIÓN

	NOMBRE	FIRMA	FECHA		
DIBUJ.	I.V.R.		05/07		
VERIF.					
APROB.					
FABR.					
CALID.					

TÍTULO:

HMJNCS-Ohana

MATERIAL: PVC

N.º DE DIBUJO: pipesLV1

A4

PESO: 50.98g

ESCALA:1:5

HOJA 1 DE 1

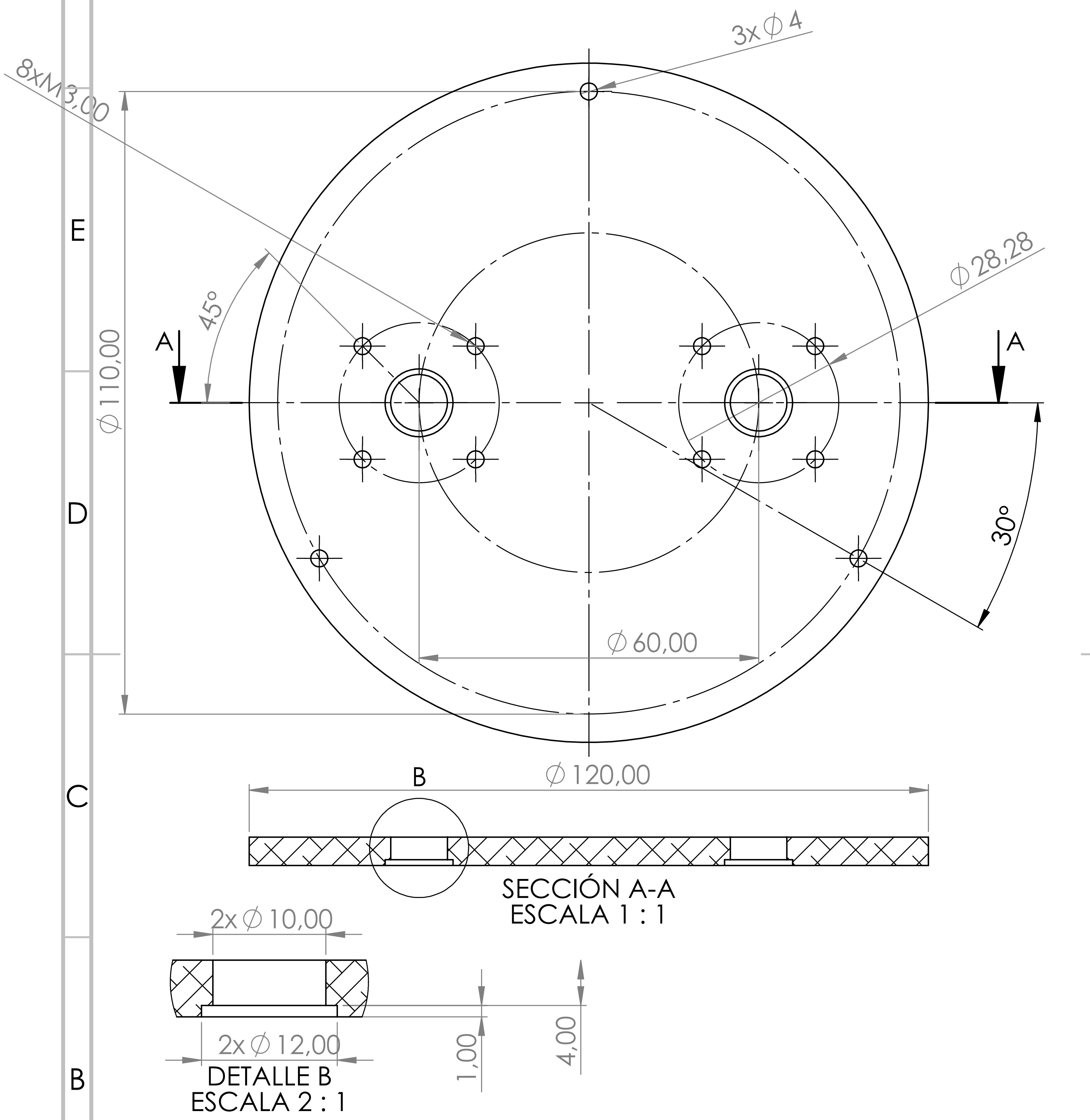

SI NO SE INDICA LO CONTRARIO: LAS COTAS SE EXPRESAN EN MM ACABADO SUPERFICIAL: TOLERANCIAS: LINEAL: ANGULAR:	ACABADO:	REBARBAR Y ROMPER ARISTAS VIVAS	NO CAMBIE LA ESCALA	REVISIÓN	

	NOMBRE	FIRMA	FECHA	
DIBUJ.	I.V.R.		05/07	
VERIF.				
APROB.				
FABR.				
CALID.				MATERIAL: Al 6063-T6
				PESO: 149.58g

TÍTULO:

HMJNCS-Ohana

N.º DE DIBUJO

Reservoir_cover

A4

ESCALA:1:1 | HOJA 1 DE 1

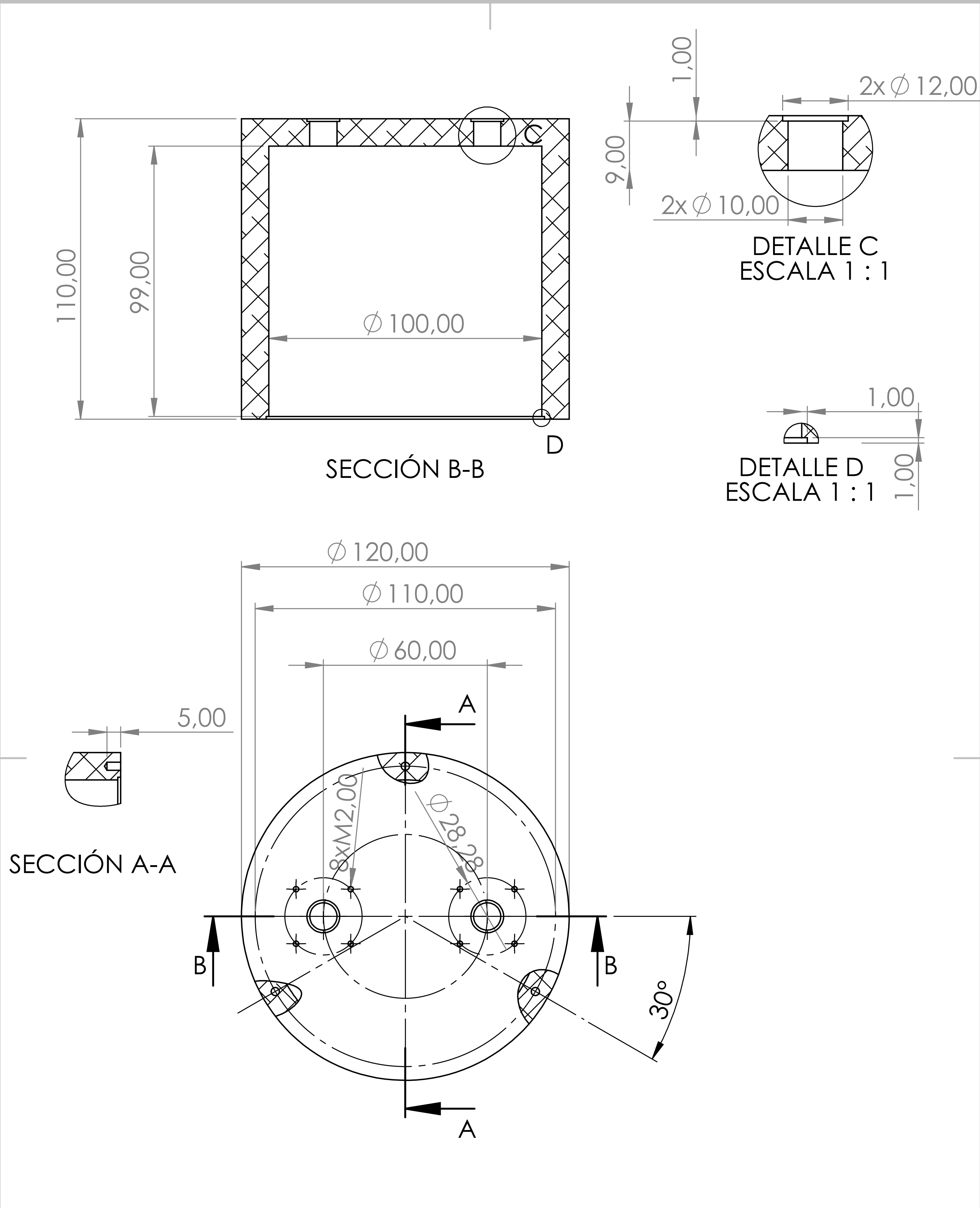

SI NO SE INDICA LO CONTRARIO: LAS COTAS SE EXPRESAN EN MM ACABADO SUPERFICIAL: TOLERANCIAS: LINEAL: ANGULAR:	ACABADO:	REBARBAR Y ROMPER ARISTAS VIVAS	NO CAMBIE LA ESCALA	REVISIÓN

	NOMBRE	FIRMA	FECHA
DIBUJ.	I.V.R.		05/07
VERIF.			
APROB.			
FABR.			
CALID.			

TÍTULO:

HMJNCS-Ohana

MATERIAL: Al 6063-T6

N.º DE DIBUJO: Reservoir_main

A4

PESO: 1232.26g

ESCALA:1:2

HOJA 1 DE 1

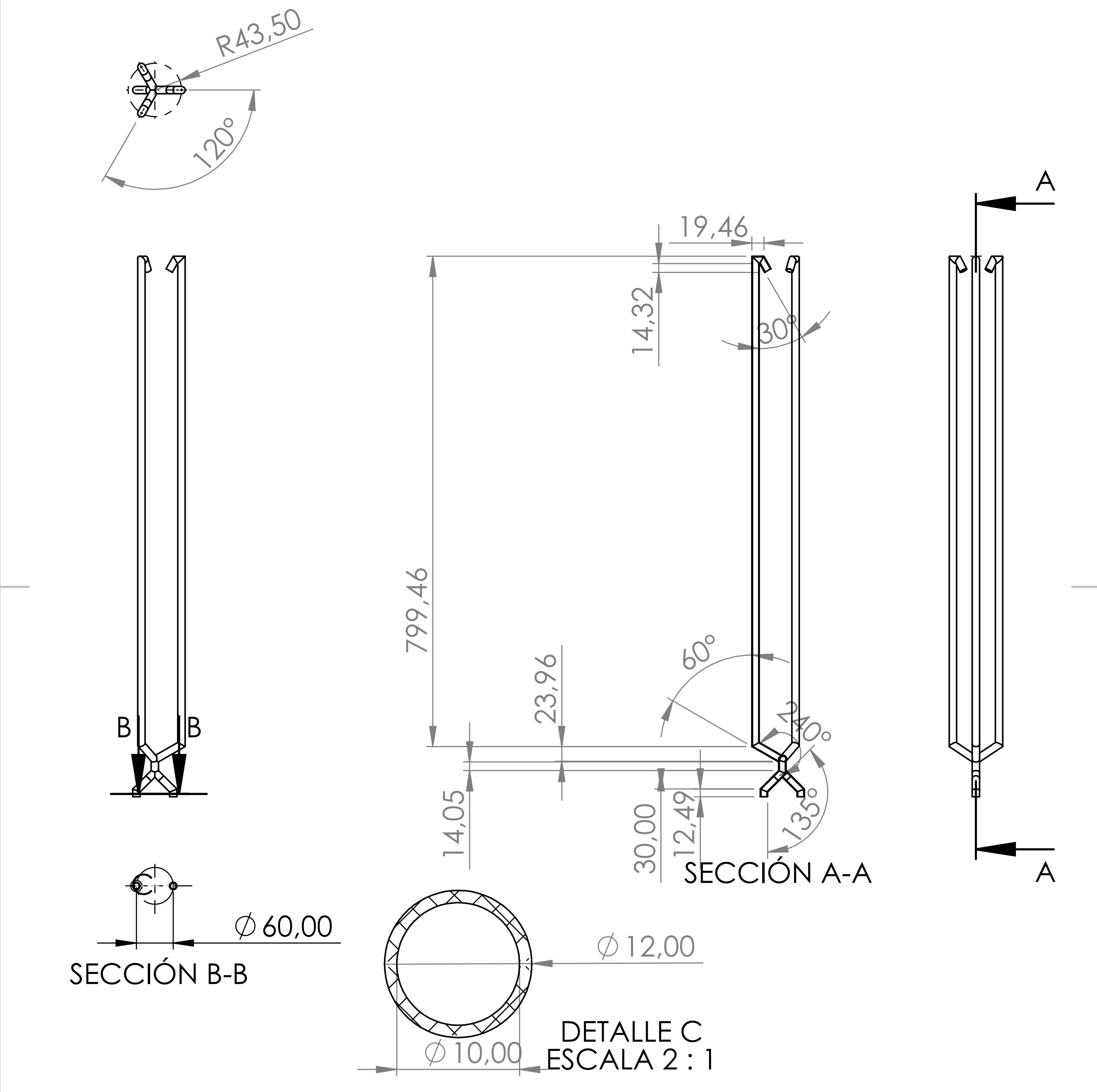

SI NO SE INDICA LO CONTRARIO: LAS COTAS SE EXPRESAN EN MM ACABADO SUPERFICIAL: TOLERANCIAS: LINEAL: ANGULAR:	ACABADO:	REBARBAR Y ROMPER ARISTAS VIVAS	NO CAMBIE LA ESCALA / REVISIÓN

	NOMBRE	FIRMA	FECHA
DIBUJ.	I.V.R.		05/07
VERIF.			
APROB.			
FABR.			
CALID.			

TÍTULO:

HMJNCS-Ohana

MATERIAL: PVC

N.º DE DIBUJO: pipesLV2

A4

PESO: 122.29g

ESCALA:1:10

HOJA 1 DE 1

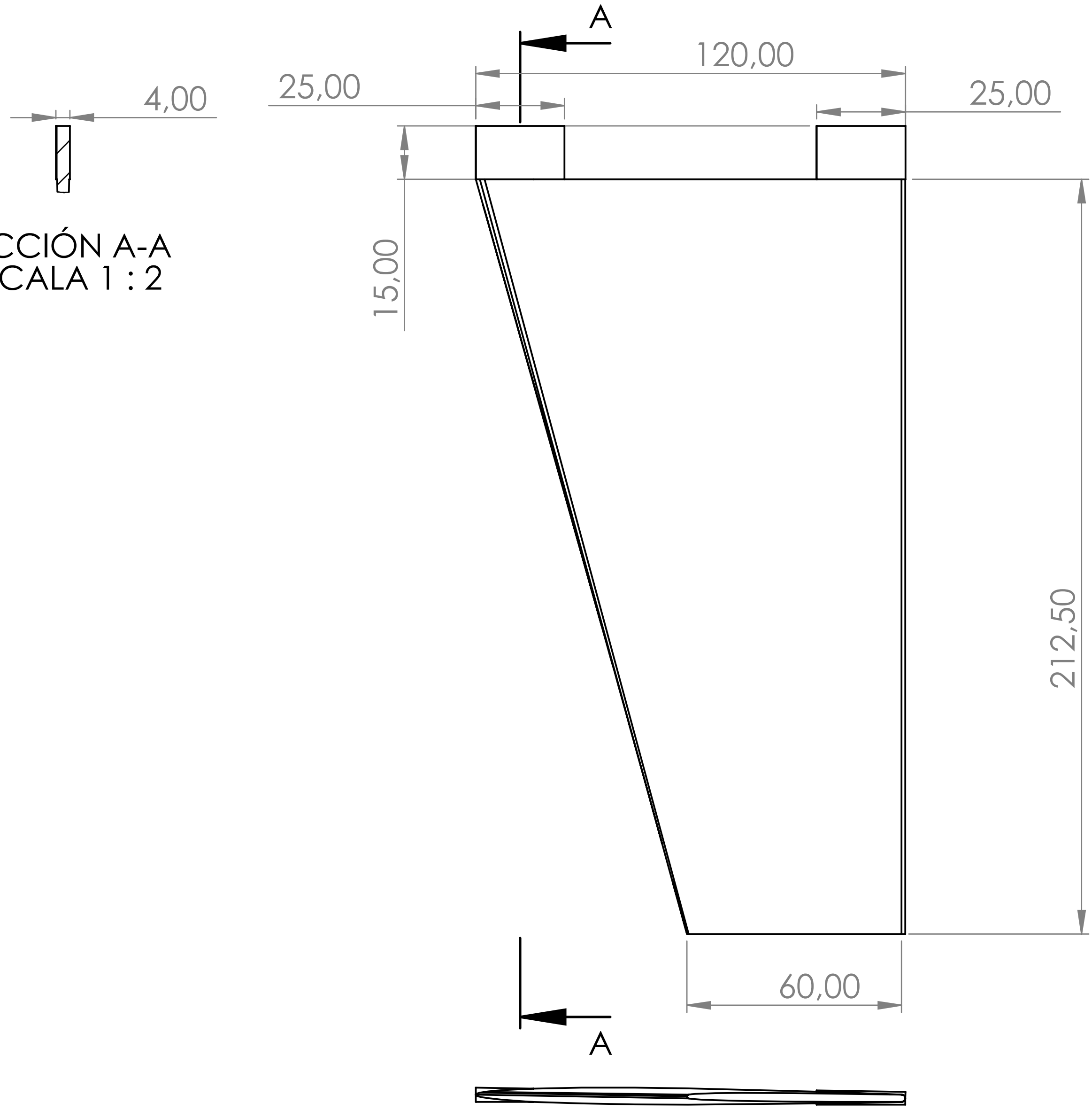

The fins's profile follows the equations:

$$L = 120 - \frac{60}{L_{fin}} z$$

$$y \begin{cases} 5t(z)\left[0.2969\sqrt{\frac{x}{L(z)}} - \frac{0.1260}{L(z)}x - 0.3516\left(\frac{x}{L(z)}\right)^2 + 0.2843\left(\frac{x}{L(z)}\right)^3 - 0.1015\left(\frac{x}{L(z)}\right)^4\right] & if\ x \leq L(z) \\ \sqrt{(0.0105t(z))^2 - (x - L(z))^2} & if\ L(z) \leq x \leq L(z) + 0.0105t(z) \end{cases}$$

SI NO SE INDICA LO CONTRARIO:
LAS COTAS SE EXPRESAN EN MM
ACABADO SUPERFICIAL:
TOLERANCIAS:
LINEAL:
ANGULAR:

ACABADO:

REBARBAR Y ROMPER ARISTAS VIVAS

NO CAMBIE LA ESCALA

REVISIÓN

	NOMBRE	FIRMA	FECHA
DIBUJ.	I.V.R.		05/07
VERIF.			
APROB.			
FABR.			
CALID.			

TÍTULO:

HMJNCS-Ohana

MATERIAL:

Epoxy Resin: 75.3%
E Glass Fiber: 24.7%

N.º DE DIBUJO

FIN_LV2

A4

PESO: 104.55g

ESCALA:1:2

HOJA 1 DE 1

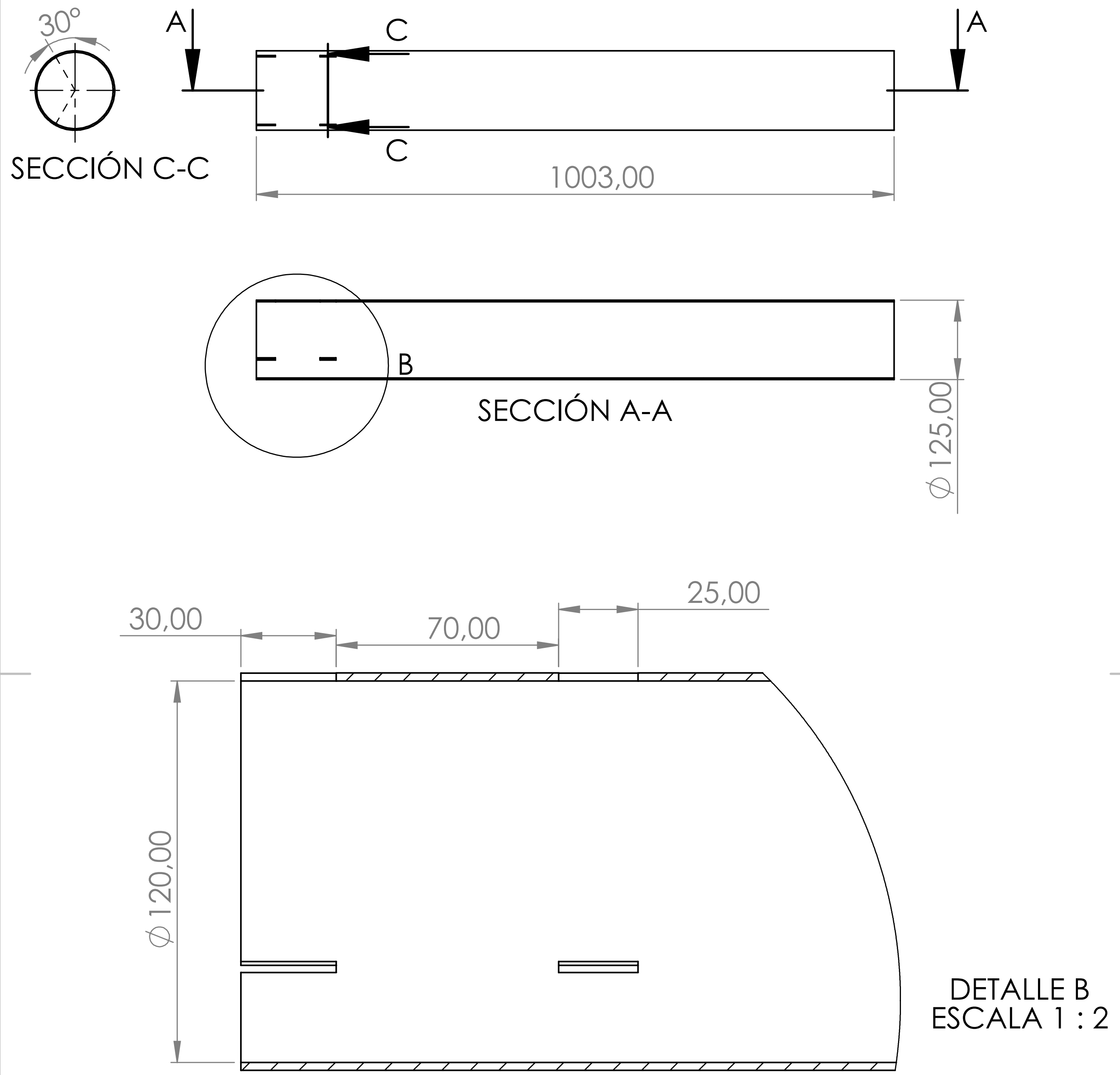

SI NO SE INDICA LO CONTRARIO: LAS COTAS SE EXPRESAN EN MM ACABADO SUPERFICIAL: TOLERANCIAS: LINEAL: ANGULAR:	ACABADO:	REBARBAR Y ROMPER ARISTAS VIVAS	NO CAMBIE LA ESCALA	REVISIÓN

	NOMBRE	FIRMA	FECHA
DIBUJ.	I.V.R.		05/07
VERIF.			
APROB.			
FABR.			
CALID.			

TÍTULO:

HMJNCS-Ohana

MATERIAL:

Epoxy Resin: 18.72%
E Glass Fiber: 81.28%

N.º DE DIBUJO

LV2_Tube

A4

PESO: 2292.16g

ESCALA:1:10

HOJA 1 DE 1

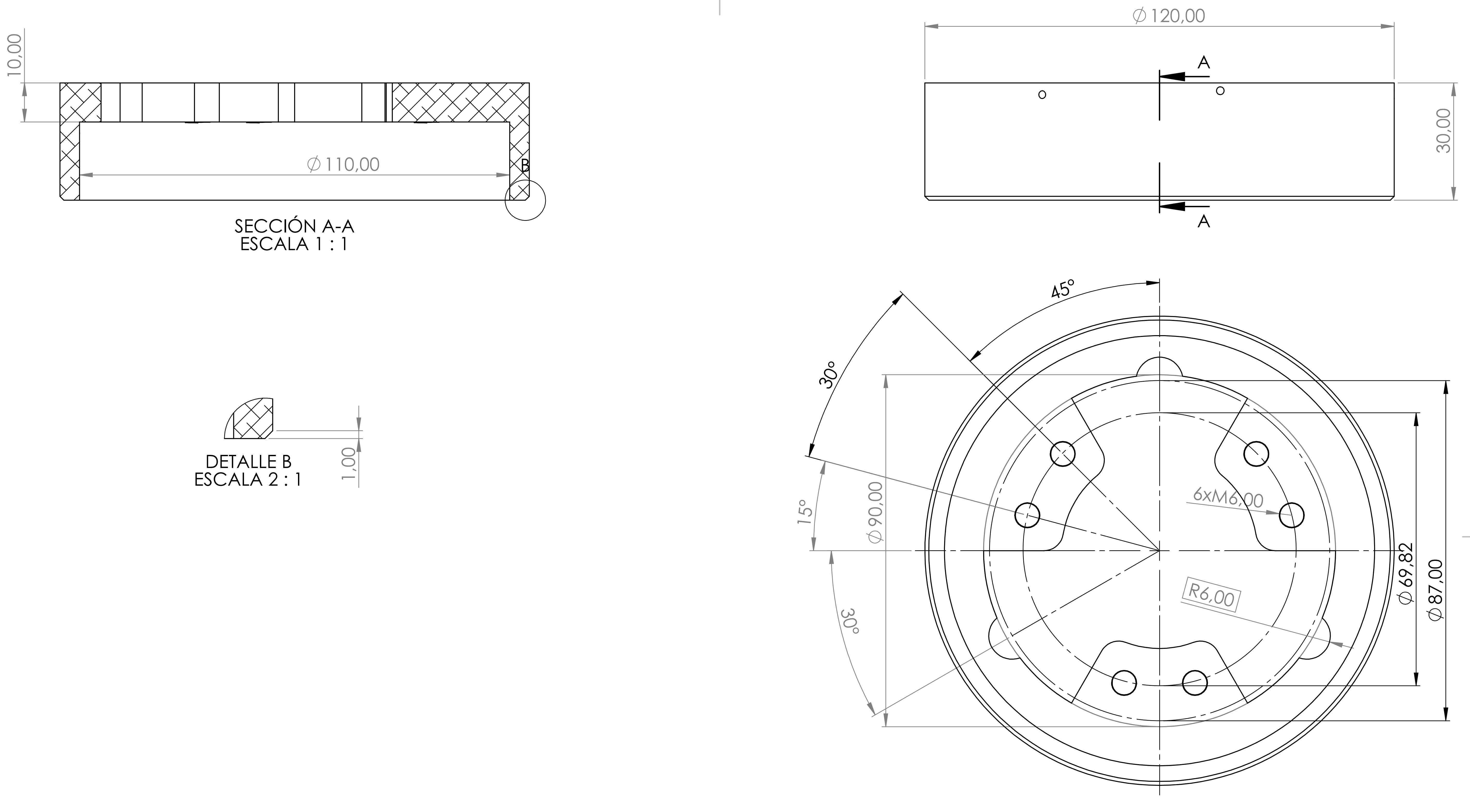

SI NO SE INDICA LO CONTRARIO: LAS COTAS SE EXPRESAN EN MM ACABADO SUPERFICIAL: TOLERANCIAS: LINEAL: ANGULAR:	ACABADO:	REBARBAR Y ROMPER ARISTAS VIVAS	NO CAMBIE LA ESCALA	REVISIÓN

	NOMBRE	FIRMA	FECHA
DIBUJ.	I.V.R.		05/07
VERIF.			
APROB.			
FABR.			
CALID.			

TÍTULO:
HMJNCS-Ohana

MATERIAL: Al 6063-T6

N.º DE DIBUJO: **motor_retainer** — A3

PESO: 280.61g | ESCALA:1:2 | HOJA 1 DE 1

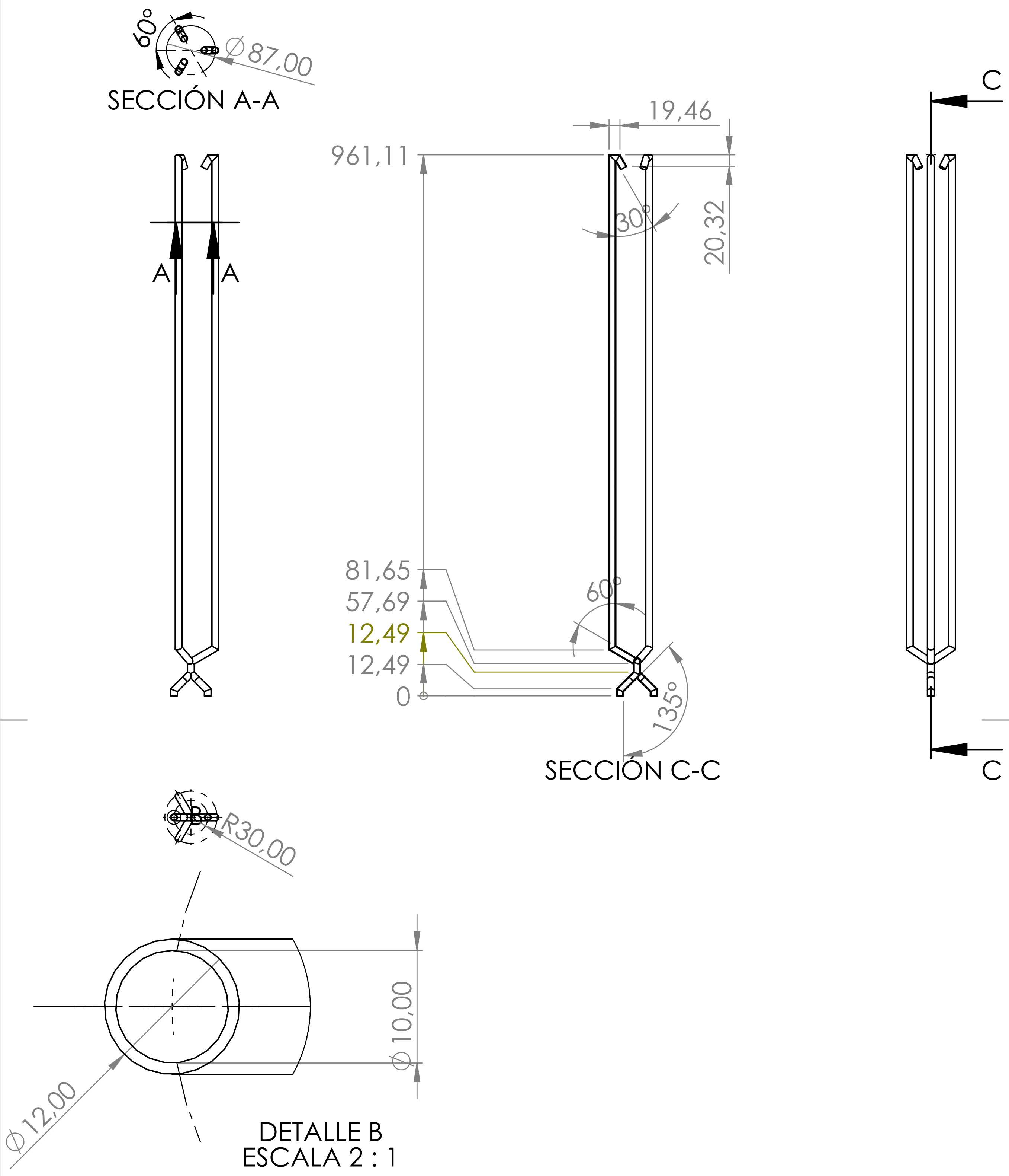

SI NO SE INDICA LO CONTRARIO:
LAS COTAS SE EXPRESAN EN MM
ACABADO SUPERFICIAL:
TOLERANCIAS:
LINEAL:
ANGULAR:

ACABADO:

REBARBAR Y ROMPER ARISTAS VIVAS

NO CAMBIE LA ESCALA

REVISIÓN

	NOMBRE	FIRMA	FECHA
DIBUJ.	I.V.R.		05/07
VERIF.			
APROB.			
FABR.			
CALID.			

TÍTULO:

HMJNCS-Ohana

MATERIAL:
PVC

N.º DE DIBUJO
pipes_LV3

A4

PESO: 133.07g

ESCALA:1:10

HOJA 1 DE 1

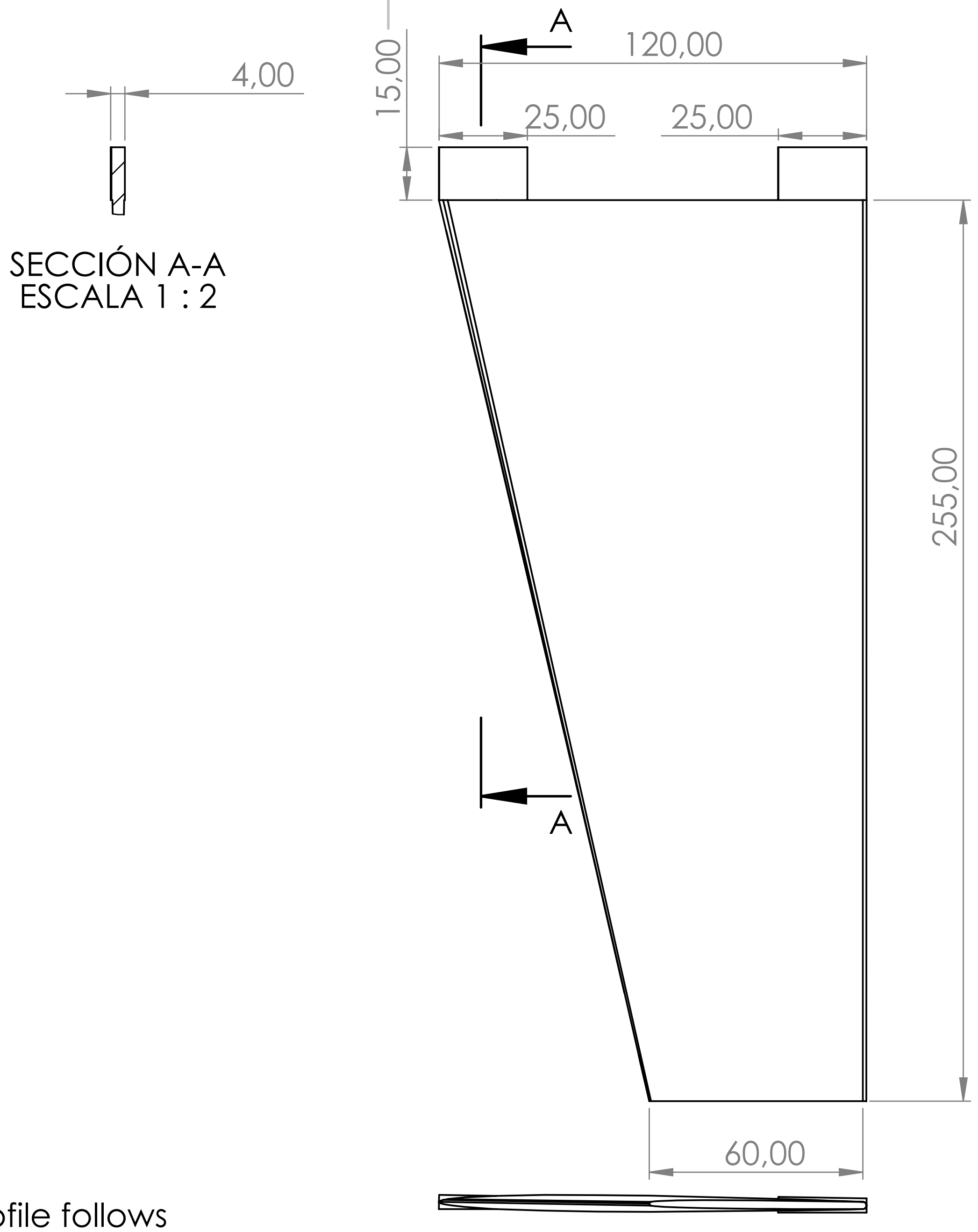

The fins's profile follows the equations:

$$L = 120 - \frac{60}{L_{fin}} z$$

$$y \begin{cases} 5t(z)\left[0.2969\sqrt{\frac{x}{L(z)}} - \frac{0.1260}{L(z)}x - 0.3516\left(\frac{x}{L(z)}\right)^2 + 0.2843\left(\frac{x}{L(z)}\right)^3 - 0.1015\left(\frac{x}{L(z)}\right)^4\right] & if\ x \le L(z) \\ \sqrt{(0.0105t(z))^2 - (x - L(z))^2} & if\ L(z) \le x \le L(z) + 0.0105t(z) \end{cases}$$

SI NO SE INDICA LO CONTRARIO: LAS COTAS SE EXPRESAN EN MM ACABADO SUPERFICIAL: TOLERANCIAS: LINEAL: ANGULAR:	ACABADO:	REBARBAR Y ROMPER ARISTAS VIVAS	NO CAMBIE LA ESCALA / REVISIÓN

	NOMBRE	FIRMA	FECHA
DIBUJ.	I.V.R.		05/07
VERIF.			
APROB.			
FABR.			
CALID.			

TÍTULO: HMJNCS-Ohana

MATERIAL: Epoxy Resin: 70.3% E Glass Fiber: 29.7%

N.º DE DIBUJO: FIN_LV3

A4

PESO: 129.26g

ESCALA: 1:2

HOJA 1 DE 1

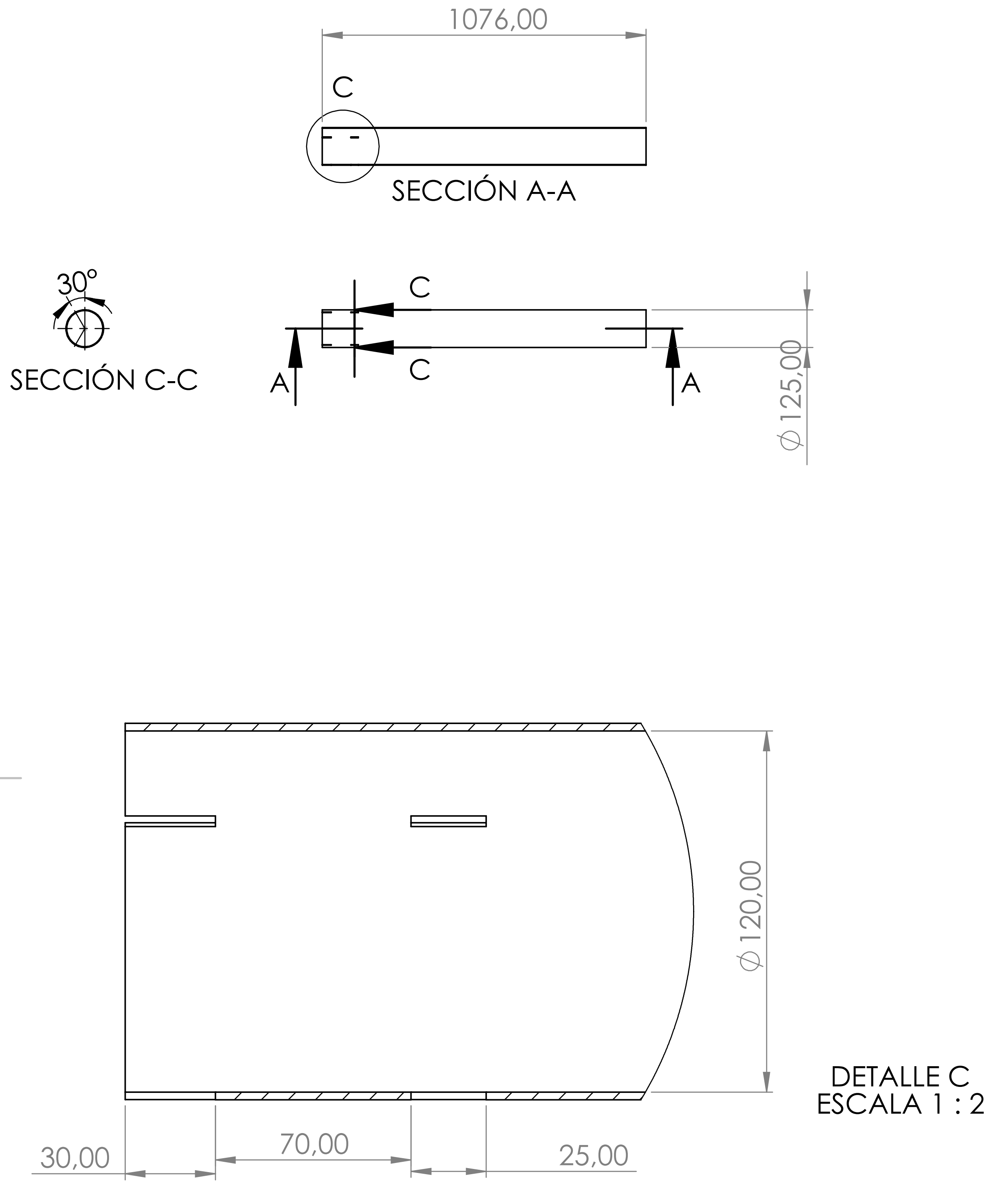

SI NO SE INDICA LO CONTRARIO: LAS COTAS SE EXPRESAN EN MM ACABADO SUPERFICIAL: TOLERANCIAS: LINEAL: ANGULAR:	ACABADO:	REBARBAR Y ROMPER ARISTAS VIVAS	NO CAMBIE LA ESCALA	REVISIÓN	

	NOMBRE	FIRMA	FECHA	
DIBUJ.	I.V.R.		05/07	TÍTULO: HMJNCS-Ohana
VERIF.				
APROB.				
FABR.				
CALID.			MATERIAL: Epoxy Resin: 18.72% E Glass Fiber: 81.28%	N.º DE DIBUJO LV3_Tube — A4
			PESO: 2458.98g	ESCALA:1:20 — HOJA 1 DE 1

DOCUMENT 3: CONDITIONS AND REQUIREMENTS

Spaceport America Cup

Intercollegiate Rocket Engineering Competition
Rules & Requirements Document

Revision History

REVISION	DESCRIPTION	DATE
Baseline	Baseline Revision Last Updated	03/06/2017
Rev. A	1. Section 1.1 revised to reflect completed transition to SA Cup 2. Section 1.3 revised to allow for minor, mid-cycle updates 3. Section 1.4 revised to reflect administrative form changes a. Separate, paper ESRA and NMSA waiver forms replaced by a single, digital form b. Individual PII release form deleted 4. Section 2.0 revised for clarity 5. Section 2.1 reorganized for clarity 6. Section 2.2 (formerly Section 2.3) reorganized and revised – most notably to reflect ESRA and SDL's official stance on the spirit and intent of encouraging mature payload interfaces via the CubeSat standard a. Section 2.2.1 (formerly Section 2.3.1) amended with clarification of allowable deviation in payload weight due to calibration differences measurement devices b. Section 2.2.2 (formerly (section 2.3.2) revised to clarify differences between payload(s) and commonly confused launch vehicle subsystems c. Section 2.2.3 (formerly Section 2.3.4) revised to eliminate option for in-situ weight addition, in favor of a point penalty d. Section 2.2.5 (formerly Section 2.3.5) revised for clarity and to distinguish between functional payloads (not necessarily required to meet CubeSat form factor) and non-functional payloads (required to meet CubeSat form factor). 7. Section 2.6.2.10 (formerly Section 2.7.2.10 amended to include additional requirement that hybrid and liquid propulsion system teams included processes and procedures for cleaning 8. Section 2.6.3 (formerly Section 2.7.3) amended to include additional requirement for prominent Team ID# marking on Poster Session materials. 9. Section 2.6.4 (formerly Section 2.7.4) amended to include still more ideas for podium session topics 10. Section 2.6.5.2 added to request insurance information from schools 11. Section 2.6.5.3 (formerly Section 2.7.5.2) revised to define single, paperless NMSA and ESRA waiver and release of liability form 12. Former Section 2.7.5.3: [paper] ESRA waiver form deleted 13. Former Section 2.7.5.4: [paper] NMSA waiver form deleted 14. Section 2.7.1 (formerly Section 2.8.1) revised to clarify Place Awards eligibility within half the category target altitude 15. Section 2.7.1.1 (formerly Section 2.8.1.1) revised to adjust value to 60 pts (formerly 100 pts) 16. Section 2.7.1.2 (formerly Section 2.8.1.2) revised to permit revision of a project's "analysis" score based on competition officials' team interactions at the SA Cup, and to shift point distribution a. "Completeness" is worth 20 pts (formerly 40 pts) b. "Analysis" is worth 140 pts (formerly 120 pts) 17. Section 2.7.1.3 (formerly Section 2.8.1.3) revised to replace SRAD	11/12/2017

REVISION	DESCRIPTION	DATE
	evaluation with strategic design decisions evaluation, and to shift point values and distribution a. Competency of design and quality of construction worth 180 pts (formerly 100) b. SRAD evaluation replaced with strategic design decisions evaluation worth 60 pts 18. Section 2.7.1.4 (formerly Section 2.8.1.4) revised to widen scoring band to ±30% of the category target altitude (formerly ±2,000 ft) 19. Section 2.7.1.6 added to codify payload requirement violation penalties 20. Section 2.7.1.7 added to codify bonus for eligible CubeSat payload(s) 21. Section 2.7.1.8 added to codify bonuses for efficient launch preparation 22. Section 2.7.3 (formerly 2.8.3) revised for clarity and amended to codify Hoult and Barrowman awards a. Section 2.7.3.3 added to codify Hoult Award for Mod & Sim b. Section 2.7.3.4 added to codify Barrowman Award for Flight Dynamics 23. Former Section 2.11: Sponsored Challenges deleted with intent to host content on ESRA or SA Cup website 24. Former Section 3.0: Non-competing demonstration flights deleted with intent to host content on ESRA website 25. Hyperlinked cross-references 26. Other sections renumbered as needed 27. General edits for spelling, grammar, and clarity	
Rev. A	1. Former Section 2.1.2 deleted in response to participant lobbying a. Individual student organizations may once again enter multiple teams into the IREC b. Each of these teams will continue to represent one project/rocket c. A student organization should not have multiple teams entered in a single IREC category 2. Section 2.1.2 (formerly Section 2.1.3) renumbered due to previous section's deletion	05/13/2018

Table of Contents

SECTION		PAGE
1.0	INTRODUCTION	6
1.1	BACKGROUND	6
1.2	PURPOSE AND SCOPE	6
1.3	REVISION	6
1.4	DOCUMENTATION	6
2.0	INTERCOLLEGIATE ROCKET ENGINEERING COMPETITION OVERVIEW	7
2.1	TEAM COMPOSITION AND ELIGIBILITY	8
2.1.1	STUDENT TEAM MEMBERS	8
2.1.2	ONE PROJECT PER TEAM	8
2.2	PAYLOAD	8
2.2.1	PAYLOAD MASS	8
2.2.2	INDEPENDENT PAYLOAD FUNCTIONALITY	9
2.2.3	PAYLOAD LOCATION AND INTERFACE	9
2.2.4	RESTRICTED PAYLOAD MATERIALS	9
2.2.5	PAYLOAD FORM FACTOR	9
2.3	FAA CLASS 2 AMATEUR ROCKET LIMITATION	10
2.4	RANGE TRACKING	10
2.5	OFFICIAL ALTITUDE LOGGING	10
2.6	PROJECT DELIVERABLES	10
2.6.1	ENTRY FORM AND PROGRESS UPDATES	10
2.6.2	PROJECT TECHNICAL REPORT	12
2.6.3	POSTER SESSION MATERIALS	14
2.6.4	PODIUM SESSION MATERIALS	15
2.6.5	ADMINISTRATIVE DOCUMENTS	16
2.7	AWARDS AND SCORING	17
2.7.1	CATEGORY "PLACE" AWARDS	17
2.7.2	JUDGES CHOICE AND OVERAL WINNER AWARD	23
2.7.3	TECHNICAL ACHIEVEMENT AWARDS	23
2.7.4	TEAM CONDUCT AWARDS	24
2.8	DISQUALIFICATION FROM CONSIDERATION FOR ANY AWARD	25
2.9	WITHDRAWAL FROM COMPETITION	25

3.0 INTERNATIONAL TRAFFIC IN ARMS REGULATIONS 25
APPENDIX A: ACRONYMS, ABBREVIATIONS, AND TERMS 26

1.0 INTRODUCTION

The Experimental Sounding Rocket Association (ESRA) and the New Mexico Spaceport Authority (aka Spaceport America; NMSA) have partnered to host and support the Spaceport America Cup (SACup), a week-long series of events which will set the background and provide structure for the world's largest university rocket engineering competition. This new host-event continues the Intercollegiate Rocket Engineering Competition's (IREC) legacy of inspiring student design teams from across the country and around the world.

1.1 BACKGROUND

The “smoke and fire,” noise, high speeds, and sleek aerodynamics of rocketry encourage students to pursue science, technology, and mathematics based careers. They have "Rocket Fever!", and competition motivates them to extend themselves beyond the classroom to design and build the rockets themselves. These students also learn to work as a team, solving real world problems under the same pressures they'll experience in their future careers.

ESRA held the first annual IREC in 2006. The competition achieved international status in 2011 when Canadian and Brazilian universities threw their hats in the ring. These schools have since been joined by others from every continent except Antarctica. In fact, the competition has roughly doubled in size every year since 2013, becoming the largest known collegiate level rocket engineering competition in the world in 2014. Attendance in 2016 included as many as 600 participants – including faculty, family, and friends of students from over 50 colleges and universities. The next year marked the start of a new era with the inaugural Spaceport America Cup. Over 1,100 students, faculty, and representatives from 22 industry partners participated in an academic conference, rocket and payload engineering competitions, and non-competing demonstration flight tests.

1.2 PURPOSE AND SCOPE

This document defines the rules and requirements governing participation in the IREC. Additional guidance for collegiate teams entered in the IRECis contained in the *IRECDesign, Test, & Evaluation Guide (DTEG)*, maintained on the ESRA website. The DTEGprovides teams with project development guidance ESRA uses to promote flightsafety. Departures from this guidance may negatively impact an offending team's score and flight status depending on the degree of severity.

IREC teams should avoid feeling constrained before seeking clarification, and may contact ESRA with questions or concerns regarding their project plans’ alignment with the spirit and intent of this document.

1.3 REVISION

It is expected the *IREC Rules & Requirements Document*may require revision from one competition to the next, based on the experiences and lessons learned by both host organizations and the participants. Major revisions will be accomplished by complete document reissue. “Real world events” may require smaller revisions to this document in the months leading up to a competition. Such revisions will be reflected in updates to the document’s effective date. The authority to issue revised versions of this document rests with ESRA and NMSA. Revisions will be approved either by ESRA, or jointly by both organizations as appropriate.

1.4 DOCUMENTATION

The following documents include standards, guidelines, schedules, or required standard forms. The documents listed in this section are either applicable to the extend specified in this document, or contain reference information useful in the application of this document.

DOCUMENT	FILE LOCATION
IREC Design, Test, & Evaluation Guide	http://www.soundingrocket.org/sa-cup-documents--forms.html
SACupIntegrated Master Schedule Document	http://www.soundingrocket.org/sa-cup-documents--forms.html
SAC Range Standard Operating Procedures	http://www.soundingrocket.org/sa-cup-documents--forms.html
IREC Entry Form & Progress Update	http://www.soundingrocket.org/sa-cup-documents--forms.html
IREC Project Technical Report Template	http://www.soundingrocket.org/sa-cup-documents--forms.html
IREC Extended Abstract Template	http://www.soundingrocket.org/sa-cup-documents--forms.html
Spaceport America Cup Waiver and Release of Liability Form	https://www.spaceportamericacup.com/2018-spaceport-america-cup-waiver.html
14 CFR, Part 1, 1.1 General Definitions	http://www.ecfr.gov/cgi-bin/text-idx?SID=795aaa37494b6c99641135267af8161e&mc=true&node=se14.1.1_11&rgn=div8
14 CFR, Part 101, Subpart C, 101.22 Definitions	http://www.ecfr.gov/cgi-bin/text-idx?SID=795aaa37494b6c99641135267af8161e&mc=true&node=se14.2.101_122&rgn=div8

2.0 INTERCOLLEGIATE ROCKET ENGINEERING COMPETITION OVERVIEW

In general, student teams competing in the IREC must design, build, and launch a rocket carrying no less than 8.8 lb of payload to a target apogee either 10,000 ft or 30,000 ft above ground level (AGL). Projects will be divided into one of the following six categories based on the type of project attempted – defined by the target apogee and selected propulsion system. Teams are permitted to switch categories as necessary prior to submitting their final Project Technical Report.

- 10,000 ft AGL apogee with commercial-off-the-shelf (COTS) solid or hybrid rocket propulsion system
- 30,000 ft AGL apogee with COTS solid or hybrid propulsion system
- 10,000 ft AGL apogee with student researched and developed (SRAD) solid rocket propulsion system
- 30,000 ft AGL apogee with SRAD solid rocket propulsion system
- 10,000 ft AGL apogee with SRAD hybrid or liquid rocket propulsion system
- 30, 000 ft AGL apogee with SRAD hybrid or liquid rocket propulsion system

SRAD propulsion systems are defined as those designed by students – regardless of whether fabrication is performed by students directly, or by a third party working to student supplied specifications – and can include student designed modifications of COTS systems. ESRA reserves the right to change the category in which a project is initially entered based on the design presented.

Multistage launch vehicles and all chemical propulsion types (solid, liquid, and hybrid) are allowed. Note that all propellants used must be non-toxic. Ammonium perchlorate composite propellant (APCP), potassium nitrate and sugar (aka "rocket candy"), nitrous oxide, liquid oxygen (LOX), hydrogen peroxide, kerosene, propane and similar substances, are all considered non-toxic. Toxic propellants are defined as those requiring breathing apparatus, special storage and transport infrastructure, extensive personal protective equipment, etc. (e.g. Hydrazine and N_2O_4).

Additional high-level design and acceptance testing requirements are contained in the DTEG, maintained on the ESRA website. ESRA uses theDTEG to promote flight safety. Departures from the DTEG may negatively impact an offending team's score and flight status, depending on the degree of severity.

Competition Officialswill evaluate competitors for Place Awards within each competition category based on the quality of required project documentation, a Poster Session held during the SACupConference, the quality of theirsystem's overall design and construction, and finally the program'soverall operational efficiency and performance demonstrated at the SA Cup. Furthermore, Competition Officials will select no less than 24 teams to present a particular aspect of their work in a Podium Session held during the SA Cup Conference. These teams are eligible to receive certain Technical Achievement Awards.

IREC teams should avoid feeling constrained before seeking clarification, and may contact ESRA with questions or concerns regarding their project plans' alignment with the spirit and intent of this document.

2.1 TEAM COMPOSITION AND ELIGIBILITY

2.1.1 STUDENT TEAM MEMBERS

IREC Teams shall consist of members who were matriculated undergraduate or graduate students (i.e. Masters or Doctoral students) during the previous academic year (e.g. former students who graduated shortly before the competition remain eligible) from one or more academic institutions (e.g. "joint teams" are eligible). There is no limit on the overall number of students per team, or on the number of graduate students per team.Students are free to participate on multiple teams, so long as each team is led by a different individual.

2.1.2 ONE PROJECT PER TEAM

Each team shall submit no more than one project into the IREC. Furthermore, no project may be entered in more than one category at the IREC. Although, as previously noted, teams are permitted to switch categories as necessary prior to submitting their final Project Technical Report. The event organizers will track and evaluate each team separately, regardless of common student membership or academic affiliation.

> *Important: Although individual student organizations may form multiple IREC teams, these teams must be entered in separate IREC categories. Finally, student organizations which form multiple IREC teams must provide a rational for the formation of multiple IREC teams within the "Any other pertinent information block" found at the bottom of each team's Entry Form and Progress Report described in Section 2.6.1 of this document. Such rational typically relates to the parent organization's overall membership size and/or diversity of work.*

2.2 PAYLOAD

2.2.1 PAYLOAD MASS

The launch vehicle shall carry no less than 8.8 lb of payload. Payload is defined as being replaceable with ballast of the same mass, with no change to the launch vehicle'strajectory in reaching the target apogee, or its' successful recovery. This payload may be assumed present when calculating the launch vehicle's stability. In other words, launch vehicles entered in the IREC need not be stable without the required payload mass on-board.

Competition officials will "weigh-in"the launch vehicle's payload(s) at the Spaceport America Cup with a scale they provide. Understanding there may be discrepancies between a team's own scale and the official one used for weigh-in, competition officials will accept payload weigh-ins as much as 5% (~0.4 lb) less than the specified minimum without penalty. For example, competition officials will not penalize a team whose payload measured 8.8 lb on the team's scale but 8.4 lb on the officials' scale. Any weight greater than the specified minimum is acceptable.

2.2.2 INDEPENDENT PAYLOAD FUNCTIONALITY

Although non-functional "boiler-plate" payloads are permitted, teams are encouraged to launch creative scientific experiments and technology demonstrations; however, launch vehicles shall be designed to deliver the payload to the target apogee and recover themselves independent of any active or passive payload function(s). For example, an active launch vehicle stability augmentation system is a launch vehicle subsystem – not a payload. Such launch vehicle subsystems will contribute to competition officials' overall evaluation of a project, and may be submitted to the SA Cup Conference Podium Session described in Section 2.6.4 of this document, but they are not payloads.

Scientific experiments and technology demonstration payloads entered in the IREC may be evaluated for awards by representatives from the Space Dynamics Laboratory (SDL) as part of the SDL Payload Challenge – an Intercollegiate Payload Engineering Competition hosted at the Spaceport America Cup. Teams wishing to enter their payload(s) into the SDL Payload Challenge should consult the SDL Payload Challenge Page on the ESRA website (http://www.soundingrocket.org/sdl-payload-challenge.html).

2.2.3 PAYLOAD LOCATION AND INTERFACE

Neither the payload's location in the launch vehicle nor its' method of integration and removal is specified; however, competition officials will weigh payload(s) independent of all launch vehicle associated systems prior to flight. Therefore, the payload(s) submitted for weigh-inshall not be inextricably connected to other, launch vehicle associated, components (e.g. the launch vehicle's recovery system, internal structure, or airframe) while being weighed. If the payload's design prevents it from being weighed completely independent of the launch vehicle, competition officials will impose a point penalty on the team in accordance with Section 2.7.1.6of this document.

2.2.4 RESTRICTED PAYLOAD MATERIALS

Payloads shall not contain significant quantities of lead or any other hazardous materials. Similarly, any use of radioactive materials shall be permitted only if deemed operationally necessary and such operational necessity is concurred with by competition officials. If approved, any such materials shall be fully encapsulated and are limited to 1 µC or less of activity. Finally, payloads shall not contain any live, vertebrate animals.

2.2.5 PAYLOAD FORM FACTOR

The following sections concern the required shape and dimensions of payload(s) submitted for weigh-in. These requirements are different if the payload is a non-functional "boiler-plate" (aka mass emulator) orif it is a functional scientific experiment/technology demonstration (i.e. those entered in the SDL Payload Challenge). Section 2.2.5.1 defines the requirements for non-functional payloads. Section 2.2.5.2defines the requirements for functional payloads.

2.2.5.1 BOILER PLATE PAYLOAD

Any launch vehicle carrying strictly non-functional, "boiler-plate" mass as it's payload shall do so in the form of one or more CubeSats, which equal no less than 3U when stacked together. Each CubeSat shall be no less than 1U in size. One CubeSat Unit (1U) is defined as a 10cm×10cm×10cm (approx. 4in×4in×4in) cubic structure. Similarly, three CubeSat Units (3U) constitute either a single structure or a stack measuring 10cm×10cm×30cm (approx. 4in×4in×12in).

2.2.5.2 SCIENTIFIC EXPERIMENT OR TECHNOLOGY DEMONSTRATION PAYLOAD

Any functional scientific experiment or technology demonstration payload and its associated structure (i.e. those entered in the SDL Payload Challenge) may be constructed in any form factor, provided the experiment/technology and its associated structure remain in compliance with Sections2.2.1, 2.2.2, 2.2.3, and 2.2.4 of this document. With special regard to compliance with Section 2.2.1, the required minimum payload mass should be achieved primarily by the experiment(s)/technology and associated support structure. The payload design may incorporate a limited amount of additional "boiler-plate" mass (perhaps as much as 2.25 lb, or just over 1/4th the required minimum) to meet the required minimum while remaining exempt from Section 2.2.5.1 above. Competition officials may impose a point penalty on any team believed to be violating the spirit and intent of this rule in accordance with Section 2.7.1.6 of this document.

Finally, despite this exemption, ESRA and SDL highly encourage teams to adopt the CubeSat standard for their payload(s) whenever possible – either as the payload structure itself, or as an adapter which the payload is mated to prior to the combined assembly's integration with the launch vehicle (such an adapter could be included in the official payload mass). To promote this encouragement, teams who's functional payloads do adopt the CubeSat physical standard will be awarded bonus points in the IREC in accordance with Section 2.7.1.7.

2.3 FAA CLASS 2 AMATEUR ROCKET LIMITATION

Launch vehicles entered in the IREC shall not exceed an installed total impulse of 9,208 pound-seconds (40,960 Newton-seconds), to meet the U.S. Federal Aviation Administration (FAA) definition of Class 2 Amateur Rocket (aka High-Power Rocket) - as per Code of Federal Regulations, Title 14 (14 CFR), Part 101, Subpart C, 101.22 Definitions.

2.4 RANGE TRACKING

Launch vehicles, and any deployable payload(s), shall carry a radio beacon or similar transmitter aboard each independently recovered assembly to aid in locating them after launch. Tracking systems usingthe Global Positioning System (GPS) or equivalent global navigation satellite systems (GNSS)and an automatic packet reporting system (APRS) are highly encouraged.

2.5 OFFICIAL ALTITUDE LOGGING

Launch vehicles shall carry a COTS barometric pressure altimeter with on-board data storage, which will provide an official log of apogee for scoring. This may either be a standalone COTS product or a feature of a COTS flight computer - also used for launch vehicle recovery system deployment.If a deployable payload is integrated on the launch vehicle, the official altitude logging system shall be mounted to the launch vehicle and not the payload.

While the on-board log is considered the primary data source for official altitude reporting, telemetry – if implemented – may be accepted under certain circumstances defined in Section 2.7.1.4of this document. If implemented, this telemetric data shall originate from the same sensor source as the official on-board data log.

2.6 PROJECT DELIVERABLES

The following sections define the deliverable materials (e.g.paperwork and presentation materials) competition officials require from teams competing in the IREC – includingas appropriate each deliverable's format and minimum expected content. Unless otherwise noted, all deliverables will be submitted to ESRA via DropBox™. A DropBox™ account is not necessary to submit these files. The unique DropBox™ link found within each relevant deliverable description will facilitatesubmission of that deliverable.

The scheduled due dates of all required deliverables are recorded in the *Spaceport America Cup Integrated Master Schedule Document*, maintained on the ESRA website (http://www.soundingrocket.org/sa-cup-documents--forms.html).

2.6.1 ENTRY FORM AND PROGRESS UPDATES

Eachteam shall inform ESRA and NMSA of their intent to compete in the IREC by completing aprovided Microsoft® Excel spreadsheet template as fully as possible at the time of submission. Teams shall submit updated versions of this spreadsheet on threespecified occasions prior to the competition. This "living document" will record changes in the project's technical characteristics during development. Competition officials understand not all technical details will be known until later in the design process. Therefore, the Entry Form and all subsequent Progress Updates prior to the final submission will be evaluated based only on their timeliness and completeness – defined as follows.

Completeness of the entry form and subsequent updates will be evaluated based on the number and type of fields completed. The template's fields are color coded to indicate the timeframe in which information is expected to be defined.

- ***RED:*** These fields shall be completed as accurately as possible in the Entry Form and all subsequent Progress Updates. These fields mostly concern the team's identifying information and the highest-level technical information. This information is expected to vary little during over the course of development.
- ***BLUE:*** These fields should always be completed "to the team's best knowledge at the time of submission", but are expected to vary with increasing accuracy and fidelity throughout development. These fields mostly concern the system's overall dimensions, and other characteristics which may be approximated early in development. Teams should begin providing such approximations no later than in the first Progress Update.
- ***YELLOW:*** Information contained in these fields may not be known or estimated reasonably until later in the project, but should populated as soon as possible. These fields mostly concern derived information, whose exact value depends heavily on earlier design decisions. Complete and accurate information is not expected in these fields until the final progress update.

IMPORTANT: Always check the template maintained on the ESRA website before submitting your Entry Form or latest Project Update to ensure you are using the latest version. Do not reformat the template, shift fields around, or type in fields not designated for user input. Competition officials uses an automation script to import this into other spreadsheets and databases for administrative purposes. This will not work properly if the template is tampered with. The template also contains embedded comments to explain some fields. Please check these comments first before contacting ESRA for assistance completing the spreadsheet.

The *Intercollegiate Rocket Engineering Competition Entry Form &Progress Update*template is available for download on the ESRA website(http://www.soundingrocket.org/sa-cup-documents--forms.html).Always check the template maintained on the ESRA website before submitting your Entry Form or latest Project Update to ensure you are using the latest version.

Teams shall submit their entry form using the Drop Box™link(https://www.dropbox.com/request/d1bZuIrnbMlanLzoLQx7), with the filename "Your Project Name_Entry Form". For example, a team named the "Reading Comprehension Rocketeers" would submit their entry form using the filename "Reading Comprehension Rocketeers_Entry Form".

Between the time when a majority of Entry Forms are received and the due date of the first progress update, ESRA will issue every team a numeric Team ID. Entries made later in the academic year should be accompanied by an e-mail addressed directly to ESRA (experimentalsoundingrocket@gmail.com), alerting the organizers to check for the late entry. Such entries will receive their Team ID shortly after receipt of the entry form. The Team ID is the competition officials' primary means of identifying and tracking all the many teams. Once assigned, any correspondence between a team and the organizers must contain that team's ID number to enable a timely and accurate response.

Teams shall submit all subsequent Progress Updates using the following Drop Box™ links, with the filename "Your Team ID_nth Progress Update". For example, a team assigned the Team ID "42" would submit their first progress update using the filename "42_1st Progress Update", their second using the filename "42_2nd Progress Update", and so on.

- First Progress Update: https://www.dropbox.com/request/C50eSdxUpbib0U9NtFZK
- Second Progress Update:https://www.dropbox.com/request/4phqwFFbfntxXAxqyE5l
- Third Progress Update: https://www.dropbox.com/request/yUqWRfNO4mZMZf5AMPic

2.6.2 PROJECT TECHNICAL REPORT

Each team shall submit a Project Technical Report which overviews their project for the judging panel and other competition officials. The Project Technical Report shall be formatted according to the style guide of the American Institute of Aeronautics and Astronautics (AIAA), using a provided Microsoft® Word document template.

The *Intercollegiate Rocket Engineering Competition Project Technical Report* template is available for download on the ESRA website (http://www.soundingrocket.org/sa-cup-documents--forms.html).Always check the template maintained on the ESRA website before drafting your Project Technical Report to ensure you are using the latest version.

On or before a specified date prior to the event, teams shall submit a digital, PDF copy of their Project Technical Report using the Drop Box™ link (https://www.dropbox.com/request/gKwrhu6vn1y16QTv6rav), with the file name "Your Team ID_Project Report". For example, a team assigned the Team ID "42" would submit the digital copy of their Project Report using the filename "42_Project Report". The event organizers will post these files in an online archive of the conference proceedings. Teams will also bring a limited number of hardcopies to the Spaceport America Cup so members of the judging panel and other competition officials may consult the contents at will during interactions with the team.

The Project Technical Report's main title is left to the team's discretion, however; the paper shall be subtitled “Team Your Team ID Project Technical Report to the Year Spaceport America Cup". For example, a team assigned the Team ID "42", competing in the 2017 IREC, would subtitle their Project Technical Report "Team 42 Project Technical Report to the 2017 Spaceport America Cup".

The Project Technical Report shall be no longer than 20 pages, not including figures, footnotes, sources, source endnotes, nomenclature lists, equations, explanations of variables, and appendices. The following sections overview the required minimum Project Technical Reportsections and appendices in the order they should appear. Additional sections, subsections, and appendices may be added as needed.

2.6.2.1 ABSTRACT

The Project Technical Report shall contain an Abstract. At a minimum, the abstract shall identify the launch vehicle's mission/category in which the team is competing, identify any unique/defining design characteristics of launch vehicle, define the payload's mission (if applicable), and provide whatever additional information may be necessary to convey any other high-level project or program goals & objectives.

2.6.2.2 INTRODUCTION

The Project Technical Report shall contain an Introduction. This section provides an overview of the academic program, stakeholders, team structure, and team management strategies. The introduction may repeat some of the content included in the abstract, because the abstract is intended to act as a standalone synopsis if necessary.

2.6.2.3 SYSTEM ARCHITECTURE OVERVIEW

The Project Technical Report shall contain a System Architecture overview. This section shall begin with a top-level overview of the integrated system, including a cutaway figure depicting the fully integrated launch vehicle and it's major subsystems – configured for the mission being flown in the competition. This description shall be followed by the following subsections. Each subsection shall include detailed descriptions of each subsystem, and reflect the technical analyses used to support design and manufacturing decisions. Technical drawings of these subsystems should be included in the specified appendix.

- Propulsion Subsystems
- Aero-structures Subsystems
- Recovery Subsystems
- Payload Subsystems

2.6.2.4 MISSION CONCEPT OF OPERATIONS OVERVIEW

The Project Technical Report shall contain a Mission Concept of Operations (CONOPS) Overview. This section shall identify the mission phases, including a figure, and describe the nominal operation of all subsystems during each phase (e.g. a description of what is supposed to be occurring in each phase, and what subsystem[s] are responsible for accomplishing this). Furthermore, this section shall define what mission events signify a phase transition has occurred (e.g."Ignition" may begin when a FIRE signal is sent to the igniter, and conclude when the propulsion system comes up to chamber pressure. Similarly, "Liftoff" may begin at vehicle first motion, and conclude when the vehicle is free of the launch rail). Phases and phase transitions are expected to vary from system to system based on specific design implementations and mission goals & objectives. No matter how a team defines these mission phases and phase transitions, they will be used to help organize failure modes identified in a Risk Assessment Appendix – described in Section 2.6.2.9 of this document.

2.6.2.5 CONCLUSIONS AND LESSONS LEARNED

The Project Technical Report shall contain Conclusions and Lessons Learned. This section shall include the lessons learned during the design, manufacture, and testing of the project, both from a team management and technical development perspective. Furthermore, this section should include strategies for corporate knowledge transfer from senior student team members to the rising underclassmen who will soon take their place.

2.6.2.6 SYSTEM WEIGHTS, MEASURES, AND PERFORMANCE DATA APPENDIX

The first Project Technical Report appendix shall contain System Weights, Measures, and Performance Data. This requirement will be satisfied by appending the Third/Final Progress Report as the first appendix of the Project Technical Report. As described in Section 2.6.1 of this document, the Third/Final Progress Report is also submitted as a separate excel file for administrative purposes.

2.6.2.7 PROJECT TEST REPORTS APPENDIX

The second Project Technical Report appendix shall contain applicable Test Reports from the minimum tests prescribed in the *IREC Design, Test, & Evaluation Guide*(http://www.soundingrocket.org/sa-cup-documents--forms.html). These reports shall appear in the following order. In the event any report is not applicable to the project in question, the team will include a page marked "THIS PAGE INTENTIONALLY LEFT BLANK" in its place.

- Recovery System Testing: In addition to descriptions of testing performed and the results thereof, teams shall include in this appendix a figure and supporting text describing the dual redundancy of recovery system electronics.

- SRAD Propulsion System Testing (if applicable): In addition to descriptions of testing performed and the results thereof, teams developing SRAD hybrid or liquid propulsion systems shall include in this appendix a fluid circuit diagram. This figure shall identify nominal operating pressures at various key points in the system – including the fill system.
- SRAD Pressure Vessel Testing (if applicable)

2.6.2.8 HAZARD ANALYSIS APPENDIX

The third Project Technical Report appendix shall contain a Hazard Analysis. This appendix shall address as applicable, hazardous material handling, transportation and storage procedures of propellants, and any other aspects of the design which pose potential hazards to operating personnel. A mitigation approach – by process and/or design – shall be defined for each hazard identified.An example of such a matrix is available on the ESRA website at (http://www.soundingrocket.org/sa-cup-documents--forms.html).

2.6.2.9 RISK ASSESSMENT APPENDIX

The fourth Project Technical Report appendix shall contain a Risk Assessment. This appendix shall summarize risk and reliability concepts associated with the project. All identified failure modes which pose a risk to mission success shall be recorded in a matrix, organized according to the mission phases identified by the CONOPS. A mitigation approach – by process and/or design – shall be defined for each risk identified. An example of such a matrix is available on the ESRA website at (http://www.soundingrocket.org/sa-cup-documents--forms.html).

2.6.2.10 ASSEMBLY, PREFLIGHT, AND LAUNCH CHECKLISTS APPENDIX

The fifth Project Technical Report appendix shall contain Assembly, Preflight, and Launch Checklists. This appendix shall include detailed checklist procedures for final assembly, arming, and launch operations. Furthermore, these checklists shall include alternate process flows for dis-arming/safe-ing the system based on identified failure modes. These off-nominal checklist procedures shall not conflict with the *IREC Range Standard Operating Procedures*. Teams developing SRAD hybrid or liquid propulsion systems shall also include in this appendix a description of processes and procedures used for cleaning all propellent tanks and other fluid circuit components.

Competition officials will verify teams are following their checklists during all operations – including assembly, preflight, and launch operations.Therefore, teams shall maintain a complete, hardcopy set of these checklist procedures with their flight hardware during all range activities.

2.6.2.11 ENGINEERING DRAWINGS APPENDIX

The sixth Project Technical Report appendix shall contain Engineering Drawings. This appendix shall include any revision controlled technical drawings necessary to define significant subsystems or components – especially SRAD subsystems or components.

2.6.3 POSTER SESSION MATERIALS

Each team shall bring to the Spaceport America Cup, a poster display which overviews their project for industry representatives, the general public, other students, and members of the judging panel. The information provided should encompass the overall project's design, testing, CONOPS, and purpose. The poster shall measure approximately 36 in × 48 in, and must be self-supporting on either an organizer provided table or team provided easel. No partitions or other structures for hanging posters will be provided. Finally, the poster shall prominently display the team's Team ID in the top, right corner, in bold, black, size 72 or larger, Arial font (or similar), on a white field.

These displays – as well as any practicable non-energetic project hardware – will be exhibited in a Poster Session held during the SA Cup Conference. One or more team members are expected to remain with the display throughout the day to answer questions and present their work toindustry representatives, the general public, other students, and competition officials. All teams will participate in the Poster Session, regardless whether or not they are additionally selected to participate in the Podium Session described in Section 2.6.4 of this document.

On or before a specified date prior to the event, teams shall submit a digital, PDF copy of their poster display using the Drop Box™ link (https://www.dropbox.com/request/wXNlo3WrL10H4wTCYbJV), with the file name "Your Team ID_Poster". For example, a team assigned the Team ID "42" would submit the digital copy of their poster display using the filename "42_Poster". The event organizers will post these files in an online archive of the conference proceedings.

2.6.4 PODIUM SESSION MATERIALS

Each team shall submit an Extended Abstract on a particular aspect of their work for competition officials and the judging panel to consider including in a Podium Session held during the SA Cup Conference. Teams whose topics are accepted into the Podium Session will be considered eligible for Technical Achievement Awards defined in Section 2.7.3of this document. The Extended Abstract shall be formatted according to the style guide of the American Institute of Aeronautics and Astronautics (AIAA), using a provided Microsoft® Word document template.

The *Intercollegiate Rocket Engineering Competition Extended Abstract* template is available for download on the ESRA website (http://www.soundingrocket.org/sa-cup-documents--forms.html).Always check the template maintained on the ESRA website before drafting your Extended Abstract to ensure you are using the latest version.

The Extended Abstract's main title is left to the team's discretion, however; the document shall be subtitled "Team Your Team ID Technical Presentation to the Year Spaceport America Cup". For example, a team assigned the Team ID "42", competing in the 2017 IREC, would subtitle their Extended Abstract "Team 42 Technical Presentation to the 2017 Spaceport America Cup".

The Extended Abstract shall be no less than 500 words long and shall not exceed two pages, not including footnotes, sources, or source endnotes. The Extended abstract should not contain any tables, figures, nomenclature lists, equations, appendices etc. The submission must include sufficient detail to demonstrate its purpose, the technical foundation for the topic discussed, any preliminary results to date, and the expected results of flight testing at the Spaceport America Cup.

The topic a team selects for their Podium Session submission should be an aspect of their launch vehicle development which they are particularly proud of, excited about, learned the most in the process of,creates new knowledge, advances the field's understanding of a particular area, presented a unique technical challenge they overcame, and/or otherwise best demonstrates the team's technical excellence and/or innovation in a particular aspect of their work. A few examples of student work from past IRECs which would have made strong Podium Session submissions include the following. (This list is intended to be thought provoking only, and is in no way intended to be either comprehensive, exclusive, or otherwise limiting.)

- Design, analysis, and testing of additively manufactured plastic fins for transonic and supersonic flight
- Design, analysis, and testing of gridfins
- Design, analysis, and testing of plasma based electrodynamic roll control actuators
- Rigorous internal ballistics analysis of a large SRAD solid rocket propulsion system
- Design, analysis, and testing of a drag reducing aerospike equipped nosecone
- Rigorous verification & validation testing of a SRAD ignition system for simultaneous activation of parallel rocket stages comprising multiple combustion cycles
- Design, analysis, and flight demonstration of automated, active telemetry transmitter tracking by a steerable, ground based antenna

- Rigorous verification & validation testing of a SRAD propulsion system, including propellant characterization and multiple hot fire tests
- Design, analysis, and testing of "rollerons" implemented for passive roll stability augmentation
- Design, analysis, and testing of an additively manufactured liquid rocket engine combustion chamber
- Progress in a regimented iterative approach to developing and implementing an active stability augmentation system
- Rigorous post-test analysis and characterization of a previously undefined hybrid rocket motor failure mode
- Design, analysis, and testing of a regenerative cooling system
- Structural design based on exquisite aerodynamic/aerothermal loads analysis
- Exquisite trajectory analysis verified by flight demonstration
- Manufacturing capabilities enabled by SRAD fiber composite filament winding technology
- Structural analysis of fiber composite laminates using non-isentropic analytic techniques

On or before a specified date prior to the event, teams shall submit a digital, PDF copy of their Extended Abstract using the Drop Box™ link (https://www.dropbox.com/request/YGTXAlERhBefXAOSlTQR), with the file name "Your Team ID_Extended Abstract". For example, a team assigned the Team ID "42" would submit the digital copy of their Extended Abstract using the filename "42_Extended Abstract". The event organizers will post these files in an online archive of the conference day proceedings.

At the same time they submit their Extended Abstract, teams shall also submit a digital, PDF copy of any slides they wish to use in their presentation using the Drop Box™ link (https://www.dropbox.com/request/JkLPyQPyhHPBrfpXOTlt), with the file name "Your Team ID_PresentationSlides". For example, a team assigned the Team ID "42" would submit the digital copy of their slide deck using the filename "42_Presentation Slides". The event organizers will post these files in an online archive of the conference proceedings.

No less than 24teams will be accepted into the Podium Session. Each presentation will be allotted 20 minutes, with an additional five minutes reserved for Q&A with judges and other audience members.Whether accepted into the Podium Session or not, all attending teams should be prepared to participate in this activity. On the conference day itself, competition officials may ask teams whose Extended Abstracts were considered "runners up" to take the place of any selected teams who fail to attend the Spaceport America Cup.

2.6.5 ADMINISTRATIVE DOCUMENTS

2.6.5.1 SCHOOL PARTICIPATION LETTER

Each team shall have the academic institution(s) in which its members are enrolled provide a signed letter toESRA, acknowledging the team's participation in the IREC at the Spaceport America Cup. The signature shall be that of a faculty member or other paid, non-student staff representative. This will affirm the team in question does in fact represent the academic institution(s)its members claim affiliation with.Academic institutions sending more than one team to the IREC need only write one participation letter, covering all their teams, but each included team must submit an individual copy of that letter. In the case of a joint team, comprised of students from multiple academic institutions, each affiliated institution must provide its own letter to the team.

An example Spaceport America Cup School Participation Letter is available for download on the ESRA website (http://www.soundingrocket.org/sa-cup-documents--forms.html).

On or before a specified date prior to the event, teams shall submit digital, PDF copy(s) of their signed school participation letter(s) using the Drop Box™ link(https://www.dropbox.com/request/JefGetTCj0jaw4RDWIqG), with the filename "Your Team ID_SchoolInitials_School Letter". For example, a team from Starfleet Academy assigned the Team ID "42" would submit the digital copy of their signed school participation letter with the filename

"42_SA_School Letter". Similarly, if this same team were one formed jointly by students from Starfleet Academy and the Vulcan Science Academy, they would submit two files. The first would use the filename "42_SA_School Letter". The second would use the filename "42_VSA_School Letter".

2.6.5.2 SCHOOL PROOF OF INSURANCE

ESRA's insurance covers ESRA, SA, and the state of New Mexico and will pay for any accidents, damaged property, and injuries related to the event. However, there is one loophole. If your flight damages a person or property, and the person or owner decides they want to sue the team for additional costs, our insurance does NOT protect you from the additional lawsuit.

While the majority of you should be covered by your university, some of you are not. If you would like to purchase additional insurance, you can go through the same company ESRA is using for $1,500. If your team is doing an exhibition launch to a higher altitude, this price will go up, and this price only covers one launch. They will negotiate costs for multiple launches and higher altitudes.

As soon as the 2018 Spaceport America Cup is done, ESRA is going to try to renegotiate the insurance a 3rd time for 2019. But in case we are unsuccessful. 2019 teams not covered under their school's insurance should budget for an additional $1,500. If ESRA is unsuccessful at negotiating with the power that be, this may be a requirement by Spaceport America for 2019, but not 2018 as it is too late for us to leverage a $1,500 penalty on the teams.

If purchasing additional insurance, contact:
Dana Smith | Assistant Vice President | JLT Aerospace (North America) Inc.
5847 San Felipe Road |Suite 2800| Houston | TX | 77057
Direct Dial: 713 325 7625 | Cell: 713 828 7319 | Fax: 713 789 0415
dana.smith@jltaerospace.com | www.jltaerospace.com

2.6.5.3 SPACEPORT AMERICA CUP WAIVER AND RELEASE OF LIABILITY FORM

Every individual attending the Spaceport America Cup – including team members, faculty advisers, and others – shall digitally sign the *Spaceport America Cup Waiver and Release of Liability Form*. Individuals who do not sign this form will be unable to participate in any activities occurring on NMSA property (ie the Spaceport).

The *Spaceport America Cup Waiver and Release of Liability Form* is available for digital signature at the following web address: https://www.spaceportamericacup.com/2018-spaceport-america-cup-waiver.html.

2.7 AWARDS AND SCORING

2.7.1 CATEGORY "PLACE" AWARDS

A First Place Award will be granted to the highest scoring, eligible team in each of the six categories defined in Section 2.0 of this document. A Second Place Award will be granted to the second highest scoring, eligible team in each category. A team is considered eligible for the place award(s) in its category after launching successfully toat least half or more its 10,000 ft or 30,000 ft target altitude – depending on category. In the event no teams meet this definition in a given category, competition officials may issue Category Place Awards at their discretion based on multiple factors – including points accrued, launches attempted, and flight performance.

Teams are permitted to switch categories as necessary prior to submitting their final Project Technical Report. For example, if an SRAD propulsion system project encounters insurmountable difficulties at any point during the academic year, the student team is free to defer work on the SRAD system and opt for a near-term COTS solution without dropping out of the competition; however, each team's project will be entered into only one competition category. For example, a single team may not compete in two categories in the same year by flying once using a

COTS motor, then again using an SRAD motor. In the event such a possibility exists for any team, the organizers highly encourage that team to compete in an SRAD rather than a COTS category.

Competition officials will award points based on their evaluation of each teams required documentation (including the Entry Form, Progress Updates, and Project Technical Report), design implementation (observed through the team's poster display and a day in the field spent prepping for launch), and demonstrated flight performance (including reported altitude and successful recovery).

2.7.1.1 SCORING ENTRY FORM AND PROGRESS UPDATE DELIVERIES

The correct, complete, and timely delivery of a team's Entry Form and subsequent Progress Updates is awarded as many as 60points – 6% of 1,000 total points possible. The Entry Form and subsequent updates are considered correct if they are submitted using the templatespecified in Section 2.6.1 of this Document. They will be considered complete if they are filled out in accordance with Section 2.6.1 of this Document. They will be considered timely if they are received no later than72 hrsafter the deadline specified in the *Spaceport America Cup Integrated Master Schedule Document*.

The 60points are divided evenly among the four submissions (i.e. the Entry Form and three subsequent Project Updates), making each submission worth 15points. The submission is awarded these points on a pass/fail basis and must meet all three criteria – correctness, completeness, and timeliness – in order to"pass". Although they will not receive points for the submission, teams which miss a 72 hr submission window are still required to make that submission as soon as possible for administrative purposes – unless that team no longer plans to attend the Spaceport America Cup.

Teams which enter the IREClater in the academic year, after the first progress report is normally due, will receive special instructions upon entry on how their Entry Form and subsequent Progress Updates will be handled.

2.7.1.2 SCORING PROJECT TECHNICAL REPORT

Timely Project Technical Reports will be awarded as many as 200 points – 20% of 1,000 points possible – for their correctness, completeness, and analysis. Only timely Project Technical Reports will be evaluated and scored. A Project Technical Report is considered timely if it is received no later than72 hrsafter the deadline specified in the *Spaceport America Cup Integrated Master Schedule Document*.Although they will not receive points for the submission, teams which miss a 72 hr submission window are still required to make that submission as soon as possible for administrative purposes – unless that team no longer plans to attend the Spaceport America Cup.

Correctness is worth 20% (40 points) of the Project Technical Report's overall point value. Correctness is defined by the it's adherence to the format/style guide specified in Section 2.6.2 of this document and upholding of basic technical editing standards. The report's correctness will be rated on a scale of 1-4 as follows – where each integer corresponds to a factor of 10 points.

> ***(4)*** *A rating of 4 indicates exemplary quality. The paper requires no substantial correction of grammatical mistakes, misspellings, mistyping, incorrect punctuation, inconsistencies in usage, poorly structured sentences, wrong scientific terms, wrong units and dimensions, inconsistency in significant figures, technical ambivalence, technical disambiguation, statements conflicting with general scientific knowledge, etc... Furthermore, the paper contains no stylistic errors deviating from the prescribed style guide.*

> ***(3)*** *A rating of 3 indicates at least average quality. The paper requires minimal correction of grammatical mistakes, misspellings, mistyping, incorrect punctuation, inconsistencies in usage, poorly structured sentences, wrong scientific terms, wrong units and dimensions, inconsistency in significant figures, technical ambivalence, technical disambiguation, statements conflicting with general scientific*

knowledge, etc... The paper may contain minimal, insubstantial deviations from the prescribed style guide.

(2) *A rating of 2 indicates no greater than average quality. Overall the paper's quality is symbolic of the proverbial "first draft". The paper requires some substantial correction of grammatical mistakes, misspellings, mistyping, incorrect punctuation, inconsistencies in usage, poorly structured sentences, wrong scientific terms, wrong units and dimensions, inconsistency in significant figures, technical ambivalence, technical disambiguation, statements conflicting with general scientific knowledge, etc... The paper deviates significantly from the prescribed style guide, or is formatted in accordance with another style guide entirely.*

(1) *A rating of 1 indicates poor quality. The paper requires numerous substantial corrections of grammatical mistakes, misspellings, mistyping, incorrect punctuation, inconsistencies in usage, poorly structured sentences, wrong scientific terms, wrong units and dimensions, inconsistency in significant figures, technical ambivalence, technical disambiguation, statements conflicting with general scientific knowledge, etc... The paper makes little or no attempt at cohesive formatting in accordance with either the prescribed or any other style guide.*

Completeness is worth 10% (20points) of the Project Technical Report's overall point value. The Project Technical Report is considered complete if it contains all minimally required content defined in Section 2.6.2 of this document. Points for completeness are awarded on a pass/fail basis, and only minor omissions or ambiguity of required information is tolerated in a passing evaluation.

Analysis is worth 70% (140points) of the Project Technical Report's overall point value. This constitutes a structured, qualitative assessment by the evaluating competition officials of the analytic rigor demonstrated by the team during the iterative down-selection, refinement, and acceptance of all project aspects. The report's analysis will be rated on a scale of 1-4 as follows – where each integer corresponds to a factor of 35 points. Furthermore, this score may be amended at the Spaceport America Cup itself, based on the evaluators' assessment of the team's conceptual understanding during any interactions.

(4) *A rating of 4 indicates exemplary quality. The paper provides adequate discussion of all key design decisions, including relevant trade space descriptions, constraints, and overall rational. Furthermore, the paper provides adequate discussion of all key verification & validation tests performed on the final design – as well as any significant progenitors – and demonstrates complete, valid conclusions were drawn from the results. Finally, the paper makes appropriate use of tables, figures, and appendices to effectively organize information and communicate it to the reader.*

(3) *A rating of 3 indicates at least average quality. The paper provides adequate discussion of mostkey design decisions, including relevant trade space descriptions, constraints, and overall rational. Furthermore, the paper provides adequate discussion of most key verification & validation tests performed on the final design, and demonstrates complete, valid conclusions were drawn from the results. Finally, the paper generally makes appropriate use of tables, figures, and appendices to effectively organize information and communicate it to the reader.*

(2) *A rating of 2 indicates no greater than average quality. Overall the paper's quality is symbolic of the proverbial "first draft". The paper provides adequate discussion of some key design decisions, including relevant trade space descriptions, constraints, and overall rational. Furthermore, the paper provides evidence of sufficient verification & validation testing performed on the final design, but does not does not consistently demonstrate complete, valid conclusions were drawn from the results. Finally, the paper would be improved by more appropriate use of tables, figures, and appendices to effectively organize information and communicate it to the reader.*

(1) *A rating of 1 indicates poor quality. The paper lacks adequate discussion of anykey design decisions, and makes little to no attempt at describing the relevant trade spaces, constraints, or overall rational. Furthermore, the paper lacks evidence sufficient verification & validation testing was performed at any point during the design process. Finally, the paper makes either no, or minimally effective, use of tables, figures, and appendices to organize information and communicate it to the reader.*

2.7.1.3 SCORING DESIGN IMPLEMENTATION

Teams will be awarded as many as 240points – 24% of 1,000 points possible – for the overall competency of design, quality of construction, and strategic design decisions exhibited by their work. Competition officials will evaluate these criteria through interactions with the teams and their systems, occurring throughout the SA Cup Conference Poster Session and all during the following day – spent making launch preparations in the field.

Competency of design and quality of construction are worth 75% (180 points) of the overall value assigned to Design Implementation. This constitutes a structured, qualitative assessment by the competition officials of the team's relative competency in the physical principals governing their design (e.g. Did the team demonstrate they know what they're doing by designingsomething likely to work with a greater or lesser degree of success – provided it is sufficiently well constructed?) and the quality with which that design was constructed (e.g. Is the finished product sufficiently well-constructed to meet the needs of the underlying design). The project's design and construction will be rated on a scale of 1-4 as follows – where each integer corresponds to a factor of 45points.

(4) *A rating of 4 indicates exemplary quality. All features of the project hardware reflect strong competency in the physical principals governing their design, and are of more than sufficient quality to operate as intended without risk of premature failure due to fatigue or reasonably expected loading. Wherever possible, the project hardware exhibits robust design characteristics – which decrease itssensitivity to reasonably expected variations in "real-world" operations. Furthermore, the overall system exhibits evidence of a strong systems engineering discipline maintained throughout development (e.g. lacking any features which are both critical systems, and yet clearly implemented as "afterthoughts" to the intended system). Finally, the overall system complies with all expectations set by the IREC, Design, Test, & Evaluation Guide.*

(3) *A rating of 3 indicates at least average quality. All key features of the project hardware reflect adequate competency in the physical principals governing their design, and are of sufficient quality to operate as intended without risk of premature failure due to fatigue or reasonably expected loading. Furthermore, the project hardware makes at least some robust design characteristics in key areas – which decrease these components' or assemblies' sensitivity to reasonably expected variations in "real world" operations. Finally, the overall system exhibits evidence of a strong systems engineering discipline maintained throughout development (e.g. lacking any features which are both critical systems, and yet clearly implemented as "afterthoughts" to the intended system). Finally, the overall system complies with all expectations set by the IREC, Design, Test, & Evaluation Guide.*

(2) *A rating of 2 indicates no greater than average quality. All key features of the project hardware reflect adequate competency in the physical principals governing their design, and are of sufficient quality to operate as intended without risk of premature failure due to fatigue or reasonably expected loading. No obvious attempts are made at robust design to decrease the system's to reasonably expected variations in "real-world" operations. Furthermore, the overall system may exhibit evidence of lapses in systems engineering discipline (e.g. operation of the overall system is facilitated by one or "field modifications" – which have become critical systems themselves, yet are clearly implemented as "afterthoughts" to the intended system).Finally, the overall system complies with the minimum expectations set by the IREC, Design, Test, & Evaluation Guide.*

(1) *A rating of 1 indicates poor quality. One or more key features of the project hardware reflect inadequate competency in the physical principals governing their design, and/or are of insufficient quality to operate as intended without risk of premature failure due to fatigue or reasonably expected loading. No obvious attempts are made at robust design to decrease the system's to reasonably expected variations in "real-world" operations. Furthermore, the overall system may exhibit evidence of lapses in systems engineering discipline (e.g. operation of the overall system is facilitated by one or "field modifications" – which have become critical systems themselves, yet are clearly implemented as "afterthoughts" to the intended system).Such a system fails to meet the minimum expectations set by the IREC, Design, Test, & Evaluation Guide.*

The team's consideration of strategic design decisions is worth 25% (60 points) of the overall value assigned to Design Implementation. This constitutes a structured qualitative assessment by the competition officials of the team's due diligence in deciding how best to implement their design – in keeping with a strategic vision they can articulate clearly. In general, teams should set strategic goals for their project which extend beyond simply excelling in a particular category in a particular IREC.ESRA places special significance on projects which leverage SRAD in a particular aspect, either to enhance the team's understanding of that subject, or to develop technology necessary for achieving a longer-term performance goal. While this evaluation can encompass a broad range of factors, the following 1-4 rating structure (where each integer corresponds to a factor of 15 points) illustrates some of the most significant factors competition officials will be coached to consider.

(4) A rating of 4 indicates exemplary strategic consideration given to the COTS and SRAD elements of the project. Interactions with team members demonstrate a clear, achievable vision for how challenges were selected to advance strategic goals, and the project's design implementation mirrors this. Furthermore, the manufacturing methods used in SRAD aspects of the project, such as additive manufacturing for example, are generally appropriate for the intended use and well understood by the team. This understanding extends not only to how the method works, but also its impact on project timelines, cost, and physical performance.

(3) A rating of 3 indicates at least average strategic consideration given to the COTS and SRAD elements of the project. Interactions with team members demonstrate a relatively clear, achievable vision for how challenges were selected to advance strategic goals, and the project's design implementation generally mirrors this. Furthermore, the manufacturing methods used in SRAD aspects of the project, such as additive manufacturing for example, are generally appropriate for the intended use and reasonably well understood by the team. This understanding extends to how the method works, and also its impact on project timelines, cost, and physical performance – in at least the most rudimentary sense.

(2)A rating of 2 indicates no better than average strategic consideration given to the COTS and SRAD elements of the project. Interactions with team members demonstrate an unrefined or questionably achievable vision for how challenges were selected to advance strategic goals, and the project's design implementation generally mirrors this. Furthermore, the manufacturing methods used in SRAD aspects of the project, such as additive manufacturing for example, are generally appropriate for the intended use, but may not be fully understood by the team. Their understanding extends in only the most limited ways to how the method works, its impact on project timelines, cost, and physical performance – and may be even more lacking in some areas.

(1) A rating of 1 indicates poor strategic consideration given to the COTS and SRAD elements of the project. Interactions with team members demonstrate little-to-no or completely unachievable vision for how challenges were selected to advance strategic goals, and the project's design implementation generally mirrors this. Furthermore, the manufacturing methods used in SRAD aspects of the project, such as additive manufacturing for example, are either impractical for the intended use or not well

understood by the team. Their understanding in severely lacking in how the method works, as well as its impact on project timelines, cost, and physical performance.

2.7.1.4 SCORING FLIGHT PERFORMANCE

Team's will be awarded as many as 500 points – 50% of 1,000 points possible – for their project's flight performance during launches at the Spaceport America Cup, demonstrated by altitude achieved relative to the target apogee and successful recovery.

The accuracy of the launch vehicle's actual apogee achieved relative to the target apogee is worth 70% (350 points) of the overall value assigned to flight performance. Precise Trajectory planning is important. Points will be awarded for apogees within ±30% of the 10,000 ft AGL or 30,000 ft target apogee according to the following formula.

$$Points = 350 - \left(\frac{350}{0.3 \times Apogee_{Target}}\right) \times \left|Apogee_{Target} - Apogee_{Actual}\right|$$

where Apogee $_{Target}$ may equal either 10,000 ft AGL or 30,000 ft AGL

Teams shall report in person to competition officials the apogee loggedby the official altitude logging system after it's retrieval and return to the designated basecamp area, prior to the end of eligible launch operations on the final launch day. The official altitude logging system is defined in Section 2.5 of this document.

If telemetry data from the official altitude logging system is available, teams may report the apogee revealed in this telemetry to competition officialsif and when a confirmation of nominal ascent and recovery system deployment events is possible. This information will be used for scoring only in the event the launch vehicle is not recovered prior to the end of eligible launch operations on the final scheduled launch day.

The successful recovery of the launch vehicle is worth 30% (150 points) of the overall value assigned to flight performance. A recovery operation is considered successful if it does not result in excessive damage to the launch vehicle. Excessive damage is defined as any damage to the point that, if the systems intended consumables were replenished, it could not be launched again safely. Competition officials will visually inspect the launch vehicle upon its return to the designated basecamp area, and award these points on a pass/fail basis.

2.7.1.5 PENALTIES FOR UNSAFE OR UNSPORTSMANLIKE CONDUCT

Teams will be penalized 20 points off their total earned score for every instance of unsafe or unsportsmanlike conduct recorded by competition officials (e.g.judges, volunteers, or staff members). Unsafe conduct includes, but is not limited to, violating the *IREC Range Standard Operating Procedures*, failure to use checklists during operations, violating NMSA motor vehicle traffic safety rules, and failure to use appropriate personal protective equipment. Unsportsmanlike conduct includes, but is not limited to, hostility shown towards any Spaceport America Cup Participant, intentional misrepresentation of facts to any competition official, intentional failure to comply with any reasonable instruction given by a competition official.

2.7.1.6 PENALTIES FOR VIOLATING PAYLOAD REQUIREMENTS

Teams will be penalized 100points off their total earned score for each of the five payload requirements described in Section 2.2 of this document in spirit or intent. These include Mass, Independent Function, Location & Interface, Restricted Materials, and Form Factor. With regard to mass, due to the allowance made for differences in measuring devices, teams will not be permitted to modify their payloads with additional mass to avoid penalty at the event.

2.7.1.7 BONUSES FOR CUBESAT BASED PAYLOADS

Teams whose payload(s) qualify for the form factor exemption described in Section 2.2.5.2 of this document, yet still adopt the CubeSat standard form factor, will be awarded 50 bonus points in addition to their total earned score.This promotes ESRA and SDL's encouragement that teams adopt the CubeSat standard for their payload(s) whenever possible – either as the payload structure itself, or as an adapter which the payload is mated to prior to the combined assembly's integration with the launch vehicle (such an adapter could be included in the official payload mass).

2.7.1.8 BONUSES FOR EFFICIENT LAUNCH PREPARATIONS

Teams whose preparedness, efficient operations, and hassle-free design permit their being launched in a timely manner will be awarded bonus points in addition to their total earned score according to the following tiered system. Launch readiness is declared when competition officials managing Launch Control receive the team's completed Flight Card. No bonus points will be awarded for launch attempts ending in catastrophic failures (CATO).

- 100 bonus points will be awarded to teams declared launch ready by the end of the designated field preparation day and flown by the end of the first launch day. They remain eligible to receive these points until the end of the first launch day, or until their first launch attempt ending in a scrub – at which point the team is no longer eligible for the 100 point bonus, but may still achieve bonus points awarded for teams declared launch ready on the first launch day.
- 50 bonus points will be awarded to teams declared launch ready and flown during the first launch day. They remain eligible to receive these points until the end of the first launch day. or until their first launch attempt ending in a scrub – at which point the team may attempt to regain eligibility by attempting a return to launch readiness by the end of the day.Otherwise, the team is no longer eligible for the 50 point bonus, but may still achieve bonus points awarded for teams declared launch ready on the second launch day
- 25 bonus points will be awarded to teams declared launch ready and flown during the second launch day. They remain eligible to receive these points until the end of the second launch day. or until their first launch attempt ending in a scrub – at which point the team may attempt to regain eligibility by attempting a return to launch readiness by the end of the day. Otherwise, the team is no longer eligible for bonus points.
- 0 bonus points will be awarded to teams declared launch ready and flown during the third launch day.

2.7.2 JUDGES CHOICE AND OVERAL WINNER AWARD

One team among the First Place Award winners in the six categories defined in Section 2.0of this document will be named the overall winner of the Spaceport America Cup: Intercollegiate Rocket Engineering Competition, and receive their own copy of the Genesis Cup trophy! A perpetual trophy rendition of the Genesis Cup is displayed in the Gateway Gallery at Spaceport America. The recipient of this prestigious award is determined by qualitative assessments of the competition officials made throughout the entire event.

2.7.3 TECHNICAL ACHIEVEMENT AWARDS

ESRA presents four awards recognizing technical achievement to deserving teams competing in the IREC. Three of these are awardedbased onthe competition officials' qualitative assessments made during the Podium Session held during the SA Cup Conference, and interactions the following day – spent making launch preparations in the field. The final award awarded to any IREC team based on flight performance.

2.7.3.1 JIM FURFARO AWARD FOR TECHNICAL EXCELLENCE

The Jim Furfaro Award for Technical Excellence recognizes a team which demonstrates exceptional overall engineering discipline and technical skill through their analyses and conclusions, project or program planning and execution, operational procedure, manufacturing processes, iterative improvement, systems engineering methodology, robust design, etc. A team is considered eligible for the Jim Furfaro Award if they are accepted into – and participate in – thePodium Session held during the conference day at the Spaceport America Cup. Deference is given to eligible teams which complete at least one launch attempt at the Spaceport America Cup. A launch attempt is minimally defined as an attempted ignition of the launch vehicle propulsion system with the intent of executing the launch vehicle's designed mission CONOPS.

2.7.3.2 DR. GIL MOORE AWARD FOR INNOVATION

The Dr. Gil Moore Award for Innovation recognizes a team whose project includes one or more features (including analytic or operational processes as well as components or assemblies) the judging panel finds genuinely "novel", "novel", "inventive", or solving a unique problem identified by the team. A team is considered eligible for the Dr. Gil Moore Award if they are accepted into – and participate in – the Podium Session held during the conference day at the Spaceport America Cup. Deference is given to eligible teams which complete at least one launch attempt at the Spaceport America Cup. A launch attempt is minimally defined as an attempted ignition of the launch vehicle propulsion system with the intent of executing the launch vehicle's designed mission CONOPS.

2.7.3.3 CHARLES HOULT AWARD FOR MODELING & SIMULATION

The Charles Hoult Award for Modeling & Simulation recognizes a team demonstrating excellence in math modeling and computational analyses. A team is considered eligible for the Charles Hoult Award if they are accepted into – and participate in – the Podium Session held during the conference day at the Spaceport America Cup. Deference is given to eligible teams which complete at least one launch attempt at the Spaceport America Cup. A launch attempt is minimally defined as an attempted ignition of the launch vehicle propulsion system with the intent of executing the launch vehicle's designed mission CONOPS.

2.7.3.4 JAMES BARROWMAN AWARD FOR FLIGHT DYNAMICS

The James Barrowman Award for Flight Dynamics recognizes a team demonstrating exquisite trajectory analysis. This will be evaluated by comparing the percent error between each teams actual and predicted apogee – the predicted apogee being a value declared prior to launch, based on a team’s trajectory analysis. The award is given to the team with the smallest percent error. All teams with successful launch attempts that provide apogee data will be eligible for this award.

2.7.4 TEAM CONDUCT AWARDS

ESRA presents two awards recognizing teams competing in the IREC whose conduct throughout the Spaceport America Cup is exemplary of goals and ideals held by the event organizers. The Spaceport America Cup should be an event where academia, industry, and the public may come together to preserve, popularize, and advance the science of rocketry in a collaborative environment energized by friendly competition.

2.7.4.1 TEAM SPORTSMANSHIP AWARD

The Team Sportsmanship Award recognizes a team which goes above and beyond to assist their fellow teams and the event organizers assure the Spaceport America Cup: Intercollegiate Rocket Engineering Competition is a productive, safe, and enjoyable experience for all involved. They may do this in many ways, such as making themselves available to lend-a-hand whenever and however they can (whether they are asked to or not), being positive role models for their fellow teams, and generally being a "force for good" in every activity in which they involve themselves. A team is considered eligible for the Team Sportsmanship Award by being present at the Spaceport America Cup.

2.7.4.2 TEAM SPIRIT AWARD

The Team Spirit Award recognizes a team which arrives at the Spaceport America Cup with proverbial (or literal) smiles on their face, a school flag in their hand, and never lets either waiver throughout the event. They show great pride in their work, learn from their mistakes, remain positive when things don't go their way, engage members of the general public with respect and enthusiasm, and show respect for invited guests by attending and participating guest speaker presentations whenever possible.A team is considered eligible for the Team Sportsmanship Award by being present at the Spaceport America Cup.

2.8 DISQUALIFICATION FROM CONSIDERATION FOR ANY AWARD

A limited number of criteria constitute grounds for disqualification from consideration for any award. These can include a failure to meet the defining IREC mission requirements recorded in Sections 2.0 through 2.5 of this document, failure to submit a Project Technical Report or third/final progress update at any time prior to the Spaceport America Cup (or otherwise failing to provide adequate project details in required deliverables), and failure to send eligible team member representatives to the Spaceport America Cup. Finally, any Team found to have accrued at least 10 safety or unsportsmanlike conduct infractions at any time during the Spaceport America Cup will be disqualified. Any individual observed committing a single, severe safety or unsportsmanlike conduct infraction may be summarily removed and barred from participation in the remainder of the Spaceport America Cup.

2.9 WITHDRAWAL FROM COMPETITION

Teams which decide to formally withdraw from the IREC at any time prior to the event must send an e-mail entitled "TEAM Your Team ID FORMALLY WITHDRAWS FROM THE Competition Year IREC" to experimentalsoundingrocket@gmail.com. For example, a team assigned the Team ID "42" would withdraw from the 2017 IREC by sending an e-mail entitled "TEAM 42 FORMALLY WITHDRAWS FROM THE 2017 IREC" to experimentalsoundingrocket@gmail.com.

3.0 INTERNATIONAL TRAFFIC IN ARMS REGULATIONS

Speakers and attendees of the Spaceport America Cup are reminded that some topics discussed at conferences could be controlled by the International Traffic in Arms Regulations (ITAR). The Spaceport America Cup is intended as an ITAR-free event. U.S. persons (U.S. citizens and permanent residents) are responsible for ensuring that technical data they present in open sessions to non-U.S. persons in attendance or in conference proceedings are not export restricted by the ITAR. U.S. persons are likewise responsible for ensuring that they do not discuss ITAR export-restricted information with non-U.S. nationals in attendance. Similarly, US personauthors of IREC Project Technical Reports as well as Podium Session submissions and associated slide decks are responsible for ensuring the content of their materials does not exceed the interpretation of "fundamental research" and the ITAR established by their affiliated academic institution(s).

APPENDIX A: ACRONYMS, ABBREVIATIONS, AND TERMS

ACRONYMS & ABBREVIATIONS	
AGL	Above Ground Level
AIAA	American Institute of Aeronautics and Astronautics
APCP	Ammonium Perchlorate Composite Propellant
APRS	Automatic Packet Reporting System
CFR	Code of Federal Regulations
CONOPS	Concept of Operations
COTS	Commercial Off-the-Shelf
ESRA	Experimental Sounding Rocket Association
FAA	Federal Aviation Administration
GPS	Global Positioning System
HPR	High Power Rocket *or* Rocketry
IREC	Intercollegiate Rocket Engineering Competition

ITAR	International Traffic in Arms Regulations
LOX	Liquid Oxygen
NAR	National Association of Rocketry
NMSA	New Mexico Spaceport Authority; aka Spaceport America
OML	Outer Mold Line
PII	Personally Identifiable Information
SAC	Spaceport America Cup
SDL	Space Dynamics Laboratory
SRAD	Student Researched & Developed
STEM	Science, Technology, Engineering, and Mathematics
TBD	To Be Determined
TBR	To Be Resolved
TRA	Tripoli Rocketry Association

TERMS	
Amateur Rocket	14 CFR, Part 1, 1.1 defines an amateur rocket as an unmanned rocket that is "propelled by a motor, or motors having a combined total impulse of 889,600 Newton-seconds (200,000 pound-seconds) or less, and cannot reach an altitude greater than 150 kilometers (93.2 statute miles) above the earth's surface".
Excessive Damage	Excessive damage is defined as any damage to the point that, if the systems intended consumables were replenished, it could not be launched again safely. Intended Consumables refers to those items which are - within reason - expected to be serviced/replaced following a nominal mission (e.g. propellants, pressurizing gasses, energetic devices), and may be extended to include replacement of damaged fins specifically designed for easy, rapid replacement.
FAA Class 2 Amateur Rocket	14 CFR, Part 101, Subpart C, 101.22 defines a Class 2 Amateur Rocket (aka High Power Rocket) as "an amateur rocket other than a model rocket that is propelled by a motor or motors having a combined total impulse of 40,960 Newton-seconds (9,208 pound-seconds) or less."
Non-toxic Propellants	For the purposes of the Spaceport America Cup: IREC, the event organizers consider ammonium perchlorate composite propellant (APCP), potassium nitrate and sugar (aka "rocket candy"), nitrous oxide, liquid oxygen (LOX), hydrogen peroxide, kerosene, propane

	and similar, as non-toxic propellants. Toxic propellants are defined as requiring breathing apparatus, special storage and transport infrastructure, extensive personal protective equipment, etc.

Tripoli requirements

Level 1 Certification allows flyers to fly High Power Rockets with a total installed impulse up to 640 newton-seconds.

Airframe - The rocket must be built by the flyer. The rocket shall have a display on the exterior identifying the calculated center of pressure. The rocket must be of "conventional rocket design". "Odd Rockets" including flying pyramids, saucers and flying spools will not be allowed for any certification flight. The rocket may be either a kit or scratch built. Scratch built rockets may contain commercially built components.

Recovery - Standard parachute recovery is required. Non-parachute recovery methods (e.g. tumble, helicopter, gliding, etc) are not permitted for certification flights. If the rocket is using dual deployment, the first recovery event may be via a drogue-less or streamer as long as the main or second event uses a standard parachute.

Motor – The certification flight must be with a single certified H or I motor (tested total impulse between 160.01 and 640.00 n-sec). Staged and/or Clustered rockets may not be used for certification flights. The flyer shall be observed by the certifying member or their designated representative during the assembly (if a reload or hybrid) and preparation of the motor.

Electronics – Electronics are not required for level 1 certification flights.

Certification Flight – Level 1 Certification flight may take place at any insured launch. The certifying member (i.e. Prefect, TRA Director, or TAP Member) must be present and witness the certification flight. The certifying member must witness the rocket ascend in a stable manner and descend in stabilized manner controlled by the recovery system.

Post-Flight Inspection – The rocket must be presented to the certifying member for inspection. If the rocket cannot be recovered, but can be inspected in place (power lines, tree, etc...) this is acceptable. The certifying member shall inspect the rocket for excessive damage. Excessive damage shall be considered damage to the point that if the flyer were handed another motor, the rocket could not be put on the pad and flown again safely. Damage caused by wind dragging will not cause a disqualification.

Non-certification – Any of the following will result in non-certification for a certification flight:

- Motor Cato
- Excessive Damage
- No recovery system deployment or tangled recovery system deployment
- Rocket drifting outside the specified launch range
- Components coming down not attached to the recovery system.
- Any other violation of TRA safety code associated with this particular flight.
- Any other legitimate reason the certifying member deems merits non-certification

Level 2 Certification allows flyers to fly High Power Rockets with a total installed impulse between 640.01 and 5120.00 n-sec.

Written Test – The written examination for level 2 shall be passed prior to a level 2 certification flight.

Airframe – The rocket must be built by the flyer. The rocket shall have a display on the exterior identifying the calculated center of pressure. The rocket must be of "conventional rocket design". "Odd Rockets" including flying pyramids, saucers and flying spools will not be allowed for any certification flight. The rocket may be either a kit or scratch built. Scratch built rockets may contain commercially built components.

Recovery - Standard parachute recovery is required. Non-parachute recovery methods (e.g. tumble, helicopter, gliding, etc) are not permitted for certification flights. If the rocket is using dual deployment, the first recovery event may be via drogue-less or streamer as long as the main or second event uses a standard parachute.

Motor – The certification flight must be with a single certified J, K, or L motor (tested total impulse between 640.01 and 5120.00 n-secs). Staged and/or Clustered rockets may not be used for certification flights. The flyer shall be observed by the certifying member or their designated representative during the assembly (if a reload or hybrid) and preparation of the motor.

Electronics – Electronics are not required for level 2 certification flights. However, prior to attempting level

3 certification, the flyer shall successfully fly at least one rocket in the Level 2 impulse range using an electronic device as the primary means of recovery system deployment. This may be their level 2 certification flight or any subsequent flight.

Certification Flight – Level 2 Certification flight may take place at any insured launch. The certifying member (i.e. Prefect, TRA Director, or TAP Member) must be present and witness the certification flight. The certifying member must witness the rocket ascend in a stable manner and descend in stabilized manner controlled by the recovery system.

Post-Flight Inspection – The rocket must be presented to the certifying member for inspection. If the rocket cannot be recovered, but can be inspected in place (power lines, tree, etc...) this is acceptable. The certifying member shall inspect the rocket for excessive damage. Excessive damage shall be considered damage to the point that if the flyer were handed another motor, the rocket could not be put on the pad and flown again safely. Damage caused by wind dragging will not cause a disqualification.

Non-certification – Any of the following will result in non-certification for a certification flight:

- Motor Cato
- Excessive Damage
- No recovery system deployment or tangled recovery system deployment
- Rocket drifting outside the specified launch range
- Components coming down not attached to the recovery system.
- Any other violation of TRA safety code associated with this particular flight.
- Any other legitimate reason the certifying member deems merits non-certification.

Level 3 Certification allows flyers to fly High Power Rockets with a total installed impulse greater than 5120 n-sec

Prerequisites for attempting Level 3 certification:

- The candidate must have successfully completed their Level 2 certification ***BEFORE*** they can commence their Level 3 certification process.
- The candidate will also need to demonstrate proficiency in flying Level 2 rockets with electronic recovery.
- **Prior to beginning construction** of an L3 certification project, your project design must be approved by your TAP members.
- The candidate needs to successfully design, build, fly and recover a rocket using a certified HPR motor in the M-O impulse range.

Airframe – The rocket must be built by the flyer. The rocket shall have a display on the exterior identifying the calculated center of pressure. The rocket must be of “conventional rocket design”. “Odd Rockets” including flying pyramids, saucers and flying spools will not be allowed for any certification flight. The rocket may be either a kit or scratch built. Scratch built rockets may contain commercially built components. Commercially available pre-fabricated fin cans, either as part of a kit or obtained separately, may not be used for level 3 certification flights.

Construction - TRA members designing or preparing to fly a level 3 project must present details of their design to 2 TAP members of their choice. ***BEFORE*** commencing construction, 2 TAP members must have signed off on the member’s certification form. TAP members should be kept informed of any changes during construction. In general, the TAP member for objectively assessing the rocket will need the following information:

- A completely filled out Pre-Flight Data Capture form
- Drawings of the rocket showing airframe components, fins, bulkheads, recovery system components, payloads, etc...
- A parts listing that includes material descriptions, adhesive types, screw sizes gauges, thicknesses, etc...
- A simplified wiring diagram of the electronic recovery system that shows the major components.
- Checklist describing: field assembly/preperation of the rocket, motor installation, recovery system preparation, launcher installation, system arming and disarming, etc.
- These items should be neatly drawn, and, if possible, lists typed. The primary preparation criteria are those drawings and lists are neat and legible. All items will be returned to the submitter if desired. A self-addressed envelope or supply postage funds to assist the TAP member with returns.

Do you have to document my build with pictures? The more pictures the better for the TAP members that are involved with your certification process. You will also need to supply at least one photograph of the builder working on project.

Motor – The certification flight must be with a single certified M or larger motor (tested total impulse greater than 5120.01 n-secs). Staged and/or Clustered rockets may not be used for certification flights.

The flyer shall be observed by the TAP member or their designated representative during the assembly (if a reload or hybrid) and preparation of the motor.

Electronics – Prior to a level 3 certification flight, the flyer shall successfully fly at least one rocket in the level 2 range using an electronic device as the primary means of recovery system deployment. Level 3 certification flights shall include at least two completely separate electronic devices, with independent power sources, wire harnesses, and ignition devices for the primary and back-up means of recovery system deployment.

Certification Flight – Level 3 Certification flight may take place at any insured launch. The TAP member must be present and witness the certification flight. The TAP member must witness the rocket ascend in a stable manner and descend in stabilized manner controlled by the recovery system.

Post-Flight Inspection – The rocket must be presented to the certifying member for inspection. If the rocket cannot be recovered, but can be inspected in place (power lines, tree, etc...) this is acceptable. The certifying member shall inspect the rocket for excessive damage. Excessive damage shall be considered damage to the point that if the flyer were handed another motor, the rocket could not be put on the pad and flown again safely. Damage caused by wind dragging will not cause a disqualification.

Non-certification – Any of the following will result in non-certification for a certification flight:

- Motor Cato
- Excessive Damage
- No recovery system deployment or tangled recovery system deployment
- Rocket drifting outside the specified launch range
- Components coming down not attached to the recovery system.
- Any other violation of TRA safety code associated with this particular flight.
- Any other legitimate reason the TAP member deems merits non-certification.